Durability of Cement Composites Reinforced with Sisal Fiber

Jianqiang Wei

Submitted in partial fulfillment of the
requirements for the degree of
Doctor of Philosophy
in the Graduate School of Arts and Sciences

COLUMBIA UNIVERSITY

2014

ABSTRACT

Durability of Cement Composites Reinforced with Sisal Fiber

Jianqiang Wei

This dissertation focuses mainly on investigating the aging mechanisms and degradation kinetics of sisal fiber, as well as the approaches to mitigate its degradation in the matrix of cement composites.

In contrast to previous works reported in the literature, a novel approach is proposed in this study to directly determine the fiber's degradation rate by separately studying the composition changes, mechanical and physical properties of the embedded sisal fibers. Cement hydration is presented to be a crucial factor in understanding fiber degradation behavior. The degradation mechanisms of natural fiber consist of mineralization of cell walls, alkali hydrolysis of lignin and hemicellulose, as well as the cellulose decomposition which includes stripping of cellulose microfibrils and alkaline hydrolysis of amorphous regions in cellulose chains. Two mineralization mechanisms, CH-mineralization and self-mineralization, are proposed.

The degradation kinetics of sisal fiber in the cement matrix are also analyzed and a model to predict the degradation rate of cellulose for natural fiber embedded in cement is outlined. The results indicate that the time needed to completely degrade the cellulose in the matrix with cement replacement by 30wt.% metakaolin is 13 times longer than that in pure cement.

A novel and scientific method is presented to determine accelerated aging conditions, and to evaluating sisal fiber's degradation rate and durability of natural fiber-reinforced cement composites. Among the static aggressive environments, the most effective approach for accelerating the degradation of natural fiber in cement composites is to soak the samples or change

the humidity at 70 ℃ and higher temperature. However, the dynamic wetting and drying cycling treatment has a more accelerating effect on the alkali hydrolysis of fiber's amorphous components evidenced by the highest crystallinity indices, minimum content of holocellulose, and lowest tensile strength.

Based on the understanding of degradation mechanisms, two approaches are proposed to mitigate the degradation of sisal fiber in the cement matrix.

In order to relieve the aggressive environment of hydrated cement, cement substitution by a combination of metakaolin and nanoclay, and a combination of rice husk ash and limestone are studied. Both metakaolin and nanoclay significantly optimize the cement hydration, while the combination of these two supplementary cementitious materials validates their complementary and synergistic effect at different stages of aging. The presented approaches effectively reduce the calcium hydroxide content and the alkalinity of the pore solution, thereby mitigating the fiber degradation and improving both the initial mechanical properties and durability of the fiber-cement composites. The role of rice husk ash in cement modification is mainly as the active cementitious supplementary material.

In order to improve the degradation resistance of sisal fiber itself, two novel, simple, and economical pretreatments of the fibers (thermal and sodium carbonate treatment) are investigated. Both thermal treatment and Na_2CO_3 treatment effectively improve the durability of sisal fiber-reinforced concrete. The thermal treatment achieves improvement of cellulose's crystallization, which ensures the initial strength and improved durability of sisal fiber. A layer consisting of calcium carbonate sediments, which protects the internals of a fiber from the strong alkali pore solution, is formed and filled in pits and cavities on the Na_2CO_3 treated sisal fiber's surface.

TABLE OF CONTENTS

LIST OF FIGURES

LIST OF TABLES

GLOSSARY

AFm	Tricalcium aluminate monosulfate hydrate
Aft	Tricalcium aluminate trisulfate hydrate
C_3A ($3CaO \cdot Al_2O_3$)	Tricalcium aluminate
C_4AF ($4CaO \cdot Al_2O_3 \cdot Fe_2O_3$)	Tetra-calcium Aluminoferrite
Cel	Fraction of cellulose left
CH ($Ca(OH)_2$)	Calcium hydroxide
CRHA	Coarse rice husk ash
Cr.I.	Crystallinity index
C_2S ($2CaO \cdot SiO_2$)	Dicalcium silicate
C_3S ($3CaO \cdot SiO_2$)	Tricalcium silicate
C-S-H ($xCaO \cdot SiO_2 \cdot yH_2O$)	Calcium silicate hydrate
CT	Tracheid and vessel element constituted as xylem
DTG	Derivative thermogravimetry
EDX	Energy Dispersive X-ray spectroscopy
ESI	Effective saturation indices
FRCC	Fiber-reinforced cement composites
FWHM	Full width half maxima
IAP	Ion activity product
ISA	Isosaccharinic acid
LCT	Lime consumption test
LS	Limestone
LSFM	Long Sisal Fiber-Reinforced Mortar
MK	Metakaolin
N7	Na_2CO_3 treatment for 7 days
N10	Na_2CO_3 treatment for 10 days
NC	Nanoclay
NCCP	Na_2CO_3 crystal particles
NFRCC	Natural fiber reinforced cement composites
PC	Portland cement
PSD	Particle size distributions
RHA	Rice husk ash
SEM	Scanning electron microscopy
SCM	Supplementary cementitious material
SCP	Short Sisal Fiber-Reinforced Cement Paste
SFRCC	Sisal fiber-reinforced cement composites
SFRC	Sisal fiber-reinforced concrete
SMA	Surface modification agent
TGA	Thermalgravimetric analysis
T_p	Post-cracking toughness
W&D	Wetting and drying cycle
XRD	X-ray diffraction
%Cr	Percentage of crystallinity
σ_f	First crack strength
σ_p	Post-crack flexural strength

This page intentionally left blank

ACKNOWLEDGMENTS

There are many people who have provided me with guidance and support throughout this hard-won journey, and to whom I owe a great deal of thanks.

First and foremost, I would like to express my deepest appreciation to my advisor and mentor, Professor Christian Meyer, who provided me with continuous support, guidance and encouragement, and who did everything to help me achieve my dreams. His refusal to accept anything but my best has made me a better researcher, thinker, writer and presenter. His perfectionism, dedication, endless advice and insight into my research made completion of this dissertation possible in three years.

I truly appreciate the consistent support of the Erbilgin Family, for providing me with the opportunity to pursue my doctorate through the Erbilgin Family fellowship at Columbia University.

I am especially grateful to Professors Huiming Yin, Shiho Kawashima, James Im and Ah-Hyung (Alissa) Park for their interest in my research, their willingness to serve on my defense committee and review this dissertation.

Additionally I would like to thank the faculty of the Fu Foundation School of Engineering and Applied Science and specifically those in the Department of Civil Engineering and Engineering Mechanics (CEEM) and Materials Science and Engineering (MS&E) Program who have contributed to my education or aided me in my research.

I am greatly appreciative of the assistance that I received from the staff of the Robert A.W. Carleton Strength of Materials Laboratory. This includes Mr. Adrian Brügger and Dr. Liming Li. Without their support and technical knowledge, I would not have been able to complete the experimental portion of my research. Additionally I would like to thank Ms. Elaine Macdonald and Mr. Scott Kelly for their countless help.

I could not have survived these past two years and eight months without encouragement, inspiration, sympathy and joy from my peers. I must express my appreciation to my friends at Columbia University including Xueyu Pang, Ying Wang, Nan Shi, Muqing Liu, Jinwoo Jang, Sung-Hwan Hang, Zhaoyi Li, Siwei Ma, Ye Qian, Chengye Xu, Jiaxing Liu, Hao Sun, Wang Yao, Sophie Zhang and Mei-Hui Lee. Their companion and help really made me live and do research work at Columbia more enjoyable. I will always cherish the friendships, which brought me limitless happiness in The City of New York.

Most importantly, I am grateful for my family for their endless love, meticulous care, and unconditional support, especially my parents, who raised me and supported me in all my pursuits. I must thank my love, Yuling, who stood by me patiently through the tough and stressful stages of my doctorate. My warm hearted thanks to my elder brother, Jianyong, and grandmother, Yunting, thousands of miles did not stop your caring for my life. Also my warmest thoughts to my grandfather, Jun Wei, who have been the mentor in my life and taught me more than I can ever possibly express in words.

It is always my greatest motivation to make you all proud!

Dedicated to my parents, Xianglan and Heping,

and your unwavering, endless love.

In memory of my grandfather, Jun Wei

This page intentionally left blank

CHAPTER 1: INTRODUCTION

This chapter provides an introduction to the development and challenges of using sisal fiber in cement composites. Section 1.1 introduces the background and objective of this research. Section 1.2 briefly reviews previous approaches to improve the mechanical properties and durability of natural fiber and natural fiber reinforced cement composites (NFRCC). Finally, Section 1.3 presents the outline of this thesis.

1.1 Background and Objective

1.1.1 Development of natural fiber reinforced cement based construction materials

As a crucial raw material for civilization, cement-based materials, e.g. concrete, are second only to water in terms of the amounts that are most commonly used by mankind (Manzano, Enyashin et al. 2012). Ranging from the 2,000-year-old Pantheon in Rome to modern skyscrapers and highways, cement composites occupy a most important position in the history of human development. An unprecedented demand and output of cement was driven by the on-going construction boom in developing nations such as China, Brazil and India. As Amato (2013) stated, if this year's expected global output of cement were somehow poured across Manhattan Island, the 3.4-billion-ton mass would solidify into a monolith about 14 meters high. The main disadvantage of cement composites are their low tensile strength and fracture toughness. In order to compensate for their poor tension behavior, they have been traditionally reinforced primarily with steel reinforcing bars. Their toughness is effectively improved with the use of uniformly distributed and randomly oriented short fibers to control the initiation and growth of microcracks (Balaguru and Shah 1992.). The desirable improvements of tensile behavior, flexural strength and toughness, and

ductility can all be realized by using fiber reinforcement. The increase in fracture energy is caused by the fiber itself and the bond between fiber and matrix. Commonly used fibers made of a variety of materials, such as steel, glass, polypropylene, and other polymeric materials, are known to lead to substantial improvements in fracture toughness. Most of these fibers have some disadvantages, though. For example, steel and carbon fibers are relatively expensive, and the environmental footprint of many synthetic fibers can be substantial. Natural fibers, on the other hand, improve the sustainability of cement composites by being renewable and considerably less costly.

The increasing environmental concern and awareness of industrial pollution are forcing the construction and manufacturing industries to search for innovative materials that are reliable, sustainable and can replace conventional synthetic fibers as reinforcement of structural materials. Natural fibers, such as sisal, jute, cotton, flax, hemp, kenaf, and so on, have already been considered as potential alternatives, given their environmental friendliness and ready availability in fibrous form and by the fact that they can be extracted from plant leaves at low cost (Silva, Chawla et al. 2008). Natural fiber reinforced composites also offer other advantages such as reduced dependence on non-renewable energy/material sources, lower pollutant emissions, lower greenhouse gas emissions, enhanced energy recovery, and biodegradability (Joshi, Drzal et al. 2004). Therefore, in the last two decades, considerable effort has been directed towards the use of various natural fibers, which are available in abundance in tropical and sub-tropical countries, as reinforcement of cement composites for producing cost-effective construction materials that promote sustainable development (Ramakrishna and Sundararajan 2005). Composites with natural fiber reinforcements are currently considered amongst the most promising structural materials in sustainable engineering technologies (Belaadi, Bezazi et al. 2013). They have served for useful purposes for a long time, but their application as concrete reinforcement is of more recent origin.

In countries where natural fibers of varying types are abundantly available, it makes economical sense to search for appropriate technologies to utilize such fibers as reinforcement of cement composites for housing and other construction. Due to their excellent mechanical properties, natural fiber-reinforced cement composites (NFRCC) constitute a new and distinct group of building materials with almost the same performance as that of conventional concrete composites reinforced with metallic, mineral or synthetic fibers (Aziz, Paramasivam et al. 1981).

Table 1.1: Properties of sisal fibers reported by different researchers (Li, Mai et al. 2000)

Density (Kg/m^3)	Moisture content (%)	Tensile strength (MPa)	Tensile modulus (GPa)	Maximum strain (%)	Diameter (μm)	Reference
1450	11	604	9.4-15.8	-	50-200	(Satyanarayana, Sukumaran et al. 1990)
1450	-	530-640	9.4-22	3-7	50-300	(Chand, Tiwary et al. 1988)
-	-	347	14	5	-	(Bessell and Mutuli 1982)
1030	-	500-600	16-21	3.6-5.1	-	(Pavithran, Mukherjee et al. 1987)
1410	-	400-700	9-20	5-14	100-300	(Kalaprasad, Joseph et al. 1997)
1400	-	450-700	7-13	4-9	-	(Nair, Diwan et al. 1996)
-	-	530-630	17-22	3.64-5.12	100-300	(Mukherjee and Satyanarayana 1984)
1450	-	450-700	7-13	4-9	-	(Kumar, Amma et al. 1995)

Sisal fiber promises to be a suitable natural reinforcement of cement composites on account of its low cost, low density, high strength and elastic modulus, no health risk, ready availability in many countries, and renewability (Li, Mai et al. 2000). A sisal plant produces between 200 and 250 leaves before flowering (Kallapur 1962) and each leaf contains approximately 700–1400 fiber bundles with a length of about 0.5–1.0 m (Oksman, Wallström et al. 2002). The sisal leaf consists of a sandwich structure composed of approximately 4% fiber, 1% cuticle, 8% dry matter, and 87% water (Mukherjee and Satyanarayana 1984). Nearly 4.5 million tons of sisal fiber are produced every year throughout the world. Tanzania and Brazil are the two main producing countries (Chand, Tiwary et al. 1988). The important properties of sisal fibers reported in the literature are summarized in Table 1.1.

1.1.2 Challenges in application and problem statement

In spite of sisal fiber's advantages, its usefulness in cement based materials is limited by the relatively low durability in alkaline environments, which means it loses strength when used as reinforcement of a cement matrix exposed to weathering (Aziz, Paramasivam et al. 1981). When exposed to the alkaline pore solution of Portland cement (PC), their mechanical properties can deteriorate due to alkaline hydrolysis, thereby compromising the durability of NFRCC (Deniel James I 2003). According to the thermalgravimetric analysis (TGA), the constituents of sisal fiber are mainly cellulose, lignin and hemicellulose (Bakare, Okieimen et al. 2010). One single natural fiber is composed of several elementary fibrils (typically 10–40), bound together by the pectin substances in the middle lamella (van Hazendonk, van der Putten et al. 1993, Baley, Busnel et al. 2006). As shown in Fig. 1.1, there are three distinct layers from outside to inside of a natural fibril: (i) the middle lamella containing pectin, hemicellulose and lignin; (ii) the primary cell wall containing hemicellulose and cellulose; (iii) the secondary cell wall consisting mainly of cellulose.

Cellulose is a linear polymer made of glucose subunits linked by β-1,4 bonds, and the basic repeating unit is cellobiose (Bergström and Gram 1984). Cellulose's stiffness and durability is supported by its formation of rigid, insoluble micro-fibril chains, integrated by the numerous intra- and intermolecular hydrogen bonds. The high tensile strength of cellulose enables plant cells to withstand osmotic pressure and is responsible for the resistance of plants to mechanical stress (Bergström and Gram 1984). The polymerization degree of cellulose in sisal fiber is around 25,000, which means the crystalline arrangement may be disrupted by the chain-ends (Gram 1983, Toledo Filho, Silva et al. 2009). The polymerization degree of hemicellulose and lignin, which are mainly in the primary wall and middle lamella, lies between 50-200 (Gram 1983) and around 60 (Word 2006), respectively. Hemicellulose, which emerges as an immense renewable biopolymer resource, is the second most abundant biopolymer in the plant kingdom, representing about 25-35% of lignocellulose biomass (Saha 2000, Kumar R. 2008, Junli, Xinwen et al. 2012), only less than cellulose. In contrast to cellulose in the main cell wall constituent, hemicellulose represents a type of hetero-polysaccharides with complex structures containing glucose, xylose, mannose, galactose, arabinose, fucose, glucuronic acid, and galacturonic acid in various amounts depending on the source (Ren and Sun 2010). The main chain is characterized by a β-1,4-linked-D-xylopyranosyl, which carries a variable number of neutral or uronic monosaccharide substituents (Joseleau 1992). Lignin is nature's most abundant aromatic (phenolic) polymer (Lora 2002), whose main function is to cement the cellulose fibers in plants. As a kind of three-dimensional network heteropolymer, lignin has a complex and non-uniform structure with aliphatic and aromatic constituents, resulting from the oxidative coupling of primarily the three p-hydroxycinnamyl alcohols (monolignols): p-coumaryl, coniferyl and sinapyl alcohols (Novo-Uzal, Pomar et al. 2012). The most common linkages formed during lignin biosynthesis are the β-O-4 ether linkages, followed by other types

of ether and C–C linkages such as α-O-4, β-β, β-5, and 5-5 (Hatfield and Vermerris 2001, Sugimoto, Akiyama et al. 2002, Nadji, Diouf et al. 2009). Because the low degradation resistance of lignin and hemicellulose that exist in the middle lamellae of the fibers and cellulose molecules in a high alkali environment (Singh 1985, Tolêdo Filho, Scrivener et al. 2000), sisal fiber gradually degrades and loses its reinforcing capacity in a cement matrix in the later stages of its service life. Therefore, the distinct cell wall structure is the cause of the excellent mechanical properties of natural fiber, with a low density, while it also leads to the poor durability of the fiber in a cement matrix.

Due to that poor durability, the cement composites suffer a decrease in post-cracking toughness when they undergo various aging processes. This durability problem is associated with an increase in fiber fracture and decrease in fiber pull-out resistance due to fiber mineralization (Flávio de Andrade Silva 2009), which is a result of precipitation of hydration products in the fiber cell walls. The degradation of natural fiber due to the alkaline pore solution in the cement matrix seriously decreases the durability and may cause premature failure of the composite.

Therefore, restraining the degradation of natural fibers in a cement matrix has been the central issue that needs to be solved before promoting the widespread application of natural fiber in various composites. Although a lot of effort has been made to improve the durability of NFRCC through fiber treatment and development of a calcium hydroxide (CH)-free matrix, the degradation and mineralization of natural fiber have still not been fully understood.

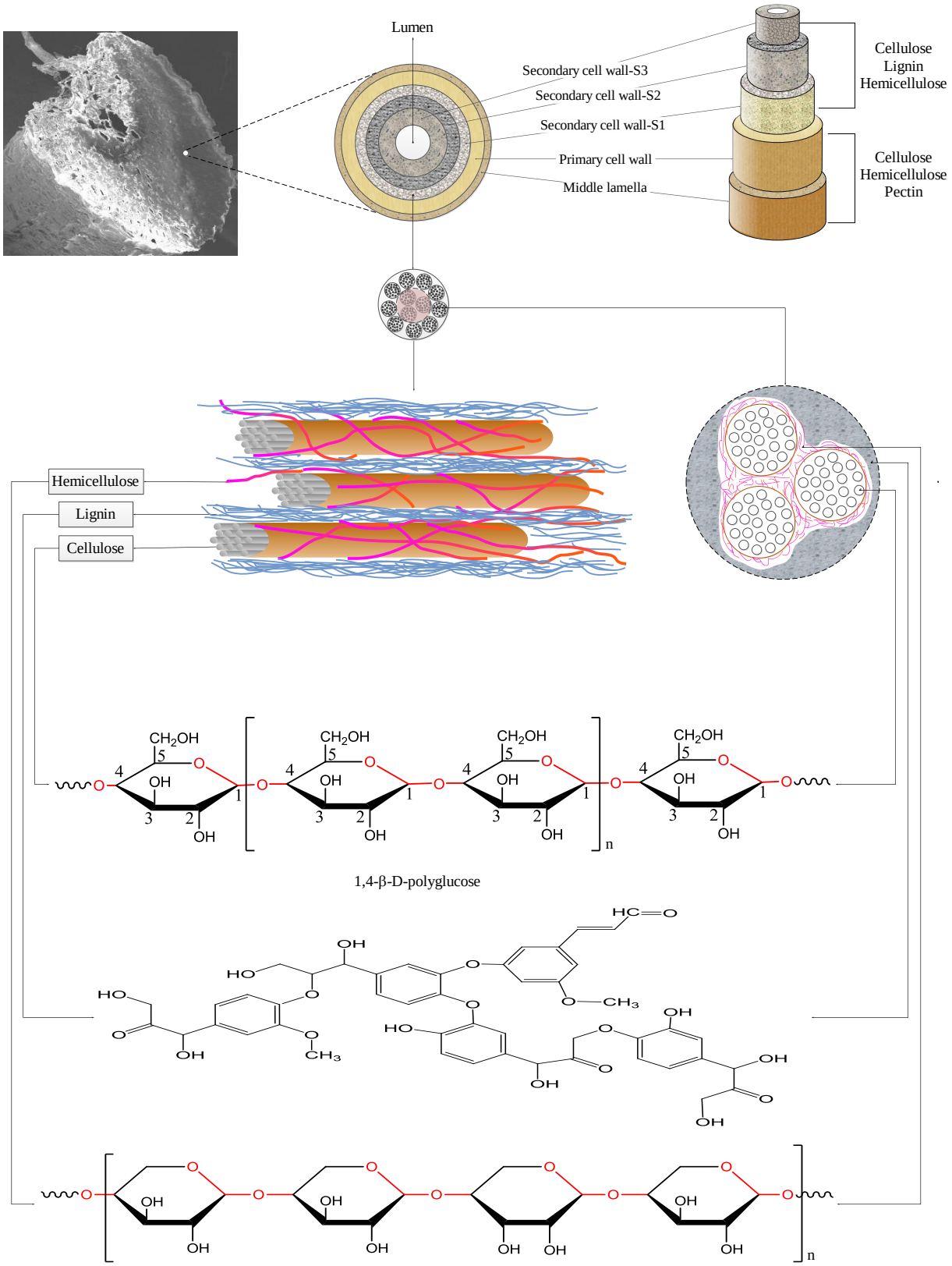

Figure 1.1: Microstructure, schematic diagram and molecular structures of natural fiber cell wall

In addition, the investigation of the degradation mechanisms and kinetics of natural fiber in the complex alkaline and mineral-rich environment of cement matrices, as characterized by hydration process, setting and hardening, strength growth, combined with hydration heat release, crystallization and the formation of micro cracks in various aggressive environments, were reported rarely. Only a few publications addressed the failure of natural fiber in cement composites. Gram (1983) and Tolêdo Filho et al. (2000) described the main aging mechanisms of natural fibers in cement based composites, i.e. the dissolution of lignin and hemicellulose in a cement pore solution and alkaline hydrolysis of cellulose molecules, which leads to the degradation of molecular chains and the reduction in degree of polymerisation and tensile strength. Besides, the crystallization of lime in the lumen and middle lamellae also decreases the fiber's flexibility and strength (Singh 1985, Tolêdo Filho, Scrivener et al. 2000). Mohr (2005) proposed a three-part progressive degradation mechanism during wetting and drying cycling, the third part of which is the fiber embrittlement due to fiber cell wall mineralization indicated by the lack of recovered toughness. Melo et al. (2013) investigated two fiber degradation mechanisms in PC composites: fiber mineralization and degradation of cellulose, hemicellulose and lignin due to the existence of calcium hydroxide and adsorption of calcium and hydroxyl ions. However, the results obtained so far have been disappointing, primarily because the intrinsic degradation kinetics and mechanisms of natural fiber and its three main components, cellulose, hemicellulose and lignin, in solid phase and pore solution of cement have not been successfully investigated. And there exists no model that can be used to predict the degradation rate of natural fiber in cement composites. Few designers would be willing to accept the risk of working with inherently unreliable reinforcement. Such difficulties could be alleviated if it were possible to build a parameterized model based on

cement hydration data to predict the fiber's deterioration degree as a function of embedment duration time.

1.1.3 Objectives and scope of dissertation

The primary objective of using NFRCC in construction is to increase the flexural strength and toughness of structural components. However, the durability of such composites exposed to various aggressive environments should be guaranteed. Yet the task of predicting the degradation degree of natural fibers as a reinforcement of cement matrices is much more difficult than merely determining the durability of the composites because this depends on many factors.

The research reported here centers on improving the durability of sisal fiber-reinforced cement composites (SFRCC). A novel approach is proposed to determine the degradation rate of the fiber and to gain an understanding of the degradation mechanisms and kinetics. Previous investigations as reported in the literature, determined the degradation of natural fiber by simply testing the mechanical properties and studying the microstructure of fiber-reinforced cement composites (FRCC). In the present work, separate studies of the composition changes, the mechanical properties and physical characterization of sisal fibers embedded in the cement matrix after accelerated aging treatment were performed to determine the degradation rate of the fibers. Such studies allow a fully rational description of the degradation mechanisms of NFRCC. Based on the previous work, three basic methods are further developed to evaluate the reliability of NFRCC in construction, i.e. (i) pretreatment of sisal fiber, (ii) modification of cement matrix, and (iii) the combination of the two. The research tasks can therefore be outlined as follows:

- Investigate the degradation mechanisms and kinetics of sisal fiber to develop a simple new model capable of predicting the degradation degree of fiber in a cement matrix and help to identify effective methods to arrest the fiber degradation.
- Propose an effective and rapid simple accelerated aging method to quantify the durability of SFRCC.
- Investigate the correlation between the degradation of sisal fiber and the degree of hydration of cement with and without supplementary cementitious materials.
- Modify the cement matrix by using single and binary supplementary cementitious materials, as well as slurry treatment, to limit the fiber degradation and to improve the durability of SFRCC.
- Develop a novel, simple fiber pretreatment approach to improve the durability of SFRCC by slowing down the degradation of sisal fiber itself and the interfacial adhesion between fiber and cement matrix.

1.2 Literature Review

1.2.1 Application of natural fiber in composites

With advantages of low cost, lightweight and excellent mechanical properties, natural fibers have the potential of offering superior alternatives to the traditional fibers as reinforcement of various composites. Joshi (2004) reviewed selected comparative life cycle assessment studies of natural fiber and glass fiber composites, and concluded that natural fiber composites are likely to be environmentally superior to glass fiber composites in most cases, for the following reasons: (1)

low environmental impacts; (2) low CO_2 emissions; and (3) end of life incineration results in recovered energy and carbon sequestration credits.

Due to their eco-friendliness and bio-degradability, natural fibers are used as a replacement of traditional fibers, such as steel, AR-glass, and polypropylene, low-density polyethylene (Joseph, Thomas et al. 1992, Joseph, Thomas et al. 1993, Joseph, Thomas et al. 1993, Joseph, Kuriakose et al. 1994, Joseph, Thomas et al. 1995, Joseph, Thomas et al. 1996), polyester (Pavithran, Mukherjee et al. 1987, Pavithran, Mukherjee et al. 1988), and styrene-butadiene rubber composites (Kumar, Amma et al. 1995). Jute fiber (P. Kumar 2004, P.K. Banerjee 2008, Das and Banerjee 2013), sisal fiber (He and Liu 2003, Oda, Leomar Fernandes Jr et al. 2012), coconut coir fiber (Suchismita , Bindu 2009, Thulsairajan and Narasimha 2011, Oda, Leomar Fernandes Jr et al. 2012, Do Vale, Casagrande et al. 2013), and hemp fiber (Delgado H 2011) have been utilized and shown to have beneficial effects as modifiers in bituminous mixes by improving the performance of pavements to meet increasing traffic loads.

Since the 1970s many countries have banned the use of asbestos, which can cause diseases such as lung cancer if inhaled. This forced researchers to search for appropriate replacements as reinforcement of brittle cement composites, such as mortar and concrete. Therefore, at the end of the 1970s (Juárez, Durán et al. 2007), a systematic evaluation of engineering properties of natural fiber was performed, including the performance of Portland-cement-based composites containing these fibers, due to their ready availability in large quantities in many countries, and as a continuously renewable resource. The reinforcing effects of natural fibers, such as sisal, coconut coir, and cotton stalk fibers, in gypsum based materials (Hernández-Olivares, Oteiza et al. 1992, Singh and Garg 1994, Li, Yu et al. 2003, Carvalho, Calil Júnior et al. 2008) were investigated in the last two decades. In 1979, Andonian et al. (1979) studied the strength and fracture properties

of cellulose fiber reinforced cement composites and suggested that the fracture toughness principally depends on the work dissipated in pulling the cellulose fibers out from the cement mortar matrix. In 1992, Coutts et al. (1992) investigated the effect of sisal pulp on the mechanical properties of cement mortar and the results indicate that the optimum formulation provides a 50-60-fold increase in fracture toughness and a doubling of flexural strength compared with that of the neat matrix. The interfacial bond strength of sisal in cement composites was studied by Bessell (1982), who concluded that the interfacial adhesion between sisal fiber and cement matrix is poor due to the water absorbtion of sisal. Swift (1979) presented a model of the flexural behavior of cement-based composites reinforced with low-modulus sisal fiber. An experimental program was carried out and confirmed the theoretical predictions of increases in flexural strength.

1.2.1 Treatment methods for improving mechanical properties of natural fiber

Due to the non-homogeneous nature and complex components of sisal fibers, several approaches to improve their mechanical properties have been studied, such as alkali treatment, H_2SO_4 treatment, conjoint H_2SO_4 and alkali treatment, benzol/alcohol dewax treatment, acetylated treatment, thermal treatment, alkali-thermal treatment and thermal-alkali treatment, and so on. The treatment of natural fiber not only improved the mechanical properties of the fiber itself, but also enhanced the interfacial bond between fiber and matrix.

Alkali treatment. The alkali treatments were carried out using various alkali solutions to partially remove the lignin, hemicelluloses and other residues from the surface of fibers (Barreto, Costa et al. 2010). Barreto (2011), Rong (2001) ,Yang (1996), Khan (2011), and Joseph (1996) studied the effect of alkali (NaOH) solution on the mechanical properties of both natural fibers and natural fiber reinforced composites. Their results show that alkali treatment directly affects the thermal and mechanical properties of natural fibers and can remove the content of natural and

artificial impurities, thereby producing a rough surface topography. Consequently, the adhesion between fiber and matrices and the mechanical properties of NFRCC were significantly improved.

H_2SO_4 treatment. Yang et al. (1996) immersed sisal fibers in solutions of 2% H_2SO_4 at 60 ℃ for different durations. Then they washed the treated fibers thoroughly with water to neutral (pH = 7) and oven dried them. The results showed that H_2SO_4 decreases fracture strength and Young's modulus of sisal fiber, and that the elongation changed insignificantly.

Benzol/alcohol dewax treatment. In benzol/alcohol dewax treatment, Yang et al. (1996) put sisal fibers in soxhlet extraction with mixed solution of benzol and alcohol with ratio of 1:1 at 80℃ for 24 h. The fracture strength and elongation at failure of sisal fiber were improved, but Young's modulus was reduced.

Acetylated treatment. Rong (2001) and Yang (1996) studied the acetylated treatment of sisal fiber. The results indicate that, compared with the untreated fiber, the treated fiber presented an improved tensile strength, rougher and uneven surface morphology, a higher interfacial bonding in epoxy, and thereby an increased flexural strength.

Organosilane coupling agent treatment. In the work reported by Rong et al. (2001), it was shown that both tensile and flexural strengths of organosilane treated fiber reinforced composites were slightly higher than those of untreated fibers because of the reaction between amine groups of the coupling agent and epoxy resin. However, the tensile strength of sisal fiber was reduced.

Cyanoethylation treatment. Rong et al. (2001) used cyanoethylation as a surface modifier to treat sisal fibers. Lower crystallinity of cellulose, tensile strength, and Young's modulus were obtained, and the elongation at break increased by 80.0%.

Thermal treatment. The works of both Rong (2001) and Yang (1996) indicate that the best heat treatment for tensile properties was 150℃ for 4 h with the result that fracture strength and Young's modulus were improved by 36% and 3.4%, respectively.

In addition, thermal-alkali treatment (Yang, Zeng et al. 1996), hornification treatment,(Claramunt, Ardanuy et al. 2011), and other treatments of natural fibers using isocyanate, dicumyl peroxide, benzoyl peroxide and permanganate (Joseph, Thomas et al. 1996), and mixed treatments (Yang, Zeng et al. 1996) were also investigated and illustrated considerable enhancement of tensile strength of fiber and the mechanical behavior of natural fiber-reinforced composites.

Compared with other treatment methods, alkali treatment is more economical, but it may reduce the fibers' tensile strength, Young's modulus and other mechanical properties. In contrast, thermal treatment can increase the strength and modulus properties of sisal fibers, and it is also economical and easy to perform. Whether this or other methods can also improve the durability of sisal fiber-reinforced cement composites is not known. To find out the most effective methods is the main objective of the work reported here.

The fiber treatment methods can be divided into two groups: a) physical treatments (thermal or cold) to improve the properties of sisal fiber, such as strength, modulus and elongation; b) chemical treatments to improve the interfacial properties between fiber and matrix and durability of sisal fiber in cement based composites.

1.2.2 Methods for improving durability of NFRCC

The deterioration of natural fiber in the alkaline-mineral environment of Portland cement composites seriously decreases the durability and can lead to premature failure of the composites.

Therefore, restraining the degradation of natural fibers in a cement matrix has been a central issue that needs to be solved as a condition before promoting the widespread application of natural fiber in various composites. Actually, the cement matrix can affect the degradation of natural fibers in three different ways:

(i) The alkaline pore water dissolves the lignin and hemicellulose of fiber, which are sensitive to $Ca(OH)_2$ and high alkalinity (Gram 1983, Tolêdo Filho, Scrivener et al. 2000).

(ii) Alkaline hydrolysis of cellulose molecules leads to degradation of molecular chains and then a reduction in the degree of polymerisation and lower tensile strength (Gram 1983, Tolêdo Filho, Scrivener et al. 2000).

(iii) Crystallization of lime in the lumen, walls of the individual fibers and middle lamellae leads to a decrease in the technical fiber flexibility and strength (Singh 1985, Tolêdo Filho, Scrivener et al. 2000).

Two basic methods were selected in the work reported in the literature to improve the durability of NFRCC:

(i) Modification of cement matrix----using pozzolanic materials as partial replacement of Portland cement (PC) to reduce or eliminate the creation of calcium hydroxide, which is the primary cause of the alkaline environment in cement. Tolêdo et al. replaced the PC by calcined clay (metakaolin (MK) and calcined waste crushed clay brick) (Silva, Melo Filho et al. 2006, Toledo Filho, Silva et al. 2009, Martin, Martins et al. 2010), or 50% of Portland cement was replaced by MK (D'Almeida, Melo Filho et al. 2009). This produced a matrix totally free of calcium hydroxide so that there was none to migrate to the fiber lumen, middle lamella and cell walls and cause embrittlement. Ground granulated blast furnace slag (Savastano Jr, Warden et al. 2003, Agopyan, Savastano et al. 2005), silica fume, fly ash, and MK (de

Gutiérrez, Díaz et al. 2005, Mohr, Biernacki et al. 2007) have similar effects. The work of Pimentel (2006), Tonoli (2010), and Soroushian (2012) shows that polymers and accelerated carbonation (CO_2 saturated environment) also contribute to an increase of durability. This modification is an effective way to improve the durability of NFRCC, but the dosage of the cementitious materials must be determined carefully in order to achieve similar or higher performance compared to the composites prepared only with ordinary Portland cement (Claramunt, Ardanuy et al. 2011).

(ii) Pretreatment of natural fiber including chemical, physical and physicochemical methods. Silane coating, hornification, autoclave, sodium silicate, potassium silicate (Cooke , Pehanich, Blankenhorn et al. 2004, Bilba and Arsene 2008, Claramunt, Ardanuy et al. 2011) have been shown to improve the mechanical properties and durability of natural fiber in cement based materials.

Compared with method (i), pretreatment of natural fiber may require more effort and higher cost, and needs to consider the compatibility between modifying agent and cement matrix, as well as its effect on the interfacial properties of fiber-cement. Therefore, it is more logical to improve mechanical properties and durability of NFRCC through modifying the hydration of cement by reducing the content of CH and the alkalinity of both solid phase and pore solution of the matrix.

1.2.3 Interfacial bond between natural fiber and cement matrix

The interfacial bond between fiber and cement matrix was also considered as an additional factor, which affects the mechanical properties of the composite. It is well known that NFRCC fail by a combination of fiber fracture and pull-out (Campbell and Coutts 1980, Coutts and Kightly 1982). However, fiber pull-out is the principal mechanism of failure (Andonian, Mai et al. 1979). Awwad (2013) showed that the use of fibers in concrete without prior treatment is not advisable

because the bond is weaker and the tensile properties are not enhanced in the presence of fibers. The interfacial bond in cement-based fiber composites can be affected by several variables such as the water/cement ratio (Savastano Jr and Agopyan 1999), porosity, fiber shape and morphology (Silva, Mobasher et al. 2011), and compaction (Cunha, Barros et al. 2010). Various other approaches to improve the bond strength have been investigated. Coutts (1979) modified the interfacial bond between wood fiber and cement matrix using coupling agents, and the results indicated that the flexural strength and fracture energy of the composites were significantly improved. According to Blankenhorn (2001), both an acrylic emulsion and alkylalkoxysilane surface treatments of natural fiber led to improvements of the bending strength of fiber–cement composites. Air curing was proposed by Coutts (1987) and the results showed that this physical method effectively improves the natural fiber-cement matrix interface properties by interlocking fibers with the growing cement hydrate needle products. As has been detailed above, several methods have been developed to improve the natural fiber-cement interfacial properties. However, these methods introduce an additional step into the mechanical property improvement process, and they are unable to prevent the deterioration of natural fiber in the alkaline environment of concrete. In this sense, it is advantageous to enhance both the interface and durability of natural fiber in concrete by a single surface treatment method.

1.3 Outline of the Dissertation

Chapter 1 introduces the concept of using natural fibers in general and sisal fibers in particular as reinforcement of cement composites. The primary challenge in realizing this concept is the degradation of mechanical properties of the fibers caused by the alkalinity of the pore solution and the high calcium hydroxide content in Portland cement matrices. A brief review of

approaches to improve the mechanical properties of natural fibers and their durability in cement composites is also included.

Chapter 2 characterizes the raw materials used and describes the experimental programs. Chemical and mineralogical compositions and readily soluble compounds of Portland cement and supplementary cementitious materials (SCM) are analyzed. The pozzolanic activity of each SCM is also determined. Physical and chemical properties of sisal fiber, as well as the molecular structures of cell walls are analyzed. The entire treatment program is divided into two parts: modification of cement matrix and pretreatment of natural fiber. Matrix modification methods and fiber pretreatment operations are presented. The methods to characterize the hydration of cement, including heat evolution, mineralogical development, portlandite and bound water content, elemental analysis of calcium silicate hydrate (C-S-H) phases and pore solution, are also given. X-ray diffraction analysis, thermogravimetric analysis and microstructure analysis (using scanning electron microscope) were performed to determine the degradation rate of natural fiber embedded in different cement-based composites. The mechanical tests, such as compression and flexure of composite beams, the tension of natural fiber, and pull-out test, are also described in detail.

In Chapter 3, the effects of 10 and 30 wt.% replacement of Portland cement by metakaolin on the cement hydration kinetics, the chemical composition of hydrate phases, development of concentration of alkali elements in the pore solution and microstructure of the cement matrix are presented and analyzed. The degradation rate of fiber was investigated by analyzing the tensile behavior of a pulled out fiber, changes of the three main fiber components, and the amount of precipitated calcium hydroxide in the fiber's lumen and cell wall. The correlations between hydration degree, alkalinity, calcium hydroxide content of cement matrix and the fiber degradation are investigated. The alkaline degradation mechanisms of natural fiber and cell wall mineralization,

due to the high alkalinity and mineral nature of both cement solid phase and pore solution, are analyzed in detail. The degradation kinetics of sisal fiber in pure cement and the effect of metakaolin are analyzed systematically, and a model to predict the degradation rate of cellulose in natural fiber, is also proposed.

Chapter 4 describes an investigation to understand the influence of different accelerated aging conditions on the degradation rate of sisal fiber in a cement matrix and the most effective aging method to test the durability of SFRCC is determined. The effect of four temperatures under dry and wet environments, as well as the wetting and drying cycles, on the decline of mechanical properties of SFRCC, and the fiber tensile strength are studied.

Chapter 5 investigates the improvement of durability of SFRCC and the mitigation of sisal fiber's degradation through modification of the cement matrix. Portland cement was partially replaced by supplementary cementitious materials, such as MK, nanoclay (NC), rice husk ash (RHA), limestone (LS), and various combinations of them. The degradation of sisal fiber in cement matrices was investigated indirectly by testing the flexural behavior of SFRCC beams, and directly by testing the uniaxial tensile properties, thermal decomposition, crystallinity indices, and microstructures of embedded fibers, characterized by means of uniaxial tensile testing, thermal gravimetric analysis (TGA), X-ray diffraction (XRD), and scanning electron microscopy (SEM), respectively.

Chapter 6 identifies thermal and Na_2CO_3 treatment and their effects on the degradation of sisal fiber and durability of sisal fiber-reinforced concrete exposed to wetting and drying cycles. The microstructure, tensile strength and Young's modulus of sisal fiber as well as the weight loss of the composite were evaluated. Of primary interest were the effects on compressive and splitting

tensile strength of sisal fiber-reinforced concrete. The mechanisms of these two treatment methods were also analyzed.

Chapter 7 summarizes the primary findings of this study. Main conclusions are provided and topics for possible further research are proposed.

CHAPTER 2: EXPERIMENTAL METHODS AND PROGRAM

2.1 Materials

Sisal fiber. In this project, two similar dry and subtly combed types of sisal fiber from Madagascar and Tanzania, without knots or other impurities, provided by Bast Fibers LLC of Creskill, New Jersey, were used. The raw sisal fiber with a beige color features an average diameter of 202.5 μm, and a moisture content of 10.4±3%. Figs. 2.1-a and b show the microstructures of surface and cross section of a sisal fiber, respectively. The fiber's rough surface promises to provide a desirable bond strength between fiber and cement matrix, but it also can easily cause the precipitation of cement hydration products on the fiber surface. The fiber used in this research was characterized with a horse-shoe shaped cross section.

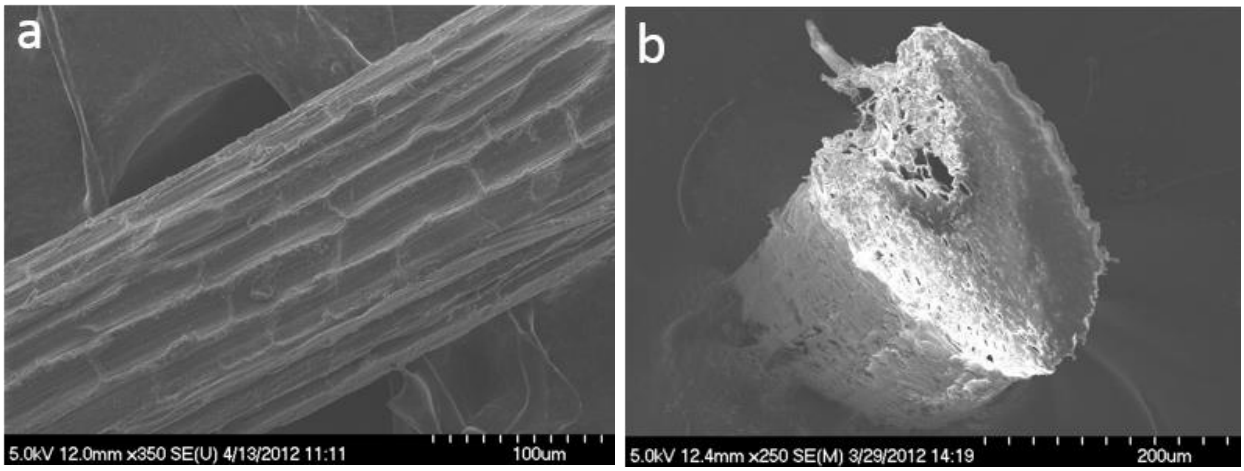

Figure 2.1: Microstructure of sisal fiber surface and cross section

Cement. Two different cements, Type I and Type III Portland cement, were used. To expedite the test program, Type III Portland cement was used to produce concrete specimens reinforced with randomly oriented short fibers. For the mortar beams reinforced with unidirectional long fibers, Type I Portland cement was selected. The chemical compositions and

particle size distributions (PSD) of the two cements are shown in Table 2.1 and Fig.2.2, respectively. The overall PSD of the two cement types are similar, but the mean particle size of Type I cement is larger than that of Type III cement. The specific surface area of Type I cement is 1.3 m^2/g. while the specific surface area, surface weighted mean and volume weighted mean of Type III are 1.72m^2/g, 3.493 μm and 12.269 μm, respectively.

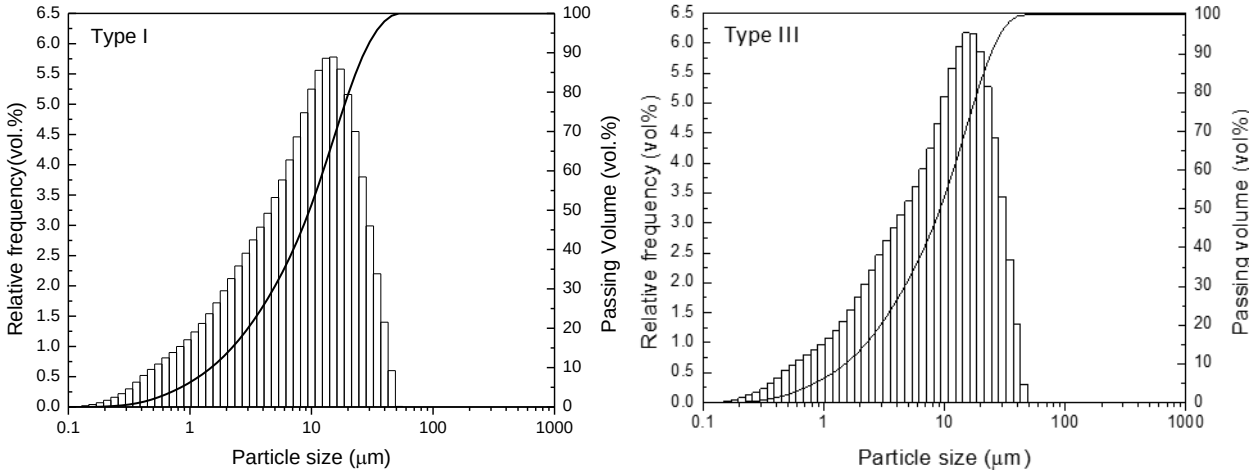

* The histogram shows the relative frequency of particles in dependence of the size (noncumulative) and the solid line shows the volume of the particles smaller than a certain size (cumulative).

Figure 2.2: Particle size distributions of Portland cement determined by means of laser diffraction

Table 2.1 Chemical and mineralogical composition of the used cement.

	Oxide composition [wt.%]		Mineralogical phase composition of Type I cement [wt.%]	
	Type I cement	Type III cement		
CaO	63.7	60.3	C_3S^a	52.4
SiO_2	12.9	16.7	C_2S^b	16.0
Fe_2O_3	7.97	8.33	C_3A^c	10.2
SO_3	5.25	3.96	C_4AF^d	8.6
Al_2O_3	4.14	3.47	Magnesite	0.3
MgO	3.50	4.52	Calcite	0.5
SrO	0.915	0.478	Periclase	0.9
K_2O	0.907	0.664	Dolomite	1.2
Na_2O	-	1.06	Anhydrite	2.3
TiO_2	0.279	0.125	Hemihydrate	2.0
ZnO	0.251	0.146	Arcanite	2.5
ZrO_2	0.119	0.0953	Ankerite	0.6
Cl	0.279	0.0548	Aphtitalite	0.4
BaO		0.131	Quartz	0.2
O	-	0.000021	Syngenite	2.0
Compton	0.98	1.30	Siderite	0.3
Rayleigh	1.19	1.41		

[a] C_3S-Tricalcium silicate, [b] C_2S-Dicalcium silicate, [c] C_3A Tricalcium aluminate, [d] C_4AF Tetra-calcium Aluminoferrite

Recycled concrete aggregate and sand. Concrete debris was obtained from a demolished building on the Manhattanville construction site in New York City. First, all major impurities were removed by hand. Next, large boulders of concrete were reduced in size with sledge hammers. In step three, the concrete was fed into a Chipmunk Jaw Crusher – Type VI, manufactured by BICO Inc., which permitted the selection of the maximum size of the output. The recycled aggregate was sieved and separated into coarse aggregate (between 4.75 mm and 12.7 mm) and fine aggregate (< 4.75 mm). In the final step, impurities such as brick were sorted out by hand again to make sure that the aggregate was as clean as possible.

Supplementary cementitious materials (SCMs). A total of 5 different SCMs were used to modify the cement matrix. These were metakaolin (MK), nano-clay (NC), two kinds of rice husk ash (RHA), and limestone (LS) powder. MK is a thermally activated alumino-silicate material with high pozzolanic activity comparable to or exceeding the activity of silica fume. Therefore it is a promising supplementary material for manufacturing high-performance concrete, owing to its effects on mechanical properties and physical behavior of the cement matrix (Caldaron and Burg 1994, Wild, Khatib et al. 1996, Coleman and Page 1997, Ding, Zhang et al. 1997, Sha and Pereira 2001, Courard, Darimont et al. 2003, Li and Ding 2003, Batis, Pantazopoulou et al. 2005, Ramezanianpour and Bahrami Jovein 2012). The reactivity of MK has been linked to its content of penta-coordinated aluminum ions that are formed during the dehydroxylation process (Rocha and Klinowski 1990, Coleman and McWhinnie 2000, Fernandez, Martirena et al. 2011, Antoni, Rossen et al. 2012) from kaolinite to MK between 600 and 800 ℃ (Murat and Comel 1983, He, Osbaeck et al. 1995). According to Ambroise (Ambroise, Maximilien et al. 1994), by mixing MK in PC, CH is quickly consumed, the microstructure is rich in C-S-H and strätlingite (C_2ASH_8), and the pore size distribution is displaced toward smaller values. Sha et al. (2002) investigated the

hydration products of PC pastes partially replaced by MK, and the results indicated that with 15% or higher MK replacement, there should be no calcium hydroxide left in the system after hydration and pozzolanic reactions are complete. Cement substitution by a combination of metakaolin and limestone was performed by Antoni et al. (2012), who showed 45% of substitution by 30% of MK and 15% of LS gives better mechanical properties at early age than neat PC and the calcium carbonate reacts with alumina from the MK, forming supplementary AFm phases and stabilizing ettringite.

Nanoclay (NC) is a new generation of processed clays that can be utilized in a wide range of high performance composites (Jahromi and Khodaii 2009). As a kind of nano-pozzolanic materials, NC can not only reduce the pore diameter and create enhanced porosity properties of the matrix at early age, but also improve the early strength of cement composites. When NC particles replace up to 2% PC, they can accelerate C-S-H gel formation at early age (Arabani, Haghi et al. 2012). Farzadnia et al. (2013) showed that the compressive strength of cement with 3% MK was increased by 24%, with increased formation of C–S–H, more consumption of CH and denser microstructure. Kawashima et al. (2013) reported that NC can considerably increase the strength of self-consolidating concrete for reduced formwork pressure and slip form paving.

Although both MK and NC can increase the degree of flocculation and floc size, they reduce the amount of CH and improve the microstructure of the cement matrix with different mechanisms. In this sense, it is of interest to modify the cement matrix using a combination of these two active clayey minerals with different chemical compositions and particle sizes. In this chapter, we studied the properties of mixes with combined additions of MK and NC, assuming that the modification on both micro- and nano scales maintains good properties and that the amount of CH can be reduced effectively with balanced flocculation. The hydration heat, mechanical properties,

microstructure, and content of CH at different ages were analyzed to investigate the effect of the two pozzolanic materials on the properties of the cement matrix. The effect of MK and NC on durability of natural fiber reinforced cement mortar and the degradation of natural fiber was evaluated by determining the flexural behaviors of composites, uniaxial tensile strength and physical-chemical properties of the embedded fibers subjected to wetting and drying cycles.

Rice husk ash (RHA) is a by-product of the burning of rice husk. More than 100 million tons rice husk are produced each year as a waste material in agricultural processes. In order to rationally dispose this renewable biomass, power plants fueled by rice husk have experienced an unprecedented development in several countries, such as Thailand, China, Philippines, India, Surinam, Malaysia, the United States, and so on. Rice husk can convert about 20% of its weight to RHA after incineration (Anwar 2001). Therefore the disposal of rice husk ash has become an important issue. Owing to the high amorphous silica content and high specific surface area, RHA has been used in construction materials as SCM to supply high pozzolanic reactivity. RHA has desirable modifying effects on properties of cement composites, such as higher compressive and flexural strengths (Zhang 1996, Rodr ́guez de Sensale 2006), enhanced workability (Habeeb 2009), declined bulk density (Hamzeh, Ziabari et al. 2013, Torkaman, Ashori et al. 2014), improved durability (Sousa Coutinho 2003, Chindaprasirt, Kanchanda et al. 2007), increased degree of cement hydration at later age (Van Tuan, Ye et al. 2011), and reduced amount of CH (Zhang, Lastra et al. 1996). However, the effect of RHA on degradation of natural fiber in the matrix of cement composites still lacks in-depth and systematic investigation.

The chemical compositions, particle size distributions (PSD), and X-ray characterizations of these cementitious materials are given in Table 2.2, Fig. 2.3 and Fig. 2.4, respectively. The main difference between MK and NC is the higher aluminide fraction in MK, and the higher silicide

fraction in NC, which also contains small amounts of reactive phases like magnesia and sodium oxide. Furthermore, NC shows overall higher amounts of CaO, ZnO and Fe_2O_3 and lower content of TiO_2 compared to MK. The main difference between the two rice husk ashes (RHA and coarse rice husk ash - CRHA) is the higher amorphous silica fraction in RHA (94.1 wt.% compared to 90.45 wt.% in CRHA), which also contains lower amounts of carbon due to the more complete incineration.

Table 2.2: Chemical and mineralogical composition of the used materials

	Oxide composition [wt.%]				
	MK	NC	RHA	CRHA	LS
CaO	0.0707	0.949	0.49	0.51	56.49
SiO_2	51.8	62.0	94.1	90.45	0.05
Fe_2O_3	4.15	6.51	0.046	0.015	0.04
SO_3	0.105	0.199	0.057	0.037	-
Al_2O_3	42.4	17.1	0.037	0.016	0.55
MgO	-	7.45	0.27	0.24	0.29
SrO	0.0397	0.0442	-	-	-
K_2O	0.218	0.0717	1.79	1.67	0.04
Na_2O	-	5.03	0.052	0.031	0.03
TiO_2	1.07	0.224	0.018	0.009	0.04
ZnO	-	0.0283	-	-	-
ZrO_2	0.0884	0.146	-	-	-
P_2O_5	-	-	0.89	0.76	-
MnO	-	-	0.13	0.07	-
Cl	0.0457	0.185	-	-	-
Carbon	-	-	2.12	6.19	
Other	0.0125	0.0628	0	0	42.47

The particle size distributions (PSD) of PC, and the SCMs measured by means of laser diffraction are shown in Fig. 2.3. As shown, the overall PSDs of NC and PC are relatively similar, but the MK shows a higher fraction of particles with a diameter smaller than 5 μm. The BET-specific surface area of MK (2.93 m^2/g) is higher than that of NC (0.873 m^2/g). The surface weighted means of MK and NC, with volume weight means of 9.632 μm and 30.751 μm, were

2.049 µm and 6.873 µm, respectively. The overall PSD of the RHA and LS are relatively similar, but RHA shows a higher fraction of particles with a diameter smaller than 3 µm compared to LS. The surface weight and volume weight means of LS are 16.46 and 50.66 µm, which are 58.37% and 36.57% greater than those of RHA, respectively. The particle size of CRHA is mainly between 11 and 300 µm, with the highest surface weight and volume weight means. Due to the occurrence of hollow and porous particles, the BET-specific surface area of RHA (0.577 m^2/g) is 77.54% higher than that of LS (0.325 m^2/g). The CRHA has a specific surface area of 0.193 m^2/g.

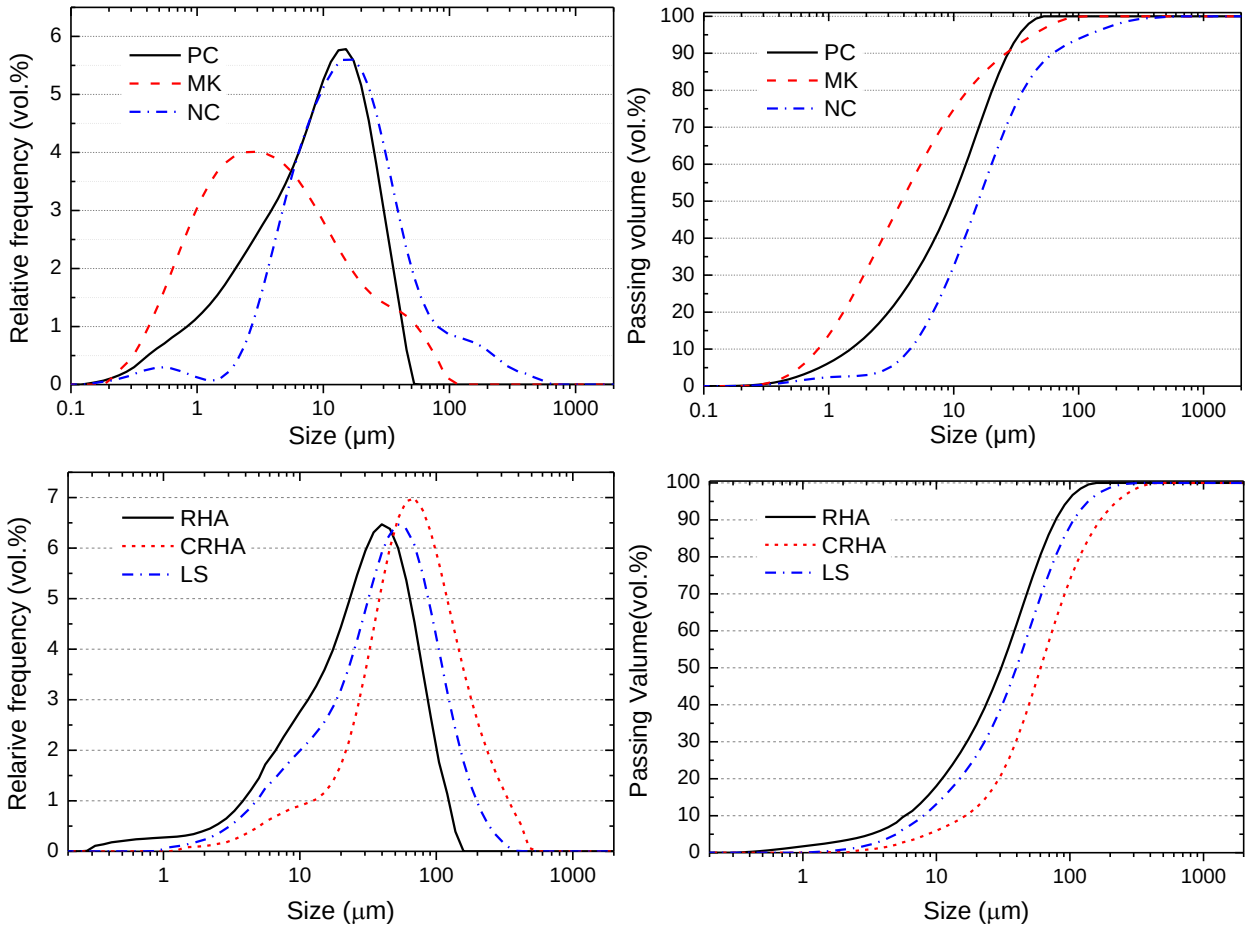

Figure 2.3: Particle size distributions of MK, NC, RHAs and LS: Relative frequency of particles in dependence of the diameter (noncumulative), volume of the particles smaller than a certain diameter (cumulative)

The XRD analysis of MK and NC is shown in Fig. 2.4. The broad humps in patterns indicate that these materials are X-ray amorphous, however, the peak positions of these two materials are different. The crystalline phases detected in MK's patterns are mainly quartz, with a small amount of sanidine, however, the main crystalline phase of NC is halloysite.

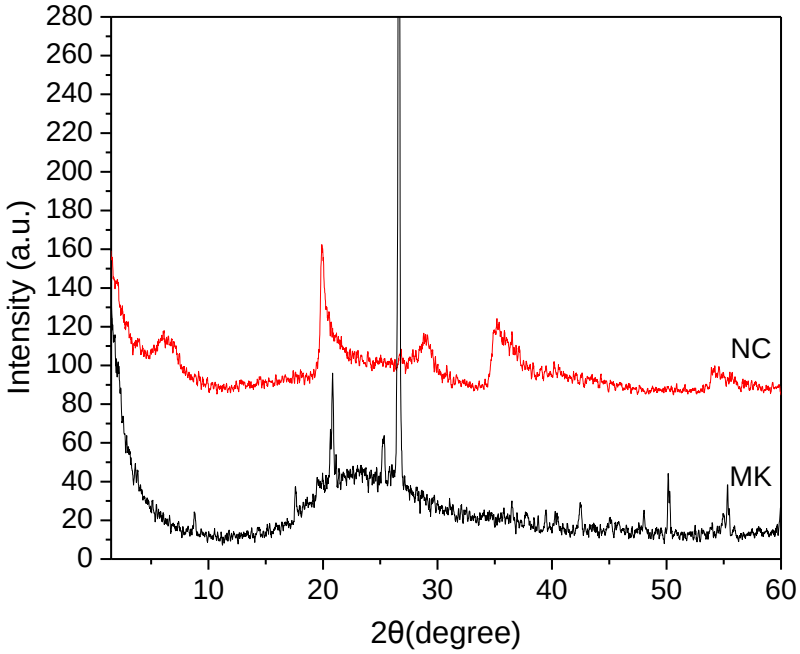

Figure 2.4: XRD pattern of MK and NC

The amounts of metakaolin (MK) and nanoclay (NC) used as partial replacement of Portland cement (PC) are given in Table 2.3. The combined substitutions in the mortar matrix resulted in total substitution levels of 10, 30, and 50%. The replacement of MK by NC increased from 0 to 5%, with increasing cement substitution level. The workability was adjusted when necessary using ADVA 408 superplasticizer up to 3 wt.% of binder, which is not enough to significantly impact the hydration kinetics of cement (Antoni, Rossen et al. 2012).

Table 2.3: Composition of MK-NC blended cements

Index	Content (%)		
	PC	MK	NC
PC	100	0	0
B10-1	90	10	0
B10-2	90	9	1
B30-1	70	29	1
B30-2	70	27	3
B50-1	50	49	1
B50-2	50	47	3
B50-3	50	45	5

Table 2.4 shows the substitution levels for cement blended with RHAs and LS, which were 5, 10, 20 and 30%.

Table 2.4: Composition of RHA-LS blended cements

	Cement (wt.%)	RHA(wt.%)	CRHA (Wt.%)	Limestone (wt.%)
PC	100	0	0	0
RHA5	95	5	0	0
RHA10	90	10	0	0
RHA20	80	20	0	0
RHA30	70	30	0	0
CRHA10	90	0	10	0
CRHA20	80	0	20	0
RHA5-LS	90	5	0	5
RHA15-LS	80	15	0	5

Surface modification agents (SMAs). Analytical grade sodium hydroxide (NaOH) and calcium hydroxide ($Ca(OH)_2$) was purchased from Sigma-Aldrich, USA. ADVA 408 superplasticizer was used to adjust the workability of the mortar when necessary. Dehydrated alcohol, acetone, and ethyl acetate, used as diluting solvent, were purchased from Thermo Fisher Scientific Inc, USA.

2.2 Mixture Proportions and Specimen Preparation

A water/cement (w/c) ratio of 0.4 and a binder-to-sand ratio of 1:1 were used for all mortar mixtures. The moisture content and water absorption capacity of the sisal fibers were considered when determining the water-solid ratio. The cement pastes were mixed with gradually added sand in a mechanical mortar mixer at 60 rpm for 2 min followed by 1 min rest and 3 min of further mixing at 120 rpm.

Three 200 mm×50 mm×12mm beams for four-point flexural test with 2% volume fraction of sisal fiber were cast for each testing point. A mortar layer of 2 mm thickness was placed at the bottom of the mold followed by a layer with half of the long unidirectional aligned fibers. A second layer of mortar of 3-4 mm thickness was placed, and a second layer of sisal fiber was uniformly distributed, followed by the third layer of mortar to fill the mold.

For compressive strength tests, 50 mm×50 mm× 50 mm cubic samples were cast in steel molds. A vibration table was used to consolidate both mortar beams and cubic samples after filling each layer of mortar. The duration and frequency of vibration were established according to ACI 544.2R. The specimens were demolded after 24 hours and immersed in CH-saturated water at 23 ± 2 ℃ for 28 days prior to accelerated aging treatment. For fiber pull-out tests, 30mm × 30mm × 300 mm prismatic specimens were prepared with a steel L-square ensuring that the sisal fibers were vertically embedded within the matrix. Epoxy super glue was applied to the free end of the fibers to prevent them from sliding in the pull-out test. The samples were demolded after 24h. Five specimens with a fiber embedment length of 30 mm per data point were tested after 7 days of curing at 23 ℃ with a relative humidity of 98%.

Fresh cement pastes prepared for chemical analysis, such as XRD and TGA, were poured into sealed bottles and then stored at 23±2 ℃ until to be tested.

For short fiber-reinforced concrete, in order to disperse the fibers uniformly, they were added by hand to the coarse aggregate and then placed into the concrete mixer and mixed for 2 minutes. Then the fine aggregate was added and mixed for another 2 min. In the third step, Type III Portland cement and water were placed into the concrete mixer and added slowly during mixing. Cylindrical specimens for compressive and splitting tensile testing were produced using 76.2 mm by 152.4 mm plastic molds. The molds were filled in three stages and consolidated on a vibration table, the time and frequency of which were established according to the recommendations of ACI 544.2R. After 24 h, the specimens were removed from the molds and placed in a curing chamber (temperature: 23 ± 2 ℃, humidity: 98%) for 7 days prior to accelerated aging treatment. Tests were conducted on two sets of specimens, plain concrete and concrete containing 0.25% mass fraction of fibers.

In addition, the durability of natural fiber-reinforced cements and mortars were mainly determined from the mechanical properties of fiber-composites, which were reasonably well understood and predictable. The strength of the composites is influenced by a number of factors, including the strength of the matrix and the matrix/fiber interfacial bond, in addition to the fiber strength (Litherland, Oakley et al. 1981). However, the strength behaviors of the natural fiber itself, which should be the foremost object of this study, is not yet fully understood. In contrast to the mechanical properties of FRCC, the strength of the fiber reinforcement provides a direct way to investigate the degradation degree of natural fiber. It is logical here to study the tensile properties of sisal fiber embedded in cement matrix as an essential approach to evaluate its degradation degree or the durability while subjected to aggressive environments. According to the "strand-in-

cement test" proposed by Litherland (1981), an improved method was developed to measure the direct tensile strength of natural fiber after being embedded in a cement matrix. As shown in Fig. 2.5, a small block of cementitious paste was cast around the middle part of a strand consisting of 10 sisal fibers. In order to remove the cement block, the strand inside the paste was wrapped with a wire mesh, which allows the matrix to contact the surface of the natural fiber. The strand outside the block was protected by epoxy resin and plasticene was used to fill and protect the edge of the block from corrosion. Three strands were prepared for each aging stage. The block around the strand was removed carefully after 5, 15 and 30 wetting and drying cycles.

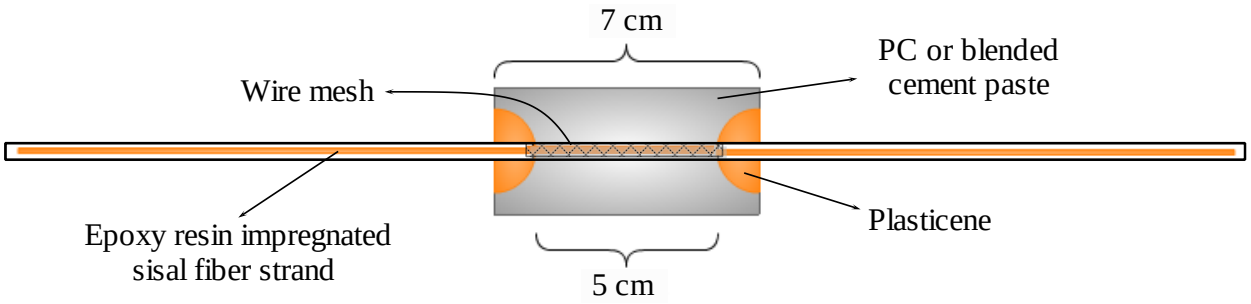

Figure 2.5: Sketch of sisal fiber strand in cement specimen

2.3 Treatment of Sisal Fiber

Thermal treatment. Sisal fibers were placed in a ventilated oven at 150 ℃ for 8 h.

Na_2CO_3 treatment. Sisal fibers were immersed in a Na_2CO_3 saturated solution for different durations: 7 days (N7), and10 days (N10). Therefore, the fibers were divided into three groups according to treatment duration. Group 1 was the control group without any treatment; Group 2

consisted of fibers treated in Na_2CO_3 saturated solution for 7 days, while fibers of Group 3 were treated for 10 days.

2.4 Test Apparatus and Procedure

2.4.1 Mechanical properties of sisal fiber-reinforced cement composites

2.4.1.1 Compressive strength and splitting tensile strength test

ASTM C109 was followed to measure the compressive strength of the mortar matrix by using an Instron 600DX 135k Universal Testing Machine. Three 50×50×50 mm cubic samples were tested for each mix and the average value was taken to be the representative strength. The relative compressive strength ratio at each curing age was calculated using the following equation:

$$I = R_b/R_{pc}*100\% \quad (2.1)$$

where I is the compressive strength ratio of the mortar; R_b is the compressive strength of the mortar; R_{pc} is the compressive strength of the control group (PC).

For concrete, each cylindrical specimen used for compressive strength testing was capped with a high-strength capping compound in accordance with ASTM C617/C617M to achieve smooth loading surfaces. Specimens were tested with an Instron 600DX universal testing machine under uniaxial load control until failure. The Instron 600DX is a load or displacement controlled hydraulic testing machine with a load capacity of 600 kN in tension and compression and a maximum crosshead displacement speed of 381 mm/min and 76.2 mm/min at full load, respectively. Then, ASTM C39 and ASTM C496/C496M were followed to determine the compressive and splitting tensile strength of cylindrical concrete specimens under load control at 1112 N/s and 44.5 N/s, respectively. Loads and displacements were recorded as functions of time to obtain complete load-deformation curves.

2.4.1.2 Flexural behavior of sisal fiber-reinforced mortar beams

Four-point bending tests were carried out on an INSTRON 5984 34k Universal Testing Machine at a crosshead rate of 0.2 mm/min to investigate the flexural behavior of sisal fiber-reinforced cement composites (Fig.2.6). Three identical specimens with a span of 150 mm were tested for each mix. The displacements at midspan were determined using LVDTs and continuously recorded together with the corresponding loads, using a 32-bit data acquisition system to obtain load-deflection curves.

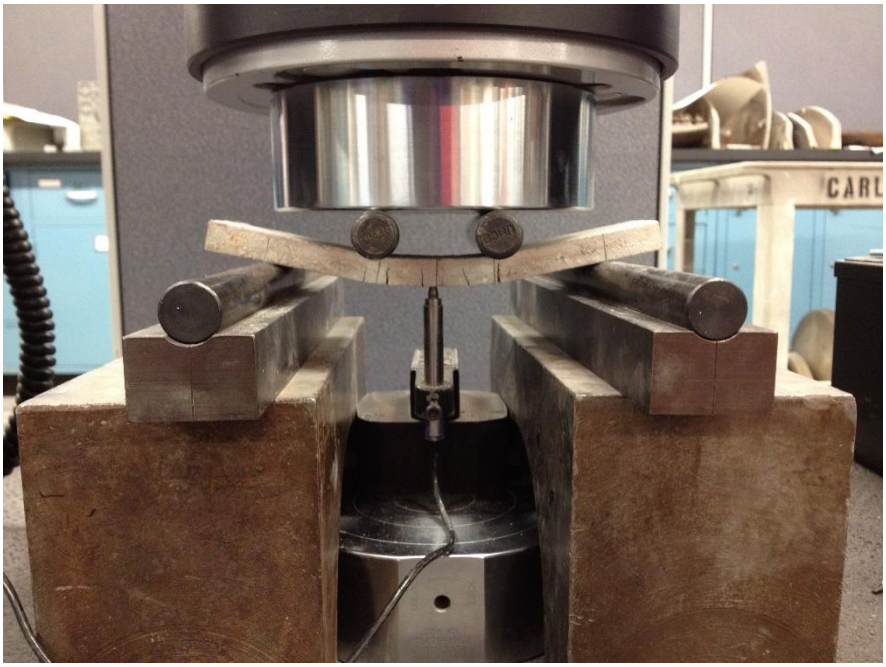

Figure 2.6: Four point bending test set-up

ASTM C1185-08(2012) (C1185 2012), ASTM C-1018 (C1018 1997) and JCI SF4 (SF4 1984) were followed to evaluate the reinforcing effect of sisal fibers by determining the toughness indices I_{30}, I_{55}, I_{85}, T_{JCI}, F_{JCI}, first crack strength (σ_f), post-crack flexural strength (σ_p), post-cracking toughness (T_p), as defined in Fig. 2.7. These were determined as follows:

(i) σ_f: According to ASTM C1018 (C1018 1997), the first crack load F_f is defined as "the point on the load-deflection curve at which the form of the curve first becomes nonlinear (Fig. 2.7)." Thus the first-cracking strength is given by Eq. (2.2):

$$\sigma_f = F_f L / bh^2 \tag{2.2}$$

where F_f is the first cracking load, L is the lower fulcrum span (150 mm), b and h are the width and thickness of the specimen, respectively.

(ii) σ_p: Determined from the maximum load (F_{max}, Fig. 2.7) of the bending test after the first crack event:

$$\sigma_p = F_{max} L / bh^2 \tag{2.3}$$

(iii) T_p: The post-cracking toughness is defined as the area under the load-deflection curve after cracking (shaded area in Fig. 2.7). The test is terminated when the deflection is 16.5 mm.

(iv) I_{30}, I_{55}, I_{85}: According to ASTM C-1018, the toughness indices I_5, I_{10} and I_{30}, were used to determine the flexural properties. Here, because of the good deformability of long fiber reinforced mortar beams, the energies required to deflect the beam to deflections of 15.5, 55 and 85 times the first cracking deflection divided by the energy to produce the first crack (area OAN, Fig. 2.7) were selected to characterize the flexural behavior of the beams.

(v) T_{max}: The ratio of deflection at maximum load (ς_{max}) divided by the first crack deflection (ς).

(vi) $T_{0.5}$: The ratio of deflection when load drops to 0.5 of the maximum load ($\varsigma_{0.5}$) divided by the first crack deflection (ς).

(vii) T_{JCI}: The energy required to deflect the mid-point of the beam up to the deflection of 1/150 of its span. Here, we use T_{JCI-10} (10/150 of L), which means the energy required to produce a deflection of ς_{JCI-10} = 10 mm.

(viii) F_{JCI-10}: Flexural toughness factor calculated from T_{JCI-10} by accounting for the beam size and span:

$$F_{JCI} = T_{JCI}L/\ bh^2\varsigma_{JCI-10} \tag{2.4}$$

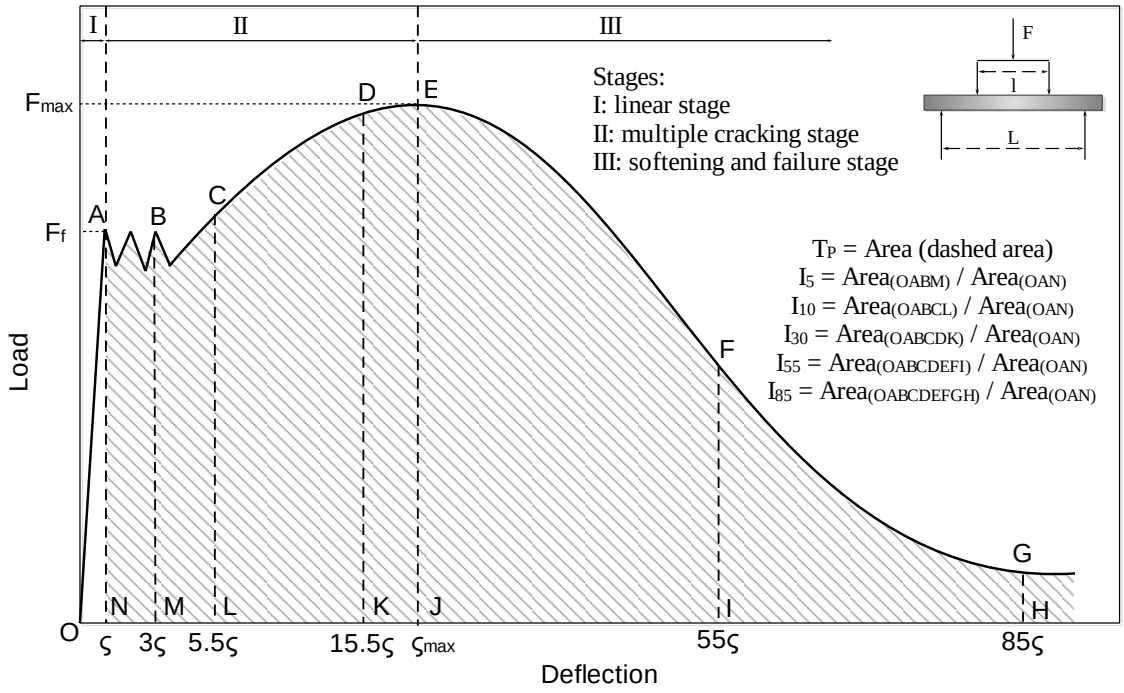

Figure 2.7: Definition of flexural strength and toughness indices

2.4.2 Fiber pull-out test

Fiber pull-out tests were performed on a micro-force Instron 5948 testing system with a loading rate of 0.2 mm/min. Fig. 2.8 shows the testing machine and a schematic drawing of the force-displacement curve of a single fiber pull-out test, which exhibits four stages. During the first

stage ($0 < F < F_d$), the interface remains intact and the linearity of the curve indicates elastic deformation of the fiber. During the second stage ($F_d < F < F_{max}$), the fiber begins to debond from the matrix through crack propagation in the interfacial zone (Liu and Nairn 1999, Zhandarov and Mäder 2005). During the third stage ($F_f < F < F_{max}$), the fiber fully debonds from the matrix through unstable crack propagation over the entire embedded length. The last stage indicates that the interfacial zone has failed and the fiber is pulled out with little resistance. In this study, the interfacial bond strength was determined from the maximum pull-out load F_{max}, as follows:

$$\tau_{max} = F_{max} / A = F_{max} / (\pi D Z_f) \quad (2.5)$$

where A is the contact area between fiber and cement matrix, F_{max} is the maximum pull-out load, D is the diameter of the interfacial zone (fiber) and Z_f = 30 mm is the length of interfacial zone or embedment length of the fiber. The pullout energy was determined as the area under the fiber pullout curve up to a pullout distance of 2 mm.

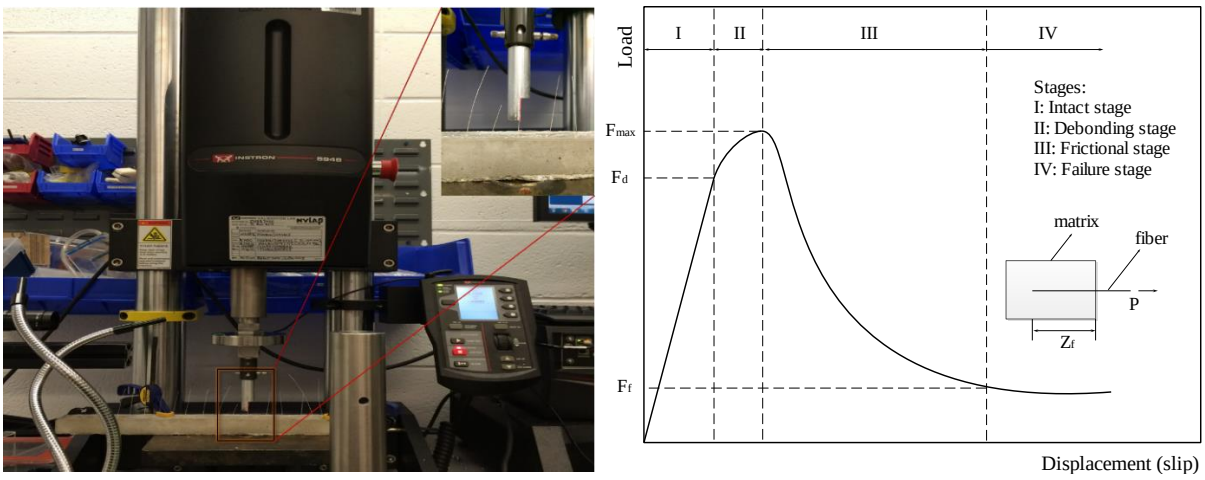

(a) Instron 5948 testing system (b) Schematic pull-out load vs. slip curve

Figure 2.8: Pullout test of sisal fiber from the cement matrix

2.4.3 Tensile properties of sisal fiber

Two fiber tension tests were used in this research. The first method used a macro-force system, as shown in Fig. 2.9-a. In order to reduce the statistical scatter of test results, bundles of five fibers each were tested using an INSTRON 5984 testing machine. The ends of each fiber bundle were glued to two aluminum foils with a rapidly hardening adhesive, such that the effective length was 20 mm to facilitate the measurements. The foils were clamped between two aluminum sheets by screws to prevent fiber slippage, Fig. 2.9-b, c. The tensile force was applied at a fixed rate of 0.5 mm/min. Strains were measured by an extensometer, Fig. 2.9-d.

(a) INSTRON 5984 testing machine

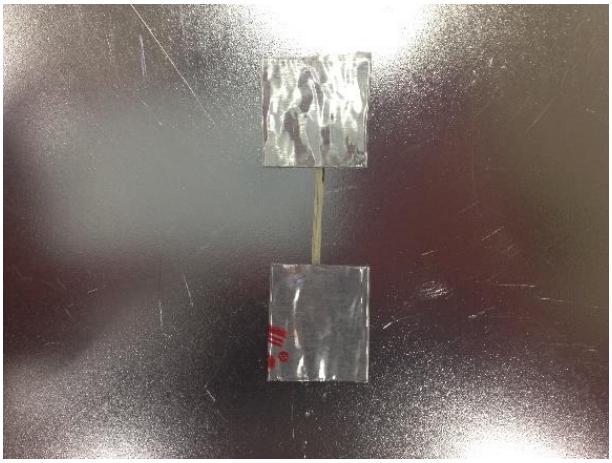

(b) Fiber bundle bonded to aluminum foils

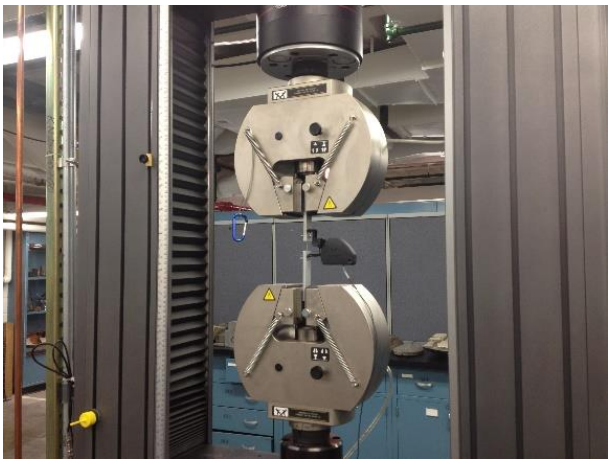

(c) Testing process

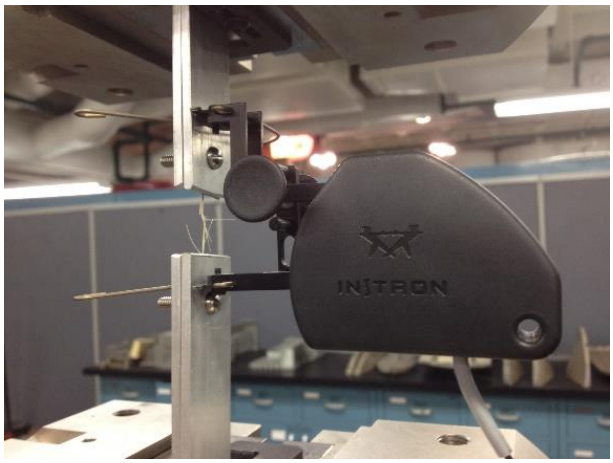

(d) extensometer and ruptured fibers

Figure 2.9: Tensile strength test of sisal fiber

The tensile strength σ_u and Young's modulus (or tensile modulus) E of raw and treated fibers were obtained as the average of five fibers in a fiber bundle and then as the average of three bundles. σ_u is the fracture strength of sisal fiber and E is calculated from the slope of the linear portion of the stress-strain curve, i.e.

$$\sigma_u = F/5A \tag{2.6}$$

$$E = \sigma_u/\varepsilon \tag{2.7}$$

where F is the failure load, A is the cross sectional area of a single fiber determined by scanning electron microscope (SEM), $\varepsilon = \Delta L/L$ is the ultimate strain of a fiber bundle, ΔL is the fiber elongation, and $L = 20$ mm.

The second method was used to test the tensile strength of a single fiber. The uniaxial tensile properties of a single raw and embedded fiber extracted from the matrices at each aging stage were tested using again the micro-force Instron 5948 testing system according to ASTM D 3822. A gauge length of 20 mm was employed and the fixed loading rate was 0.2 mm/min. The ultimate load and elongation at break of the sisal fibers were recorded. The cross sectional area A was calculated from the diameter of fiber by assuming the fiber's cross sections are in round shape. SEM was used to determine the diameter of each fiber to calculate the cross sectional area and to determine the stress-strain curves. Twenty single fibers were tested for each group.

Because of the non-homogeneous nature of sisal fibers, especially of those exposed to alkaline attack and mineralization in cement, the data of the tensile tests exhibited considerable scatter. Therefore, the two-parameter Weibull distribution model was followed to analyze the tensile test results. The probability function of this double-parameter distribution is given by:

$$f(x) = m(x)^{m-1} \exp(-x^m) \tag{2.8}$$

where f(x) is the frequency distribution of the variable x, and m is the Weibull modulus, which indicates the scatter of test data: as m gets larger, the distribution narrows.

By defining the variable x as σ/σ_0 and integrating both sides, the failure probability P can be calculated using Eq. (2.9):

$$P = 1 - \int_{\sigma/\sigma_0}^{\infty} f(\frac{\sigma}{\sigma_0}) d(\frac{\sigma}{\sigma_0}) \quad (2.9)$$

where σ is the measured failure stress and σ_0 is a normalizing parameter and defined as characteristic strength. The failure probability function also can be expressed by

$$P = 1- \exp[-(\sigma/\sigma_0)^m] \quad (2.10)$$

By taking the logarithm of both sides twice, it yields:

$$\ln\ln[1/(1-P)] = m\ln\sigma - m\ln \sigma_0 \quad (2.11)$$

or

$$\ln[-\ln(1-P)] = m\ln\sigma - m\ln \sigma_0 \quad (2.12)$$

It can be seen that the relationship between $\ln\ln[1/(1-P)]$ and $\ln\sigma$ is linear and the Weibull modulus and characteristic strength can be determined by plotting the straight line. m is the slope and σ_0 is the intercept at $\ln\ln[1/(1-P)] = 0$, which means $P = 1- (1/e) = 0.63212$.

Actually, the failure probability P can be evaluated from the probability index:

$$P = R/(N+1) \quad (2.13)$$

where R is the number of fibers broken at a certain stress σ, and N is the total number of sisal fibers that have been tested (here N=20).

2.4.4 Chemical composition and physical properties of sisal fibers

2.4.4.1 Moisture content and water absorption

Four steps are needed to extract sisal fiber from Agave sisalana: (i) cutting and receiving clean sisal leaves, (ii) extracting primordial sisal fiber from the leaves, (iii) drying sisal fiber (air drying or artificial drying), (iv) carding the fibers to remove knots and other impurities. Although the fiber has been dried during this process, the moisture content is still high, due to sisal's molecular structure, lumen and hygroscopic features. Official methods proposed by the Association of Official Analytical Chemists (AOAC) (William 1975) were followed to determine the moisture content of sisal fiber in quintuplicate: 20 grams fiber were oven dried to constant weight in a circulating air environment at 110 ℃. Then the fibers were removed from each ceramic crucible and cooled in a glass desiccator. The moisture content was determined by the average of weight loss ratios calculated as follows:

$$\omega = 100\% \times (W_i - W_d)/W_i \tag{2.14}$$

where ω is the moisture content in percent, W_i is the initial weight of sisal fiber, and W_d is the residual weight of sample after drying and cooling.

Unlike moisture content, the water absorption of natural fiber has a direct influence on the reinforcing performance and durability of the fiber in the cement matrix. Fibers absorb water, accompanied by volume expansion, from the cement composite during the mixing and casting process up to a dynamic equilibrium. During the hardening process, the cement recaptures some of that water from the fibers to form a high alkaline pore solution in the space between matrix and fiber caused by drying shrinkage, which, in turn accelerates the deterioration of natural fiber.

Each sample of 10.0 g sisal fiber was soaked in tap water, NaOH solution (pH=13) and $Ca(OH)_2$ solution (pH=13) and then placed in the curing box with temperatures of 23±2 ℃, 50 ℃

and 70 ℃ and relative air humidity of 85%. The fibers were weighed every 10 minutes, until they reached a moisture absorption balance. The water absorption was calculated according to Eq. (2.15):

$$\delta = 100\% \times (W_b - W_i)/W_i \quad (2.15)$$

where δ is water absorption in percent, W_b is the weight of sample at the moisture absorption balance, and W_i is the initial weight of sisal fiber.

2.4.4.2 Holocellulose (cellulose and hemicellulose) and lignin contents

Cellulose, which is the main structural component of all plant cell walls, consists of approximately 10,000 glucose β-D-glucopyranose residues per average molecule linked together by (1→4)-glycosidic bonds to long, linear macromolecules with a low degree of polymolecularity (Goring 1962, Marx-Figini 1963, Marx-Figini and Schulz 1963, Marx-Figini and Schulz 1963, Timell 1967) (as shown in Fig.1.1). Cellulose and hemicelluloses are the major components of the secondary layers of the cell wall in lignocellulosic fibers (Timell 1967). The hemicelluloses are present in the surface layer as adhesives to strengthen the bonds between individual fibers in a three-dimensional network of lignocellulosic (Dahlman, Jacobs et al. 2003, Sun, Sun et al. 2004). Lignin is an amorphous, three-dimensional, polyphenolic polymer, built up of phenylpropane units, most of which are located in the middle lamella. The remaining part is located throughout the secondary wall, where it interpenetrates and encrusts the cellulose micro fibrils and the hemicelluloses. Cellulose, hemicelluloses, and lignin can be classified from a morphological point of view as framework, matrix, and encrustation substances, respectively (Wardrop 1964). More vividly, their relationship is similar as that among ossature, connective tissue and muscle of the human body. The content of these three compositions determines the mechanical properties and stiffness of fiber and its degradation rate. The procedure used to determine the content of cellulose,

hemicellulose and lignin according to the methods proposed by Xu et al. (2006) and Viera et al. (2007) and illustrated in Fig. 2.10, was followed. The lignin content was determined using the Klason method (Browning 1967), and the cellulose content was obtained as the sum of α and β cellulose, while the content of the hemicellulose was determined as the mass sum of hemicellulose A and B.

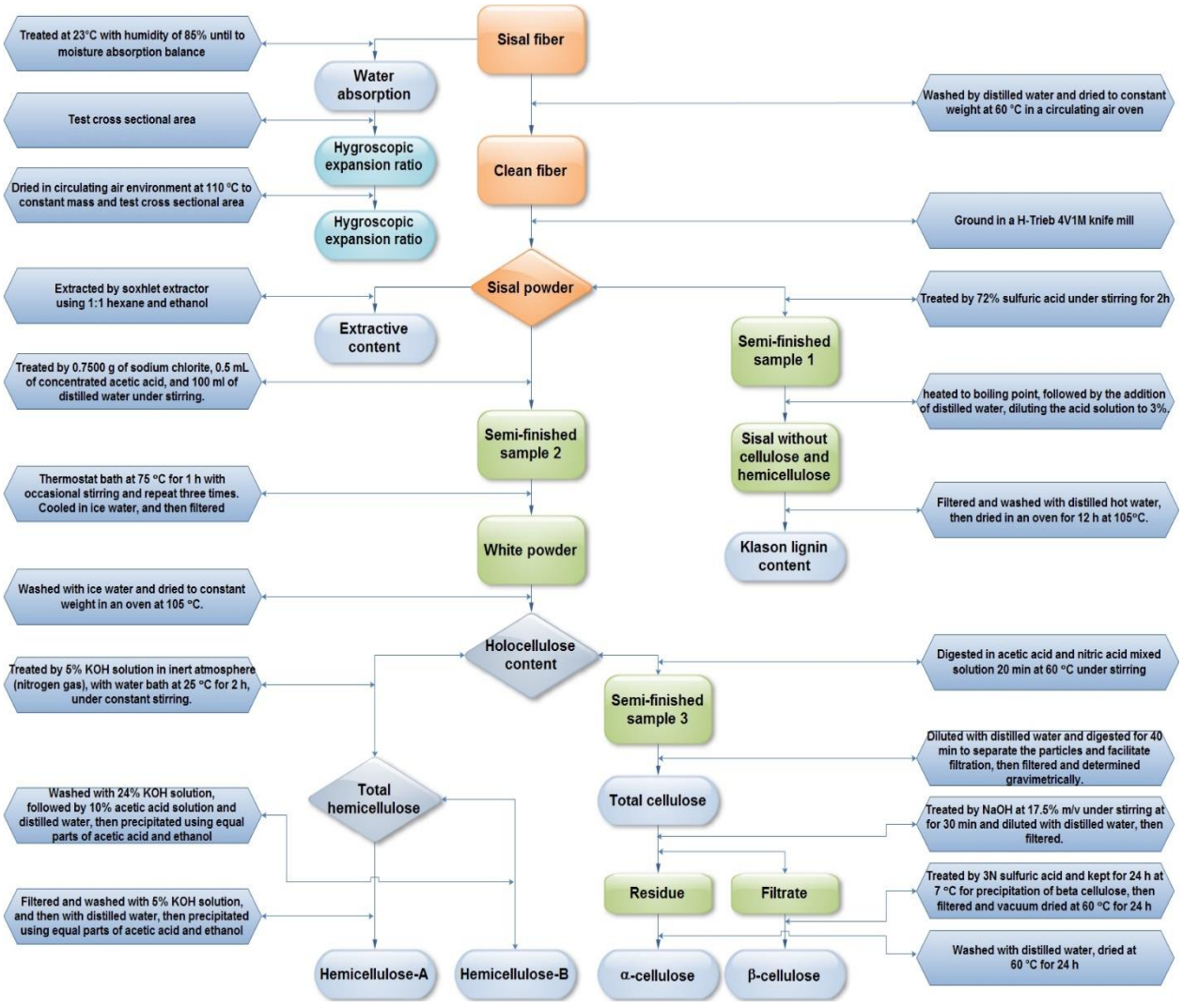

Figure 2.10: Flow chart of chemical composition and physical property analysis of sisal fiber

2.4.5 Thermal analysis

Thermogravimetric analysis (TGA) was carried out to measure the content of calcium hydroxide and bound water in cement hydration products using a TA Instruments Q50 Thermogravimetric Analyzer. Components of sisal fibers embedded in a cement matrix for accelerated aging were analyzed using a Perkin Elmer Pyris1 Thermogravimetric Analyzer at a heating rate of 20 ℃/min from room temperature to 700 ℃ in an N_2-atmosphere. The measured content of calcium hydroxide (CH) is expressed as percentage of the dry sample weight at 500 ℃ as follows (De Weerdt, Haha et al. 2011, Deschner, Winnefeld et al. 2012):

$$CH = [(W_{400}-W_{500})/W_{500}] \times M_{Ca(OH)2}/M_{H2O} = [(W_{400}-W_{500})/W_{500}] \times 4.11 \quad (2.16)$$

where M is the molar mass; W_n is the dry sample weight at the temperature n ℃.

The non-evaporable water content (W_{ne}) was determined as the difference between the mass measurements at 800 ℃ and 105 ℃, normalized by the mass at 800 ℃, and corrected for the ignition losses of the unhydrated cement powder and the substitution cementitious materials:

$$W_{ne} = (W_{105}-W_{800})/W_{800} - (f_c \times IL_{uc} + f_{MK} \times IL_{MK} + f_{NC} \times IL_{NC}) \quad (2.17)$$

where M is the molar mass; W_n is the dry sample weight at the temperature n ℃; f_c, f_{MK}, f_{NC} are the mass fractions of cement (PC), metakaolin (MK) and nanoclay (NC) in the dry mix, respectively; IL_{uc}, IL_{MK}, IL_{NC} are the ignition losses of unhydrated cement, MK and NC, respectively.

2.4.6 X-ray diffraction

The crystallinity fraction of sisal fiber and crystallization degree of cement at each age were analyzed by X-ray diffraction (XRD) carried out on ground powders with an X_2 Scintag X-Ray

diffractometer in a θ-2θ configuration using CuKα source (λ =1.54 Å) at -40 kV and 35 mA. The cement and sisal samples were scanned in step mode with a step size of 0.02° (2θ) in the angular range of 5–25 ºand 5-45 º, respectively. Four indices were calculated from the X-ray diffraction spectra of sisal fibers embedded in the cement matrices after aging: the percentage of crystallinities using the peak height method (Segal, Creely et al. 1959) ($\%Cr_1$) and deconvolution method (Hult, Iversen et al. 2003, Garvey, Parker et al. 2005, He, Cui et al. 2008, Fernandes, Mano et al. 2013) ($\%Cr_2$), crystallinity index (Cr.I.), and crystallite size (L).

The percentage of crystallinity ($\%Cr_1$) was calculated using the following equation (Vijay K. Kaushik 2012):

$$\%Cr_1 = I_{002}/(I_{002}+I_{am}) *100\% \quad (2.18)$$

where I_{002} is the maximum intensity of diffraction of the (002) lattice peak at 2θ = 22.5 º. And I_{am} is the intensity of diffraction contributing to the amorphous fraction, which is taken at a 2θ angle between 18˚ and 19˚ where the intensity is a minimum (Mwaikambo and Ansell 2002, Roncero, Torres et al. 2005, Dasong Dai 2010).

The percentage of crystallinity ($\%Cr_2$) was determined by the amorphous peak areas under the diffraction X-ray plot and was calculated based on Eq. (2.19) (Fernandes, Mano et al. 2013):

$$\%Cr_2 = (A_c/A_t) \times 100\% \quad (2.19)$$

where A_c is the area below the diffraction peak of the (002) plane (peak at 2θ = 22.5 º) and the (101) and $(10\bar{1})$ plane (peak at 13–18 º), and A_t is the area below the whole region of the XRD spectra representing the amorphous (Ramli, Kwan et al. 2013) and crystalline material in the samples.

The crystallinity index (Cr.I.), which expresses the relative degree of crystallinity (Segal, Creely et al. 1959), was evaluated by using the following equation (Le Troedec, Sedan et al. 2008, Elenga, Dirras et al. 2009, Dasong Dai 2010, Roy, Chakraborty et al. 2012):

$$Cr.I = (I_{002}-I_{am})/I_{002} \quad (2.20)$$

where, I_{002} and I_{am} have the same meaning as in Eq. (2.18).

The crystallite size in the (002) plane of sisal fiber was calculated by using Scherrer's formula (Hindeleh and Johnson 1980, Elenga, Dirras et al. 2009, Roy, Chakraborty et al. 2012):

$$L = k\lambda / (\beta\cos\theta) \quad (2.21)$$

where k = 0.89 is Scherrer's constant; β is the peak's full width half maxima (FWHM); λ is the wavelength of X-ray beam (1.54 Å) and θ is the angle of diffraction.

2.4.7 Morphology and energy dispersive X-ray spectroscopy (EDX) analyses

The micro-analysis of sisal fibers and the composite's fracture surface were performed on a Hitachi 4700 scanning electron microscope (SEM) under an accelerating voltage ranging from 10 kV to 20 kV. Energy Dispersive Spectroscopy (EDS) was used to determine the element composition of cement hydration products, focusing on the characterisation of calcium silicate hydrate (C–S–H), with a beam voltage of 10 kV to reduce the interaction volume of the electron beam with the nonconducting phases.

2.4.8 Pozzolanic activity of SCMs

The pozzolanic activity of supplementary cementitious materials (SCMs) was investigated using the lime consumption test (LCT). In LCT, 10 g of chemical grade calcium hydroxide (CH)

were mixed with 5g of SCM or their combination at a w/b ratio of 3. After mixing, samples were sealed in plastic vials. The CH content after 7 days was determined by a TGA technique.

2.4.9 Characterization of solid phase and pore solution of hydrated cement matrix

The hydration of Portland cement is a complex process, which affects the setting, hardening, crystallization, release of hydration heat, and so on. The four principal constituents, calcium silicates (C_3S and C_2S), aluminate (C_3A), and ferrite (C_4AF), with other minor minerals such as calcium sulphates (gypsum, anhydrite and/or hemihydrate), calcite, calcium oxide, magnesium oxide, Na- and K-sulphates, react with water to form various hydration products such as C-S-H, portlandite, ettringite, calcium monosulphoaluminate or calcium monocarboaluminate (Lothenbach and Winnefeld 2006). Solid phase assemblage and the development of elemental concentration of pore solution are two measures to evaluate the hydration degree of cement. The hydration studies were carried out on paste samples of the pure PC and blends containing 10 wt.% and 30 wt.% of MK.

2.4.9.1 Kinetics of hydration

The heat flow of the hydration for each paste was measured by a TAM Air iso-thermal calorimeter to 25 ℃. According to ASTM C305, pastes with a water/cement ratio of 0.5 were mixed by hand with a spatula for 1 min at a temperature of 23±2 ℃. For each measurement, 5 g of each sample were cast in glass cylinders using plastic dropper within 2 min after initial contact of cement and water. Then the sealed samples were placed in the calorimeter, which records the hydration heat flow of the sample up to 50 h.

2.4.9.2 Solid phase

Many different solid phases are formed during the hydration of cement and these phases are changing with time (Andersson, Allard et al. 1989). The phase compositions of the solid not only affect the mechanical properties, porosity, and shrinkage, but also determine the degree of mineralization and decomposition of natural fiber. In addition, the solubility behaviors of the solid phases directly determine the elemental concentrations, alkalinity, as well as the saturation indices of the pore solution, which in turn affect the stability of the solid phase. The solid phases of PC and blends were analyzed by means of XRD (in a θ-2θ configuration using CuKα source in step mode with step size of 0.02° (2θ) at -40 kV and 35 mA), TGA (at a heating rate of 20 ℃/min from room temperature to 750 ℃ in an N_2-atmosphere), SEM-EDX (in electron microscope model with 15 kV electron beam, which produces a maximum interaction depth around 1 μm) and collected solubility data to characterize the crystallization, C-S-H composition, porlandite and bound water content, and solubility of solid phases.

2.4.9.3 Pore solution

There are four steps to form cement pore solution throughout the entire hydration process: (i) from mixing water to continuous phase (with suspended cement); (ii) then it converts to a rather complex alkali- and sulfate bearing solution; (iii) followed by discontinuous pore solution; (iv) at last the pore solution is formed with continued reaction of cement components (Barneyback Jr and Diamond 1981). The pore solution chemistry is of prime importance for understanding trace element mobility and migration processes in cement (Andersson, Allard et al. 1989). This can be grossly divided into three stages (Loon and Glaus 1997): (i) dissolution of NaOH and KOH (with pH around 13.4), (ii) dissolution of $Ca(OH)_2$ (pH falls to 12.5), and (iii) dissolution of C-S-H gels (pH remains above 12.5). The high alkalinity and content of Ca^{2+} in the pore solution are well

known to be the main factor accelerating the degradation of cellulose and lignin. An inductively coupled plasma optical emission spectroscope was used to determine the concentration of K, Na, Si and Ca at different ages. The pore solution of hardened samples was obtained by the suspension method (Hidalgo, Garcia et al. 2005, Bach, Coumes et al. 2012), and the pH of the pore solutions, which was used to calculate the free OH^- concentrations, were tested by a pH electrode.

2.4.10 Accelerated aging condition

The durability of sisal fiber-reinforced cement composites was characterized by the reduction of mechanical properties of specimens subjected to two kinds of aggressive environments: hot water treatment and wetting/drying cycles, which can accelerate the deterioration of both sisal fiber and the cement matrix. The methods to determine the most effective and rapid simple accelerated aging conditions to quantify the durability of sisal fiber in cement based materials are discussed in Chapter 4.

For both the drying and wetting cycles, a ventilated oven was used: the specimens were submerged in sealed tap water at 70 ℃ and then dried at 70 ℃. In order to determine the duration of wetting and drying cycles, which means the time needed for full saturation and drying, a hysteresis mass change as a function of time was investigated. Increase and decrease of specimen mass subjected to wetting and drying cycles were measured every 10 min until the mass became constant (mass change was less than 1% in 3 consecutive measurements).

CHAPTER 3: AGING MECHANISMS AND DEGRADATION KINETICS OF NATURAL FIBER IN THE MATRIX OF CEMENT COMPOSITES

3.1 Introduction

The degradation mechanisms and kinetics of natural fiber in the complex alkaline and mineral-rich environment of cement matrices have been rarely reported in the literature. It is well known that the cement matrices are governed by the hydration process, setting and hardening, strength growth, combined with hydration heat release, crystallization and the formation of micro cracks in various aggressive environments. Only a few publications address the failure of natural fiber in cement composites. Gram (1983) and Tolêdo Filho et al. (2000) described the dissolution process of lignin and hemicellulose in a cement pore solution and alkaline hydrolysis of cellulose molecules. This leads to the degradation of molecular chains and the reduction in degree of polymerisation and tensile strength, which are the main aging mechanisms of natural fibers in cement based composites (Tolêdo Filho, Scrivener et al. 2000). Besides, the crystallization of lime in the lumen and middle lamellae also decrease the fiber's flexibility and strength (Singh 1985, Tolêdo Filho, Scrivener et al. 2000). Mohr et al. (2005) proposed a three-part progressive degradation mechanism during wetting and drying cycling, such as fiber cement debonding and reprecipitation of hydration products within the void space at the former fiber-cement interface, while the third part is the fiber embrittlement due to fiber cell wall mineralization indicated by the lack of any toughness. Almeida Melo et al. (2013) investigated two fiber degradation mechanisms in PC composites: fiber mineralization and degradation of cellulose, hemicellulose and lignin due to the existence of calcium hydroxide and adsorption of calcium and hydroxyl ions. However, the

results obtained so far have been disappointing, primarily because the intrinsic degradation kinetics and mechanisms of natural fiber and its three main components, cellulose, hemicellulose and lignin, in the solid phase and pore solution of cement have not been successfully investigated systematically. And there exists no model that can be used to predict the degradation rate of natural fiber in construction materials. Few designers are willing to accept the risk of working with inherently unreliable reinforcement. These difficulties could be alleviated if it were possible to build a parameterized model based on cement hydration data to predict the fiber's deterioration degree as a function of embedment duration.

This chapter describes the investigation of cement hydration over a time span of up to 600 days, and its effect on the durability of natural fiber to analyze the degradation mechanisms and kinetics of natural reinforcement in a cement matrix. The effects of metakaolin on cement hydration and degradation rate of sisal fibers were also studied by analyzing surface morphology, crystallinity index, thermal and uniaxial tensile characteristics of the raw and embedded fibers. The two-parameter Weibull distribution model was applied to deal with the scatter of tensile properties of the sisal fibers. The individual cellulose fiber-cells are linked together by means of the middle lamella (Toledo Filho, Silva et al. 2009). The mineralization of cell wall, the peeling off and alkaline hydrolysis of amorphous regions of cellulose in sisal fiber were parameterized based on the test data from cement hydration to predict the long-term degradation degree of sisal fibers in a cement matrix.

3.2 Characterization of Raw Materials

For comparison, 10 wt.% and 30 wt.% Portland cement (PC) was replaced by metakaolin (MK) to study its effect on cement hydration and fiber degradation. The chemical compositions of

the PC and MK determined by means of X-ray fluorescence (XRF) are shown in Table 3.1. Portland cement and concrete are essentially alkaline because Portland cement reacts with water to produce solutions which are oversaturated with $Ca(OH)_2$ (CH). But there are also small and variable percentages of Na_2O and K_2O present as minor components in cement minerals or as sulfates, which readily form NaOH and KOH solutions as the cement aluminate and ferrite hydrate to absorb the sulfate ions (Lawrence 2003). There are two kinds of alkalis in cement: readily soluble alkalis and alkalis that remain solid. The readily soluble alkalis are assumed to correspond to the alkali sulphates present in the clinker, while the remaining alkalis are assumed to be present as minor constituents in solid solution within the major clinker phases (Pollitt and Brown 1969, Deschner, Winnefeld et al. 2012). Therefore concentrations of readily soluble alkalis in distilled water were measured after an equilibration time of 10 min, at a water/solid ratio of 0.1, to evaluate the distribution of alkalis in the pore solution. In addition, the mineralogical compositions of PC and MK were analyzed by quantitative XRD, and are also shown in Table 3.1.

Table 3.1: Chemical and mineralogical composition and readily soluble compounds of PC and MK

Chemical, mineralogical composition				
XRF-analysis [wt%]			Mineralogical phase composition of cement [wt%]	
	MK	PC		
CaO	0.0707	63.7	C_3S[a]	52.4
SiO_2	51.8	12.9	C_2S[b]	16.0
Fe_2O_3	4.15	7.97	C_3A[c]	10.2
SO_3	0.105	5.25	C_4AF[d]	8.6
Al_2O_3	42.4	4.14	Arcanite	2.5
MgO	-	3.50	Anhydrite	2.3
SrO	0.0397	0.915	Hemihydrate	2.0
K_2O	0.218	0.907	Syngenite	2.0
TiO_2	1.07	0.279	Dolomite	1.2
ZnO	-	0.251	Calcite	0.5
ZrO_2	0.0884	0.119	Other	2.3
Cl	0.0457	-	Readily soluble alkalis of cement [wt%]	
Compton	0.86	0.98	Na_2O	0.07
Rayleigh	1.24	1.19	K_2O	0.85

[a] Tricalcium silicate; [b] Dicalcium silicate; [c] Tricalcium aluminate; [d] Tetra-calcium Aluminoferrite

The particle size distributions of PC and MK, measured by means of laser diffraction, are shown in Fig. 3.1. As shown, the overall PSD of both PC and MK are in micron size. The median particle size of cement ranges from 1 to 40 μm and its specific surface area, surface weighted mean and volume weighted mean are 1.7 m^2/g, 3.5 μm and 12.3 μm, respectively, but MK shows a higher fraction of particles smaller than 6 μm compared to PC. The BET-specific surface area of MK (2.93 m^2/g) is larger than that of PC (0.873 m^2/g), which means it can modify a cement matrix both in compositions of hydration products and microstructure as pozzolanic substitution material and fine filler.

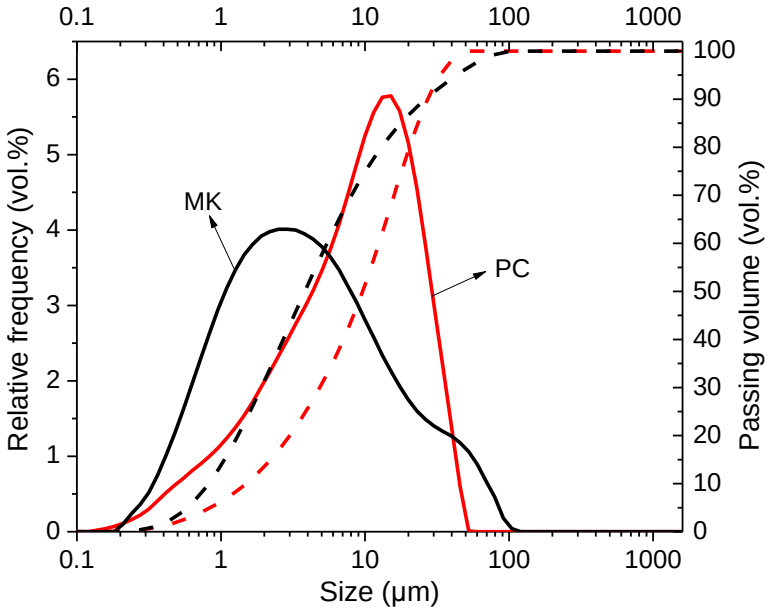

* The solid lines show the relative frequency of particles as functions of the size (noncumulative)
** The dashed lines show the volume of the particles smaller than a certain size (cumulative).

Figure 3.1: Particle size distributions of the cement and MK measured by means of laser diffraction

3.3 Solid Phase of Cement Matrix

3.3.1 Hydration reaction and kinetics

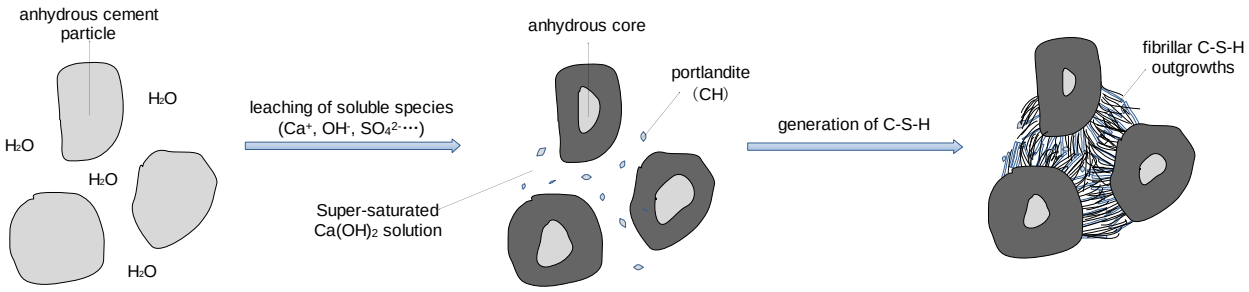

Figure 3.2: Schematic representation of the early stages of C_3S hydration (Ridi, Fratini et al. 2011)

When anhydrous cement is mixed with water, several exothermic reactions take place both simultaneously and consecutively, as schematically shown in Fig. 3.2 (Ridi, Fratini et al. 2011). The alkaline super-saturated calcium hydroxide solution, containing some other ions such as Na^+, K^+, SO_4^{2-}, is the precursor of the pore solution, which plays an important role in accelerating the degradation of natural fibers. Portlandite, which forms in the subsequent hydration and causes the mineralization of the fibers, is another factor determining the degradation rate of natural fiber in a cement matrix. Although the reaction rate and duration vary and depend on the mixing method, components, and particle size, it is well known that there are five main steps in the hydration process according to the curve of heat evolution versus time: pre-induction period, induction period, acceleration period, deceleration period and diffusion period (or stabilization period). In the pre-induction period, the very first minutes after the adsorption of water on the surface of the dry cement powder particles, a small fraction of the silicate and aluminate phases dissolves leading to the production of a $Ca(OH)_2$ supersaturated solution (Ridi, Fratini et al. 2011) and release of a

lot of ions (Bensted and Barnes 2002), and a strong heat evolution is generated by the quick conversion of aluminate phases (Ridi, Fratini et al. 2011). With the lowest heat evolution, the induction period is actually the interval between the first aluminate phase's conversion and silicate phase's conversion. Characterized by the silicate and aluminate hydrated phases' precipitation, nucleation and growth of portlandite and calcium silicate hydrates, the hydration of cement starts the two most important periods: the acceleration and deceleration periods. These two periods are accompanied by a strong heat evolution, the highest saturation level of Ca^{2+}, final set, crystallization of $Ca(OH)_2$ and end up with the formation of hydrates and a decrease of heat generation. The transition from the deceleration period to the diffusion period is somewhat arbitrary (Bensted and Barnes 2002). During the diffusion period, both the hydration heat release and saturation of Ca^{2+} tend to be stable, because its chemical rate is mainly determined by the diffusion of reacting species from the solution through the hydrated phases, to reach the anhydrous grains (Ridi, Fratini et al. 2011).

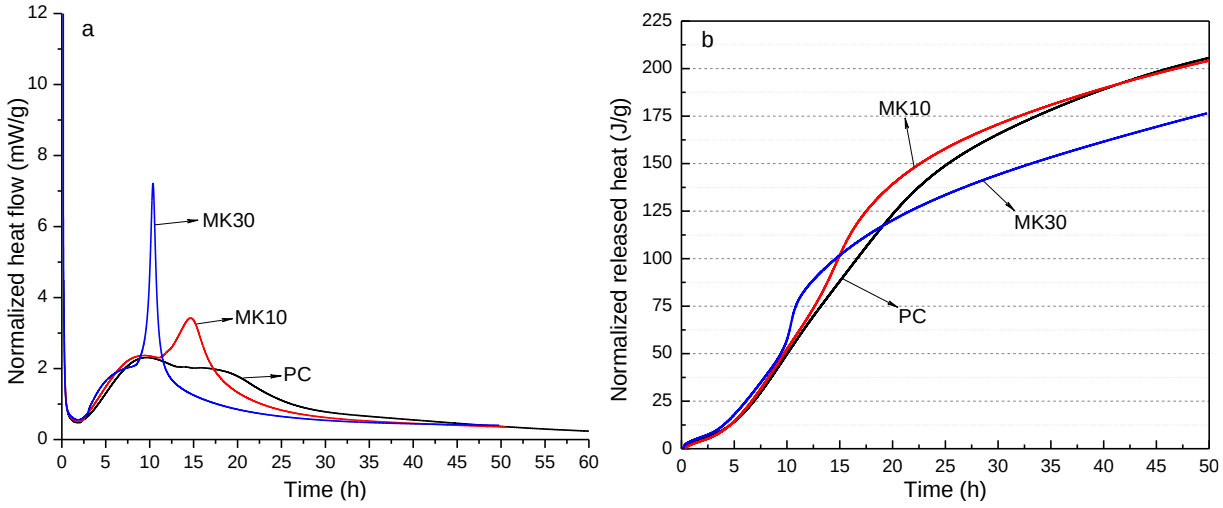

* MK10-10% weight replacement of PC by MK; MK30-30% weight replacement of PC by MK

Figure 3.3: Normalized specific heat flow and released heat of PC and PC-MK blend with a w/b ratio of 0.5 at 25 ºC

The development of normalized specific heat flow of hydration of neat PC and PC-MK blends at early age (up to 50 h) is shown in Fig. 3.3. Each curve represents the average of two measurements, the error of which is less than 0.2 mW/g. From the curves, it can be seen that the heat flow of each blend is almost the same in the first two hydration periods, while the main differences occur during the acceleration, deceleration and diffusion periods. There are two peaks (shoulders) on the PC curve, namely a silicate and an aluminate peak, due to the silicate reaction, and tricalcium aluminate reactions to form ettringite and subsequently conversion into monosulfate, respectively. There are at least three contributions of SCMs to the hydration heat of Portland cement: providing extra space for the hydration products, enhanced nucleation, and the reaction between SCMs and clinkers of cement (Lothenbach, Scrivener et al. 2011). The silicate reaction was impacted slightly by the addition of MK: the acceleration period occurred earlier and the slope during the acceleration period increased with the addition of MK, which means MK not only increased the release of heat of cement hydration during this period but also provided extra nucleation sites for C-S-H (Lothenbach, Scrivener et al. 2011, Antoni, Rossen et al. 2012). The effect of MK on the aluminate reaction was much more significant: with the increasing addition of MK, the second peak occurred much earlier and became much narrower and higher (the maximum second heat flow: 7.22 mW/g for MK30, 3.43 mW/g for MK10, and 1.98 mW/g for PC). Because of the low C_3A amount, the second shoulder peak was lower than the silicate peak for plain PC, but the opposite held for PC-MK blends. Corresponding to the second formation of ettringite, besides the nucleation role, the aluminates originating from MK also possibly participate in the reaction at this stage (Antoni, Rossen et al. 2012). The improvement in both silicate and aluminate reactions cause a higher hydration heat release at early hydration time, which can be found in the curves of Fig. 3.3-b before 15 h. However, the total released heat is reduced, especially

for MK-30, due to the rapid chemical reaction and quick end of both, the acceleration and deceleration period.

3.3.2 Mineralogical analysis

As shown in Fig. 3.4, the XRD pattern of PC identifies the crystalline phases: ettringite and portlandite after 1 day hydration. The patterns of PC at 28 days and 90 days show a growing quantity of portlandite and less ettringite, which suggests the high amount of alkalinity and transformation of AFt to AFm in the process of hydration. In blends involving MK10 and MK30, gypsum was found, along with less ettringite and portlandite at early age. After 90 days of hydration, no ettringite was detected in any blend. The quantities of ettringite phase and portlandite phase decreased with increasing SCM amount at all ages due to the dilution of cement and pozzolanic activity of MK. The development of the main crystalline alumina phases are also reflected in the XRD patterns. Amounts of hemicarboaluminate increased with increasing MK at early age. Monocarboaluminate started to increase slightly in PC after 28 days of hydration. The results show that MK effectively reduces the CH at early age accompanied by the consumption of AFt and continues at later age.

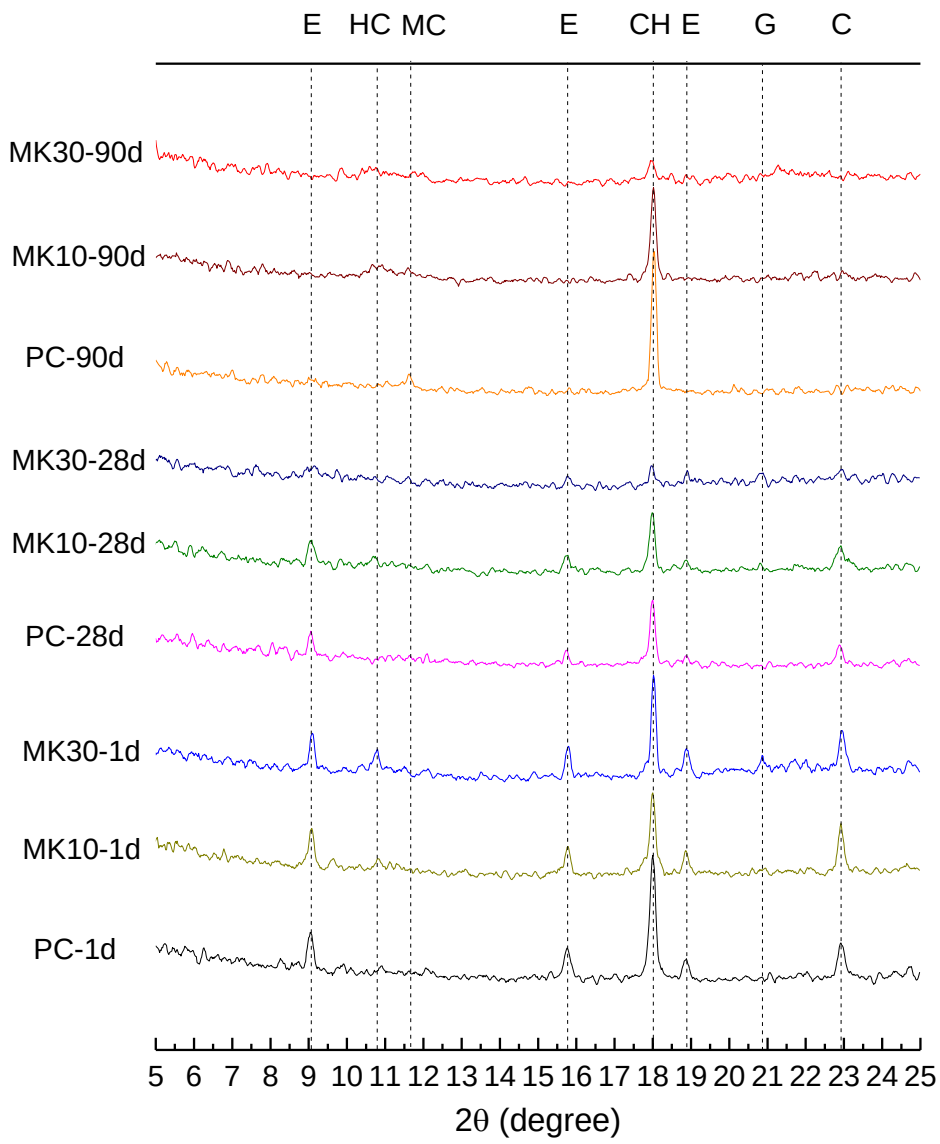

* E-ettringite, HC-hemi carbonate, CH-calcium hydroxide (portlandite), G-gypsum, MC-monocarboaluminate, C-calcium carbonate.

Figure 3.4: XRD patterns for PC, MK10 and MK30 at 1, 28, and 90 days

3.3.3 Portlandite and bound water content

The TGA and derivative thermogravimetry (DTG) curves of the investigated samples after 28 and 90 days of hydration are shown in Figs. 3.5-a and b, respectively, in which three peaks due to thermal decomposition can be found: ettringite (105 ℃), AFm (175 ℃) and CH (starting at 455 ℃). The differences between curves for neat PC and PC-MK blends around 105 ℃ at 28 days are

impressive, which indicates that the addition of MK effectively reduces the ettringite content. There are no strong peaks signifying the decomposition of ettringite in the curves in Fig. 3.5-b, which means this phase has been completely consumed or transformed after 90 days of hydration. This result is in good agreement with the analysis of the XRD patterns of Fig. 3.4. However, the amount of AFm ($3CaO \cdot Al_2O_3 \cdot CaSO_4 \cdot nH_2O$) increased with the blending of MK due to its high content of aluminum phases. The amounts of AFt and AFm phases depend on the content of C_3A (tricalcium aluminate) and ferrite phases in the original cement and the degree of hydration (Hewlett 2004). If there is excess C_3A, when the gypsum phase has been depleted in the first step of the hydration process, AFt will transfer to AFm, therefore the amount of AFt is reduced significantly with the increase of MK indicated by both XRD and TGA/DTG analysis. The strength of peaks shown in the curves indicate that the content of CH in MK30 is much lower than that of PC, which also agrees well with the results of the XRD analysis.

Fig. 3.6 summarizes the bound water and CH contents of PC and blends normalized to the mass of dry PC after 28 and 90 days of hydration. The differences between PC and PC-MK indicate that the substitution of MK for cement results in a considerable consumption of CH. With the 10 wt. % and 30 wt. % partial replacement of PC by MK, the amounts of BW and CH were reduced by 24.49% and 50.29% at 28 days, and 33.79% and 61.90% after 90 days, respectively, due to the pozzolanic reaction, which is a positive sign for improving the durability of natural fiber in a CH-free cement matrix.

The generation of bound water of pure PC declines with time, which is probably related to the reduction of stabilization of water rich hydration products, such as ettringite and monocarbonate (Deschner, Winnefeld et al. 2012), as seen in the XRD patterns. The replacement of PC by MK also results in a significant reduction of bound water content at both 28 days and 90

days. However, MK30 shows a slightly higher bound water content than MK10, and increase with time, probably as a result of formation of more water rich AFm phase.

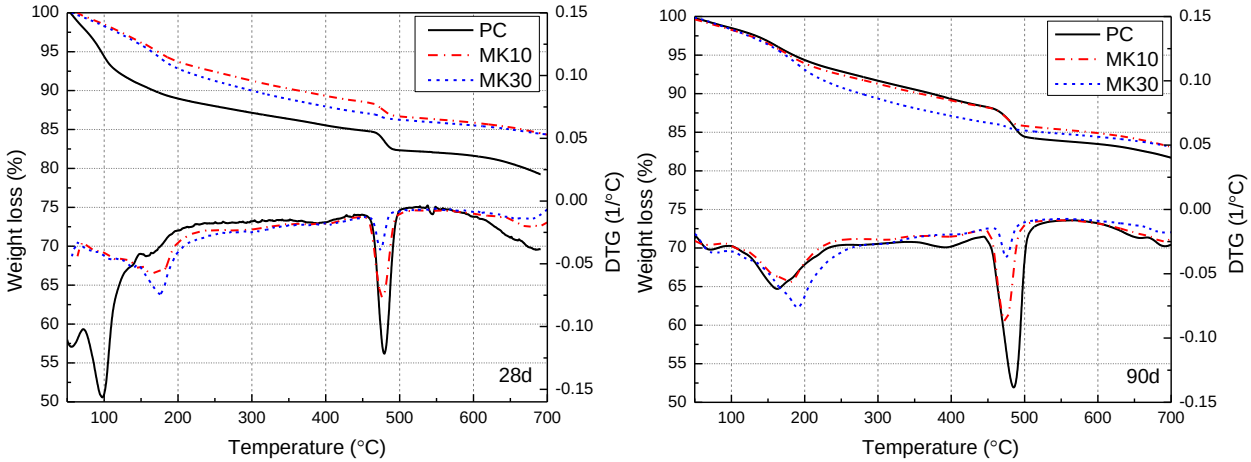

* The upper curves correspond to the relative weight loss and the lower ones are their derivation.

Figure 3.5: TGA (DTG) curves of PC, MK10 and MK30 after 28 days and 90 days of hydration

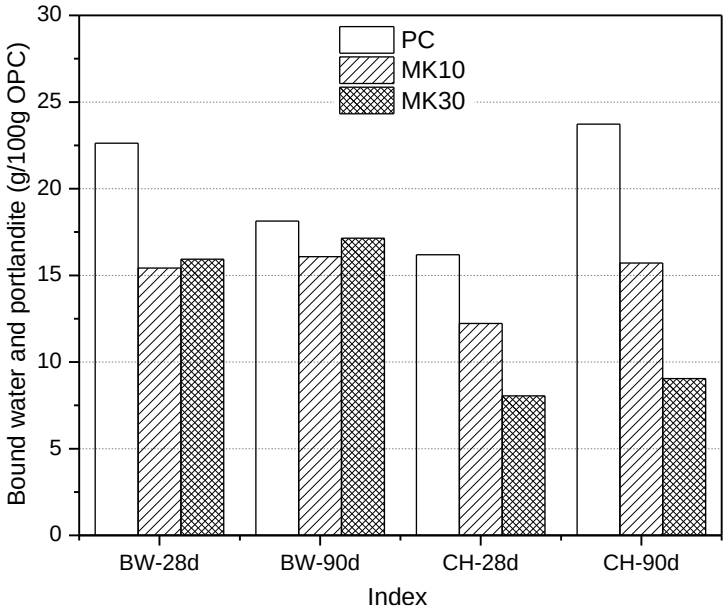

Figure 3.6: Content of normalized bound water and portlandite determined by TGA after 28 days and 90 days hydration

3.3.4 Elemental analysis of C-S-H phases

Microanalytical investigations of the hydrate phases of PC and MK blended PC were carried out in the SEM with EDX to characterize the main amorphous phase (C-S-H) at different hydration ages. Both the inner and outer hydration products were targeted by X-ray under an accelerating voltage of 15 KeV and a working distance of 12.0 mm for local chemical analysis. Due to the interaction of electrons with the specimen and the intergrowth of hydrates, the detected X-rays of one spot often are the results of the signal of mixtures of phases (Deschner, Winnefeld et al. 2012), so the absolute values of individual microanalyses (or single atomic ratios) are less useful than are plots of the atomic ratios (Ramlochan, Thomas et al. 2004). In order to assure statistical accuracy of the phase composition, more than 50 EDX spot analyses were taken from each specimen. Then the elements of the C-S-H phase were determined by plotting the Al/Ca distribution as a function of Si/Ca atomic ratio as shown in Fig. 3.7-a and b, respectively.

The effective element ratios of the materials were determined by two lines. The Al/Si ratio of C-S-H was determined by the slope of a solid line, which is drawn through the points with the lowest Al/Ca ratio and represents mixed analyses of portlandite and C-S-H without AFm or ettringite. The dashed line was drawn from AFm element point (0, 0.5) and through the upper bound of distribution of Al/Ca atomic ratio. The range of Ca/Si ratios of C-S-H was roughly represented by the interior zone with dense bulk data points along the two lines. The discrete points with much lower Si/Ca ratio or higher Al/Ca ratio are due to deviations of EDX spectra caused by the pores (Deschner, Winnefeld et al. 2012), or thin C-S-H which is not sufficiently thick to minimize the contribution of adjacent phases (Ramlochan, Thomas et al. 2004).

The calculated Ca/Si and Al/Si ratios of C-S-H in PC after 300 days and 600 days are 1.85 ± 0.3 and 0.07, respectively, and the mean value of Ca/(Si+Al) is 1.73. In order to analyze the

effect of MK on hydration of the cement matrix from an early age, the plot of Al/Ca versus Si/Ca atomic ratio of MK blended PC was obtained from the EDX investigation carried out on samples at 28 days and 300 days. From the bulk data points, it can be directly found that the addition of 30 wt. % MK strongly increased the Al/Ca of C-S-H phase, due to the high content of SiO_2 and Al_2O_3 in MK. The Al/Si ratio of C-S-H is also improved from 0.07 to 0.313, which is close to the Al/Ca values of ettringite. The calculated Ca/Si ratio is slightly reduced to 1.42±0.25, due to the introduction of silicate by MK. The mean Ca/(Si+Al) is 1.08, which is obviously reduced through blending the MK.

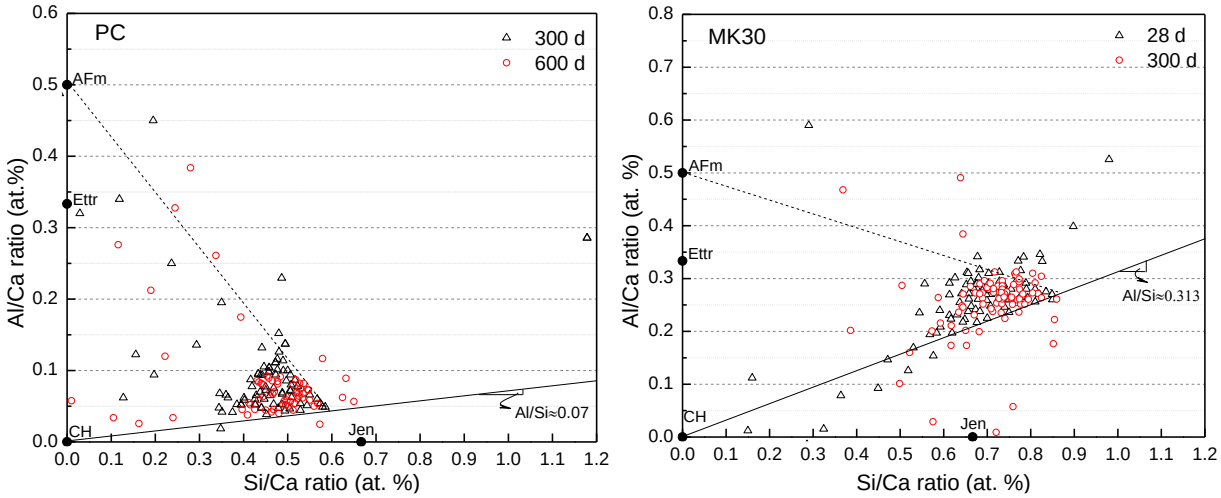

* CH-Calcium Hydroxide; Jen-Jennite; Ettr-Ettringite; AFm-Alumina-Ferric oxide-mono-sulfate.

Figure 3.7: Plot of Al/Ca as a function of Si/Ca ratios (in atomic percentage) of the EDX points analysis obtained on PC and MK-PC samples at different ages (28 days, 300 days, 600 days)

3.4 Pore Solution of Cement Matrix

As the liquid phase in the cement matrix, the alkaline pore solution, which contains a large number of ions from the soluble substance of the cement matrix, is another major reason for degradation of natural fiber, because this mineral-rich fluid can soak and infiltrate into the middle lamella and lumen of the fiber, and directly corrode cellulose, hemicellulose and lignin. The

existence of ions, especially OH^- and Ca^{2+}, in the pore solution is a major cause of the degradation of natural organic matter. The results in the literatures (Gram 1983, Singh 1985) show that CH causes more severe erosion of natural fibers than a NaOH solution with same alkalinity. In the presence of Ca^{2+}, a primary cation in cement pore water, isosaccharinic acid (ISA) will be the main degradation product (Blears, Machell et al. 1957, Machell and Richards 1960). The development of PC pore solution chemistry, such as the pH value, ions concentration as a function of hydration time, and the effect of supplementary cementitious materials on pore solution chemistry, has been a major focal point of research for several years as an index of cement hydration. The concentrations of each element depend on the dissolution of portlandite, alkali sulphates, aluminate phase and the consumption of calcium sulphate, which involve some chemical states of equilibrium as follows (D. Garvin 1987, Kulik 2002, Lothenbach and Winnefeld 2006):

Ettringite $Ca_6Al_2(SO_4)_3(OH)_{12}\cdot 26H_2O \Leftrightarrow 6Ca^{2+} + 2Al(OH)_4^- + 3SO_4^{2-} + 4OH^- + 26H_2$ (3.1)

Portlandite $Ca(OH)_2 + 2H^+ \Leftrightarrow Ca^{2+} + 2H_2O$ (3.2)

Calcite $CaCO_3 + H^+ \Leftrightarrow Ca^{2+}HCO_3^-$ (3.3)

Anhydrite $CaSO_4 \Leftrightarrow Ca^{2+} + SO_4^{2-}$ (3.4)

Gypsum $CaSO_4\cdot H_2O \Leftrightarrow Ca^{2+} + SO_4^{2-} + 2H_2O$ (3.5)

Syngenite $K_2Ca(SO_4)\cdot 2H_2O \Leftrightarrow 2K^+ + Ca^{2+} + 2SO_4^{2-} + H_2O$ (3.6)

Tobermorite-I&II $5(Ca(OH)_2)\cdot 6(SiO_2)\cdot 5(H_2O) + H_2O \; 5Ca^{2+} + 6SiO(OH)_3^- + 4OH^-$ (3.7)

Monosulfate $3CaO(Al_2O_3)\cdot(CaSO_4)\cdot 12(H_2O) \Leftrightarrow 4Ca^{2+} + 2Al(OH)_4^- + SO_4^{2-} + 4OH^- + 6H_2O$ (3.8)

The pozzolanic reaction, caused by metakaolin, consumes calcium hydroxide in cement hydration products, which in turn, affect the pH value and ion concentration of the pore solution:

$$Ca(OH)_2 + MK \rightarrow C\text{-}S\text{-}H + \text{crystalline products } (C_3AH_6,\ C_4AH_{13},\ C_2ASH_8, \text{ etc.}) \quad (3.9)$$

According to the elemental concentration levels and their effects on alkalinity and mineralization, the pH values and five element concentrations, such as K, Na, Ca, Si and OH^-, of pore solution gained from neat PC and PC blended with 30 wt. % MK were investigated, as shown in Fig. 3.8-a and b, respectively.

From Fig. 3.8-a, it can be found that in neat PC, all the concentrations in pore solution remained relatively stable except Ca, since they are controlled by the consumption of $CaSO_4$ phases and the formation of portlandite (Deschner, Winnefeld et al. 2012). Caused by the consumption of the gypsum through reaction with C_3A (Rothstein, Thomas et al. 2002) and the depletion of the calcium sulphates (Deschner, Winnefeld et al. 2012), the concentration of calcium decreased rapidly after 6h, and that of silicon and OH^- increased considerably at the same time. Although there were also slight increases, the effects of the above-mentioned reactions on concentrations of Na and K were not significant. However, the rapid reactions with calcium hydroxide and sulphates gave rise to the continuous dissolution of C_3A, which led to the increase of OH^- and high pH value in pore solution, and in turn reduced the concentration of Ca, because of the reverse reaction as shown in Eq. (3.2). These changes of concentrations in pore solution at early age have interactions and correlate with the silicate reaction and the second aluminate reaction as shown in Fig. 3.3-a. The development of pH values of pore solution in PC and MK-30 are shown in Fig. 3.8-c. Correlating with the changes of concentrations, the pH of PC stays at a level of 13.1 ± 0.1 for the first 10h, then rises up to 13.7 ± 0.06, and increases slightly with hydration for a long time.

The development of concentrations in pore solution in MK-30 is different from that of PC. Except Si, all initial concentrations of elements are reduced due to the dilution effect through

replacing cement by MK and its high content of Al_2O_3, which contributes to the first aluminate reaction. Due to the strong second aluminate reaction in blends of PC-MK shown in Fig. 3.3-a, there is an obvious reduction in concentration of Ca after 8h and it keeps decreasing even after long hydration times because of the consumption of portlandite by the pozzolanic reaction with MK. The concentration of OH^- is also reduced by mixing MK and continues to decrease with the hydration time, not only because of less readily soluble alkalis in the matrix caused by the dilution effect, but also due to the binding of alkalis in the additional amounts of C-S-H generated by the pozzolanic reaction (Duchesne and Be ŕube ´1995). As shown in Fig. 3.7, by blending 30 wt. % MK, the Ca/Si and Ca/(Si+Al) ratios of C-S-H phase were reduced by 7.57% and 36.24%, respectively. This also means the C-S-H in MK-30 binds much more alkalis than neat PC (Hong and Glasser 1999, Deschner, Winnefeld et al. 2012). The pH of pore solution in MK-30 blends was 12.9 ± 0.1 during the first 8h, and then decreased to 12.7 ± 0.08 after the deceleration and stabilization period of hydration.

According to the analysis above, the substitution of PC by MK, which results in lower concentrations of OH^- and Ca in the pore solution, is helpful in improving the durability of natural fiber.

Fig. 3.8-d shows the calculated effective saturation indices (ESI) of portlandite, ettringite and monosulfate as functions of hydration time in neat PC and MK-30 blends. As an index showing whether water tends to dissolve or precipitate a particular mineral (shown as Eqs. (3.1)-(3.8)), the ESI is defined as:

$$ESI = \log (IAP/K_{sp}) \tag{3.10}$$

where IAP is an ion activity product, and K_{sp} is a solubility product.

IAP and K_{sp} have the same form: both of them are calculated from the product of free ion, however, K_{sp} is an equilibrium constant in terms of activities of reactants and products at equilibrium, and IAP involves the actual (measured) activities. If IAP = K_{sp}, ESI=0, which means the solution is in equilibrium with the mineral; if IAP < K_{sp}, ESI < 0 pore solution is undersaturated with the mineral and reaction is proceeding from left to right (dissolution); for IAP > K_{sp}, ESI > 0, i.e. the pore solution is supersaturated with the mineral and reaction is proceeding from right to left (precipitation).

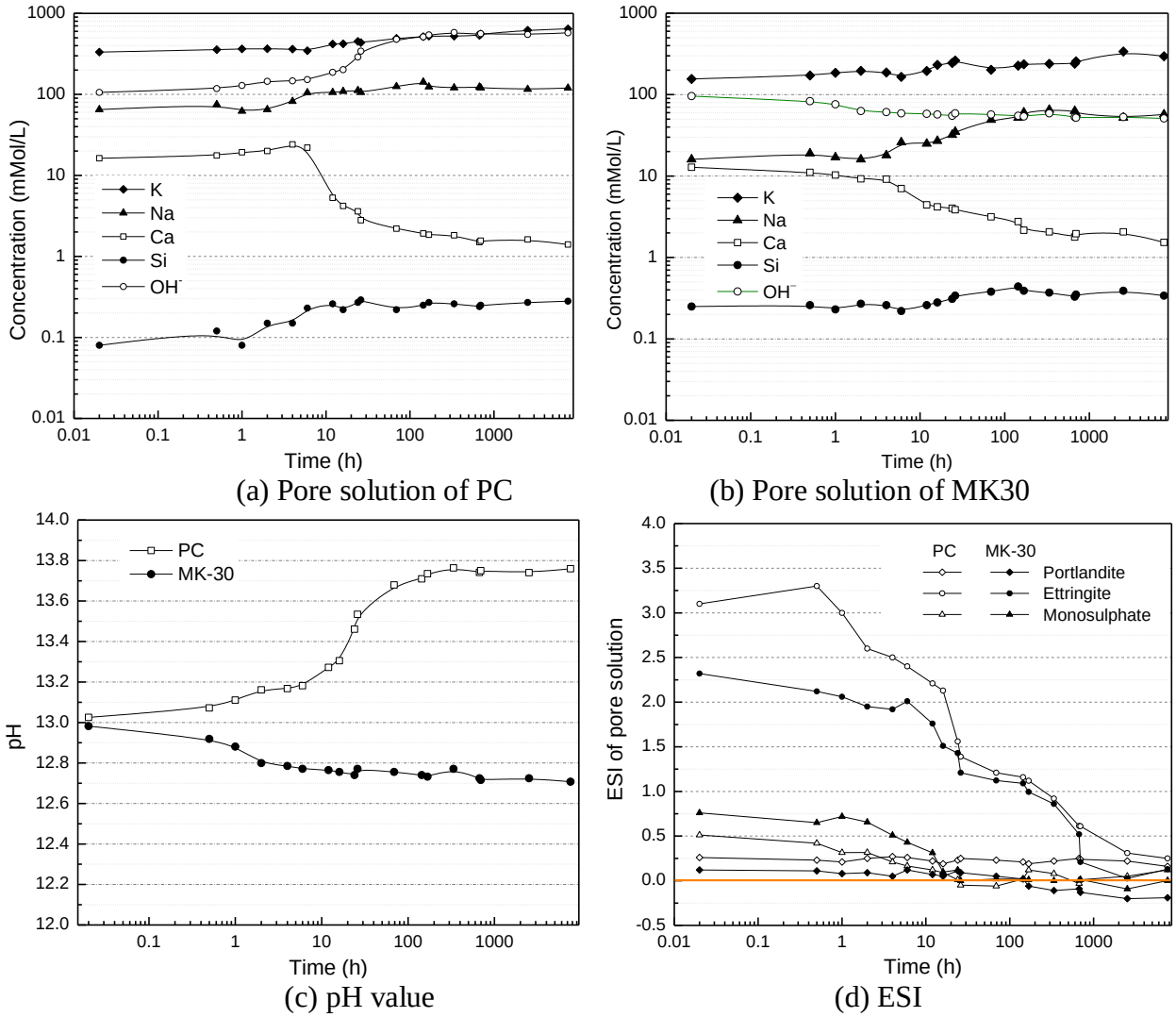

Figure 3.8: Elemental Concentrations, pH value, and ESI of pore solutions for PC and blends

The ESI of portlandite in PC is 0.25±0.09 from the time of mixing to 317 days, which means the pore solution of neat PC is supersaturated at a low level for portlandite over the whole hydration time. The slight oversaturation of portlandite was also found in the pore solution of the MK-30 blend at early age. However, after 7 days, the ESI decreased to be negative, so the portlandite was undersaturated for the remaining hydration age, which can also be correlated with the results of XRD of analysis of solid phase shown in Fig. 3.4. The ettringite in the pore solution of neat PC dropped strongly from a high level to a slight supersaturation with the increase of hydration time. The same trend was also found in the solution of MK-30, but the oversaturation degree of ettringite was much lower than that of neat PC throughout the experiment. The ESIs show that pore solutions in both PC and MK-30 were oversaturated with respect to monosulphate at early age, and then decreased to an equilibrium level after 1 day.

3.5 Autogenous Shrinkage

Hydration of Portland cement is accompanied by a chemical shrinkage (Lura, Jensen et al. 2003): not only hydration of the main clinker minerals but also the secondary reactions, including formation of ettringite, result in the shrinkage of paste (Jensen 1993). The autogenous shrinkage, which depends on surface tension of the cement gel particles, capillary tension in the pore fluid, autogenous relative humidity (self-desiccation), and so on, coupled with drying shrinkage of natural fiber, creates the interstitial fluid space between fiber and matrix. Fig. 3.9 shows the evolution of autogenous shrinkage of PC and paste blended with 10 wt. % and 30 wt. % MK, with w/b of 0.5, as a function of hydration time. It can clearly be seen that, due to the substitution of tetracalcium aluminate hydrate (C_4AH_{13}) by a lower density gehlenite hydrate (C_2ASH_8) (Wild, Khatib et al. 1998) caused by the pozzolanic reaction of MK, the autogenous shrinkage decreased with increasing amount of MK. The autogenous shrinkage of PC was up to 1.67 mm/m, while the

values of MK-10 and MK-30 were 1.13 mm/m and 0.65 mm/m, which means the substitution of 10 wt. % and 30 wt. % MK resulted in reductions of autogenous shrinkage by 21.56% and 61.08%, in four months, respectively. This positive effect is verified by results in the literature (Gleize, Cyr et al. 2007) on autogenous shrinkage of cement-based materials containing MK. The smaller autogenous shrinkage is helpful to reduce the interstitial fluid space and to prevent the automatic stripping of natural fiber in a hardened cement matrix. It can be predicted that the substitution of MK for PC can alleviate the degradation and improve the durability of natural fiber not only by chemical modification, but also through physical action.

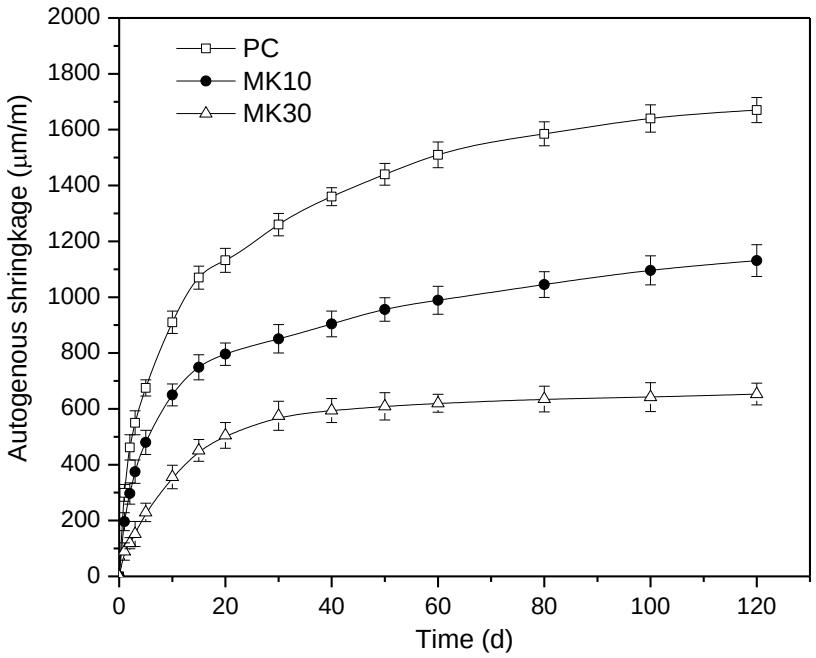

Figure 3.9: Effect of MK on autogenous shrinkage of cement pastes

3.6 Compressive Strength

Due to the pozzolanic reactions, substitution of MK not only modified the hydration of cement matrix of both solid and liquid phases, but also improved the mechanical properties. Fig.

3.10 shows the compressive strength of PC samples with and without MK. At early age (1 day), the strength of blends rose at the beginning, then decreased with further increase of MK content. There was an increase of 6.55% for MK10, but a reduction of 37.17% for MK-30 due to the dilution of the cement. After 1 day, MK-30 exhibited the fastest strength gain, and MK10 also gained higher strength than neat PC at all ages. Beyond 7 days, MK-30 achieved the highest compressive strength, and after 28 days, the strength of the MK30 blend reached 117.08% of the neat PC, while the replacement of 10 wt. % of PC by MK resulted in 5.89% higher compressive strength values compared to neat PC. The higher early strength of MK-10 might be related to the high content of Al_2O_3 in MK, which helps to accelerate the hydration and hardening of cement. This is consistent with the hydration heat flow as shown in Fig. 3.3. After the first day, in MK-30, the pozzolanic reactions became predominant compared to the dilution effect, and so the compressive strength showed a substantial increase.

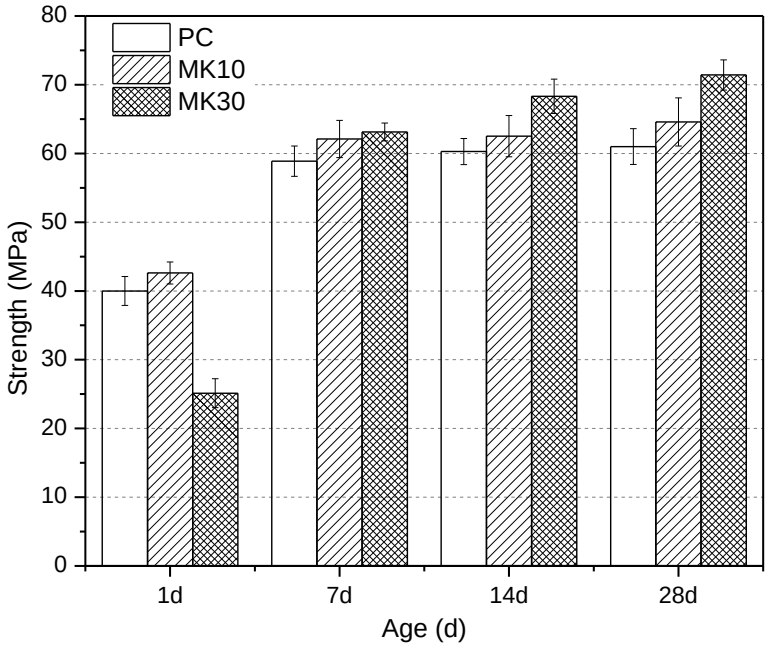

Figure 3.10: Effect of MK on compressive strength of cement mortar

3.7 Chemical Composition and Moisture Content of Natural Fiber

As shown in Table 3.2, the chemical composition of natural fiber includes pectin, extractive, lignin, hemicellulose, and cellulose contents, among which cellulose is the major component and the one that provides strength and stability. The content of cellulose in sisal, jute, bamboo and flax fibers is much higher than hemicellulose, lignin and other components, however, its content in coir is much lower, which is almost the same as lignin. As mentioned earlier, cellulose is the main structural component in cell walls, so the lower content of cellulose in coir fiber explains its relatively low tensile strength compared to the other four kinds of fiber. Due to the special structure of vegetable fiber as shown in Fig. 1.1, lignin and pectin are the first two components which encounter degradation in aggressive environments. The degradation of lignin, pectin and hemicellulose determine the separation degree of single cellulose fibers. Therefore, the contents of these three components mainly affect the durability of natural fiber in a cement matrix at early age. Coir has the highest content of lignin, pectin and hemicellulose. Flax fiber contains the lowest amount of lignin. The smallest amounts of pectin, extractive and moisture were all found in bamboo fiber, which accounts for its high tensile strength. According to the data of Table 3.2, sisal fiber was selected as a representative to determine the degree of degradation and loss of tensile strength, as well as the durability of natural fiber-reinforced cement composites (NFRCC).

Table 3.2: Chemical composition of natural fiber

Component (%)	Natural fiber				
	Sisal	Jute	Coir	Bamboo	Flax
Lignin	12.3	13.6	35.1	10.3	5.4
Holocellulose	81.9	83.4	54.3	87.8	86.3
Cellulose	68.2	69.3	38.2	73.9	69.1
Hemicellulose	13.7	14.1	16.1	13.9	17.2
Extractive	2.4	1.5	2.9	1.1	4.7
Pectin	1.3	0.9	5.3	0.4	1.6
Moisture & other	3.2	0.6	2.4	0.4	2.0

3.8 Water Absorption of Sisal Fiber

Three sisal fiber strands with different initial weight were soaked in tap water, sodium hydroxide solution and calcium hydroxide solution, with pH value of 13.0, under room temperature, 50 ℃ and 70 ℃. The mass changes in different solutions under the three temperatures are shown in Table 3.3. The fibers soaked in tap water and $Ca(OH)_2$ solution yielded the lowest and highest water absorption ratios, respectively, at all three temperatures. Compared with that soaked in tap water, the fiber's water absorption ratio in $Ca(OH)_2$ solution was 5.07% higher. It also can be seen that the moisture absorpion capacity of fibers rises with increasing temperature. It is well known that natural fibers encounter more serious attack in alkaline solution under higher temperature, which promotes the hydrolysis of amorphous materials in fibers. The difference of the fiber's water absorption ratio in $Ca(OH)_2$ and NaOH solutions is due to the mineralization caused by penetration and precipitation of minerals rich in Ca. Lignin, hemicelluloses and pectin act as chemical and physical barriers to the penetration of Ca ions into the fibers (Gustavo Henrique Denzin Tonoli 2010). Although non-cellulose materials' degradation proceeds in both solutions, the mineralization in natural fiber only occurs in $Ca(OH)_2$ solution.

Table 3.3: Water absorption ratio of sisal fiber

Temperature (℃)	Water absorption ratio, δ (%)		
	Tap water	$Ca(OH)_2$ solution	NaOH solution
23	152.96	160.71	156.83
50	155.16	165.12	158.66
70	159.71	169.30	160.19

3.9 Durability of Sisal Fiber Reinforced Cement Composites

It has been well known that the most important contribution of fiber-reinforcement in cement composites is not to strength but to the flexural toughness of the material. In order to analyze the

degradation of sisal fibers in a cement matrix and the durability of SFRCC, the flexural behavior was investigated according to ASTM C1185 - 08(2012), ASTM C-1018 and JCI SF4.

The effect of MK on the flexural properties of SFRCM and its durability as a function of wetting and drying cycles are shown in Fig. 3.11. Conflicting results are found concerning first crack strength results for sisal fiber-PC-MK composites. Mohr et al.(Mohr, Biernacki et al. 2007) found that, prior to cycling, the MK composites exhibited lower first crack strength than the control. The results obtained in our investigation, shown in Fig. 3.11-a, exhibit similar behavior as that found for compressive strength: the initial first crack strength of fiber reinforced cement mortar was improved due to the presence of MK. MK-10 and MK-30 gave 9.05% and 34.33% higher strength than that of PC, respectively. However, the improvement of durability cannot be detected from the first crack strength of MK-10 and MK-30. After 5 cycles, the first crack strength of PC increased slightly, and then decreased with additional wetting and drying cycles. The increase in density of the matrix around and the fiber embrittlement due to migration of hydration products from the matrix to the fiber cell walls could be the main factors contributing to the increase of the first crack strength and reduction of toughness, by reducing the flexibility and deformation capacity of the fibers. Stronger, more rigid and brittle fibers, and improved bond strength, are known to lead to composites with higher strength and lower ductility (Tolêdo Filho, Scrivener et al. 2000). Over the range of wet /dry cycles investigated here, the decrease of first crack strength for MK-10 and MK-30 are 3.41% and 2.90%, which are similar as those of the control. First crack strength depends mainly on characteristics that govern matrix strength and is minimally dependent on fiber parameters such as type, size and amount (Johnston and Skarendahl 1992). Therefore, first crack strength mainly reflects the bending properties of the cement matrix while the degradation

of fiber in cement depends on the properties in the multiple cracking stage and softening and failure stages shown in Fig. 2.5.

Fig. 3.11-b illustrates the peak flexural strength results of the investigated samples. The initial peak strength of sisal fiber reinforced mortar, before wetting and drying exposure, was improved by 21.23% and 35.73% for Mk-10 and MK-30, respectively. The changes in peak strength values for all three groups due to wetting and drying cycles were more obvious than those of the first crack strength, and sisal fiber reinforced neat cement mortar gave the sharpest drop. After 5 wetting and drying cycles, the strength of PC decreased by 11.23%, and additional cycling led to more significant decreases. After 30 cycles, the peak strength of PC dropped to 34.71% of the initial strength, whereas the decrease of peak strength for MK-10 was 23.20%. Compared with PC, the MK-30 suffered much smaller changes: after 30 cycles, the peak strength was still 87.69% of the initial strength, which means that the substitution of 10wt.% and 30 wt. % MK improved the durability of sisal fiber reinforced mortar by 64.47 % and 81.15%, respectively, as measured by the post crack strength of samples subjected to wetting and drying cycles.

Fiber reinforcement in cement based composites not only results in a large increase in bending strength, but also in a considerable increase in energy absorption capability. After cracking of the matrix, the cracks cannot propagate without stretching and debonding of the fibers. As a result, a large additional amount of energy is absorbed before ultimate failure of the specimen (Al-Ghamdy, Wight et al. 1994). Toughness is one of the most important performance indicators for fiber-reinforced cement composites. Post-cracking toughness results are shown in Fig. 3.11-c, which illustrate that flexural toughness is most sensitive to wetting and drying cycles. The substitution of 10 wt. % and 30 wt. % MK in cement led to 23.38% and 44.67% improvement in initial post-cracking toughness, respectively. Under progressive cycling, sisal fiber reinforced PC

mortar encountered the most significant drop in fracture toughness. After 5, 15, and 30 cycles, the toughness of PC decreased by 17.49%, 53.83% and 82.63%, respectively. The cement substitution by MK not only improved the initial post-cracking toughness of SFRCC, but also effectively delayed the degradation of the composite when subjected to progressive cycling. Up to 30 cycles, the toughness of MK-10 and MK-30 decreased by only 25.35% and 14.38%, which means the durability of fiber reinforced mortar was improved by 69.32% and 82.60%, respectively. From these results, it can be concluded that MK improves the durability of SFRCC mainly in the latter two stages of the load-deflection behavior, especially in the softening and failure stage.

Fig. 3.11-d illustrates the modified toughness index I_{55} of the investigated samples. Over the range of wetting and drying cycles, the degradations of I_{55} for sisal fiber reinforced PC, MK-10 and MK-30 are 65.77%, 33.16% and 10.80%, respectively. Similar changes were also found for the modified JCI toughness index (Fig. 3.11-f). After 30 wetting and drying cycles, the final T_{JCI-10} and F_{JCI-10} for the three groups were 39.35%, 78.50%, and 85.52% of their initial values. The JCI-toughness of MK-10 was comparable to the control prior to cycling, but MK-30 still performed better.

The deflection ratios T_{max} and $T_{0.5}$ are also effective measures of toughness and deformation capacity under applied loads. From Fig. 3.11-e, it can be seen that, compared with T_{max}, $T_{0.5}$ shows even more serious decline. T_{max} for SFRCM decreased by 66.67% after 30 cycles, whereas the corresponding decreases for MK-10 and MK-30 are only 31.88% and 16.81%, respectively. After aggressive cycling, the MK-30 still performed better than the control prior to cycling. Due to the embrittlement of sisal fiber in the cement matrix caused by the rich CH in both pore solution and solid phase, the deformation capacity of SFRCM decreased significantly when subjected to wetting and drying cycles. However, this degradation was effectively restrained by substitution of MK for

PC. The durability of SFRCM as measured by $T_{0.5}$ was improved by 57.85% and 77.39% for MK-10 and MK-30, respectively. The final deformation capacity of MK-30 was comparable to the unexposed control prior to cycling.

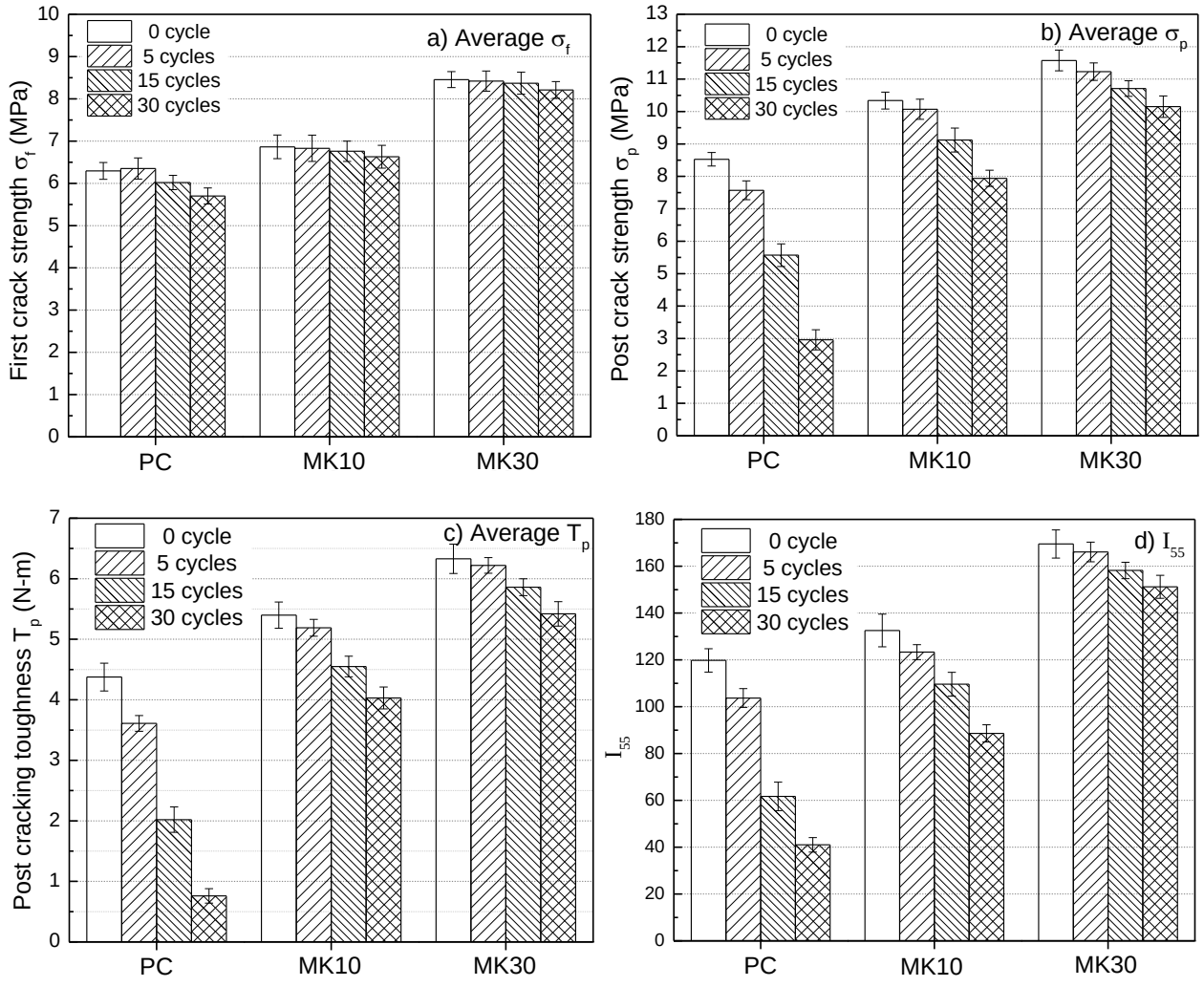

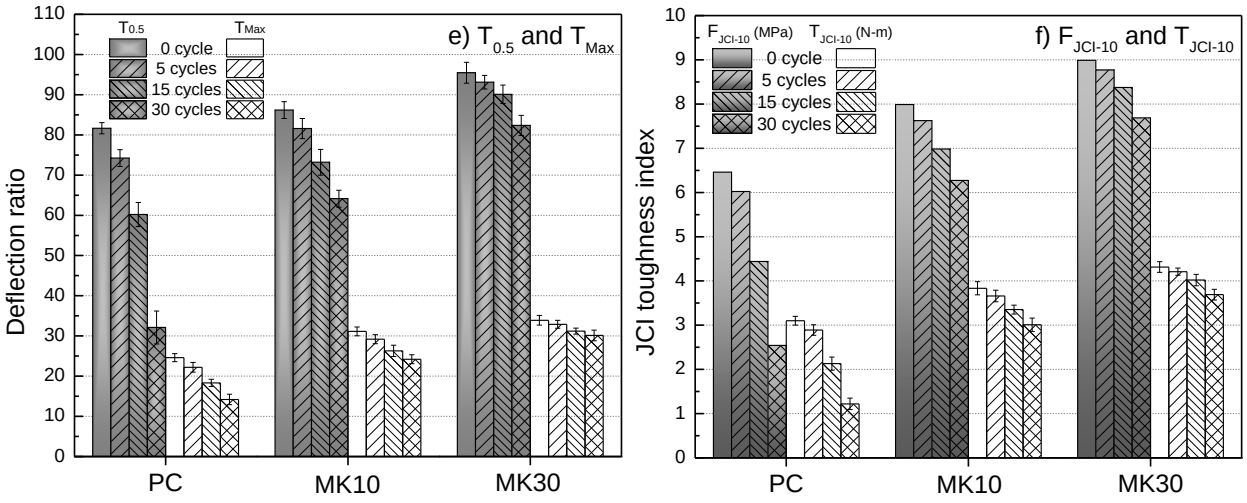

Figure 3.11: Flexure test results. (a) Average first crack strength (MPa), (b) Average post-crack flexural strength (Mpa), (c) Average post-cracking toughness (N-m), (d) I_{55}, (e) T_{JCI-10} and T_{JCI-10}, (f) T_{max} and $T_{0.5}$

Fig. 3.12 shows the effects of the pH value of cement pore solution and CH content of the composite prior to cycling on the post-cracking toughness after 30 cycles. It can be seen that both toughness T_p and strength σ_p of SFRCM drop with increases of alkalinity and CH content. When the CH content was greater than 10, sisal fibers suffered serious degradation due to mineralization and alkali hydrolysis caused by pore solution with high alkalinity. The initial CH content in the composite plays a significant role in minimizing degradation during wetting and drying cycling (Mohr, Biernacki et al. 2007), because the CH precipitation is a dominant factor in natural fiber-cement composite degradation (Mohr, Biernacki et al. 2006). Therefore, controlling the pH value of the pore solution and CH content at a relative low level by using pozzolanic supplementary materials is an effective way to counter the degradation of natural fiber.

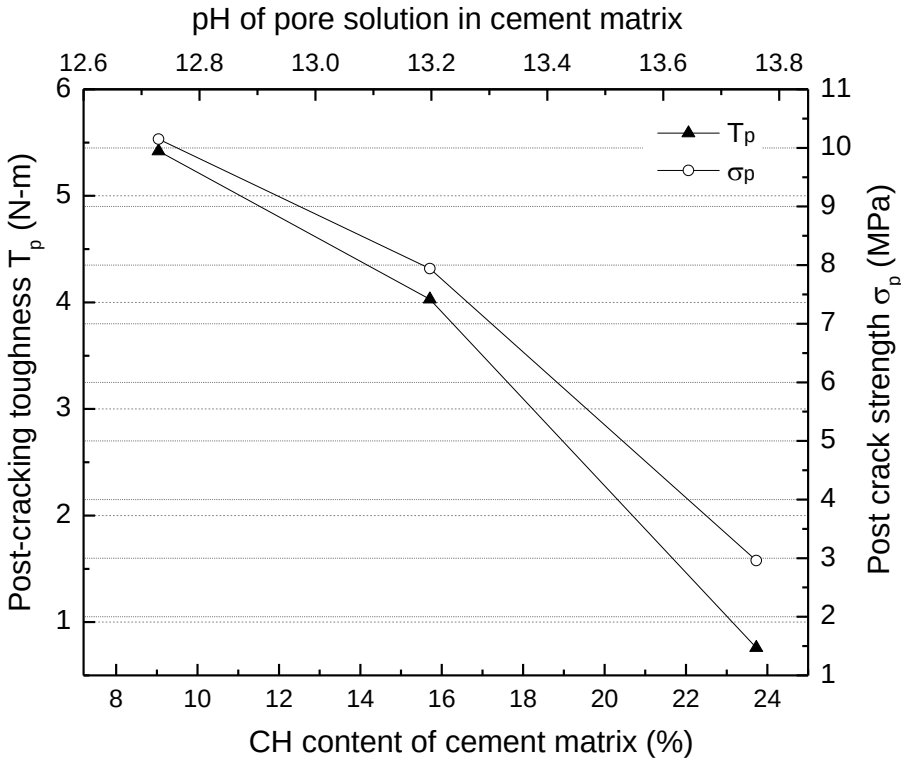

Figure 3.12: Effect of calcium hydroxide and pH value, measured prior to cycling (90d), on composite post-cracking strength and toughness, measured after 15 wet/dry cycles

3.10 Degradation of Sisal Fiber

3.10.1 Tensile strength

Fig. 3.13 shows the stress-strain curves obtained by uniaxial tensile testing of selected sisal fibers. It can be seen that the tensile strength of the embedded fiber in MK30 after 5 wetting and drying cycles is slightly higher than that of a raw fiber. The reason for this increase is the removal of non-cellulosic materials and impurities, which remain dispersed in interfibrillar regions of natural fibers (Gu 2009). The rearrangements of fibrils and close packing of cellulose chains in natural fibers result in preferable tensile deformation, better load sharing behaviors and higher tensile strength and elongation at break in the stretched state (Bledzki and Gassan 1999, Ray and Sarkar 2001, Roy, Chakraborty et al. 2012). However, the tensile strength of fibers embedded in

PC and MK10 are lower than those for the control group. All fibers, especially the ones pulled out from PC, suffer degradation in strength when subjected to aging conditions.

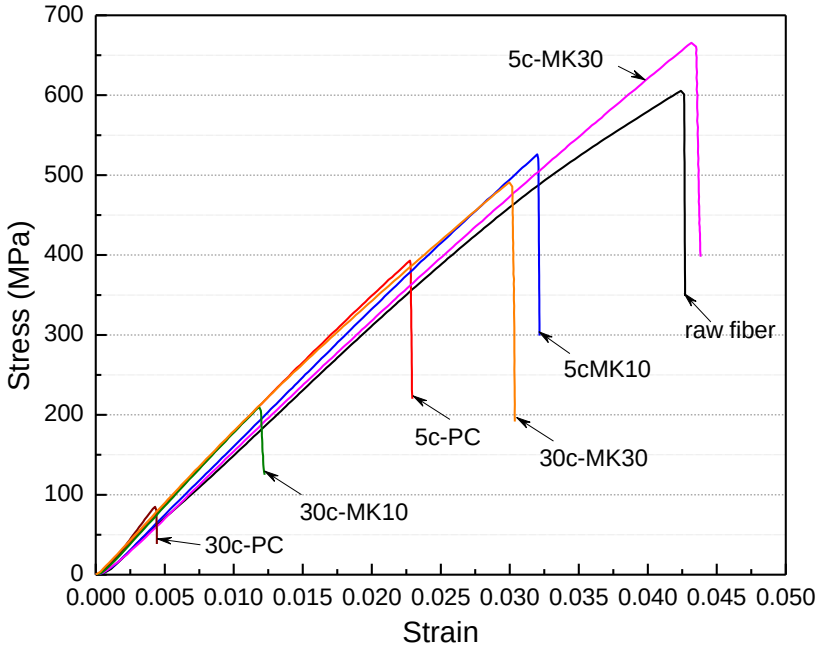

Figure 3.13: Stress–strain curve of tensile test on sisal fibers

The decreasing strength and gradually increased Young's modulus indicate that the mineralization and alkaline hydrolysis in natural fiber are the cause of a higher stiffness and brittleness. The hemicellulose and lignin in natural fiber have two consequences. On one hand they increase the interfibrillar space and disperse the fibrils. On the other hand, they protect the main structural component of the fibers, cellulose, against the alkaline attack. Without non-cellulose materials as protective coating, cellulose chains encounter corrosion directly from the pore solution of high alkalinity. Another phenomenon shown in Fig. 3.13 is that the degradation degree of sisal fiber decreases with increasing replacement of PC by MK, which indicates that MK effectively

reduces the alkalinity of the pore solution and improves the durability of natural fibers in a cement matrix by improving cement hydration.

Tensile test results for sisal fibers are difficult to analyze due to wide scatter, therefore a statistical approach is essential for assessing their tensile properties (De Rosa, Kenny et al. 2010). A Weibull distribution analysis of the data was performed (Fig. 3.14) which shows a good fit with the statistical analysis of experimental data with $R^2 \geq 0.95$.

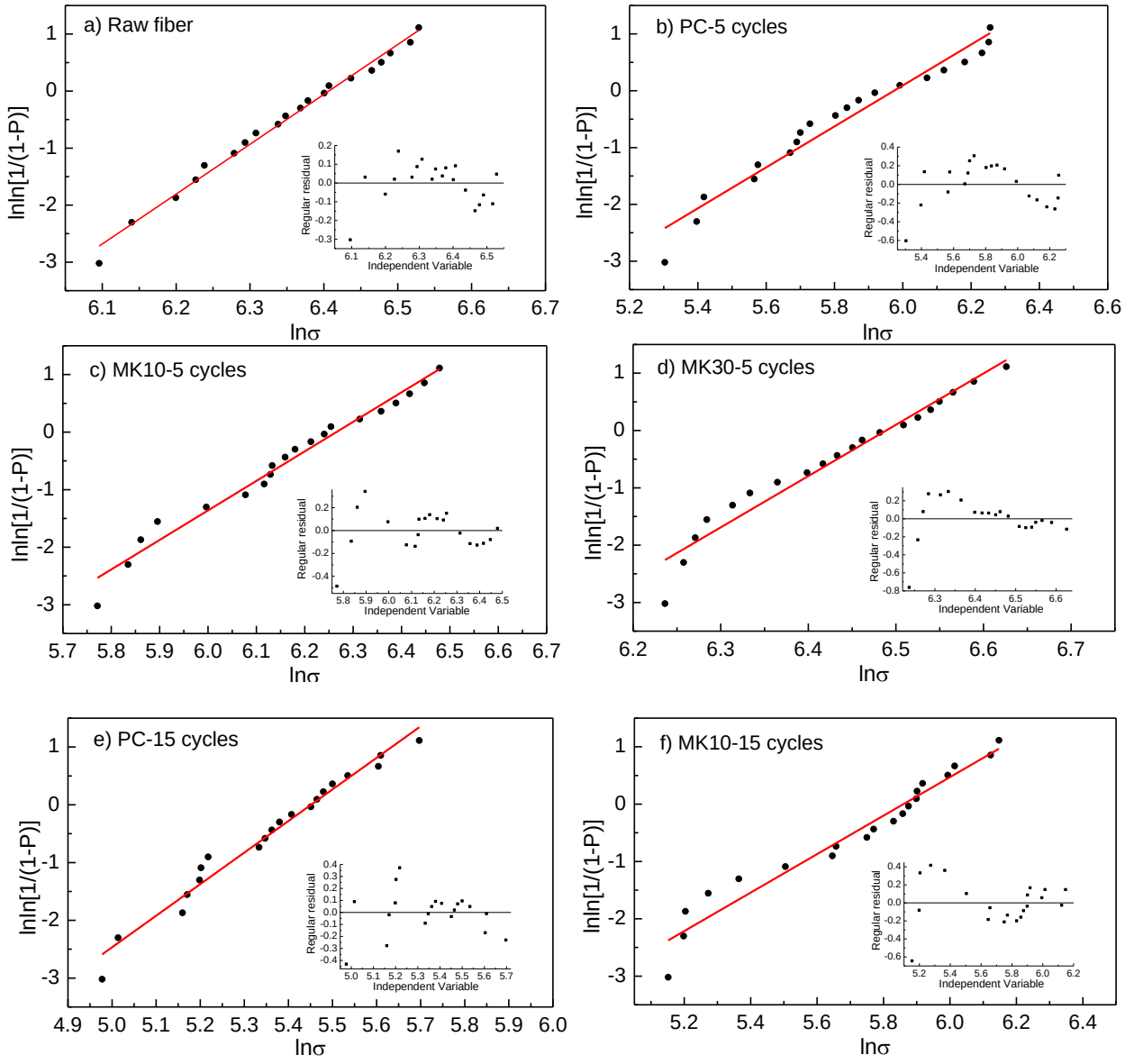

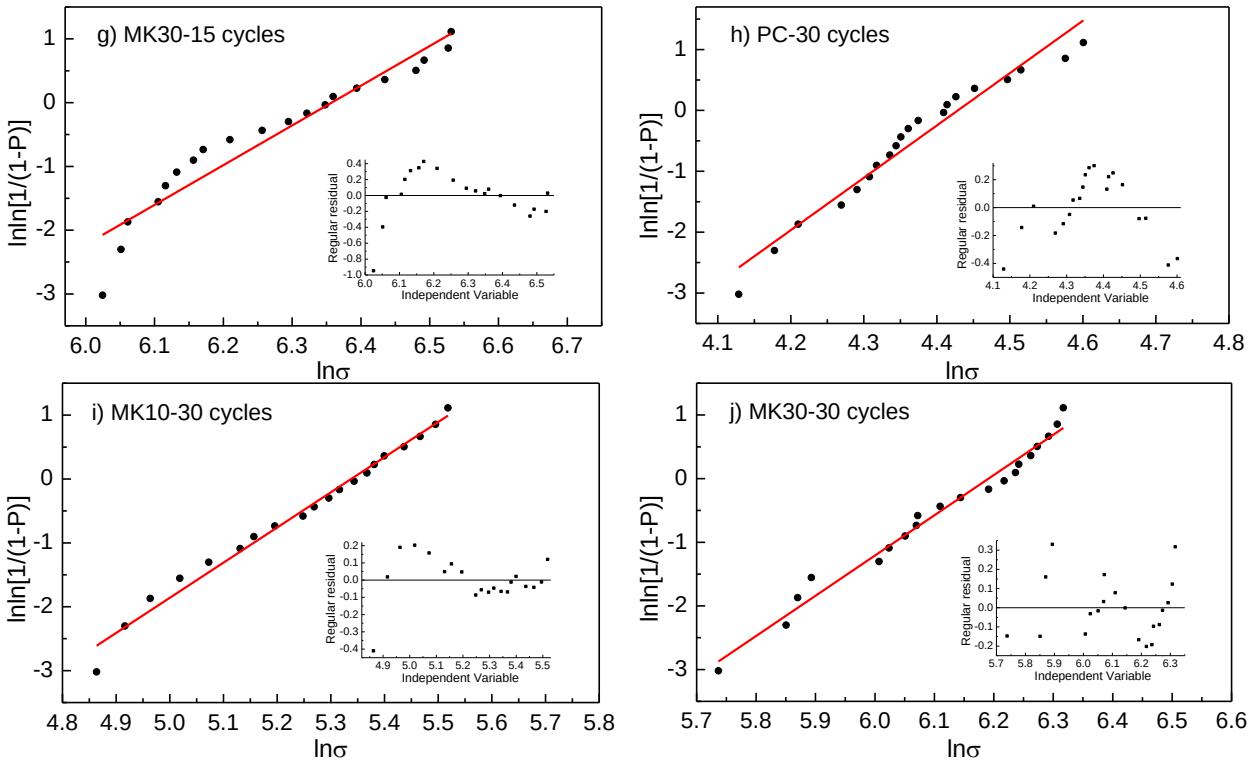

Figure 3.14: The Weibull plots of raw fiber and fibers embedded in PC and blends (MK10, MK30) subjected to 5, 15, and 30 wetting and drying cycles

Weibull modulus, characteristic strength and the average Young's modulus of sisal fibers are given in Table 3.4. The results show that the Weibull modulus decreases and then gradually increases with increasing characteristic strength, which indicates that the data of a single fiber tensile test are concentrated when the tensile strength is high or low, and apparently inconsistent for strengths inbetween. After 5 wetting and drying cycles, sisal fibers suffer a severe alkali attack from the neat cement matrix, however, the situation improves in MK modified cement blends. Compared with raw fiber, the fibers embedded in neat PC and MK-10 have 35.11% and 13.19% lower tensile strength, respectively, but a slightly improved strength is obtained for the fibers embedded in MK-30. The cause is the slight removal of hemicellulose and lignin from the fibers due to the mild alkaline environment (low CH content (Fig. 3.6) and low pore solution alkalinity (Fig. 3.8-c)) of a matrix created by blending 30wt.% MK. Because of the high alkalinity of the

pore solution and high CH amount in the PC matrix, the fiber pullout from a neat PC matrix shows the lowest tensile strength and elongation at break at every step of aging. After 30 wetting and drying cycles, the tensile strength of fibers embedded in PC decreased by 86.17%. However, MK10 and MK30 decrease the fiber's strength by only 65.67% and 37.52%, respectively, compared with the raw fiber.

The effect of MK on the durability of natural fibers is also evidenced by the fiber's maintained deformability in the cement matrix after aging as indicated by Young's modulus. As can be seen in Table 3.4, after 5 cycles of aging, the deformability is reduced only slightly, and the tensile strength of fibers embedded in MK30 is about the same as that of raw fiber. The fibers embedded in a neat PC matrix yield the highest Young's modulus, due to the alkaline corrosion. After 30 wetting and drying cycles, Young's modulus of fiber in PC increases by 28.51%, however, that of fiber embedded in MK30 increases by only 6.49%.

Table 3.4: The Weibull parameters and deformability of sisal fibers in tensile test

Sample	Number of cycles	Weibull Modulus m	Characteristic Strength σ_0 (MPa)	R^2	Young's modulus E (GPa)
Raw fiber	0	8.74	605.86	0.98934	15.4
PC	5	3.60	393.15	0.95462	17.26
MK10	5	5.13	525.97	0.97302	16.44
Mk30	5	8.95	607.32	0.95387	15.42
PC	15	5.47	133.06	0.97124	18.66
MK10	15	3.36	350.67	0.94849	17.15
MK30	15	6.23	576.74	0.94594	16.07
PC	30	8.60	83.82	0.95378	19.79
MK10	30	5.50	208.04	0.98462	17.73
MK30	30	6.32	378.53	0.97777	16.40

Both mineralization and alkaline hydrolysis of non-cellulose materials in fibers cause the increased stiffness and brittleness. The formation of ettringite/monosulphate layers in the lumen cavity and CH re-precipitation in the center of the lumen (Tonoli, Rodrigues Filho et al. 2009) significantly increase the stiffness of natural fiber, evidenced by the increased Young's modulus of fibers in Table 3.4 and thus affect the embrittlement of composites. Due to the alkaline hydrolysis of hemicellulose and lignin, the content of cellulose crystal chains, which are the framework of natural fibers, become the main structural component. The increased crystallinity indicates that the lower amount of phenolic polymer and amorphous components, and as a result, stiffness and embrittlement of natural fiber were enhanced.

3.10.2 X-ray diffraction

As mentioned earlier, quantifying crystalline properties is a logical approach to evaluate the effects of mineralization and alkaline hydrolysis on the properties of natural fibers. It is evident from the literature that natural fibers are a semi-crystalline material and the tensile strength and elastic modulus have an evident relationship with its crystal content. Here, the intensity of the ($\bar{1}10$), (110), and (002) peaks and the amorphous scatter between 18 ºand 19 ºwere measured. The percent crystalline materials of the fibers were expressed as "percentage of crystallinity" ($\%Cr_1$ and $\%Cr_2$), "crystallinity index" (Cr.I.) and "crystallite size" (L) as shown in Eq. (2.18)-Eq. (2.20).

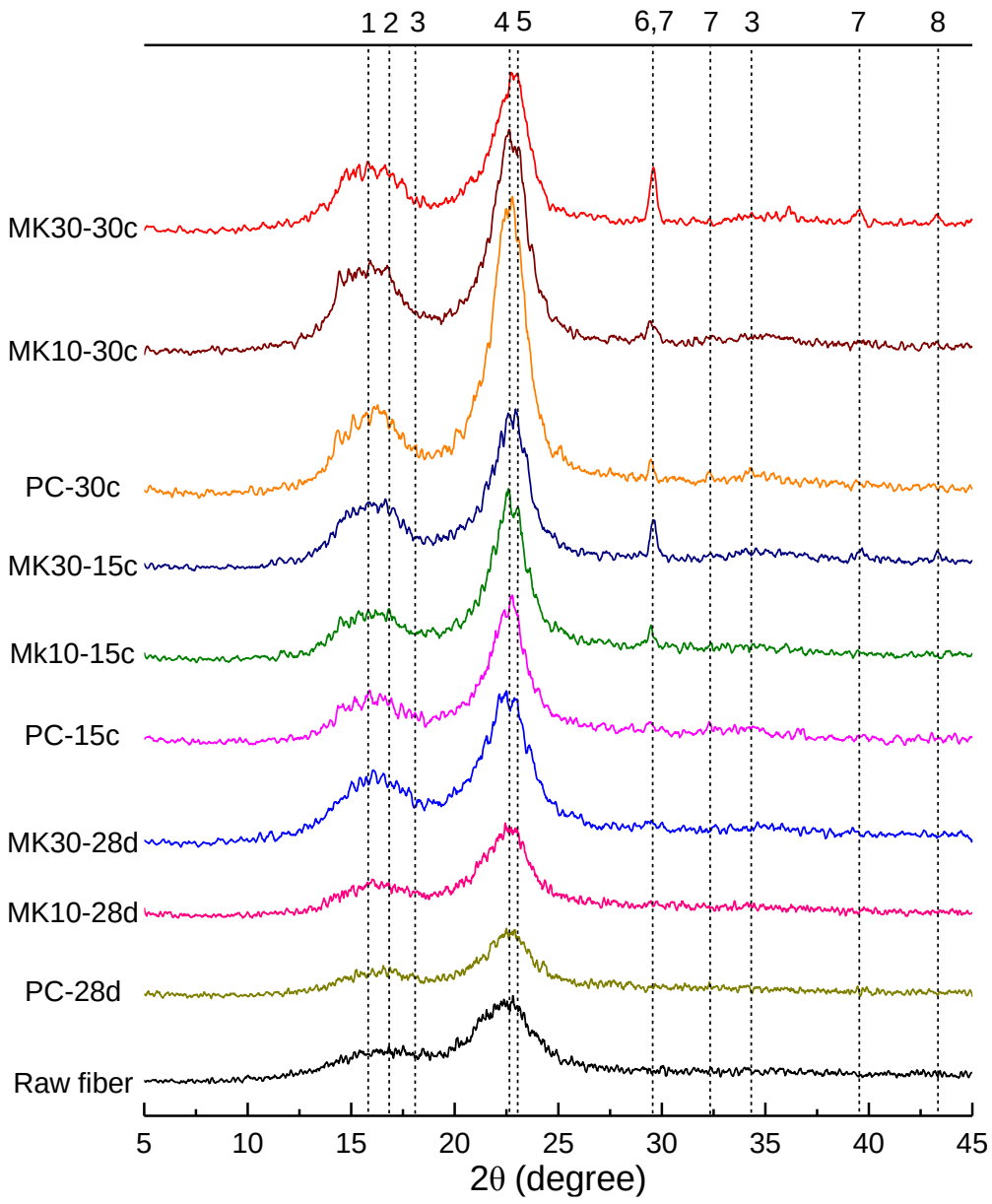

* 1, 2, 4: cellulose crystallographic plane ($\bar{1}10$), (110) and (002); 3: $Ca(OH)_2$; 5: ettringite; 6: $CaCO_3$; 7: C_2S, C_3S; 8: MgO.

Figure 3.15: XRD pattern of the raw fiber and embedded fibers before (28d) and after 5 (5c), 15 (15c) and 30 (30c) wetting and drying cycles

Fig. 3.15 shows the XRD diagrams of the raw sisal fiber and that embedded in PC, MK10 and MK30 samples after 5, 15 and 30 wetting and drying cycles. It can be seen that cellulose has a crystalline nature with an intensive peak at $2\theta \approx 22.5^{\circ}$ corresponding to the (002) lattice plane and

a broad peak between 13 °and 18 °corresponding to the ($\bar{1}$10) and (110) lattice planes. Peaks of ettringite are found in all fibers except the raw one, while the peaks of CH are only detected in fibers embedded in a neat PC matrix. These results agree fairly well with the modification effect of MK in cement as shown in Figs. 3.4-3.6. Due to the dilution effect and pozzolanic activity of MK, CH and ettringite are effectively consumed in the matrix. Therefore less re-precipitation of these two hydration products occurs in the lumen of natural fibers. $CaCO_3$ and MgO peaks were detected in the x-ray patterns of the embedded fibers by 15 cycles of wetting and drying cycles, and become stronger after 30 cycles.

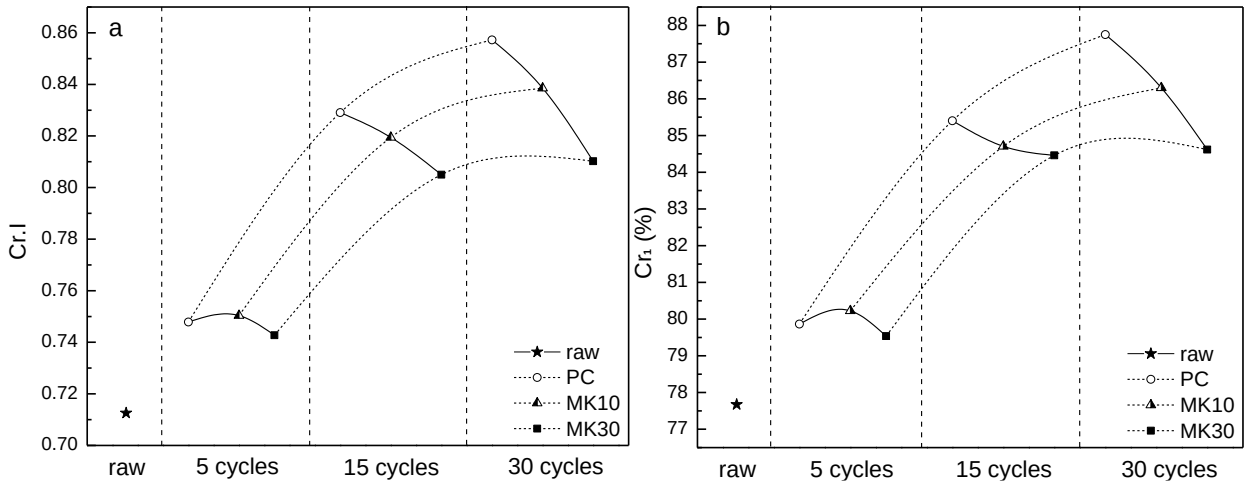

Figure 3.16: Crystallinity index and percentage of crystallinity of the embedded sisal fiber as functions of MK content and exposure duration

Figs. 3.16-a and b show the Cr.I. and %CR_1 of sisal fiber as functions of MK content and duration of aging, respectively. It can be seen that the crystallinity index of raw fiber is around 0.71 and increases at different rates with the aging duration of all three matrices. For the samples exposed to 5 cycles of aging, fibers embedded in MK10 have the highest crystallinity index and percentage of crystallinity. This is caused by the different degradation rates of the amorphous and

crystal components of the embedded sisal fibers in slight alkaline environment. The severe deterioration of the lignin and hemicellulose and the detainment of cellulose increase the crystallinity indices. Due to the highest alkalinity and CH amount in the neat PC matrix, the fibers embedded therein have a bigger Cr.I and % Cr_1 than those embedded in MK10 and MK30 for longer aging durations. After 30 wetting and drying cycles, the crystallinity index and crystallinity percentage of fiber embedded in neat PC were 20.31 and 12.97% higher than those of raw fiber, respectively. Therefore, these fibers have the highest content of cellulose crystals, which means the amorphous materials encountered serious attack in the PC matrix. At every stage of aging, the fiber embedded in MK30 has the lowest crystallinity index, although it present a dramatic increase from the raw fiber, and the Cr.I and % Cr_1 increase by only 0.65% and 0.19% from 15 to 30 wetting and drying cycles. The results agree well with the single fiber's tensile test data and flexural properties of sisal fiber reinforced cement mortar as analyzed above.

Table 3.5 shows sisal fibers' percentage of crystallinity (%Cr_2) and crystal size, which is calculated from their corresponding peak position and the full width of the peak at its half maximum height (FWHM) using the deconvolution method. Curve-fitting and deconvolution processes of XRD spectra were carried out to separate diffraction peaks using Gaussian functions. An important assumption for this analysis is that increased amorphous contribution is the main contributor to peak broadening, however, in addition to crystalline disorder, there are other intrinsic factors that influence peak broadening, such as crystallite size and non-uniform strain within the crystal (Park, Baker et al. 2010). Therefore, the regularity of these data is not significant as Cr.I and %Cr_1, or even inconsistent. Therefore, in future work, Cr.I and %Cr1 should be selected to characterize the crystallinity and degradation degree of the embedded sisal fiber. However, it still can be seen that after accelerated aging, the embedded fibers show bigger crystallite size than

raw fiber. Fibers pullout from PC and MK30 give the smallest crystallite size and crystallinity percentage after 30 cycles of aging, respectively.

Table 3.5: Calculated and observed crystalline parameters of sisal fiber

Curing or Exposure duration	Samples	Peak position (2θ)	FWHM* (β) (2θ)	L (nm)	%Cr_2
-	Raw fiber	16.81 22.31	4.89 3.37	1.62 2.38	41.2
5 cycles	PC	16.47 22.53	4.88 2.66	1.63 3.01	36.64
	MK10	16.59 22.48	4.28 3.19	1.85 2.51	42.12
	MK30	16.43 22.47	4.38 3.15	1.81 2.54	47.56
15 cycles	PC	16.46 22.56	4.37 2.64	1.82 3.04	39.62
	MK10	16.53 22.61	4.60 2.49	1.73 3.22	42.47
	MK30	16.21 22.63	4.04 2.53	1.97 3.17	45.28
30 cycles	PC	16.47 22.59	4.58 2.30	1.73 3.48	49.72
	MK10	16.08 22.61	4.14 2.38	1.92 3.36	50.22
	MK30	16.17 22.67	4.14 2.40	1.92 3.34	45.02

* Full width of the peak at its half maximum height.

3.10.3 Thermal gravimetric analysis

The results of a thermalgravimetric analysis (TGA and DTG) of sisal fibers are shown in Fig. 3.17. They present similar thermal degradation behaviors of raw fiber and fibers embedded in matrices of PC, MK10 and MK30 after 30 wetting and drying cycles between room temperature and 600 ℃. As analyzed in previous work (Wei and Meyer 2014), there are three main stages of weight loss: (i) slight weight loss from 50 to 110 ℃ due to evaporation of moisture in the fibers; (ii) weight loss for decomposition of hemicelluloses and the main part of lignin under temperature between 270 and 360 ℃; (iii) the maximum weight loss under higher temperature accompanying

the degradation of cellulose and the rest of lignin. The extensive range of the degradation of the lignin in two or three stages (Jakab, Faix et al. 1997, Sun, Lu et al. 2001) make the analysis more difficult. In addition, the DTG curves of selected samples show that the ranges of each stage shift for fibers with different degradation degree. For the first stage, the original sisal fiber shows a moisture content of 3.14%, which is higher than that of fibers embedded in the cementitious matrices. The reason for the high moisture content of raw sisal fiber is its water-absorption capacity in the warm and humid air (25.5 ℃, CO_2 concentration of 514 ppm and humidity of 10.5%) in this study. Although the fibers absorbed water from fresh cement paste when they were embedded into the matrix, they gradually lost water due to the high water demand of the matrix, especially the cement-MK composites. The accelerated aging ended with drying, which also accounted for the lower moisture contents of pulled out fibers than those of raw fibers. The degradation and damage of cell walls also caused a reduction of water retention. Therefore, the fibers embedded in the PC matrix encountered the most serious corrosion after accelerated aging treatment and showed a lower moisture content (0.97%) than those of fibers pulled out from MK10 (1.62%) and MK30 (1.56%). For the second stage, the raw fiber and fiber pulled out from MK10 presented evidence of independent weight loss as shown in the DTG curves. For fibers pulled out from MK30 and PC matrices, the second stage merged with the thermal decomposition peak of cellulose. For the raw fiber, in stage 2, the mass loss was 19.73%, while fiber pulled out from MK30, MK10 and PC matrices yielded a mass loss of 15.39%, 12.62%, and 8.99%, respectively. This indicates that hemicellulose and lignin of sisal fiber are sensitive to the alkalinity and CH amount of the cement matrix. These two amorphous components encountered the most serious degradation in a PC matrix, while the MK10 and MK30, with reduced alkalinity of pore solution and less portlandite in solid phase, showed slightly less corrosion of sisal fiber.

As depicted in Fig. 3.17, the raw sisal fiber and the fiber embedded in MK30 experienced pronounced degradation processes starting at around 300 ℃, while for fibers pulled out from the MK10 and PC matrices slightly less pronounced degradation processes occurred at 280 ℃ and 260 ℃, respectively. The main decomposition step occurred in the range of 260 ℃ to 490 ℃ for the raw fiber; 270 ℃ to 460 ℃ for fiber embedded in MK30; 255 ℃ to 455 ℃ and 250 ℃ to 410 ℃ for fiber embedded in MK10 and PC, respectively. In this stage the cleavage of the glycosidic linkages of cellulose reduces its polymerization degree, leading to the formation of CO_2, H_2O and a variety of hydrocarbon derivatives (Bourbigot, Chlebicki et al. 2002). The decomposition profiles indicate slight thermal stability differences for the samples. The DTG peaks were centered at 421 ℃, 411 ℃, 407 ℃ and 385 ℃ for the original fiber and fibers pulled out from the matrix of PC, MK10 and MK30, respectively, as presented in Fig. 3.17-b. As the DTG peaks shifted to lower temperatures with decreasing crystallite size, thermal stability of sisal fiber was reduced. In stage 3, the raw fiber and fibers pulled out from MK30, MK10 and PC yielded weight losses of 52.8%, 38.28%, 31.79%, and 28.75%, respectively. Compared with the effect on hemicellulose and lignin, MK's effectiveness in slowing down the degradation of cellulose in natural fiber was slightly lower. This was caused by the specific structure of sisal fibers and the complex mechanisms of degradation. Lignin and hemicellulose are more sensitive to the alkaline pore solution and are in direct contact with the hydration products of the matrix, therefore, their degradation is more impressionable than that of cellulose. The pore solution can infiltrate the cell wall of the fiber and cellulose encounters alkali hydrolysis even though the lignin and hemicellulose are only partially decomposed. In addition, the precipitation of calcium hydroxide among cellulose micro fibrils, through the gap of lignin and hemicellulose, also accelerates the embrittlement and decomposition of cellulose.

The continued loss of mass at higher temperatures is due to the thermal decomposition of residual cellulose and lignin of fiber. However, the significant differences between the raw fiber and the embedded fibers in the temperature range of 500 to 600 ℃ indicate the existence of precipitation of portlandite phase in cell walls of sisal fiber. The mass loss of raw fiber after the main decomposition step was 3.04%, while the fibers embedded in MK30, MK10 and PC matrices experienced a weight loss of 5.79%, 6.43%, and 13.94%, respectively. Assuming the weight losses for residual components of each sample are the same between 500 and 600 ℃, the extra weight loss of the embedded fiber after the main decomposition step can be considered to serve as the amount of portlandite precipitated in cell walls. The fiber embedded in the pure PC matrix yielded a portlandite amount of 10.9%. However, MK30 (2.75%) and MK10 (3.39%) indicate a considerable inhibiting effect on the mineralization of fiber. This also confirms the important roles of lignin and hemicellulose as protective barriers to the infiltration of pore solution and precipitation of portlandite in cell walls of natural fiber.

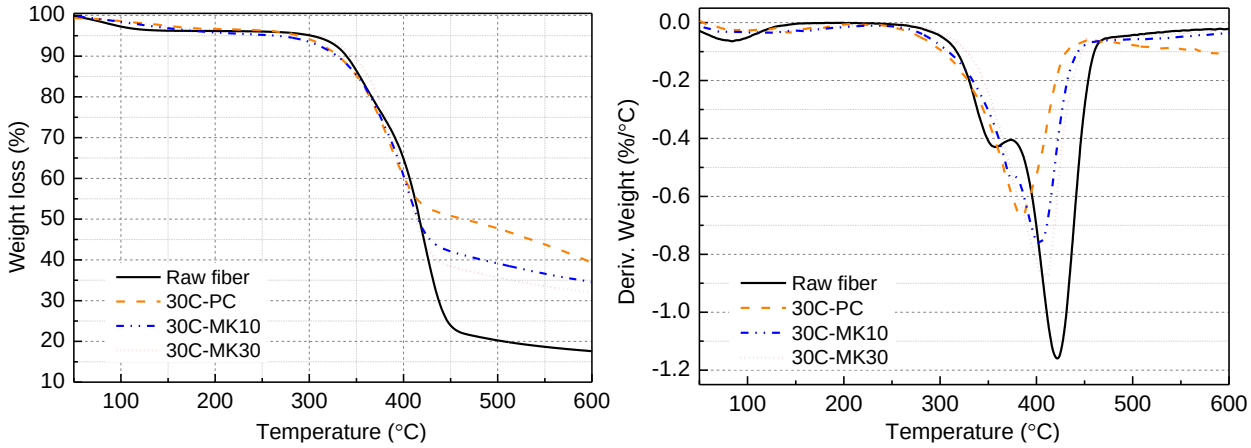

Figure 3.17: TGA and DTG curves of original sisal fiber and fibers pulled out from the matrix of PC, MK10 and MK30 after 30 wetting and drying cycles

3.10.4 Microanalysis

A microstructure analysis was carried out of the fracture surfaces of sisal fiber reinforced cement samples to investigate the effect of aggressive environments on the degradation of sisal fiber. Figs. 3.18-a and b show micrographs of sisal fiber in a cement matrix after 7 and 28 days curing, respectively, without accelerated aging. It can be seen that the sisal fiber embedded in PC, at an early age, still remained intact without indication of mineralization on the surface or defects caused by corrosion. In contrast, after 28 days of hydration, a stripping space was found around the fiber due to the autogenous shrinkage and dry shrinkage of both cement and fiber. The fiber still kept its initial appearance, except for small signs of mineralization on the fiber surface. The crack on the fiber surface and stripping of single cellulose micro-fibrils shown in Figs. 3.18-c and d, were the result of fiber degradation in PC after 15 cycles of aging. This was caused by the alkaline hydrolysis of lignin and hemicellulose due to the deposition of cement hydration products, especially calcium hydroxide, as part of the alkaline degradation process. As shown in Figs. 3.18-e, f and g, hemicelluloses and lignin were decomposed almost completely after 30 cycles in the aggressive environment. The sisal fiber's surface was fully decomposed and the lumen was saturated with the hydration products of cement. This caused the hydrolysis of cellulose through peeling-off reaction, chemical stopping reaction, physical stopping reaction, and alkaline hydrolysis consisting the degradation mechanisms. The three main components of natural fiber, lignin, hemicellulose and cellulose, were decomposed progressively from the surface to the inside. As a result, the fibers lost their reinforcement capacity in cement based materials. Fig. 3.18-h shows the sisal fiber pulled out from a MK30 sample after 30 cycles of wetting and drying, from which two remarkable observations could be made, in contrast to the neat PC sample (Fig. 3.18-g): (i) the stripping space between fiber and matrix was reduced by replacing 30 wt. % of PC by MK due to the decreased autogenous shrinkage of the cement matrix (Fig. 3.9) and less drying

shrinkage of sisal fiber in the low alkaline pore solution due to the pozzolanic reaction and dilution effect of MK; (ii) the fiber still retained its initial morphology with a good integrity, except for a slight defect on the surface, which was also due to the low alkalinity of the pore solution and low content of portlandite in the solid phase of the matrix because of the pozzolanic reaction of MK in the cement. This is also the reason for the reduction of flexural strength of sisal fiber reinforced PC and the retention of flexural behavior of MK30 specimens after accelerated aging (Fig. 3.11).

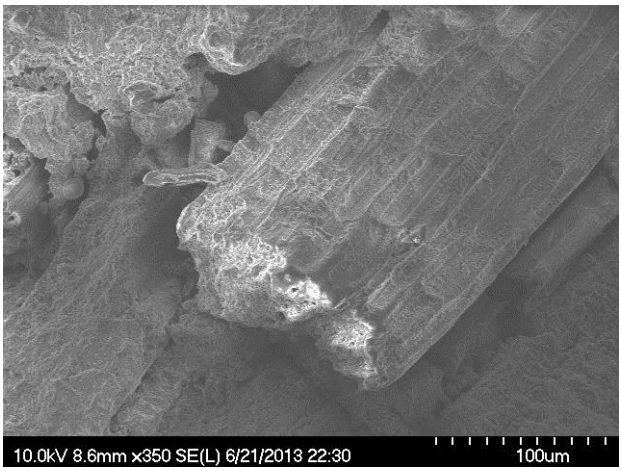

(a) 7 days

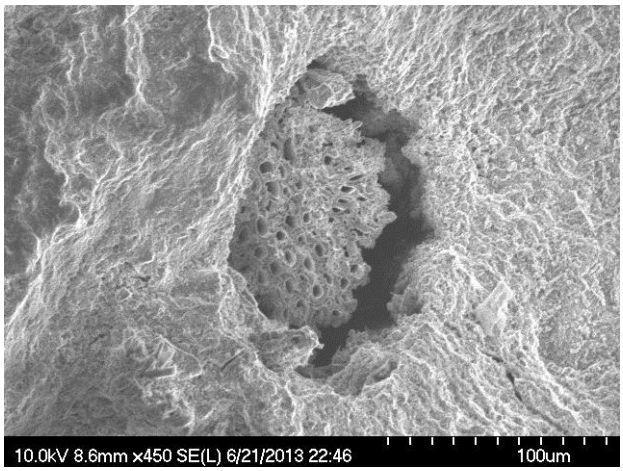

(b) 28 days

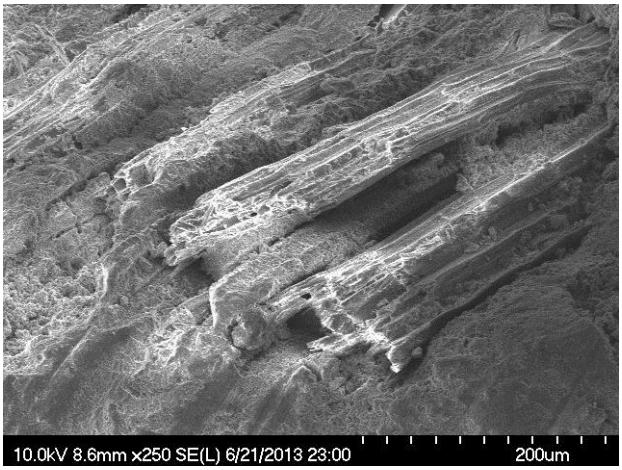

(c) PC-15c

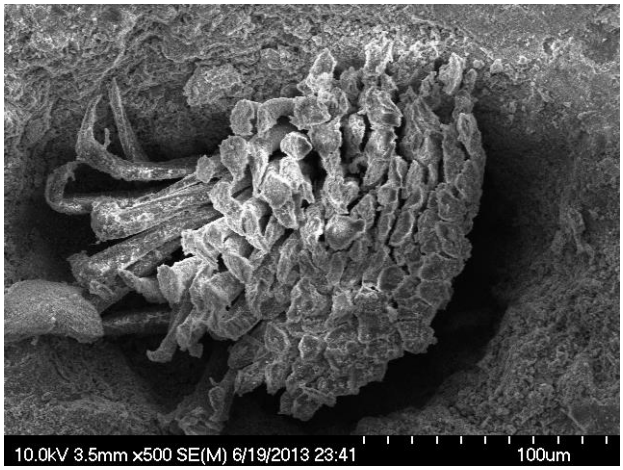

(d) PC-15c

(e) PC-30c

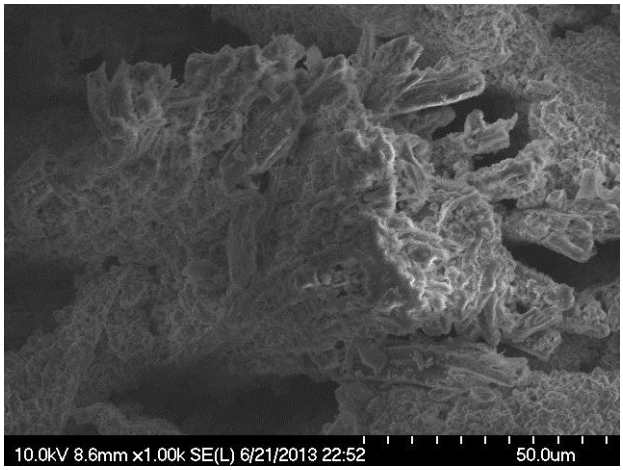

(f) PC-30c

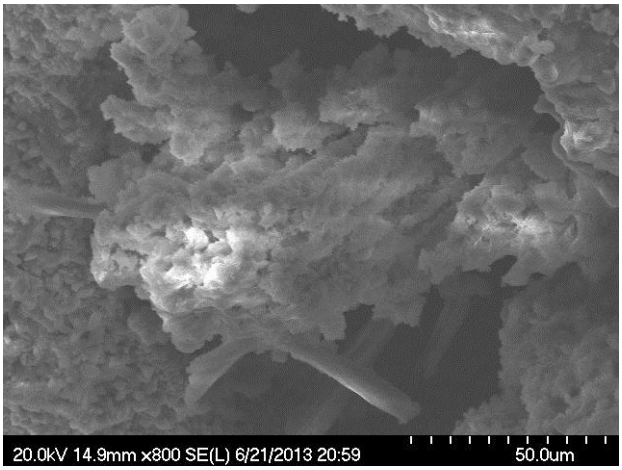

(g) PC-30c

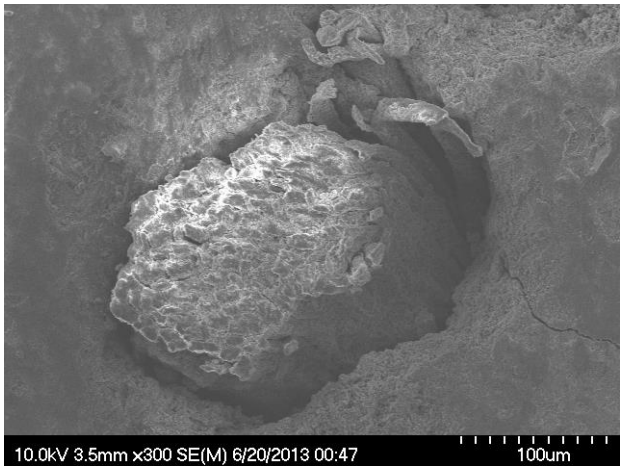

(h) MK30-30c

Figure 3.18: SEM micrographs of the fracture surface of the aged sample with sisal fiber

3.11 Degradation Mechanisms

3.11.1 Cellulose

As shown in Fig. 1.1, cellulose molecular chains are ordered into strands of approximately 40 cellulose microfibrils, which have a diameter of 35 Å, through inter- and intra-molecular hydrogen bonding(Kennedy, Phillips et al. 1985). These microfibrils are not homogeneous, consisting of crystalline and amorphous regions. As the vulnerable spots, the amorphous regions are most prone to degradation in the alkaline environment (Haas, Hrutfiord et al. 1967). Fig. 3.19

shows the microfibrillic structure of cellulose, from which it can be seen that in amorphous regions cellulose molecules have a non-reducing end and a reducing one, along with repeating glucose units. The reducing and non-reducing ends feature original C4-OH and C1-OH groups, respectively. The reducing end is a latent aldehyde, like an aldehyde function, responds to both reduction and oxidation processes and plays a key role in the alkaline degradation (Loon and Glaus 1997). Therefore, the alkali degradation of cellulose mainly depends on the reducing end in amorphous regions.

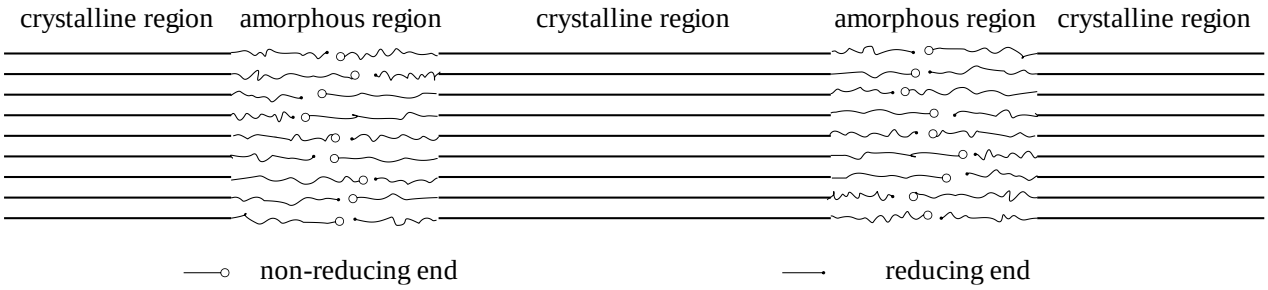

Figure 3.19: Diagrammatic sketch of microstructure of cellulose micro-fibrils

According to the analysis of previous investigators (Ziderman and Bel-Ayche 1978, Blazej, Kos ƙ et al. 1985, Ziderman and Belayche 1986, Theander and Nelson 1988, Loon and Glaus 1997) the alkali degradation of cellulose comprises four processes: peeling-off reaction, chemical stopping reaction, physical stopping reaction, and alkaline hydrolysis. Peeling-off reaction is a kind of endwise chain depolymerization which is accompanied by the release of glucose units from the cellulose molecules caused by β-elimination at the C-4 carbon atom. The main degradation products generated by peeling-off reaction is 3-deoxy-2-C-(hydro-xymethyl)-pentanoic acid (ISA) (Pavasars, Hagberg et al. 2003). If β-elimination occurs at other positions, two stopping reactions occur: chemical stopping reaction and physical stopping reaction. In the chemical one, the hexose

units remain attached to the cellulose molecules and the reducing end group is converted to an alkali stable end group (metasaccharinic acid), which terminates the depolymerization. In the physical stopping reaction, the reducing end group reaches the crystalline region of the cellulose, which is inaccessible to alkali (Haas, Hrutfiord et al. 1967). Alkaline hydrolysis is accompanied by the cleavage of glycosidic bonds in cellulose, and leads to the production of new reducing end groups, which creates favorable conditions for the above three decomposition mechanisms. In principle, this would enable complete degradation of cellulose (Pavasars, Hagberg et al. 2003). The crystalline regions of cellulose are much more stable than the amorphous region in alkali, and provide strength of cellulose fiber. Generally, the degradation of cellulose can be simply generalized as the disconnection of discrete cellulose nano-crystals caused by decomposition of reducing ends in amorphous regions.

3.11.2 Hemicellulose

Different from the highly uniform polyglucan structure of cellulose, hemicelluloses represent a type of hetero-polysaccharides with complex structures containing glucose, xylose, mannose, galactose, arabinose, fucose, glucuronic acid, and glacturonic acid in various amounts, depending on the source (Ren and Sun 2010). As shown in Fig. 1.1, hemicelluloses do not serve as load-bearing component in the cell wall of natural fiber, but they bind and fix the cellulose micro-fibrils to make the fiber more stable. Probably no chemical bonds exist between cellulose and hemicellulose, but mutual adhesion is provided by hydrogen bonds and van der Waals forces (Charles, Stephen et al. 2004). In other words, the content of holocellulose (including hemicellulose and cellulose) determines the rigidity and strength of natural fiber. Hemicelluloses are usually divided into four general groups of structurally different polysaccharide types: (1) xyloglycans (xylans); (2) manno glycans (mannans); (3) xyloglucans (XG); and (4) mixed-linkage

β-glucans (Ebringerova, Hromadkova et al. 2005). All hemicelluloses are amorphous and lack the crystalline regions that can be found in cellulose, thus making them less mechanically protected against degradation reactions during chemical pulping (Sjöström 1993). Therefore hemicellulose is much easier degraded in the alkaline environment of a cement matrix.

3.11.3 Lignin

Lignin functions as cuticle or glue in the cell wall of natural fiber giving it structure and protecting the fiber against microbial or chemical degradation of the polysaccharides. Unlike cellulose and hemicellulose, lignin is a non-carbohydrate aromatic heteropolymer or phenolic polymer that is derived from the oxidative coupling of three different phenylpropane building blocks (monolignols): p-coumaryl alcohol, coniferyl alcohol, and sinapyl alcohol (Lu and Ralph 2010, Abdel-Hamid, Solbiati et al. 2013). Lignin and hemicellulose have one characteristic in common: they are both amorphous, which means lignin is also easy to undergo the alkaline hydrolysis. The alkaline hydrolysis of α-O-4 bonds and free phenolic hydroxyls results in the formation of α-alcohols (1-guaiacylethanol, 1-guaiacylpropanol) (Erdtman 1972). The cleavage of β-0-4 ether bond is one of the most important reactions of alkaline delignification (Madzhidova, Dalimova et al. 1996). When free hydroxyls are present on neighboring α- or γ-carbon atoms or if there is a CO group in the α-position, structural units of lignin of the nonphenolic β-ether type are capable of undergoing alkaline hydrolysis, and lead to the formation of guaiacol, guaiacylpropane, 3-guaiacylpropanol, and p-hydroxyphenylpropane (Adler 1964, Gierer 1964). The alkaline degradation products of lignin, which have been investigated in several publications, are mainly protocatechuic acid, vanillic acid catechol, oxalic, and other simple aliphatic acids (Phillips 1934), as well as a dark, amorphous, humin-like “lignic acid” which is the cause of the darkening effect of alkaline treated sisal fiber, especially under high temperature.

Fig. 3.20 is a diagrammatic sketch showing the alkaline degradation of natural fiber in a cement matrix, due to the high alkalinity of cement solid phase and pore solution. There are four steps: (i) Degradation of lignin and part of hemicellulose, which leads to the exposure of holocellulose in the pore solution and solid phase of the matrix; (ii) In this step, degradation occurs mainly on hemicellulose, which causes the decrease of integrity and stability of the cell wall of natural fiber; (iii) After the degradation of lignin, hemicellulose and intra-molecular hydrogen bonding, there remains no binding for cellulose micro-fibrils, and as a result cellulose fibers disperse in the pore solution of the matrix, which in turn, accelerates the degradation of cellulose; (iv) The last step is the failure of cellulose micro-fibrils, which is caused by alkaline hydrolysis of amorphous regions containing non-reducing end, as shown in Fig. 3.19, and leads to the complete degradation of natural fiber. As the degradation proceeds, the hydration products, such as soluble C-S-H and portlandite, gradually infiltrate into the cell wall, which in turn leads to mineralization and embrittlement of the natural fiber.

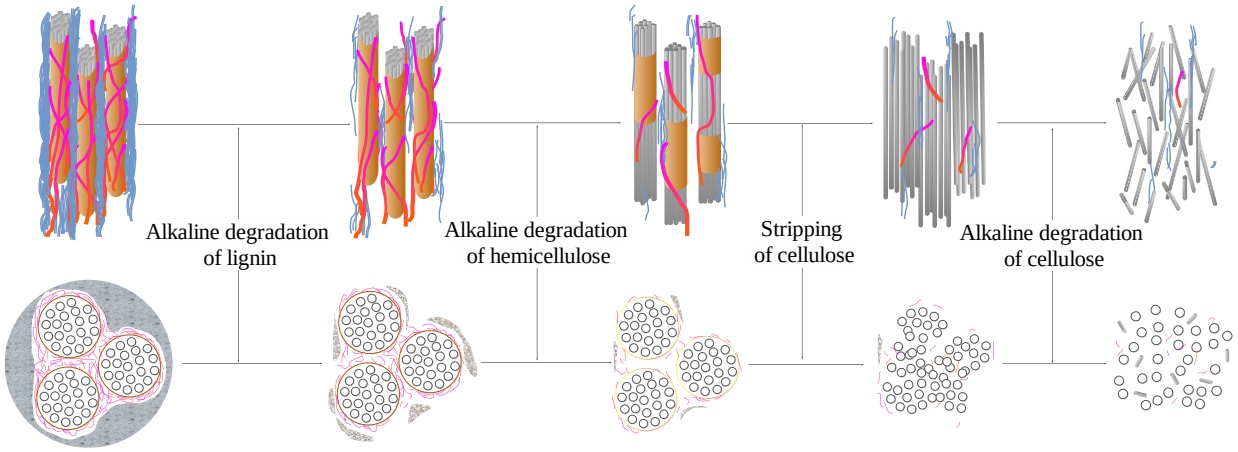

Figure 3.20: Diagrammatic sketch of natural fiber's alkaline degradation process

3.11.4 Mineralization

Except for the alkali hydrolysis of the three main components, cell wall mineralization is also an important degradation mechanism which leads to the fiber embrittlement and the reduction of strength and strain capacity. Caused by the migration of hydration products to lumens and to the middle lamella, and volume variation in these fibers due to their high water absorption, fiber mineralization is sensitive to the CH amount of the matrix (Toledo Filho, Silva et al. 2009). In contrast to the reviews presented in articles (Tolêdo Filho, Scrivener et al. 2000, Mohr, Nanko et al. 2005, Toledo Filho, Silva et al. 2009), two mineralization mechanisms are proposed in this study: CH-mineralization and self-mineralization. Caused by the migration of hydration products (calcium hydroxide) to lumens and to the middle lamella, and volume variation, CH-mineralization indicates that the CH content of the matrix and Ca^{2+} concentration in the pore solution contribute to the degradation of natural fiber. However, self-mineralization demonstrates the hydrolysis rate of amorphous components (lignin and hemicellulose), therefore the contribution of alkalinity of the matrix to the fiber degradation can be determined. It is well known that the precipitation of hydration products, likely calcium hydroxide, within the fiber cell wall structure is the main reason for cell wall mineralization (Mohr, Nanko et al. 2005). As shown in Fig. 3.13, sisal fibers suffered brittle fracture without any plastic deformation, therefore, it is logical to characterize the deformability of sisal fiber using the tensile modulus. Combining the results of TGA and tensile test of the embedded sisal fibers, Fig. 3.21-a shows the effect of precipitated CH amount on Young's modulus of fiber. It can be seen that the precipitation of CH in the cell wall significantly reduces the deformability of sisal fiber. The crystallization of CH through nucleation and growth processes in the cell wall not only seriously damage the bonding between the various components but also corrode cellulose micro-fibrils, thereby the strength was significantly reduced. Unlike CH-mineralization, slight hydrolysis of lignin and hemicellulose has no effect on Young's modulus of

sisal fiber. However, when Cr.I exceeds 0.80, the deformability of the fiber is reduced, which is evidenced by the increased Young's modulus as shown in Fig. 3.21-b. This indicates that Young's modulus of natural fiber mainly depends on the cellulose, which is the primary structural component of cell walls. However, lignin within the fiber cell wall acts as a barrier to pore solution ingress/egress and by its very presence prevents precipitation of mineral phases within the fiber cell wall, thereby minimizing fiber mineralization (Mohr, Biernacki et al. 2006). In order to restrain the degradation of natural fiber in the cement matrix, both amorphous components (lignin and hemicellulose) and cellulose should be protected by reducing the OH- concentration of pore solution in the matrix.

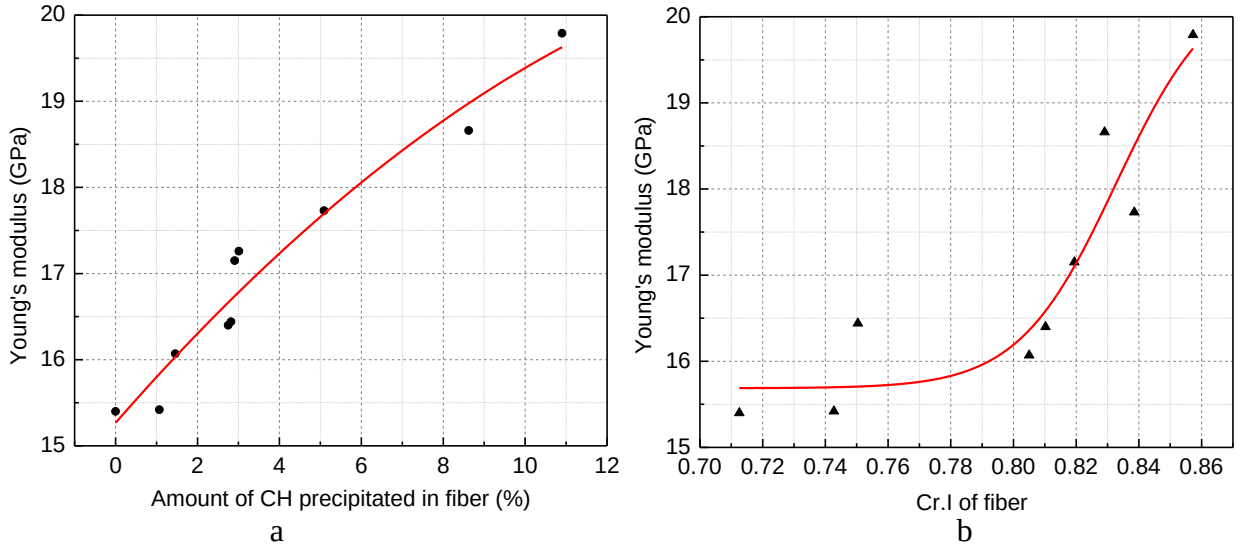

Figure 3.21: Effect of CH precipitation (a) and Cr.I (b) on Young's modulus of sisal fiber

3.12 Degradation Kinetics

The degradation kinetics of natural vegetable organics, especially cellulose, in an alkaline medium have been studied by several investigators. Due to the interaction effect between degradation processes in alkaline degradation, alkaline hydrolysis of cellulose cannot be studied

separately from the peeling off reaction because the hydrolysis products new reducing end groups, which initiate a peeling off reaction (Van Loon and Glaus 1998). Franzon et al. (1957) studied the alkaline degradation of cellulose under different temperatures and presented that the degraded fraction of cellulose can be described by a logarithmic relationship with the number of glucose units and reaction duration. Lai and Sarkanen (1967) arrived at a similar conclusion with the following equation:

$$\ln(Cel) = -k \cdot \beta \cdot t \tag{3.11}$$

where Cel is the fraction of cellulose left, k is the pseudo-first-order reaction rate constant, β the average number of glucose units peeled off, and t is the reaction time.

According to Franzon at al. (1957), $K \cdot \beta$ has a value of 3.6×10^{-10} h^{-1} in 1.25 M/L OH- with a constant number of glucose units peeled off for each break ($\beta = 65$). According to the linear dependence of $k \cdot \beta$ on the concentration of OH^- for $0 < [OH^-] < 2$ M/L proposed by Lai and Sarkanen (1967):

$$K_{1.25} \cdot \beta / 1.25 = k_{C[OH^-]} \cdot \beta / C[OH^-] \tag{3.12}$$

$k \cdot \beta$ under a certain OH^- can be calculated as follows:

$$k_{C[OH^-]} \cdot \beta = K_{1.25} \cdot \beta \cdot C[OH^-] / 1.25 = 2.88 \times10^{-10} \cdot C[OH^-] \tag{3.13}$$

where $C[OH^-]$ is the concentration of OH^-.

In the peeling off reaction, the reducing end group is split off from the cellulose chain, resulting in the formation of an intermediate product G_e, which reacts further to give the ultimate degradation products, such as isosaccharinic acid, lactic acid, formic acid, and acetic acid (Whistler and BeMiller 1958, Machell and Richards 1960, Lai 1991). At a constant OH- concentration, when

t = 0, the mole fraction of glucose units is eliminated, and G_e can be calculated as follows (Loon and Glaus 1997):

$$G_e = G_{r0} \cdot (k / k_t) \cdot (1-e^{-k_t \cdot t}) \quad (3.14)$$

where, G_{r0} is the initial reducing end group content at t = 0, k_t is the total rate constant for chain termination (k_t = k' + k_{cr}, where k_{cr} is the formal rate constant of termination caused by inaccessibility and k' is the pseudo first order reaction rate constant for the chemical stopping reaction.)

As shown in Fig. 3.8, OH^- concentrations of pore solutions for PC and MK30 follow a nonlinear relationship with the hydration time of cement:

$$C[OH^-]_{PC}\ (mMol/L) = 561.55 - 437.05 / (1+ t^{1.8} / 473.08) \quad (3.15)$$

$$C[OH^-]_{MK30}\ (mMol/L) = 54.69 + 36.73 / (0.873 + t^{1.168}) \quad (3.16)$$

Substitution of Eqs. (3.15) and (3.16) in Eq. (3.13) gives:

$$k_{PC} \cdot \beta = 2.88 \times 10^{-7} \cdot [561.55 - 206759.6 / (473.08 + t^{1.8})] \quad (3.17)$$

$$k_{MK30} \cdot \beta = 2.88 \times 10^{-7} \cdot [54.69 + 36.73 / (0.873 + t^{1.168})] \quad (3.18)$$

Substitution of Eqs. (3.17) and (3.18) in Eq. (3.11) gives:

$$\ln (Cel_{PC}) = - 2.88 \times 10^{-7} \cdot [561.55 - 206759.6 / (473.08 + t^{1.8})] \cdot t \quad (3.19)$$

$$\ln (Cel_{MK30}) = - 2.88 \times 10^{-7} \cdot [54.69 + 36.73 / (0.873 + t^{1.168})] \cdot t \quad (3.20)$$

As analyzed in the degradation mechanisms section (section 3.11), the alkali degradation of cellulose comprises peeling-off reaction and alkaline hydrolysis, therefore, the overall degradation of cellulose can be expressed by combining Eq. (3.11) and (3.14) (Loon and Glaus 1997):

$$Y = (1 - G_e) \times Cel \quad (3.21)$$

where Y is the fraction of remaining cellulose.

Substitutions of Eqs. (3.14) and (3.19) in Eq. (3.21) give the cellulose left of fiber embedded in the PC matrix:

$$Y_{PC} = \{1 - G_{r0} \bullet (k_1 / k_t) \bullet [1\text{-}\exp(-k_t \bullet t)]\} / \exp\{ 2.88 \times 10^{-7} \bullet [561.55 - 206759.6 / (473.08 + t^{1.8})] \bullet t \} \quad (3.22)$$

Substitution of Eqs. (3.14) and (3.20) in Eq. (3.21) gives the cellulose left of fiber embedded in the matrix of MK30:

$$Y_{MK30} = \{1 - G_{r0} \bullet (k_1 / k_t) \bullet [1\text{-}\exp(-k_t \bullet t)]\} / \exp\{ 2.88 \times 10^{-7} \bullet [54.69 + 36.73 / (0.873 + t^{1.168})] \bullet t \} \quad (3.23)$$

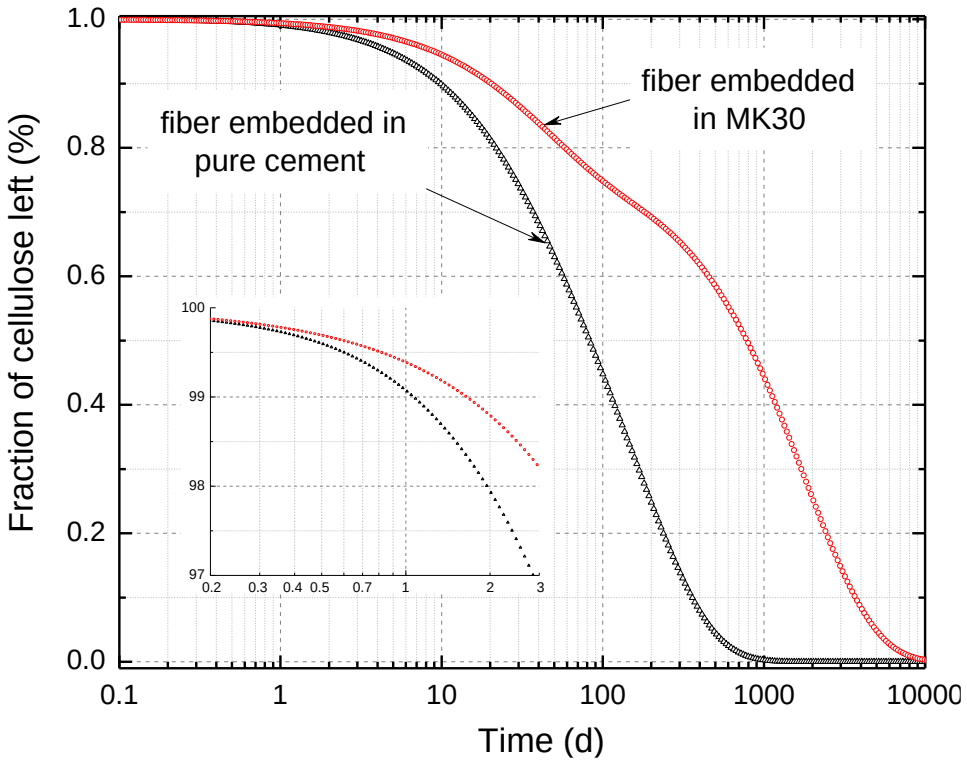

Figure 3.22: Degradation of cellulose in sisal fiber at 25 ºC in the matrix of pure PC and MK30

The initial reducing end group mole fraction $(G_r)_0$ is defined as the initial number of end groups in the cellulose divided by the initial number of all glucose units (Ziderman and Bel-Ayche 1978). Donald and Bjorn (Haas, Hrutfiord et al. 1967) reported the mole fraction $(G_r)_0$ to be 6.25 $\times 10^{-3}$ for hydrocellulose I and 2.98 $\times 10^{-3}$ for hydrocellulose II which are the reciprocals of the initial number-average degree of polymerization as determined by viscosity. Here, an initial reducing end group mole fraction of 0.004 (which means, on average, there is one reducing glucose end group per 250 glucose units), was selected as calculated in Aldrich cellulose macromolecule (Pavasars, Hagberg et al. 2003). Fig. 3.22 shows the overall degradation of cellulose as a function of time in the matrix of pure Portland cement and MK30 under 25 ℃ (with an assumption of k_1 = 0.04 and k_t = 0.0007). It can be seen that cellulose encounters more severe degradation in PC than if embedded in the matrix of MK30 from the beginning. The difference becomes apparent after the first day. Because of the rapid rise of OH^- concentration in the pore solution, cellulose of the fiber embedded in PC experiences a sharp linear decrease after 10 days and completely deteriorates after around 2 years of exposure. In contrast, two shoulders are found on the curve of cellulose in MK30, which means that the cellulose experiences four steps of degradation: primary stage, initial acceleration stage, decelerating stage, and final acceleration stage. In the primary stage (within the first day), only 0.62% of cellulose is decomposed due to the low initial reducing end group mole fraction and slow peeling-off reaction. After the first day of immersion, the degradation of cellulose shows a slight acceleration until 60 days. In this stage, the peeling-off reaction, the rate of which is 10^8 times faster than that of alkaline hydrolysis (Van Loon and Glaus 1998), dominates the degradation rate. Between 60 days and 110 days of immersion, the degradation rate of cellulose decelerates as a result of the peeling reaction being inhibited by a combination of physical and chemical stopping reactions. These are caused by the crystalline regions and the formation of

metasaccharinic acids (Humphreys, Laws et al. 2010). This removes the reducing end groups and blocks subsequent peeling of the chain. The alkali hydrolysis of mid-chain scission of amorphous portions of the cellulose leads to a release of new end groups, which in turn promotes the alkali hydrolysis of cellulose. As a result, cellulose encounters a second accelerated degradation stage until the complete deterioration after 27.4 years of corrosion. The slow degradation rate in each phase, especially at the end of the decelerating stage and, owing to the 30wt.% replacement of Portland cement by MK, significantly slows down the deterioration of cellulose of sisal fiber in the cement matrix. After 80 days of embedment, the sisal fiber in the PC matrix loses half of its cellulose, while in the matrix of MK30, only 23% cellulose is decomposed. The time needed to completely degrade the cellulose in MK30 is 13 times longer than that in the matrix of pure cement, which can also account for the better tensile strength of pull-out sisal fiber from MK30 (Table 3.4) and the considerable durability of sisal fiber reinforced MK30 samples, as shown in Fig. 3.11.

3.13 Summary

The presented work analyzed the degradation kinetics and mechanisms of sisal fiber in cement matrices. The cement hydration was proposed to be a crucial cause of deterioration of natural fiber in the alkaline and mineral-rich environment of cement. Investigated were the effects of the replacement of 10 wt.% and 30 wt.% of PC by metakaolin ultra-fine powder on the hydration kinetics; the chemistry of hydrate phases and pore solution; the shrinkage and microstructure of blended cement; the degradation rate of sisal fiber in cement matrices; and the durability of sisal fiber reinforced cement based composites. The comprehensive investigation of the solid and liquid phases during the hydration of pure cement and the two blended cements with different amounts of metakaolin, as well as the separate study of the component changes, mechanical properties and physical characterization of sisal fiber pull-out from the matrix after accelerated aging, allows the

qualitative description of the degradation mechanisms of natural reinforcement in cement based materials. Specifically, the following observations were made.

(1) From the heat evolution data it can be seen that the heat flows of neat PC and PC-MK develop similarly during the pre-induction and induction periods. The main differences occur during the acceleration, deceleration and diffusion periods. Compared with silicate reactions, the effects of MK on the aluminate reactions of cement are much more significant. The second peak of the heat release curve occurs much earlier and becomes narrower and higher. Although improvements in both silicate and aluminate reactions cause a faster hydration heat release at early ages, the total released heat was reduced by blending PC with MK.

(2) The results of XRD and TGA investigations indicate that, due to the pozzolanic reaction, substitution of MK resulted in a significant reduction of CH, ettringite and bound water of the matrix. With the 10 wt. % and 30 wt. % replacement of PC by MK, CH was reduced by 24.49% and 50.29% after 28 days, and by 33.79% and 61.90% after 90 days, respectively. The calculated Ca/Si and Al/Si ratios of C-S-H in PC after 300 days and 600 days were 1.85 ± 0.3 and 0.07, respectively, with a mean value for Ca/(Si+Al) of 1.73. The EDX investigation at 28 days and 300 days showed that the addition of 30 wt. % MK significantly increased the Al/Ca of C-S-H phase, due to the high content of SiO_2 and Al_2O_3 in MK. However, the Ca/Si and Ca/(Si+Al) ratios of C-S-H phase were reduced by 7.57% and 36.24%, respectively.

(3) By blending 30wt.% MK, element concentrations of Si were increased, however the concentrations of K, Na, Ca, Si and OH^- of the pore solution in the matrix were significantly reduced. The ESI results indicate that the pore solution of neat PC was supersaturated for portlandite during the entire hydration time, while the pore solution of MK30 was

undersaturated for CH, therefore both the alkalinity and mineral environment of the cement matrix were effectively relieved.

(4) The autogenous shrinkage of PC was as high as 1.67 mm/m, while the values for MK10 and MK-30 blends were 1.13 mm/m and 0.65 mm/m, respectively. This means the substitution of 10 wt. % and 30 wt. % MK resulted in reductions of autogenous shrinkage by 21.56% and 61.08%, after four months, respectively. After 7 days, MK30 gave the highest compressive strength, and after 28 days, the strength of blends reached 117.08% of the neat PC, while the replacement of 10 wt. % of PC by MK resulted in 5.89% higher compressive strength values compared to neat PC. With hydration of cement, the pozzolanic reactions become predominant compared to the dilution effect, therefore the compressive strength was increased substantially.

(5) The chemical composition of sisal fiber is made up of pectin (1.3%), extractive (2.4%), lignin (12.3%), hemicellulose (13.7%), and cellulose (68.2%), among which cellulose is the main structural component in cell walls. Compared to fibers that were soaked in tap water, the water absorption ratio of fibers immersed in $Ca(OH)_2$ solution was 5.07% higher, and the moisture absorption capacity of fibers increased with increasing temperature.

(6) The durability of sisal fiber reinforced cement based composites was assessed by the flexural behavior of samples subjected to wetting and drying cycles. After 30 cycles, the substitution of 30 wt. % MK improved the durability of sisal fiber reinforced cement mortar by 81.15%, 82.60%, 83.58%, 76.13%, 74.79%, and 77.39%, as measured by post crack strength, flexural toughness, I_{55}, $T_{JCI\text{-}10}$ ($F_{JCI\text{-}10}$), T_{max} and $T_{0.5}$, respectively. Therefore, controlling the pH value of the pore solution and the CH content at a relatively low level by using pozzolanic supplementary material is an effective way to arrest the degradation of natural fiber.

(7) The degradation of sisal fiber was also studied separately by tensile behavior testing, crystallinity characterization, and components analysis. Compared with raw fiber, the tensile strength of fiber embedded in PC decreased by 86.17%, after 30 wetting and drying cycles. However, in MK10 and MK30 blends, the fiber's strength decreased by only 65.67% and 19.37%, respectively. Due to the decomposition of the amorphous phases (lignin and hemicellulose) of sisal fiber, the crystallinity of fibers increased after embedment. After 30 wetting and drying cycles, the crystallinity index and crystallinity percentage of fiber embedded in neat PC were 20.31 and 12.97% higher than those of raw fiber, respectively. However, the crystallinity index of the fiber embedded in MK30 showed only an increase of 13.7%. Compared to fibers embedded in PC, sisal fiber in MK30 showed much higher amounts of lignin, hemicellulose and cellulose. The precipitation of portlandite in cell walls of natural fiber was also effectively restrained, due to the protective barriers role of lignin and hemicellulose. The microstructure analysis of the fracture surface of sisal fiber reinforced cement after wetting and drying cycles also verified the better fiber integrity in MK30, compared with that in PC.

(8) The alkali degradation of cellulose mainly depends on the reducing ends in amorphous regions and can be simply generalized as the disconnection of discrete cellulose nano-crystals caused by decomposition of reducing end through four processes: peeling-off reaction, chemical stopping reaction, physical stopping reaction, and alkaline hydrolysis. Lignin and hemicellulose are amorphous and easily undergo the alkaline hydrolysis. Four interactional alternate steps were summarized: (i) Degradation of lignin and part of hemicellulose leading to the exposure of holocellulose; (ii) degradation of hemicellulose causing the decrease of integrity and stability of cell walls; (iii) degradation of intra-molecular hydrogen bonding

leading to the dispersion of cellulose microfibrils; (iv) alkaline hydrolysis of amorphous regions containing non-reducing ends, and as a result, complete degradation of cellulose micro-fibrils. As the degradation proceeded, the hydration products, such as soluble C-S-H and portlandite, gradually infiltrated into the cell wall, which in turn led to mineralization and embrittlement of natural fiber.

(9) Cell wall mineralization was found to be an important degradation mechanism which leads to the fiber embrittlement and the reduction of strength and strain capacity. In contrast to the reviews presented in the literature, two mineralization mechanisms are proposed in this study: CH-mineralization and self-mineralization. The crystallization of CH through nucleation and growth processes in cell walls not only seriously damage the bonding between the various components but also corrode cellulose micro-fibrils, which leads to increased brittleness and reduction of strength. The self-mineralization indicates that the slight hydrolysis of lignin and hemicellulose has no significant effect on Young's modulus of sisal fiber, however, when Cr.I exceeds 0.80, the deformability of fiber is reduced considerably. This demonstrates the barrier role played by lignin and hemicellulose by preventing cell walls from precipitation of mineral phases.

(10) Based on the data for OH^- concentrations of pore solutions for PC and MK30 as functions of hydration time, the overall degradation of cellulose in PC and MK matrices was estimated by involving two processes: peeling-off reaction and alkaline hydrolysis. Cellulose of the fiber embedded in PC showed a linear decrease after 10 days until complete deterioration at about 2 years of embedment. Four steps of fiber degradation were found in the curve of cellulose degradation embedded in the MK30 matrix: primary stage, initial acceleration stage, deceleration stage, and final acceleration stage. The low degradation rates, especially the

existence of the deceleration stage, indicate that the 30wt.% replacement of Portland cement by MK significantly slows down the deterioration of cellulose of sisal fiber. The time needed to completely degrade the cellulose in MK30 is 13 times longer than that in the matrix of pure cement.

The results demonstrate that natural fibers undergo serious degradation in the cement matrix due to the mineralization of cell wall, peeling-off reaction and alkaline hydrolysis of amorphous components (lignin, hemicellulose) of fiber and the amorphous regions of cellulose. The blending of metakaolin significantly restrains this degradation by reducing both mineralization and the alkaline hydrolysis reactions. The degradation model indicates the effect of alkalinity of cement pore solution on the decomposition of cellulose and can be used to predict the failure of natural fiber. Because of the uncertainties of the kinetics data and the lack of parameterization of mineralization, further investigation of the natural fiber degradation in cement matrices is necessary. The effects of temperature, concentration of Ca^{2+}, water/cement ratio, as well as different aggressive aging conditions on mineralization, peeling-off reaction, and alkaline hydrolysis of lignin and hemicellulose, especially the cellulose, need to be studied in more detail.

CHAPTER 4: DETERMINATION OF ACCELERATED AGING CONDITIONS FOR SISAL FIBER-REINFORCED CEMENT COMPOSITES (SFRCC)

4.1 Introduction

In spite of much research on the mechanical characteristics of sisal fiber as reinforcement of cement based composites, their durability under different aging conditions (Table 4.1), and treatment methods to improve their durability, it is still unknown how various influence factors contribute to the deterioration of sisal fiber and what are the most effective accelerated aging conditions to evaluate their durability in a relatively short period of time. Essentially, to characterize the degradation of sisal fiber in a cement matrix and to determine the most effective accelerated aging conditions, four main aspects should be studied and compared: (i) knowledge of the mechanical properties of pure cement paste subjected to accelerated aging conditions (ii) knowledge of the mechanical properties of FRCC subject to accelerated aging conditions, (iii) interfacial behavior between fiber and the cement matrix, (iv) tensile strength loss of strands of sisal fiber in cement subjected to the same aggressive environments.

According to the summary of the accelerated curing methods of SFRCC in Table 4.1, the effect of temperature and humidity of the aggressive environment have not yet been considered. In the present study, SFRCC and sisal fiber strands-cement specimens were subjected to seven different accelerated curing conditions, the details and designations of which are presented in Table 4.2.

Table 4.1: Overview of durability investigations of sisal fiber and sisal fiber-cement composites

Study object	Composite	Treatment medium*					Aging conditions**	Reference
		1	2	3	4	5		
sisal fiber	-	●	●	●	●		RT	(Toledo Filho, Scrivener et al. 2000) (Ramakrishna and Sundararajan 2005)
		●	●	●			W&D	(Ramakrishna and Sundararajan 2005)
sisal-cement composites	CH free paste	●					W&D	(Toledo Filho, Silva et al. 2009)
		●					HT	(Soroushian, Won et al. 2012)
		●					W&D	(Soroushian, Won et al. 2012)
		●					F&T	(Soroushian, Won et al. 2012)
		●					WDC	(Soroushian, Won et al. 2012)
	mortar	●		●			RT	(Toledo Filho, Scrivener et al. 2000, Toledo Filho, Ghavami et al. 2003, G. Ramakrishna 2010)
		●					W&D	(Berhane Z 1987, Gram HE 1987, Toledo Filho, Scrivener et al. 2000, Toledo Filho, Silva et al. 2009)
						●	AH	(Toledo Filho, Scrivener et al. 2000, Toledo Filho, Ghavami et al. 2003)
	concrete	●					RT	(Gram 1983)
		●					HT	(Bergström and Gram 1984)
		●					W&D	(Gram 1983, Bergström and Gram 1984)
						●	AH	(Gram 1983)

* 1-Tap water; 2-Solution of calcium hydroxide; 3-solution of sodium hydroxide; 4-Cement saturated water; 5-Ambient humidity.

** RT-Room Temperature; HT-High Temperature; W&D-wetting and drying cycles; F&T-freezing–thawing cycles; WDC-repeated wetting–drying-carbonation, AH-ambient humidity.

Here we report on the durability of sisal fiber-reinforced cement mortar and paste, and sisal fiber strands embedded in a cement matrix subjected to seven exposure conditions. The degradation of sisal fiber was characterized by tensile strength loss when subjected to aging and component analysis through thermo gravimetric analysis (TGA), crystallinity through X-ray diffraction (XRD), and microanalysis through scanning electron microscopy (SEM).

Table 4.2: Aggressive conditions of sisal fiber and the composites

Aggressive conditions	Classification	Temperature (℃)	
D50	Hot-dry	50	
D70		70	
D90		90	
S50	Hot- soak	50	
S70		70	
S90		90	
W&D	Wetting and drying cycles	wet	dry
		70	70

4.2 Durability of Long Sisal Fiber-Reinforced Mortar (LSFM)

It is well known that the most important contribution of fiber-reinforcement in cement composites is not to strength but to the flexural toughness. In order to analyze the degradation of fiber in a cement matrix and the durability of fiber reinforced cement mortar, the flexural behavior was investigated according to ASTM C1185 - 08(2012), ASTM C-1018 and JCI SF4. Before reaching the peak load, the formation of micro cracks, which are arrested by the bridging action of fibers, is the main mechanism that works until the density of microcracks reaches a saturation level when the composite is no longer able to withstand additional tension (Karihaloo and Wang 2000). Fig. 4.1 shows the typical load-deflection curves of sisal fiber-reinforced mortar subjected to wetting and drying cycles.

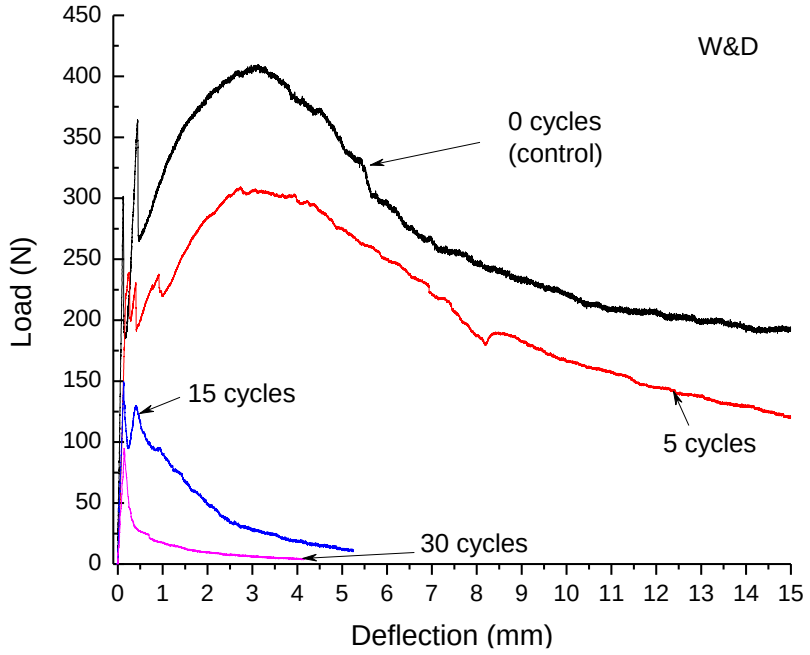

Figure 4.1: Typical load-deflection curves for LSFM subjected to cycles of wetting and drying

Quantitative values for the flexural parameters are shown in Table 4.3. The post-cracking strength σ_p gradually decreases with increasing aging duration. For both hot-dry and hot-soak aggressive conditions, the strength loss rate increases with increasing temperature. Therefore, sisal fiber encounters a more severe alkali attack in a cement matrix at higher temperatures. Among the hot-dry treated specimens, the samples treated in D90 yielded the minimum flexural strength σ_p for each aging duration. After 100 days, D90 beams showed a post-cracking strength of 1.95 MPa, which is 10.14%, 51.13%, and 77.14% lower than those of aged specimens treated by D70, D50, and that of unaged beams without aging treatment, respectively. A similar trend was also detected in hot-soak treated samples. Compared with the control samples, the sisal fiber-reinforced cement mortar encountered a strength loss of 86.05%, after being treated in S90 for 100 days. Compared with flexural strength loss, a more noticeable influence of temperature on degradation of sisal fiber is detected from the toughness loss of the beams. After 100 days, samples treated in D90, D70,

and D50 yielded 89.23%, 71.03%, and 52.31% lower post-cracking toughness T_p, respectively, than that of the control group. For hot-soak aggressive treatment, S90 showed the worst ultimate toughness, which was 39.59%, 66.19%, and 86.05% lower than those of S70, S50, and the control group, respectively. For JCI-toughness and deflection index $P_{0.5}$, the samples treated in D90 and S90 also gave the lowest value for each aging duration.

The results indicate that temperature is the main factor influencing both the deterioration of sisal fiber in a cement matrix and degradation of SFRCC. And the accelerated aging conditions should be defined with a temperature of 70 ℃ or higher.

The differences of flexural properties between hot-dry and hot-soak treatment indicate the effect of humidity on the degradation rate of SFRCC. It can be seen that at each temperature the soaked samples yielded lower flexural strength and toughness than those exposed to dry aggressive conditions. The samples treated in both D90 and S90 show considerable degradation after 100 days. The flexural strength, post-cracking toughness, $P_{0.5}$ and JCI toughness of S90 treated beams are 38.97%, 76.19%, 59.59% and 86.67% lower, respectively, than D90 treated specimens. In addition, S70 has a similar effect on flexural properties compared with D90 treated beams. Although temperature is the main factor determining the degradation rate of sisal fiber in a cement matrix, the humidity has an enhancing accelerated impact. By comparison, it appears that the most effective statical aggressive condition is the soak treatment at a temperature higher than 70 ℃.

For the samples exposed to wetting and drying cycles, the change of humidity has a significant effect on accelerating the degradation rate of the sisal fiber. A duration of 42 h per cycle was determined according to the mass change: 15 h immersion in tap water at 70 ℃, followed by 25 h drying in an oven under 70 ℃, between which there were twice 1 h periods of air drying under 23 ℃ with 10% humidity. Among the aged samples, the W&D treated samples encountered

the sharpest drop in flexural strength and toughness. After 30 wetting and drying cycles, the post-cracking strength and toughness of the beams declined by 86.52% and 99.08%, respectively, which are 3.36% and 64.0% lower than those of S90. It's notable that the time for 30 W&D cycles is 52.5 days, which is almost half of the final duration of hot-dry and hot-soak treatment.

Table 4.3: Durability of LSFM determined by four-point flexural indices

Aggressive condition	Temperature ℃	Duration /Number of cycles	σ_p (MPa)	T_p (N-m)	T_{JCI} (N-m)	$P_{0.5}$
Control	23±2	0	8.53	3.90	3.10	82.02
D50	50	10d	8.37	3.61	2.96	76.34
		30d	6.29	3.05	2.13	55.07
		60d	4.61	2.37	1.77	34.12
		100d	3.99	1.86	1.09	20.22
D70	70	10d	6.73	3.29	2.52	62.30
		30d	4.34	2.43	1.89	42.44
		60d	3.22	1.97	1.36	27.92
		100d	2.17	1.13	0.75	19.63
D90	90	10d	4.59	2.81	2.14	52.25
		30d	3.13	1.23	1.41	32.10
		60d	2.64	0.77	0.92	18.62
		100d	1.95	0.42	0.45	10.12
S50	50	10d	8.19	3.47	2.82	62.33
		30d	6.07	2.89	2.06	47.53
		60d	4.24	2.09	1.43	28.62
		100d	3.52	1.53	0.87	17.13
S70	70	10d	6.53	2.95	2.19	49.66
		30d	4.12	2.26	1.52	31.15
		60d	3.04	1.76	1.02	19.06
		100d	1.97	0.95	0.57	10.05
S90	90	10d	3.76	2.51	2.01	44.23
		30d	2.86	1.08	1.16	23.29
		60d	1.95	0.53	0.43	11.76
		100d	1.19	0.10	0.06	4.09
W&D	70	5c	6.42	2.66	2.20	47.49
		15c	2.70	0.20	0.19	12.40
		30c	1.15	0.036	0.035	3.26

From the comparison of strength and toughness between the initial and aged samples, it can be concluded that the most effective approaches for accelerating the degradation of natural fiber in cement composites is to soak the samples at a temperature higher than 70 ℃ and the W&D treatment.

4.3 Durability of Short Sisal Fiber-Reinforced Cement Paste (SCP)

Fig. 4.2 illustrates typical three-point load-deflection curves of selected sisal fiber-reinforced cement pastes subjected to the seven aggressive conditions of various durations. Overall, similar as the LSFM, the bending strength and toughness of SCP also decrease with aging. Two more notable observations can be made from the load-deflection curves: the increasing flexural modulus and the loss of post-cracking behavior of samples treated in hot-soak and W&D. Natural fiber's embrittlement due to fiber cell wall mineralization in a cement matrix (Mohr, Nanko et al. 2005), not only leads to the decline of its reinforcing effect but also causes the increase of the flexural modulus of the cement matrix. Compared with LSFM, due to the fiber length and arrangement, the post-cracking behavior of SCP is unremarkable. However, the slight load increase or strength reserve after cracking still indicate some ductility of the beams and reinforcing capacity of the short fiber. The decline or disappearance of post-cracking behaviour not only demonstrates the increasing brittleness of SCP, but also indicates the degradation of sisal fiber. Table 4.4 summarizes the flexural indices of SCP in three-point bending test. As expected, the declining rates of flexural strength and toughness parameters are directly proportional to the temperature of the aggressive conditions. It can be seen that, after 150 days of hot-dry aging, the beams treated in D90 yield minimum strengths, which are 36.94%, 54.79%, and 86.04% lower than those of samples treated by D70, D50, and the control group, respectively. Similar trends can also be found in toughness (T_f) and flexural strain at failure (ϵ_f), after 100 days. The D90 treatment led to declines

of these two indices by 93.66%, and 81.36%, respectively. For hot-soak treatment, the increase of temperature led to a severe degradation of sisal fiber in a cement matrix as evidenced by the significant decline of strength and toughness. Compared to those of D90, at the duration of 100 days, the SCPs treated by S90 caused a decline of bending strength, toughness and flexural strain by 49.60%, 73.54%, and 48.08%, respectively. The results verify the conclusion obtained for LSFM that the most effective static aggressive condition should be the soak treatment at a temperature higher than 70 ℃.

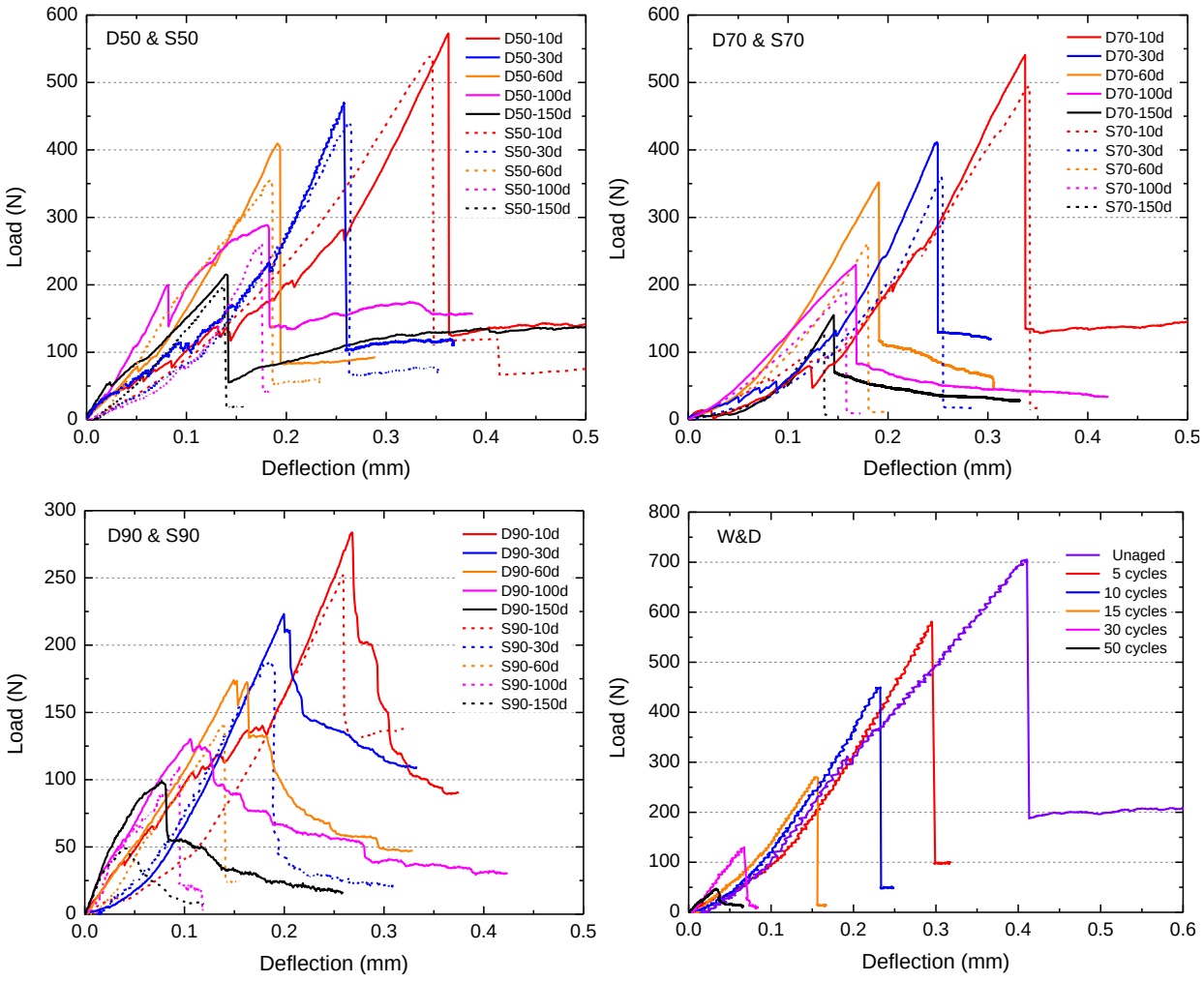

Figure 4.2: Effect of temperature and humidity on the flexural strength of SCP

Compared with LSFM, the degradation of flexural properties of SCP is mild, but it still illustrates that W&D is the most effective aggressive condition for accelerating the degradation of natural fiber. After 50 wetting and drying cycles, the flexural strength, toughness and deflection of SCP experienced a decline by 93.37%, 99.16%, and 91.94%, respectively, which are 5.81%, 49.65%, and 16.67%, of those of S90.

Although the flexural modulus does not direct correlate with the deterioration of sisal fiber, it is an indicator of increase of fiber brittleness, caused by the precipitation of cement hydration products in fiber walls. Except for the alkali hydrolysis of fiber amorphous components, cell wall mineralization is another degradation mechanisms of natural fiber in a cement matrix. Increased mineralization of the fibers leads to higher embrittlement of the composite after accelerated aging (Tonoli, Rodrigues Filho et al. 2009).

Both, the four-point flexural test of LSFM and three-point bending test of SCP, indicate that the most effective static approach to accelerate the degradation of natural fiber in cement composites is to soak the samples or change the humidity at 70 ℃ and higher temperature. The W&D treatment has a more aggressive effect on strength and toughness decline of the samples, therefore, it is the most feasible one to assess the durability of NFRCC within a short period of time. However, due to the sharp decrease of strength and toughness, the properties of the treated specimens are not steadily. On one hand, the duration of each wetting and drying stage should be defined logically, on the other hand, the number of cycles needs to be determined carefully. In contrast, although the hot-soak treatment (S70 or S90) shows a relative modest impact on degradation of fiber and needs more time to determine the durability, the samples' properties experience gradually stable declines, therefore easier to control and determine the degradation rate.

Table 4.4: Durability of SCP determined by three-point flexural indices

Aggressive condition	Duration/number of cycles	σ_f (MPa)	T_f (N-mm)	ϵ_f	E_f (GPa)
Control	0	7.09	170.59	0.00558	1.17
D50	10d	5.78	96.31	0.00493	1.27
	30d	4.74	58.27	0.00350	1.35
	60d	4.13	42.46	0.00264	1.57
	100d	2.91	33.89	0.00249	1.17
	150d	2.19	24.76	0.00192	1.15
D70	10d	5.47	83.17	0.00459	1.19
	30d	4.15	40.64	0.00340	1.22
	60d	3.56	36.30	0.00259	1.38
	100d	2.31	30.56	0.00228	1.01
	150d	1.57	14.43	0.00198	0.79
D90	10d	2.86	46.68	0.00364	0.78
	30d	2.26	34.42	0.00272	0.83
	60d	1.76	26.89	0.00204	0.86
	100d	1.31	25.91	0.00145	0.96
	150d	0.99	10.81	0.00104	0.95
S50	10d	5.44	89.43	0.00471	1.15
	30d	4.43	49.51	0.00361	1.23
	60d	3.58	35.01	0.00253	1.42
	100d	2.62	15.70	0.00238	1.10
	150d	1.99	12.52	0.00188	1.06
S70	10d	4.99	63.32	0.00465	1.07
	30d	3.63	29.35	0.00346	1.05
	60d	2.62	18.11	0.00244	1.07
	100d	1.91	13.44	0.00215	0.89
	150d	1.33	5.43	0.00185	0.72
S90	10d	2.54	31.99	0.00353	0.73
	30d	1.89	18.47	0.00259	0.77
	60d	1.42	9.42	0.00190	0.74
	100d	1.10	5.28	0.00130	0.85
	150d	0.499	2.86	0.00054	0.92
W&D	5c	5.85	69.18	0.00402	1.46
	10c	4.57	42.66	0.00316	1.44
	15c	2.74	17.73	0.00214	1.28
	30c	1.30	4.67	0.00092	1.42
	50c	0.47	1.44	0.00045	1.05

4.4 Degradation of Sisal Fiber in the Cement Matrix

Beside the strength and toughness loss of fiber-reinforced cement composites, the degradation of the tensile properties of fibers embedded in a cement matrix is a more direct indicator of the deterioration rate of fiber. Fig. 4.3 shows the Weibull plots of the raw and embedded fibers subjected to various aggressive conditions. Although with non-homogeneous structures, the raw sisal fiber showed the highest concentration degree of test data. For hot-dry treatment, test data exhibited an increase of scatter with increasing aging duration. This indicates that only partially embedded fibers encountered severe degradation while the other fibers still had considerable tensile strength. On the other hand, the opposite was true for W&D treatments. Due to the serious deterioration of partially embedded fibers, the test data present a low concentration degree at early aging stage. With increasing number of cycles, the data begin to increase to a high concentration caused by the general decline of tensile strength of all embedded fibers. However, the data of embedded fiber subjected to hot-soak treatment show a neutral trend: the concentration of data decreases at first and then generally increases. The fibers with intact surface present better degradation resistance, whereas the fibers with surface defects are prone to high precipitation of calcium hydroxide in cell walls. The inside lignin and hemicellulose easily encounter alkali hydrolysis, which further leads to the stripping of cellulose micro-fibrils. The low ultimate tensile strength and high concentration degree of test data of embedded fibers indicate that all embedded fibers suffered severe alkali attack and mineralization in the cement matrix exposed to W&D cycles.

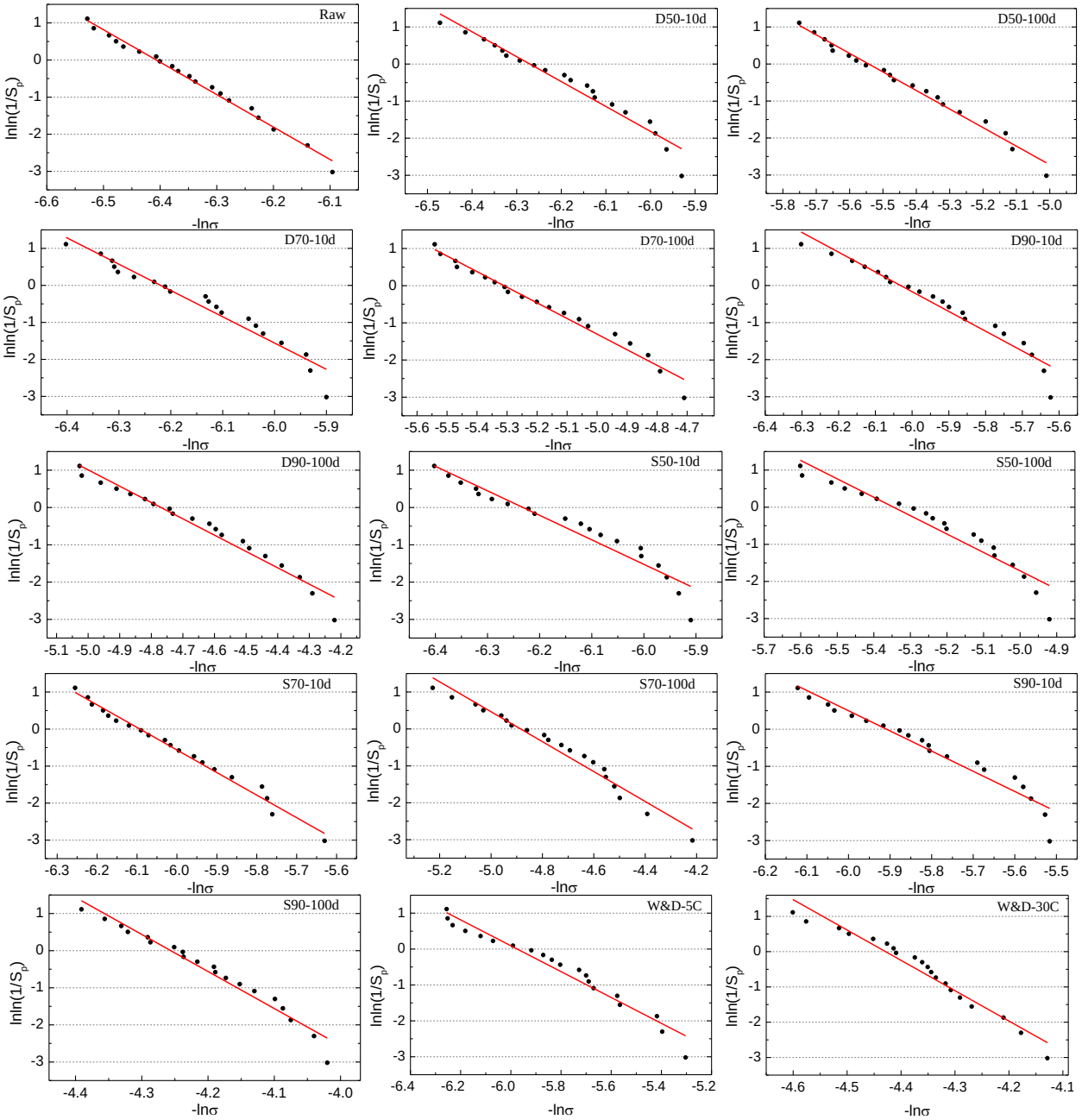

* D: hot-dry, S: hot-soak, C: number of wetting and drying cycles

Figure 4.3: The Weibull plots of raw fiber and embedded fibers after 10 and 100 days static treatment, and 5 and 30 wetting and drying cycles

Table 4.5 summarizes the Weibull parameters and Young's modulus, which is used to assess the deformability of sisal fibers in this study. It can be seen that, for static aging conditions, the rate of strength loss of sisal fibers gradually increases with increasing temperature. The embedded

sisal fibers subjected to hot-dry and hot-soak conditions at 90 ºC (D90 and S90) had the minimum tensile strength, i.e. 19.45%, and 11.64% of the strength of raw fiber, respectively.

Table 4.5: The Weibull parameters of sisal fibers in tensile test

Treatment	Duration	Weibull Modulus, m	R^2	Characteristic Strength, σ_0 (MPa)	Young's modulus, E (GPa)
Raw fiber	0	8.74	0.9893	605.88	15.41
D50	10 d	6.72	0.9525	528.67	16.59
	30 d	6.05	0.9423	376.52	17.27
	100d	5.01	0.9844	255.36	17.46
D70	10 d	7.10	0.9479	502.42	16.67
	30 d	6.17	0.9516	341.33	17.59
	100 d	4.21	0.9763	202.32	17.63
D90	10 d	5.33	0.9443	416.31	16.42
	30 d	4.21	0.9626	291.64	17.71
	100 d	4.38	0.9646	117.86	17.86
S50	10 d	6.57	0.9249	508.69	16.82
	30 d	4.29	0.9633	346.47	17.71
	100 d	4.96	0.9166	209.73	17.82
S70	10 d	6.10	0.9851	442.58	16.43
	30 d	4.37	0.9235	313.67	17.69
	100 d	4.55	0.9643	132.29	17.89
S90	10 d	5.44	0.9389	368.13	17.75
	30 d	4.99	0.9511	190.29	17.87
	100 d	9.98	0.9615	70.54	19.54
W&D	5 c	3.60	0.9546	393.15	17.27
	15 c	4.56	0.9491	133.06	17.98
	30 c	8.60	0.9538	83.82	19.79

The soak treatment accelerated the degradation of sisal fiber. The embedded fibers subjected to S50 and S70 yielded similar strength as those of D70 and D90, respectively. Therefore, agreeing well with the flexural properties of LSFM and SCP, the tensile strength of the embedded fibers encountered the most severe degradation in S90 for the static aggressive conditions. For the continuous W&D treatment, after 30 cycles, the embedded fibers present a similar degradation

degree as that of S90. The Young's modulus of sisal fiber increased with the decreasing tensile strength. However, the embedded fibers treated by W&D presented higher Young's modulus than those of S90, which indicates that the change of humidity promotes the mineralization of fiber walls.

4.5 Crystallization

The crystallinity indices of sisal fibers were determined by means of X-ray diffraction. Fig. 4.4 shows the XRD patterns of the raw sisal fiber and the embedded fibers subjected to hot-dry, hot-soak, and W&D conditions. The results indicate that sisal fiber's crystallization mainly depends on cellulose, which presents an intensive peak at $2\theta \approx 22.5^{\circ}$ corresponding to its (002) lattice plane and a broad peak ranging from 13º to 18º corresponding to the ($\bar{1}10$) and (110) lattice planes. Compared with the raw sisal fiber, the pulled out fibers show recognizable narrow peaks with higher intensity, due to the decomposition of amorphous components (lignin and hemicellulose) in the alkaline environment of cement. Due to the removal of amorphous components (Sinha and Rout 2009), both crystallite size and crystallinity index of the fibers increased. With increasing temperature and humidity, the main peaks of sisal fiber sharpen gradually. After 30 cycles of wetting and drying, the main peaks of sisal fiber embedded in pure cement showed the highest intensity, which means that the fiber encountered the most severe alkali attack in the cement matrix.

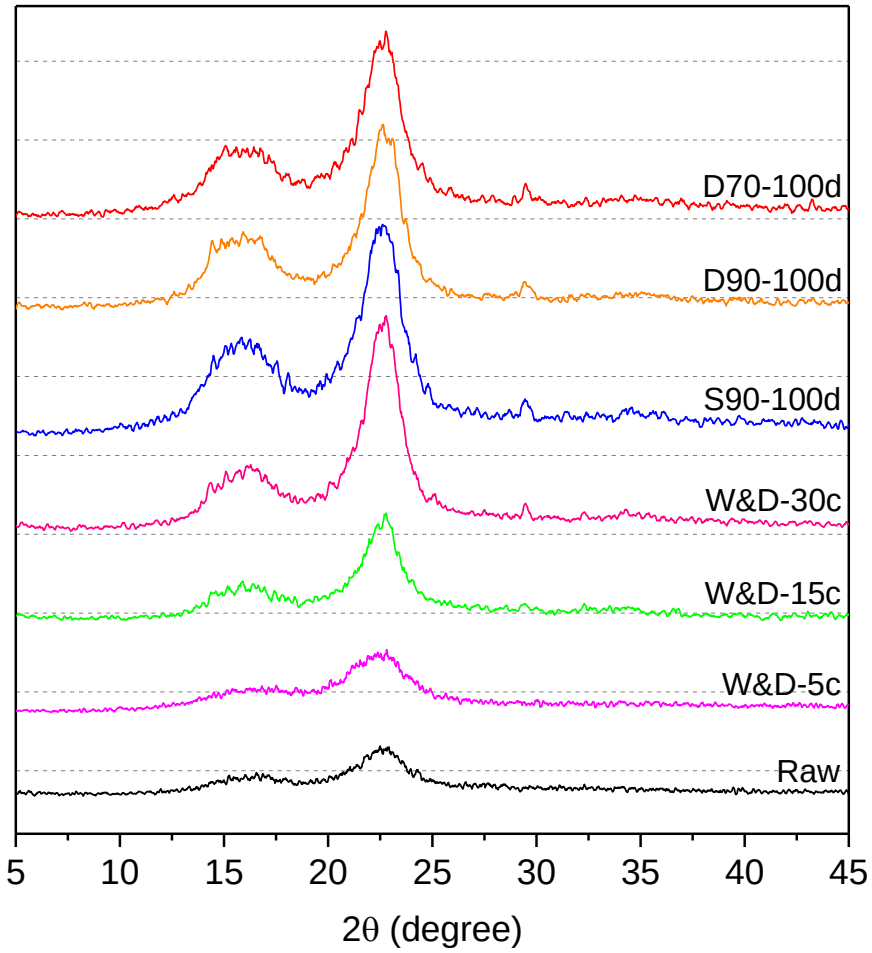

Figure 4.4: XRD pattern of the raw and embedded sisal fibers

The crystallinity index (Cr.I.), percentage of crystal (%Cr), and crystallite size (L), calculated from the corresponding diffraction peaks and their full width at half maximum (FWHM) using the deconvolution method, are summarized in Table 4.6. Although the crystallite size is affected by non-uniform strain, crystalline disorder, and some other uncertain factors, it still can be seen that the crystallite sizes for cellulose crystals of embedded fibers become bigger than those of raw sisal fiber, and increase with aging duration. For statical aggressive treatment, the increase of temperature accelerates the alkali hydrolysis of lignin and hemicellulose, as expected. The fiber treated by D90 shows 1.55% and 1.91% greater %Cr and Cr.I., respectively, than those of D70. The soak treatment further accelerates the degradation of fiber evidenced by the increased

crystallinity indices from D90 to S90. For W&D, both the Cr% and Cr.I. increase with increasing wetting and drying cycle numbers. As indicated in Fig. 4.4, the fibers subjected to 30 wetting and drying cycles, present the highest crystallinity indices %Cr and Cr.I., which are 11.70% and 18.92% greater than those of the raw fiber, respectively.

Table 4.6: Calculated crystalline parameters of sisal fiber

Aggressive conditions	Duration /Number of cycles	Peak position (2θ)	FWHM(β) (2θ)	L (nm)	%Cr	Cr.I.
Unaged	0	16.68 22.41	4.58 3.69	1.73 2.17	77.67	0.7126
W&D	5 c	16.61 22.56	4.11 3.37	1.93 2.38	79.70	0.7553
	15 c	16.46 22.56	4.37 2.64	1.82 3.03	85.29	0.8276
	30 c	16.47 22.59	4.58 2.30	1.73 3.48	86.76	0.8474
S90	100 d	16.16 22.53	4.35 2.69	1.88 3.16	86.54	0.8391
D90	100 d	16.08 22.61	4.14 2.38	1.98 3.58	85.97	0.8177
D70	100 d	16.21 22.56	4.47 2.60	1.83 3.27	84.66	0.8021

4.6 Thermal Analysis

Fig. 4.5 shows the overall thermal decomposition process of raw and embedded sisal fibers in the form of TGA and DTG curves. Due to the moisture evaporation and thermal decompositions of hemicellulose and cellulose, three weight loss stages are detected in both the TGA and DTG curves in the following temperature ranges: (i) from 50 to 110 ºC, (ii) between 270 and 360 ºC, and from 335 to 500 ºC. As shown in Table 3.2, the main chemical component of sisal fiber is cellulose (>65%), which is also the main structural component of natural fiber's cell walls.

According to the analysis of other investigators (Ziderman and Bel-Ayche 1978, Blazej, Kosík et al. 1985, Ziderman and Belayche 1986, Theander and Nelson 1988, Loon and Glaus 1997) the alkali degradation of cellulose comprises four processes: peeling-off reaction, chemical stopping reaction, physical stopping reaction, and alkaline hydrolysis. The content of residual cellulose is an effective measure to evaluate the degradation degree of sisal fiber. A distinct DTG peak that corresponds to the sharp loss of weight in the TGA curve, due to the decomposition of cellulose, can be observed for each sample. However, the "shoulder", normally caused by the thermal decomposition of hemicellulose, is only visible in the DTG curves of the raw sample and the embedded fibers treated by D90 and S90. The sample exposed to 30 wetting and drying cycles encountered a severe alkali hydrolysis of hemicellulose, and consequently its hemicellulose's shoulder peak is overlapped in the cellulose main peaks (Yao, Wu et al. 2008).

It is a challenge to accurately calculate the content of lignin from the TGA curves of natural fiber due to the extensive temperature range covering two or three stages (Jakab, Faix et al. 1997, Sun, Lu et al. 2001). Different from the sharper DTG peaks of cellulose and the "shoulders" of hemicellulose, the DTG curve for lignin presents three broad exothermal steps: the first one from 280 to 390 ºC, the second one at the higher temperature of 420 ºC, and a long tail beyond 500 ºC (Brebu and Vasile 2010).

In Fig. 4.5, it can be seen that the embedded fiber subjected to W&D encounters cellulose and hemicellulose decompositions of 43.34% and 8.09% after 30 cycles, which are 41.60% and 40.95% lower, respectively, than that of the raw fiber. After 100 day treatments of D90 and S90, the fibers encountered cellulose content losses of 53.22% and 47.37%, which are 28.28% and 36.17% lower than the control group, respectively, but higher than that of W&D treated fibers.

With the assumptions that the long tail of the curves beyond 500 ºC is caused by the thermal

decomposition of lignin and that each sample decomposed the same amount of lignin, the extra weight loss of embedded fibers at the temperature range from 500 ºC to 600 ºC beyond the raw fiber is due to the decomposition of CH, which precipitates in the cell walls of sisal fiber and features a high decomposition temperature. After 30 wetting and drying cycles, the embedded fibers show a mean CH precipitation of 5.91%, which is 241.62% and 351.15% greater than those of embedded fibers treated by S90 and D90 for 100 days. Therefore, sisal fiber encountered the most severe alkaline attack in W&D treatment evidenced by the minimum cellulose content and highest amount of precipitated CH caused by the high CH content of the matrix.

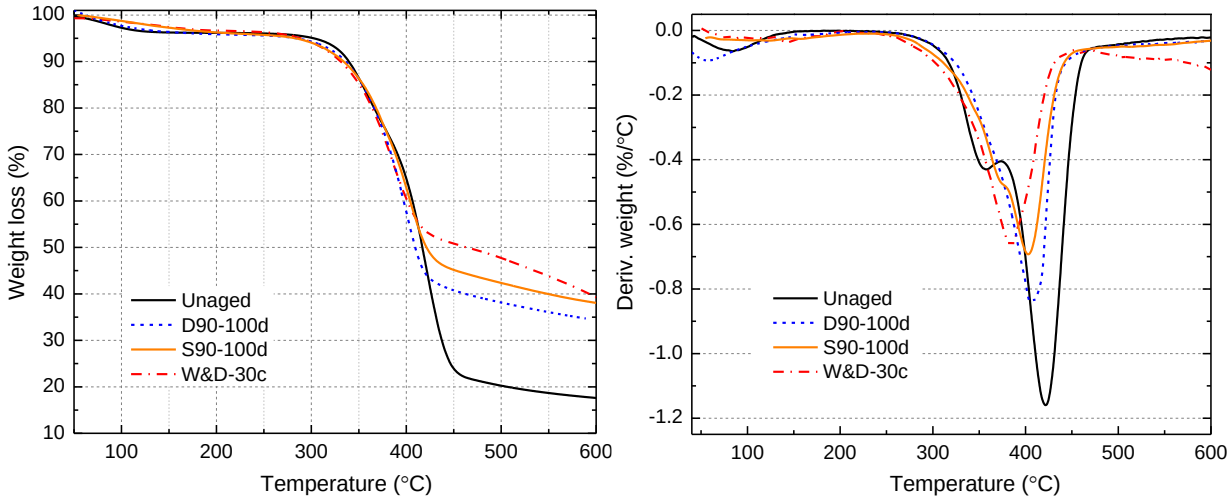

Figure 4.5: TGA and DTG curves of the raw sisal fiber, the embedded fiber subjected to D90 and S90 for 100 days, and that treated by 30 wetting and drying cycles

4.7 Microanalysis

The micro-analysis of typical fracture surfaces of SCP after curing for 28d, D90 and S90 for 100 d, and W&D for 30 cycles was performed by using SEM to study the effect of aggressive conditions on the degradation degree of sisal fiber in a cement matrix. As shown in Fig. 4.6, before accelerated aging, the sisal fiber, pulled out from the cement matrix, still maintained an intact outer

surface except for small amount of cement hydration products and a sign of stripping of partial cellulose microfibrils. After 100 days of D90 aging, cracks and stripping of cellulose micro-fibrils, caused by the alkaline hydrolysis of amorphous components and the slight deposition of cement hydration products, are detected on the fiber cross sections. S90 leads to a more severe fiber degradation than D90: the hemicelluloses and lignin were decomposed almost completely after 100 days. Sisal fiber's surface was fully decomposed, but the inside cellulose microfibrils were intact, which still ensured some reinforcing effect of sisal fiber. After 30 wetting and drying cycles, the sisal fibers have totally deteriorated. The decomposition of amorphous components (lignin, hemicellulose, and pectin) led to a considerable migration and precipitation of hydration products of cement into fiber cell walls. As a result, the cellulose micro-fibrils were partially dispersed and filled by calcium hydroxide and calcium silicate hydrate (C-S-H). From the microstructure of embedded sisal fibers, it is reasonable to again reach the conclusion that both S90 and W&D create effective accelerated aging conditions to determine the durability of sisal fiber-reinforced cement composites.

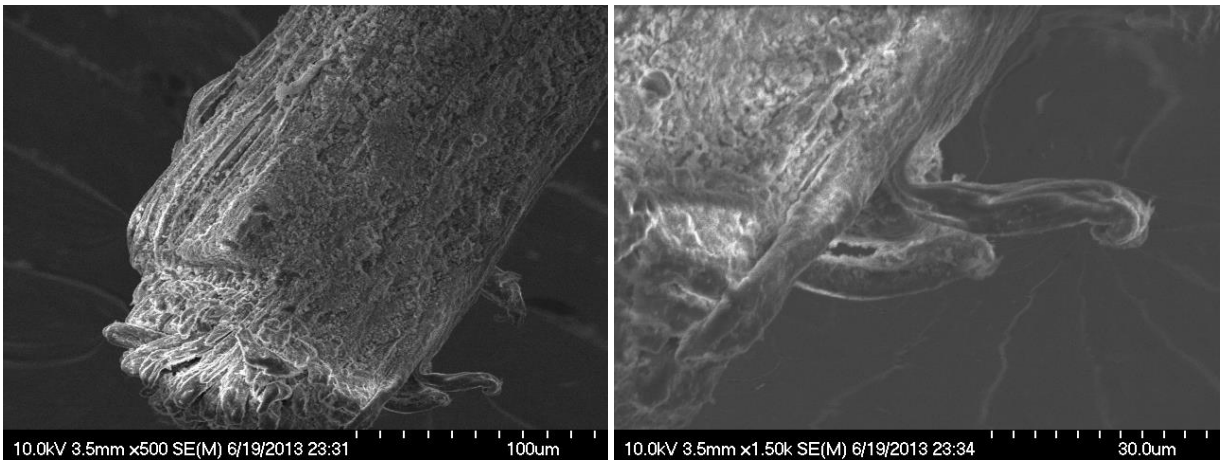

Curing for 28d

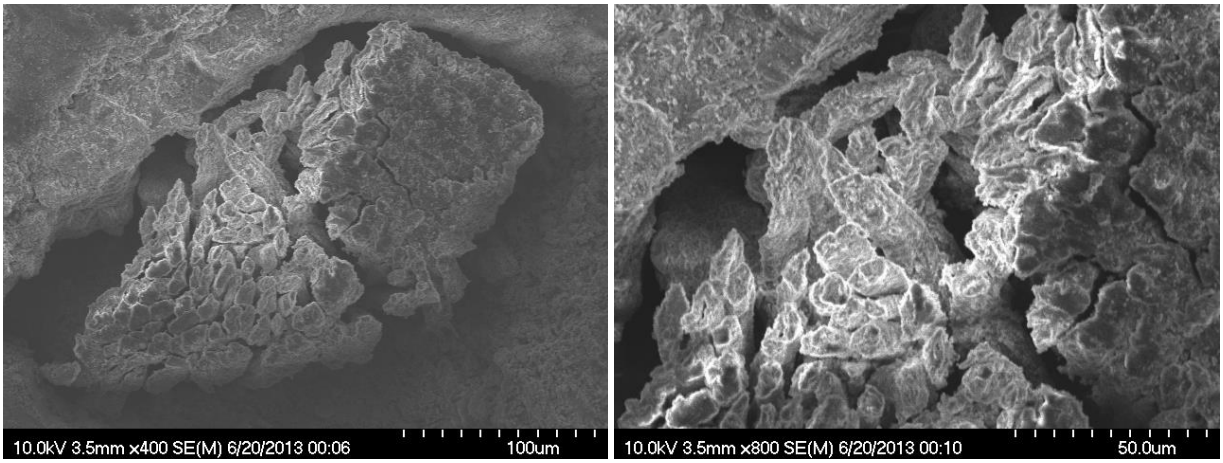

D90-100d

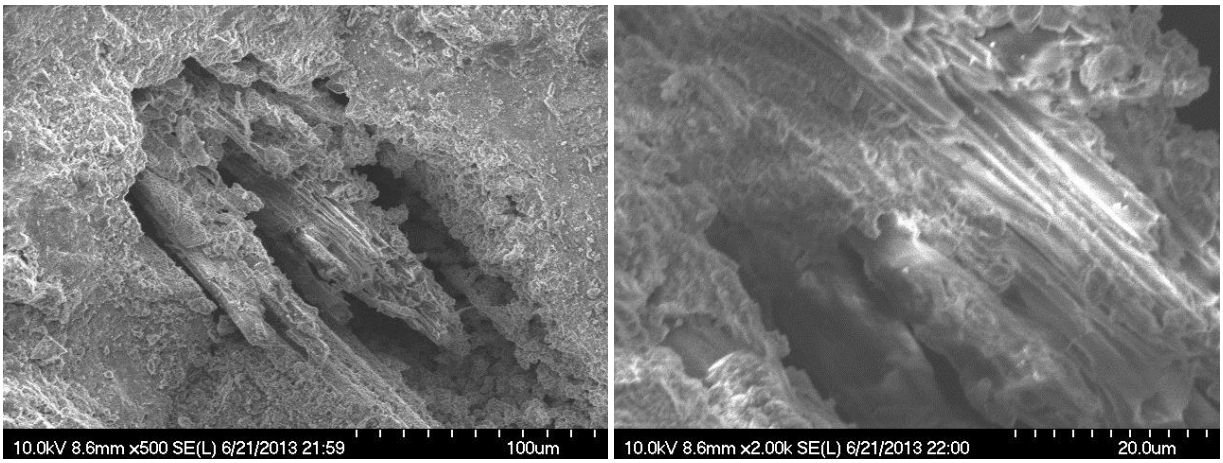

S90-100d

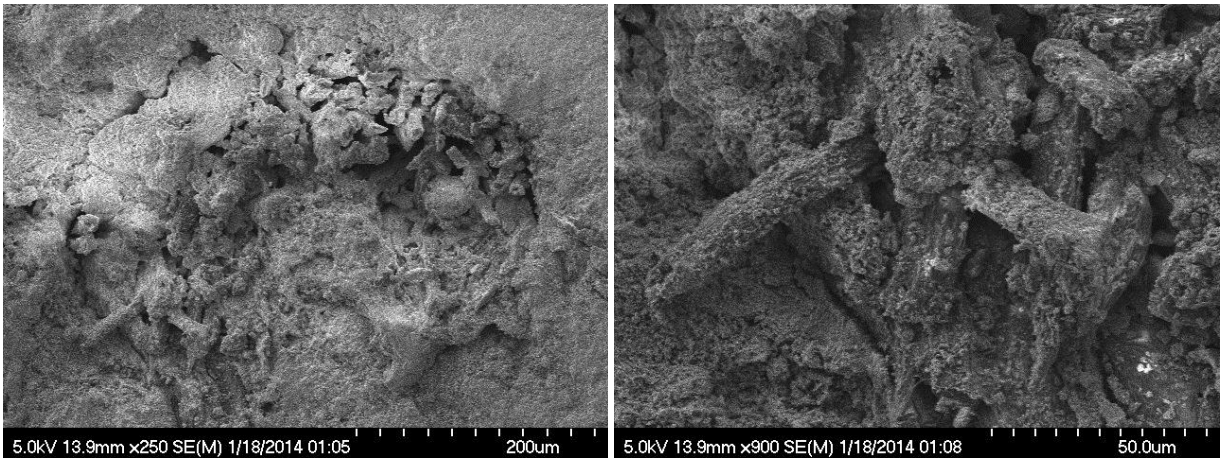

W&D-30c

Figure 4.6: SEM micrographs of the fracture surface of sisal fiber reinforced cement paste with curing of 28 days, D90 and S90 treatment for 100 days, and 30 W&D cycles

4.8 Summary

The effects of seven accelerated aging conditions on the deterioration of sisal fiber and the durability of sisal fiber-reinforced cement composites were investigated through testing the flexural properties of mortar and paste beams, uniaxial tensile strength, crystallinity index, thermal decomposition of the embedded fibers and the analysis of fracture surface microstructures.

Both of the four-point flexural testing of LSFM and three-point bending test of SCP indicate that the most effective static approach for accelerating the degradation of natural fiber in cement composites is to soak the samples or change the humidity at 70 ºC and higher temperature. The W&D treatment has a more aggressive effect on strength and toughness decline of the samples. Therefore, it is logical to determine the durability of natural fiber-reinforced cement composites within a reasonable short time using these treatments. However, due to the sharp decrease of strength and toughness, it is difficult to precisely predict the durability of SFRCC. The embedded fibers with S90 aging for 100 days experienced similar degradation rates as those of 30 W&D cycles in tensile strength. The W&D treatment had a more accelerating effect on both the alkali hydrolysis of fiber's amorphous components and the mineralization of fiber cell wall indicated by the highest crystallinity indices and minimum content of cellulose.

The microstructure of fracture surfaces indicated that the sisal fiber encountered the most severe alkali attack and precipitation of hydration products in the cement matrix after 30 wetting and drying cycles. The results indicate that the cyclic changes of humidity at relative high temperature (≥ 70 ºC) accelerate the degradation of natural fiber in cement matrix more effectively than the static aggressive conditions. In the following chapters, the durability of sisal fiber-reinforced cement composites and the fiber degradation will be determined after being treated by wetting and drying cycles as accelerated aging conditions.

CHAPTER 5: ARRESTING THE DEGRADATION OF SISAL FIBER IN CEMENT COMPOSITES THROUGH MODIFICATION OF CEMENT MATRIX

5.1 Introduction

This chapter reports the results of an investigation carried out to understand the influence of cement matrix modification on the durability of sisal fiber-reinforced cement composites (SFRCC) and the degradation of sisal fiber in the cement matrices. The effects of partial replacement of Portland cement by two rice husk ashes (RHA) with different degrees of fineness (RHA and CRHA) and the combinations of metakaolin (MK) and nanoclay (NC) on the durability of SFRCC were investigated by determining the flexural strength and toughness of samples subjected to wetting and drying cycles. In contrast to previous studies as reported in the literatures, a separate investigation of the degradation rate of the embedded sisal fibers after accelerated aging treatment was performed to determine their tensile properties, component change, crystallinity indices, and microstructures, characterized by means of uniaxial tension test, thermal gravimetric analysis (TGA), X-ray diffraction (XRD), and scanning electron microscopy (SEM), respectively. A two-parameter Weibull distribution model was used to enable an accurate prediction of tensile strength of the embedded sisal fibers. In order to illustrate the "filler effect" of RHA in cement, which potentially promotes cement hydration by the seeding effect, additional samples with a replacement of 5 wt. % of RHA by limestone (LS) powder with similar fineness were studied.

5.2 Pozzolanic Activity of MK and NC

In a test for pozzolanic activity 100 g of SCM was mixed with 10 g of chemical grade calcium hydroxide (CH) with a water/blend ratio of 0.5. The samples were cast in sealed bottles at 23 °C and the hydration was stopped by solvent exchanging with acetone and washing with diethylether. The samples were investigated by means of TGA in an N_2-atmosphere after 7 days of reaction. The pozzolanic activity of SCM was determined by measuring the amounts of CH consumption between 425 and 525 ºC.

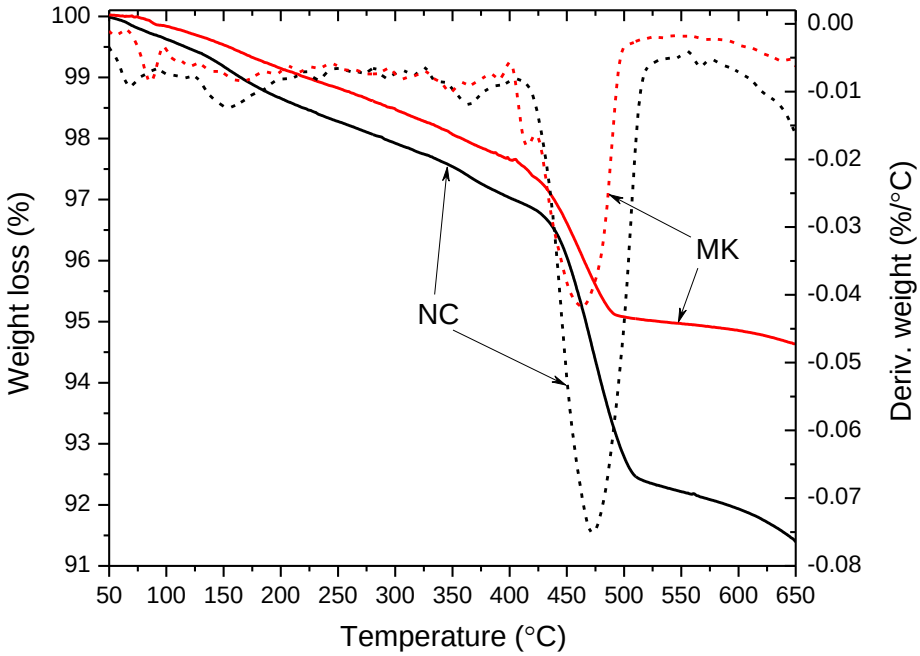

* TGA: solid line, DTG: dash lines

Figure 5.1: TGA and DTG curves of MK and NC in the reactivity test with portlandite after 7 days

Fig. 5.1 shows the TGA and DTG curves of the two samples, from which it can be seen that the weight loss of NC-CH blend is 93.94% greater than that of the MK-CH blend. This indicates that after 7 days of reaction, MK consumed more CH than NC did. The difference in activity

between MK and NC can be due to the variation in their chemical composition and particle size. As shown in Table 2.2 and Fig. 2.3, MK has an Al_2O_3 content of 42.4wt.%, which is 147.95% greater than that of NC. In addition, the specific surface area of MK is 235.62% larger than that of NC. This speeds up the pozzolanic reaction and helps to effectively consume CH in the cement matrix.

5.3 Cement Substitution by Combination of MK and NC

The amounts of metakaolin (MK) and nanoclay (NC) used as partial replacement of Portland cement (PC) are given in Table 2.3. The combined substitutions in the mortar matrix resulted in total substitution levels of 10, 30, and 50%, with increasing replacement of MK by NC.

5.3.1 Heat of hydration

The generation of specific heat flow and released heat of hydration normalized to PC content up to 50 h are shown in Fig. 5.2-a and b, respectively. These curves indicate that the hydration heat of the various blends are similar during the first two hydration periods, i.e. the pre-induction period and the induction period. The main differences are found during the acceleration and deceleration periods. From the peak values of heat flow and peak positions, it is easy to identify the replacement level of PC by supplementary cementitious materials: the peaks become narrow and high and appear earlier with increasing replacement ratio. Similar differences are also identified in the normalized released heat curves: higher blending levels lead to earlier “knees” of the curves and less released heat. There are two peaks (shoulders) in each curve, which indicate the silicate

reaction, and tricalcium aluminate reactions to form ettringite and subsequent conversion into monosulfate, respectively.

In neat PC, due to the low C_3A content (10 wt.% as shown in Table 2.1), the second shoulder peak is lower than the silicate reaction peak. With the increasing replacement of PC by MK, which is rich in aluminide, the second shoulder becomes more sharp and higher than the shoulder of silicate reaction. Corresponding to the second formation of ettringite, besides playing a nucleation role, the aluminates originating from MK also possibly participate in the reaction at this stage (Antoni, Rossen et al. 2012). Due to the dilution effect, the heights of the silicate shoulders of hydration heat flow curves gradually decrease with increasing PC replacement. Another role of MK and NC is as filler in the blends. This affects the aluminate reaction, which speeds up C_3A hydration, more so than the silicate reaction (Le Saoût and Ben Haha 2011).

The contribution of NC to hydration heat is also identified from the curves: due to the lower Al_2O_3 content, the replacement of MK by NC leads to a lower peak value and later peak position in the heat flow curves, and less released heat. With the increasing ratio of NC at each PC replacement level, the released heat declines further, because of the quick end of both acceleration and deceleration periods. Because of the fineness of MK, it provides a considerable amount of new surface area for heterogeneous nucleation of hydrates, such as C-S-H and monocarboaluminate. This illustrates that the early age (< 20 h) hydration of cement is significantly affected by both physical and chemical features of MK, i.e. fine particle size distribution for its role as “filler”, and high mineral amount of aluminate for its pozzolanic activity. The presence of NC not only relieves the rapid hydration, but also reduces the total released heat, through adjusting the “filler” size and balancing the Ca-Si-Al ratio of the blends.

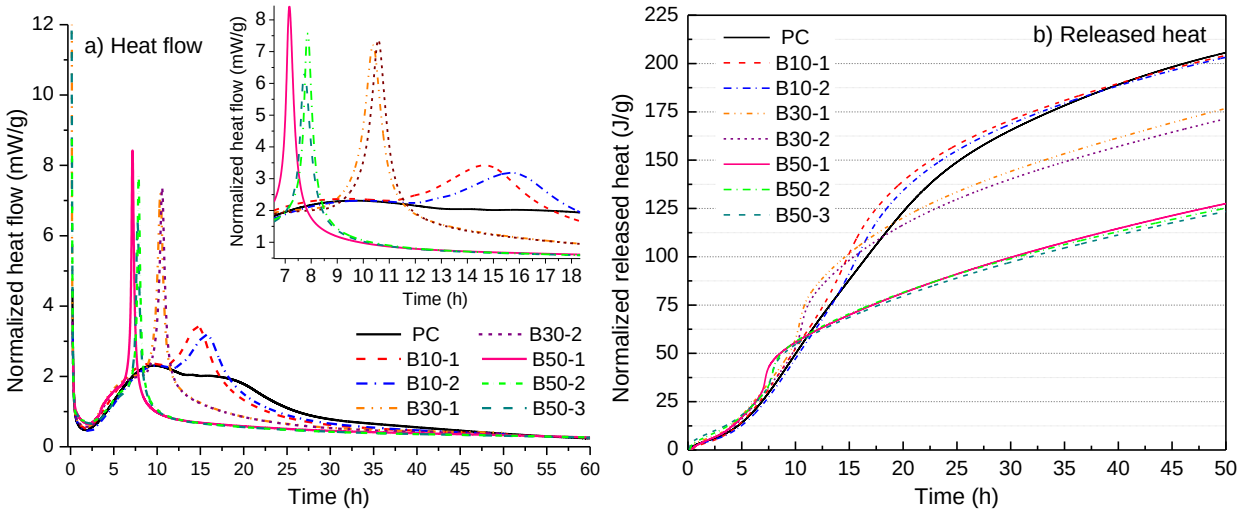

* PC: neat cement; B10-1: 90% cement +10% MK; B10-2: 90% cement +9% MK+1%NC; B30-1: 70% cement+29%MK+1%NC; B30-2: 70% cement+27%MK+3%NC; B50-1: 50%cement+49%MK+1%NC; B50-2: 50%cement+47%MK+3%; B50-3: 50%cement+45%MK+5%NC. (Table 2.3)

Figure 5.2: Normalized specific heat flow and released heat of blends with a w/b ratio of 0.5 at 25 ºC

5.3.2 Mineralogical analysis of the hydration products

XRD patterns of the hydration products of the examined cements after 1 day, 28 days and 90 days are shown in Fig.5.3. It can be seen that the hydration products of neat cement are ettringite, hemi carbonate, calcium hydroxide and calcite. In the samples with 10% replacement materials (B10-1 and B10-2), the amounts of CH and ettringite were reduced as the hydration proceeded. The differences between B10-1 and B10-2 indicate that, at early age (1 day), the combination of MK and NC had no effect on the amount of ettringite, while the CH was consumed less than that of pure MK modified cement. After 28 days and 90 days, in B30-1 and B30-2, the amounts of CH, ettringite and portlandite were significantly reduced, and the amounts of gypsum, hemi carbonate and AFm were increased with increasing NC content. When 50% of the cement was replaced by a combination of MK and NC, ettringite and calcium hydroxide could not be identified, and the amount of gypsum decreased with an increase of the NC ratio. It can be concluded that gypsum forms only at low replacement levels of MK by NC, such as in mixes B10-1, B30-2, and B50-1.

With increasing NC ratio, both the contents of calcite and hemicarbonate started to decrease after 28 days. The results indicate that the combination of MK and NC can improve the hydration process and reduce the amount of alkaline hydration products. The content of ettringite and portlandite decreased with the increase of MK and NC, and a CH-free cement matrix was obtained in the B50 series. The signal of gypsum is more obvious in B50-1, however, it was reduced with an increase of the NC ratio. In B50-2 and B50-3, ettringite, hemi carbonate, portlandite, and gypsum could not be identified, especially after 90 days of hydration.

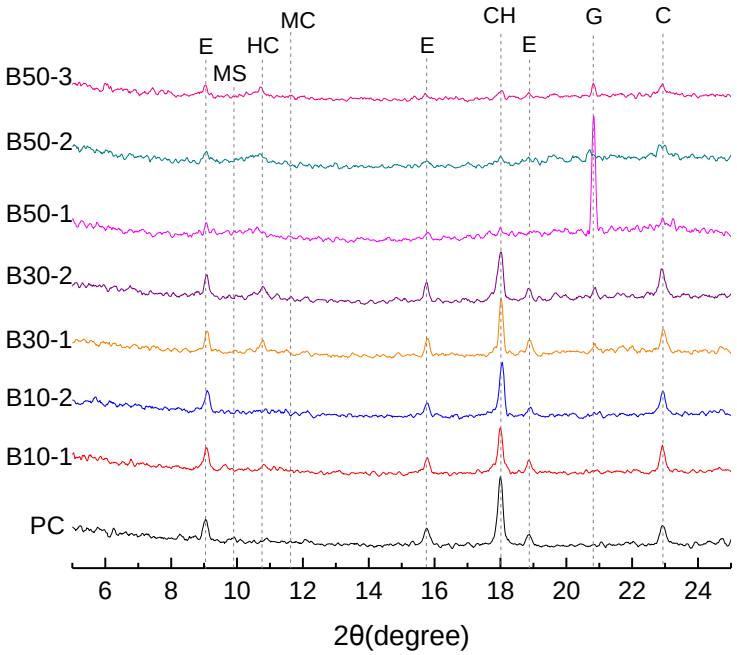

1 day

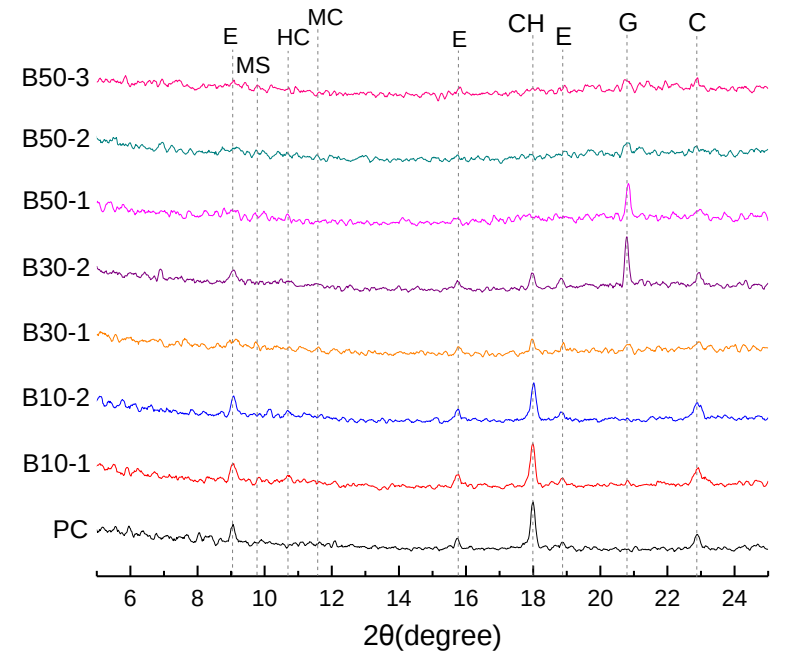

(b) 28 days

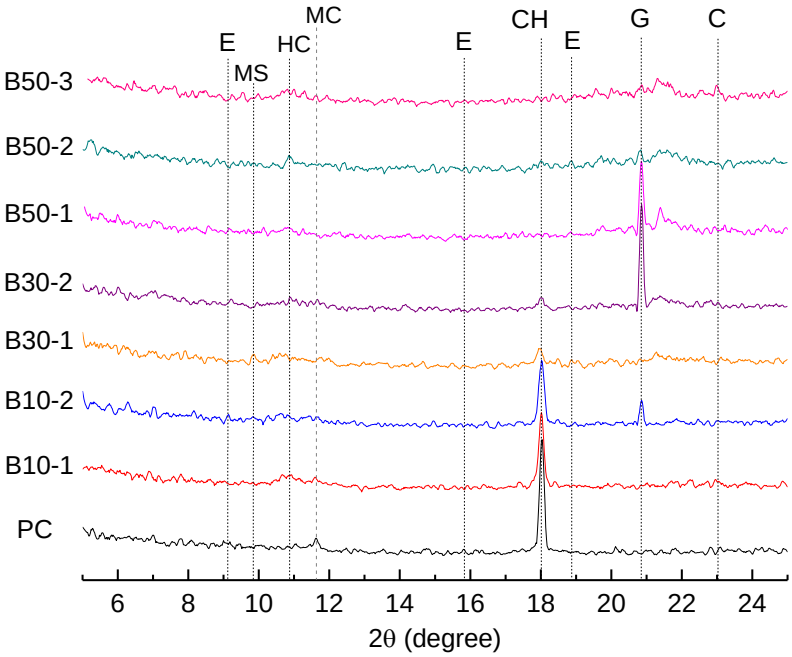

(c) 90 days

* E-ettringite, MS-monosulphate, HC-hemi carbonate, CH-calcium hydroxide, G-gypsum, MC- monocarboaluminate C-calcium carbonate.

** PC: neat cement; B10-1: 90% cement +10% MK; B10-2: 90% cement +9% MK+1%NC; B30-1: 70% cement+29%MK+1%NC; B30-2: 70% cement+27%MK+3%NC; B50-1: 50%cement+49%MK+1%NC; B50-2: 50%cement+47%MK+3%; B50-3: 50%cement+45%MK+5%NC. (Table 2.3)

Figure 5.3: XRD patterns of the investigated samples after 1 day, 28 and 90 days of hydration

5.3.3 Characterization of hydration products by thermogravimetric analysis

5.3.3.1 Analysis of TGA and DTG curves

By adding MK and NC, a higher degree of cement hydration as indicated by both hydration heat flow curves and XRD analysis was observed at early ages. In other words, these materials had an accelerating effect on the hydration of cement, which is the result of four mechanisms: (i) high pozzolanic reactivity of metakaolin to form C-S-H, (ii) the formation of carboaluminates caused by aluminates from metakaolin, (iii) high silica contents of MK and NC which shorten the induction period of cement pastes through reduced concentration of calcium ions via fast pozzolanic reactivity (Stein and Stevels 1964, Korpa, Kowald et al. 2008), (iv) acceleration of hydration facilitated by the filler effect of MK and NC powders, which provide large surface areas for early precipitation of cement hydration products (Wu and Young 1984). These processes enable MK and NC to improve the early age strength of cement and to consume CH, thereby reducing the alkalinity of the matrix and improving the durability of natural reinforcement.

TGA and DTG analyses of each blend after 1, 7, 28, 60, 90, and 300 days of hydration were performed on the TA Q50 thermo gravimetric analyzer. Figs. 5.4 a-d show the curves of selected samples after 28 and 90 days. At 28 days, PC peaks at about 100 ºC, which is linked to the decomposition of ettringite and C–S–H. This peak is higher than that of blends containing MK and NC, suggesting a higher amount of C-H-S and stabilization of ettringite. The amounts of C-S-H and ettringite in B50 blends are higher than those of B10s and B30s. Although no hemicarbonate and monocarbonate are observed in early age curves, mass loss caused by these two minerals can be clearly seen after 28 days of hydration with a rising trend.

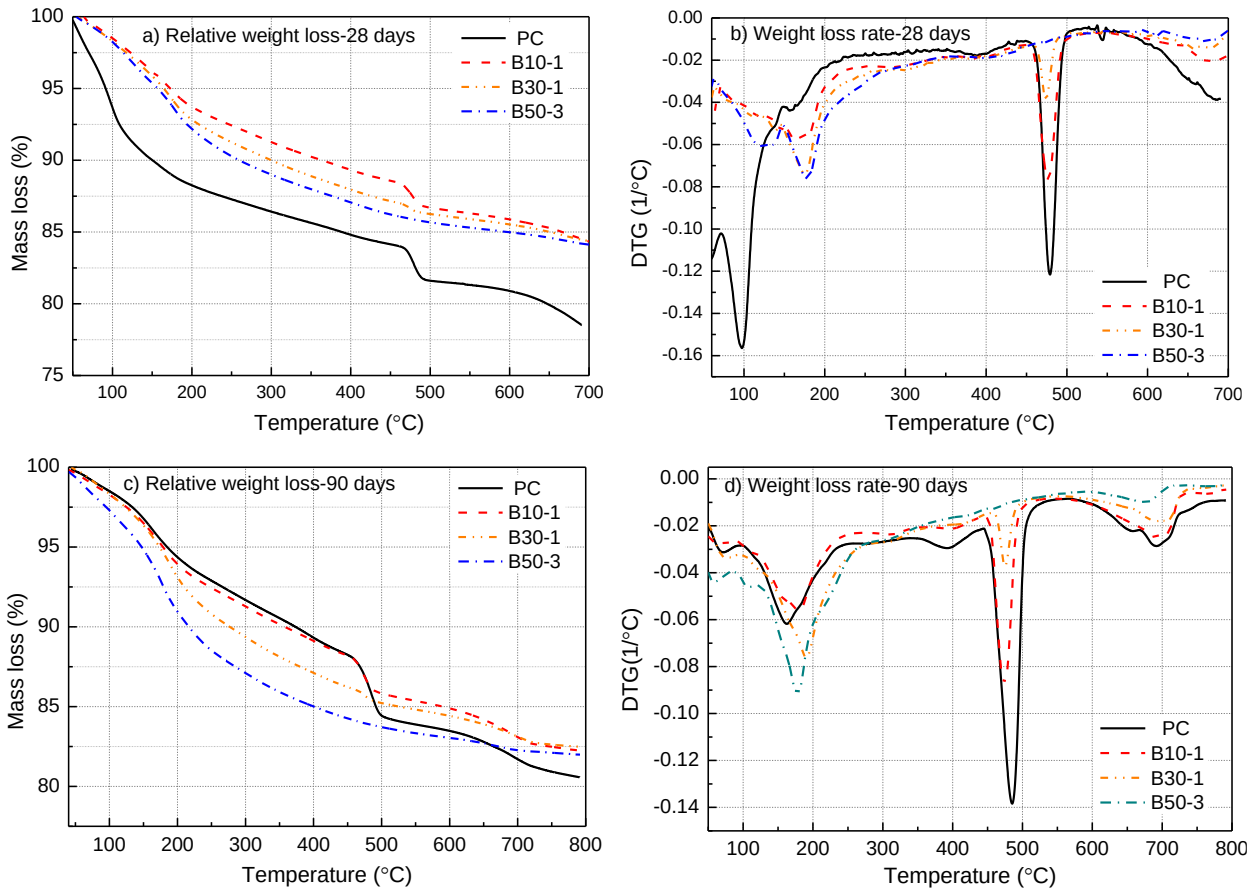

Figure 5.4: TGA and DTG curves of selected blends after 28 and 90 days

The results illustrate that MK and NC have beneficial effects on the formation of hemicarbonate and monocarbonate at 28 days, however, the amounts of these two hydration products in PC were higher than from B10 blends after 90 days. The height of the calcium carbonate peak decreased with increasing MK and NC contents at all hydration ages, confirming the increased consumption of CH and $CaCO_3$ to form carboaluminate phases in MK and NC modified pastes. The most significant effect of MK and NC on the hydration products of cement is given by the changed amount of CH. The amount of portlandite of neat PC is highest at each age and increases as hydration proceeds. Both MK and NC had beneficial effects on reducing the amount of CH. When the replacement of PC is up to 50%, the amounts of portlandite of the pastes

show a downtrend with hydration time. Compared with MK, NC is more efficient in reducing portlandite from cement pastes.

5.3.3.2 Bound water and CH contents

Figs. 5.5-a and b show the development of non-evaporable water contents (W_{ne}) and the CH contents as functions of hydration time, normalized with respect to the mass fractions of cement (m_c) in the pastes. It can be seen that for all the blends, a major fraction of the water was bound in the first 28 days, especially during the first 7 days of hydration. Neat PC paste had the highest CH and bound water content, but the lowest normalized W_{ne} after 300 days of hydration among all the pastes considered in this study. The enhancement in reactivity of cement provided by metakaolin and its own reaction at early ages resulted in the metakaolin modified paste showing a higher normalized bound water content than the neat PC paste (Vance, Aguayo et al. 2013). B10-1 and B10-2 showed lower normalized W_{ne} than neat PC at early ages of hydration and lower CH amounts at all ages. The normalized W_{ne} contents of pastes had a similar distribution pattern as hydration heat: three clearly distinguishable W_{ne} levels were identified for the three levels of replacement of PC. B50 blends had the highest normalized non-evaporable water contents at all hydration ages and B30s had a moderate increase of W_{ne} compared with PC and B10s. The increased normalized W_{ne} content in pastes is attributed to three factors: (i) the contribution of high aluminates and silica contents for reaction, (ii) the enhanced hydration of the PC in pastes due to accelerated hydration reaction caused by pozzolanic activity of MK and NC, (iii) dilution effects of MK and NC in pastes promoting the further hydration of cement. At each cement replacement level, increasing replacement of MK by NC led to higher bound water amounts before 90 days of hydration. Although after 90 days, the non-evaporable water in all blends kept increasing slightly, the pastes with higher NC content had a lower W_{ne}.

Fig.5.5-b shows that CH contents of PC, B10s and B30s increased at first and then tended to stabilize with hydration time. The turning point appears earlier with increasing replacement of PC by MK and increasing replacement of MK by NC. B50-1 kept an approximately constant amount of CH at all ages. The portlandite contents of B50-2 and B50-3 decrease with hydration time, which is evidence of the beneficial effects of MK and NC on consuming CH in cement pastes. Due to the high content of Al_2O_3, MK showed a higher pozzolanic activity than NC at early stages, therefore the CH contents of B10-1, B30-1 and B50-1 were lower than those of B10-2, B30-2, and B50-3, respectively, for the first 7 days of hydration. It is also important to note that NC has a higher portlandite consumption ability than MK at later hydration processes, because of its higher SiO_2 content.

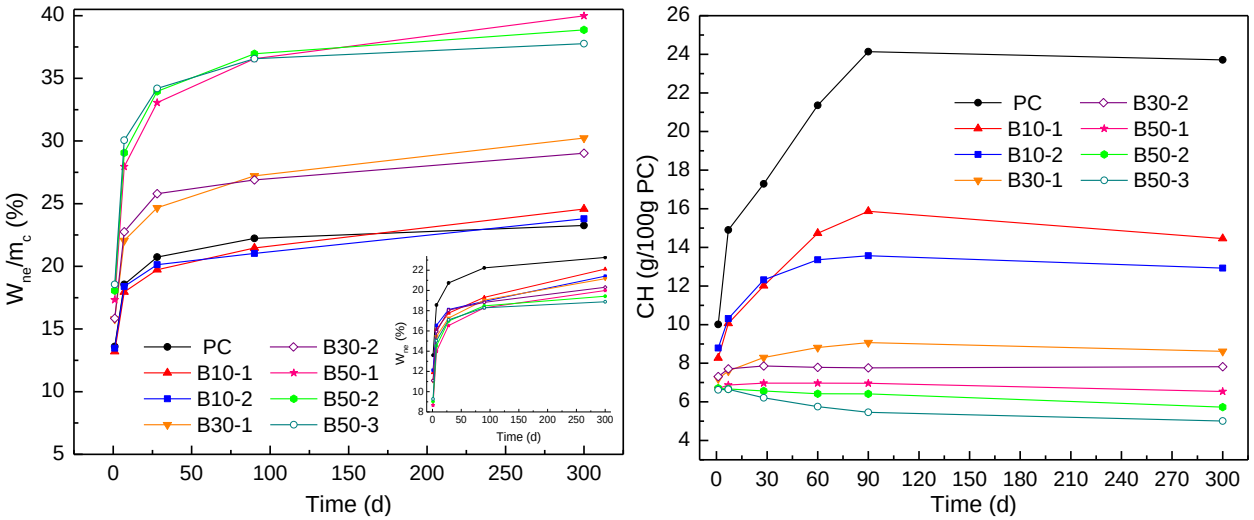

(a) Non-evaporable water (b) Portlandite

Figure 5.5: Contents of non-evaporable water and portlandite normalized to the PC content in the blends after hydration times up to 300 days

5.3.4 Analysis of C–S–H composition by SEM-EDX

Microanalytical investigations of the main phase (C-S-H) of PC, B10-1, B30-1, and B50-3 were performed on SEM-EDX under an accelerating voltage of 15 KeV and a working distance of 12.0 mm for local chemical analysis. Due to the interaction of electrons with the specimen and the intergrowth of hydrates, the detected X-rays of one spot often are the results of the signal of mixtures of phases (Deschner, Winnefeld et al. 2012), so they cannot represent the real phase composition of C-S-H. In order to guarantee statistical accuracy of the phase composition, more than 50 EDX spot analyses were taken from each specimen. Figs.5.6-a to d show the Al/Ca versus Si/Ca atomic ratio of PC after 300 and 600 days of hydration, and those of B10-1, B30-1, and B50-3 after 28 and 300 days of hydration. As mentioned in Chapter 3 (Section 3.3.4), two lines were used to determine the effective element ratios of the C-S-H in the cementitious matrices.

From Fig.5.6-a, it can be seen that, after 300 days and 600 days hydration, the C-S-H of pure Portland cement yields Ca/Si and Al/Si ratios of 1.85±0.3 and 0.07, respectively, with a mean Ca/(Si+Al) of 1.73.

It's well known that when materials rich in amorphous silica (pozzolans) are added to the Portland cement, they react with the $Ca(OH)_2$, liberated during the formation of C-S-H by the hydration of C_3S and β C_2S, thereby generating an extra production of C-S-H with higher Si/Ca ratio (Neville and Aïtcin 1998). The plot in Fig. 5.6-b indicates that B10-1 generated a C-S-H phase with a Ca/Si ratio of 1.685±0.235 and an Al/Si ratio of 0.108, and a Ca/(Si+Al) ratio which is 12.14% lower than that of PC. Due to the high Al_2O_3 and SiO_2 contents of MK, the Ca/Si and Ca/(Si+Al) ratios decrease with the increasing cement replacement level. The Ca/Si, Al/Si, and the mean Ca/(Si+Al) ratios of C-S-H in B30-1 are 1.64±0.25, 0.28, and 1.28, respectively. Although the Al/Si ratio detected in C-S-H of B50-3 is the highest among the four samples, the increasing

speed slows down due to the replacement of MK by NC, which has lower Al_2O_3 content and higher content of amorphous silica than MK. As shown in Fig. 5.6-d, the C-S-H of B50-3 yields an Al/Si ratio of 0.49, and the Ca/Si ratio is 14.94% and 24.95% lower than those of B30-1 and PC, respectively.

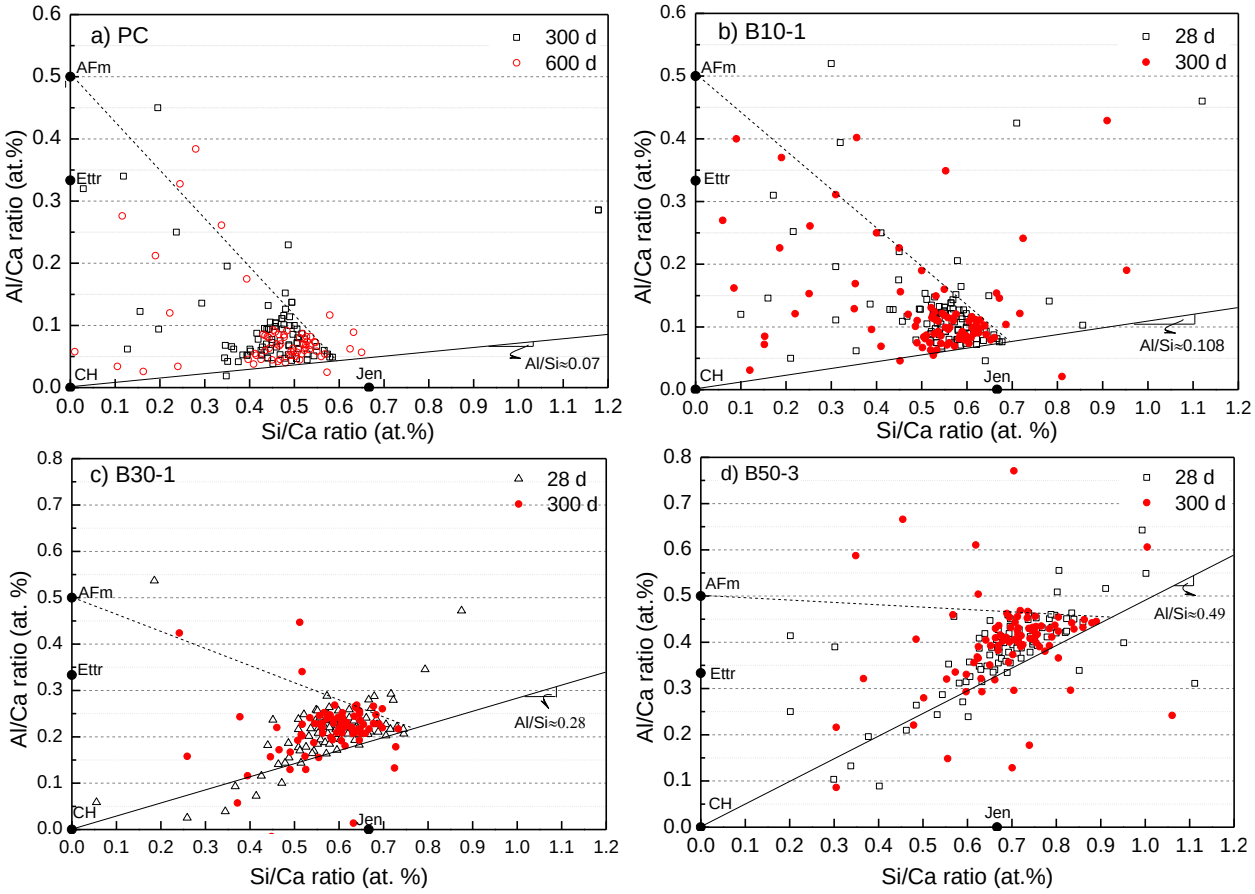

* CH-Calcium Hydroxide; Jen-Jennite; Ettr-Ettringite; AFm-Alumina-Ferric oxide-mono-sulfate

Figure 5.6: Plot of Al/Ca as a function of Si/Ca ratios (in atomic percentage) of the EDX points analysis obtained on selected samples with 15 kV (1 µm) focused on hydrate phases

5.3.5 Compressive strength

For the blended systems, parabolic isoresponse curves were obtained at 1, 7, 14 and 28 days to characterize the maximum compressive strength achieved by a replacement of Portland cement by MK (0-50 wt.%), NC (0-5wt.%) and a combination of the two (Fig. 5.7). The maximum 1-day

compressive strength, which was 6.55% higher than the strength of PC, indicated by the stationary point was obtained for the replacement of 10% MK. And the zone outlined by the 41 MPa iso-line showed that the same strength level can be achieved by combinations with MK between 4% and 12% and 0.3% or less nanoclay. B10-2, which contains 9% of MK and 1% of NC, also had a compressive strength close to that of PC. The result shows that 10% partial replacement of cement by MK or the combinations of 1% or less NC and MK improves the early strength of cement based composites. The optimal 7-day compressive strength was achieved by B10-2 (PC with 9% MK and 1% NC). At 14 days, among the samples, B30-1 yielded the highest compressive strength, which was 14.53% greater than that of PC. From the iso-line, it can also be seen that the partial replacement of PC by combinations of 25 % or less MK and 1.5% or less nano clay achieved the same strength as PC. Actually the strengths of B10-1 and B30-2 were 1.82% and 2.13% higher than that of PC. However, the compressive strength of this blend decreased with the increase of MK and NC at higher replacement levels. The effect of NC on strength was detected noticeably at 28 days. Compared with the 14-d strength, the peak value of compressive strength was achieved by a composition with the same MK content but higher replacement by NC.

The weight of the samples decreased with increasing MK and NC substitution at each age, therefore the isoresponse curves for specific strengths are similar as those for compressive strengths but tend to reach peak values with higher MK and NC contents. From Fig. 5.8, it can be seen that the maximum 1d specific strength was reached by B10-1, as the case for compressive strength. At 7 days, unlike the compressive strength, the specific strength of PC was lower than that of B10-1 and the sample with 1wt.% NC replacement of cement by NC. The optimal specific strength was obtained with B10-2, however, the isorespone of 0.026 N-m/kg indicates that the same strength can also be obtained with a replacement of cement by 20 or 25 wt.% MK combined

with 0.5-1.0 wt.% NC. The differences between 14 day and 28 day strengths not only indicate the enhancing role of NC after early age of the hardening process, but also show the effect of MK and NC on the decline of matrix density.

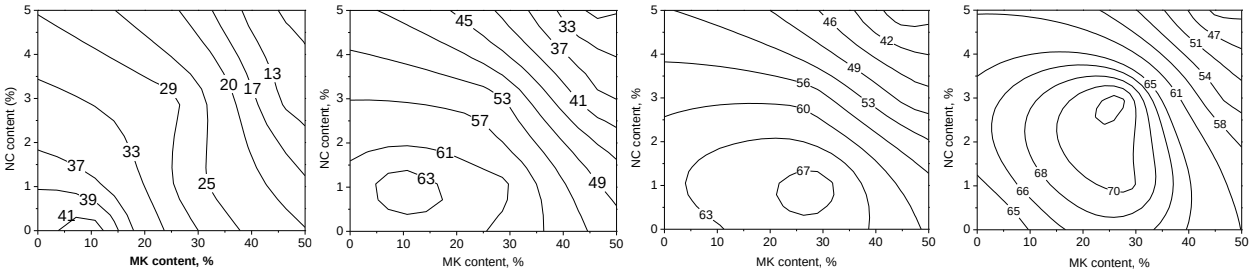

Figure 5.7: Isoresponse curves for compressive strength (MPa).

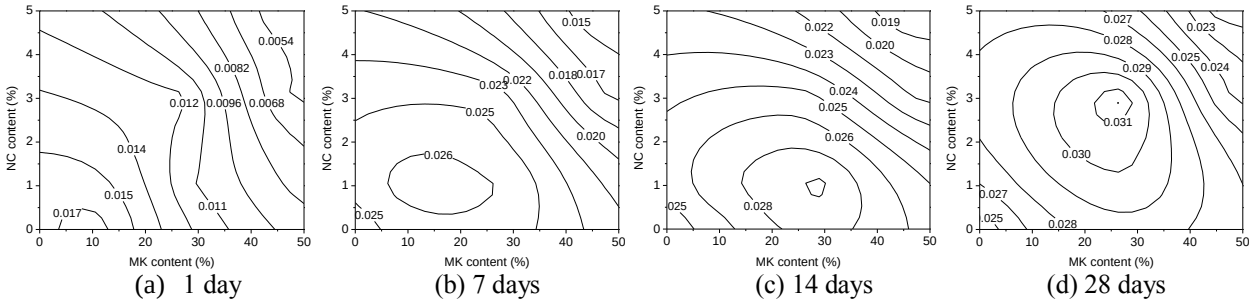

Figure 5.8: Isoresponse curves for specific strength (N-m/kg)

Fig. 5.9 shows the calculated compressive and specific strength ratios at each curing age. It can be seen that the compressive strength of B10-1 was higher than that of PC at each curing age, and B10-2 showed a higher strength than B10-1 after 7 days. Although the 1 day strength of B30-1 was much lower than that of PC, it experienced a sharp rise at early age and yielded a higher strength than PC after 7 days. Due to the low Al_2O_3 content but higher amorphous silica amount of NC, B30-2 did not reach the 1-day strengths of B30-1 and PC until 28 days. The 28 days strength of B50-1 was similar to that of PC, however, the strength decreased with increasing replacement of MK by NC. Compared with the regular compressive strength, the specific strengths of B10 and

B30 blends exceeded that of PC at early age (7 days of curing), and B50-1's specific strength exceeded that of PC at 14 days. Although B50-2 still had a lower strength than B50-1, it reached a similar specific strength as PC at 28 days. Both the optimal 28 day compressive strength and specific strength were obtained by B30-2.

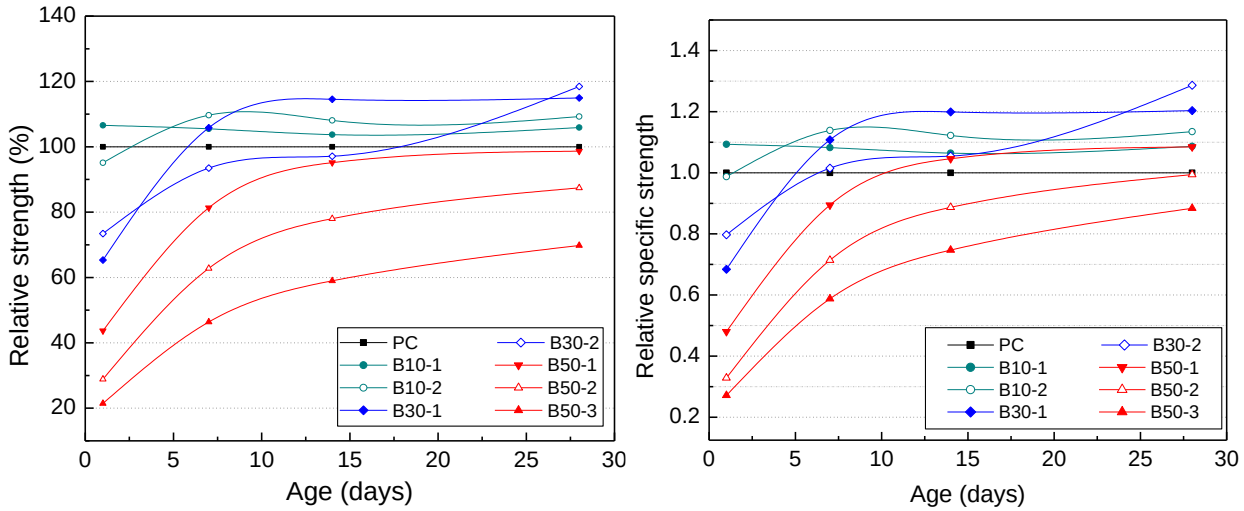

(a) Relative strength (b) Specific strength

* The relative strength ratiod were calculated according to Eq. (2.1) in Chapter 2.

Figure 5.9: Relative and specific strengths of the examined cements as functions of curing age

3.5 Interfacial bond strength and energy between fiber and matrix

Under tension, natural fiber reinforced cement composites fail by a combination of fiber fracture and pull-out (Campbell and Coutts 1980, Coutts and Kightly 1982). The final mechanical behavior of a composite material depends to a great extent on the adhesion between the reinforcing fiber and the surrounding matrix (Benzerzour, Sebaibi et al. 2012). Fig. 5.10-a shows the effect of binary blend of MK and NC on the interfacial bond strength between sisal fiber and the cement matrix. It can be seen that bond strength increases with the increasing replacement of PC by MK up to 30 wt. %, then gradually decreases. PC gave the lowest interfacial bond strength of 0.321 MPa, and B10-1, B10-2 provided 29.60% and 48.27% greater bond strength than neat PC. The

maximum bond strength between sisal fiber and matrix (0.743 MPa) was achieved by B30-2, which increased the strength by 131.46%. B30-1 and B50-1 also gave considerable enhanced bond strengths, which were 102.80% and 117.13% higher than that of PC. As MK and NC increased further, cement was diluted and the degree of flocculation was reduced as evidenced by the decrease of compressive strength. Therefore, B50-2 and B50-3 matriceshad lower bond strength than B30-2.

A similar trend can be found in the pull-out energy as shown in Fig. 5.10-b. The average pull-out energy obtained in this study ranged between 6.31×10^{-3} N•m for PC and 18.7×10^{-3} N•m for blend B30-2 which constitutes an increase of 196.35%. B50-1 also shows a substantial improvement. The pullout energy provides a better measure of interfacial properties than the fracture energy of fiber-reinforced cement-based materials (Benzerzour, Sebaibi et al. 2012). Therefore, it can be predicted that B30-1 and B50-1 with their high matrix compressive strength and considerable interfacial bond with sisal fiber, will yield higher flexural properties than other blends.

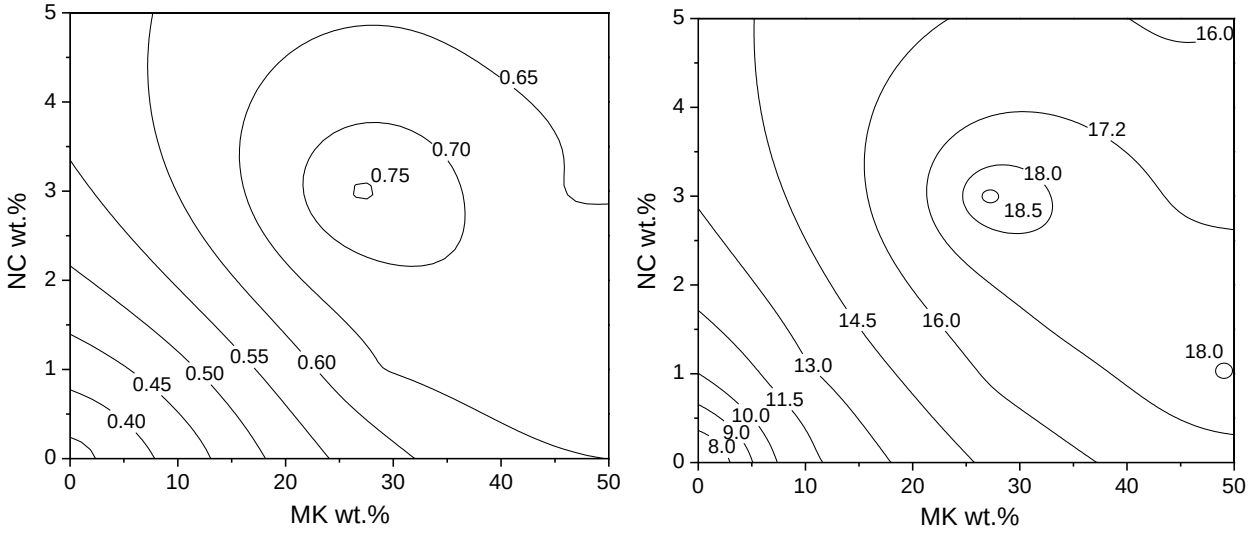

(a) bond strength (b) pull-out energy

Figure 5.10: Isoresponse curves for bond strength (MPa) and pull-out energy (N•mm × 10^{-3})

5.3.6 Determination of accelerated aging conditions

Fig. 5.11 shows the hysteresis curves of mass change as a function of duration in wetting and drying cycles for each blend. It can be seen that the saturation of PC and B50 samples took about 5 h, while samples of B10 and B30 needed more time (up to15 h). Similar results were obtained for drying. In order to subject each sample to the same aggressive treatment, a duration of 42 h was selected for each wetting and drying cycle: 15 h immersion in tap water at 70 ºC and 25 h drying in an oven at 70 ºC, with 1 h air drying under 23 ºC and 10% humidity between each half-cycle.

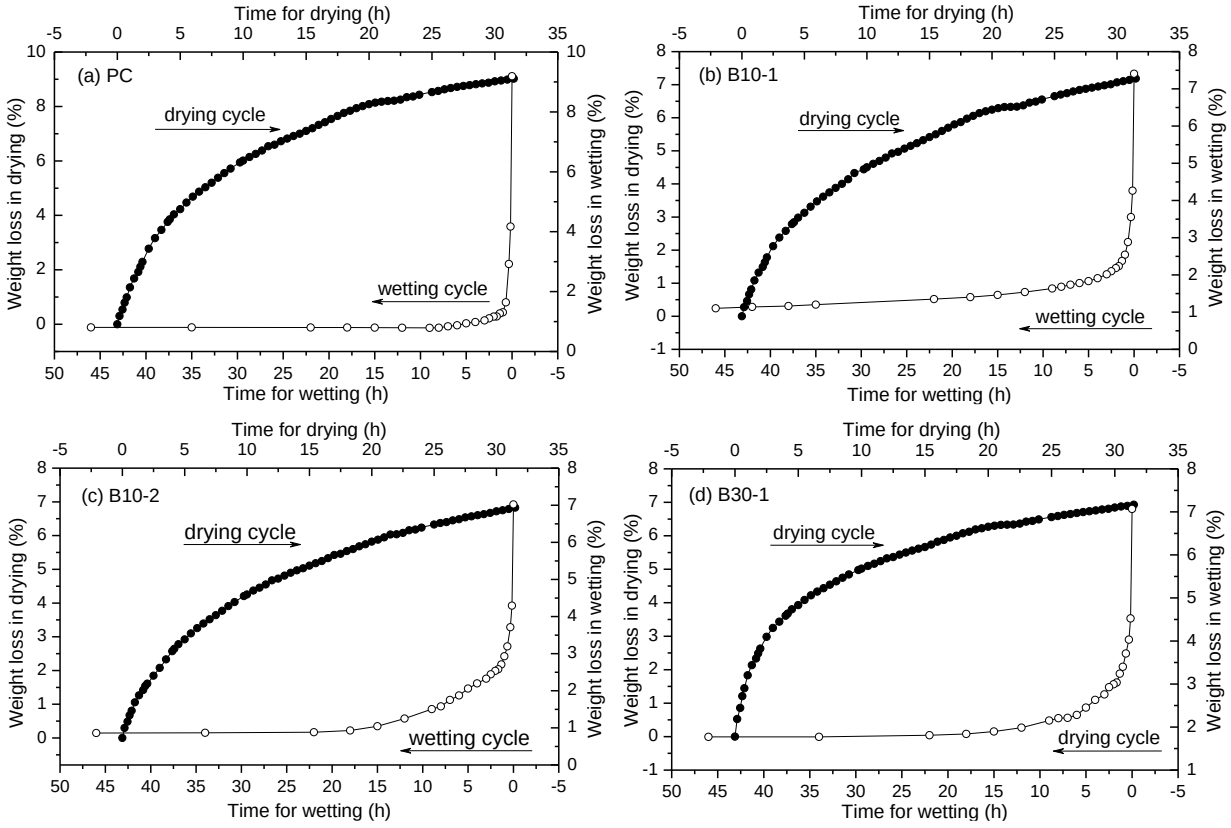

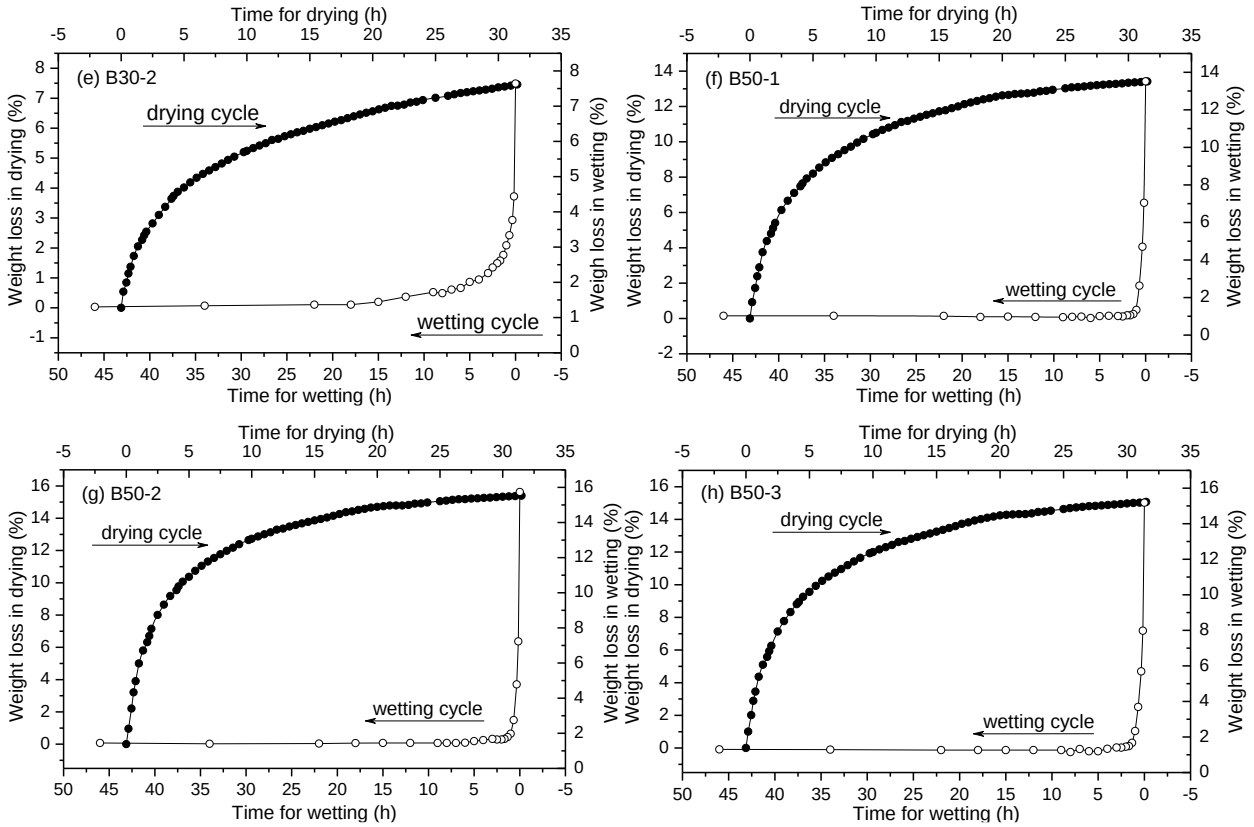

Figure 5.11: Weight loss of samples subjected to the first wetting and drying cycles

5.3.7 Durability of composites

ASTM C-1018 and ASTM C1185-08(2012) were followed to evaluate the reinforcing effect of sisal fiber and the simultaneous substitution of MK and NC for PC by determining the load-deflection curves after a certain number of wetting and drying cycles. Fig. 5.12 illustrates typical load-deflection curves of each blend after 0, 5, 15, 30, and 50 wetting and drying cycles. Overall, the composites reinforced with the sisal fibers exhibited superior mechanical properties and ductile behaviour. However, due to the increasing replacement of cement by MK and NC, the peak loads and the corresponding deflections ς_{max} increased at first and then gradually decreased. Therefore, the post cracking shoulders became broad at first and then narrow after B30-2. It can be seen that the flexural strength and toughness of sisal fiber reinforced PC samples encountered the sharpest decline with increasing numbers of cycles. After 15 wetting and drying cycles, the post-cracking

toughness was almost non-existent. With the increasing level of cement replacement by MK and NC, the decrease of flexural properties was effectively slowed down. Although B30-2 yielded an optimal flexural strength and toughness among the samples before aging, its durability declined much more rapidly than that of B50 blends. In the B50 series, the durability increased with increasing replacement of MK by NC, which is opposite to the initial flexural properties of the samples before aging. Therefore, the combined partial substitution of MK and NC for Portland cement not only increases the initial mechanical properties of sisal fiber reinforced cement mortar, but also significantly improves the durability of the composites by reducing the alkaline degradation of the fiber in modified matrices.

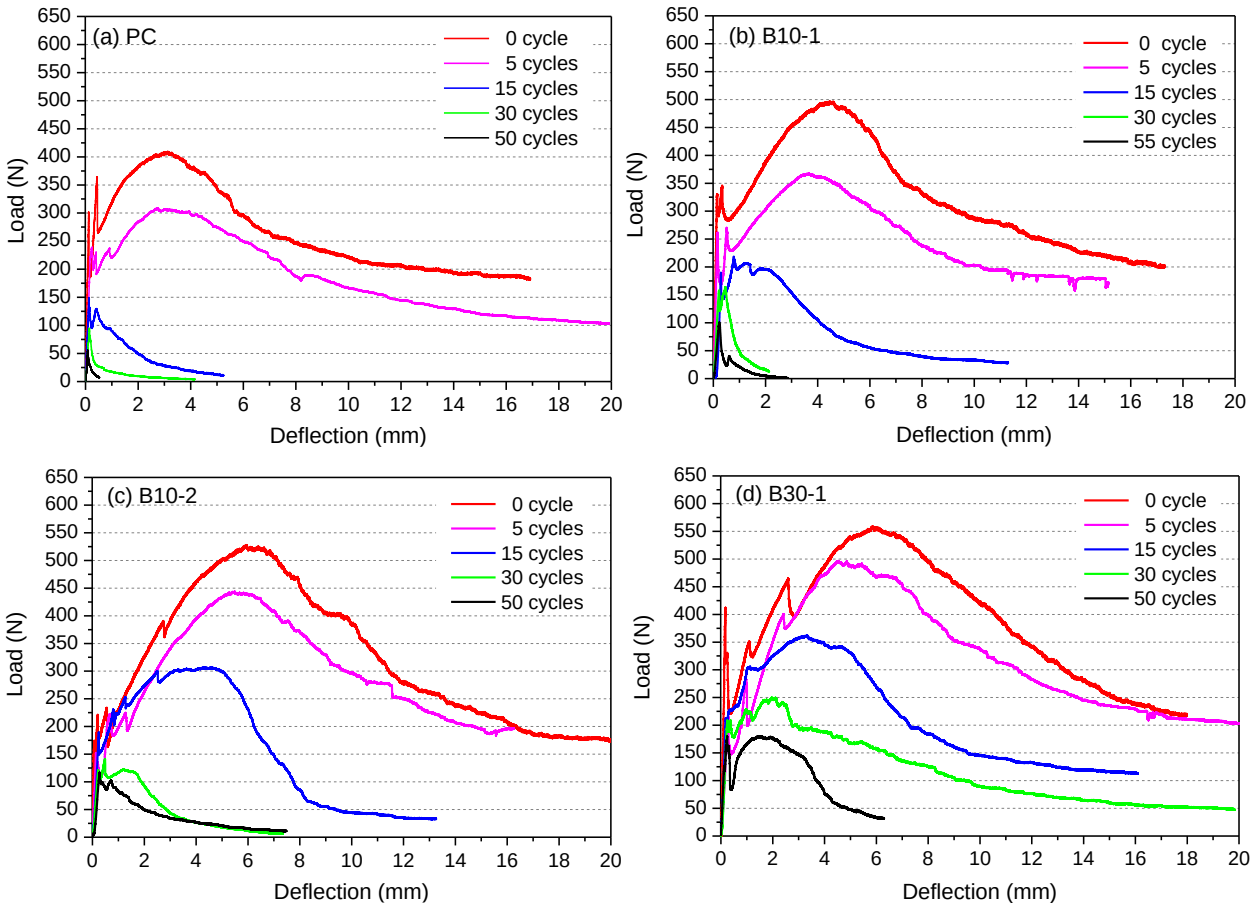

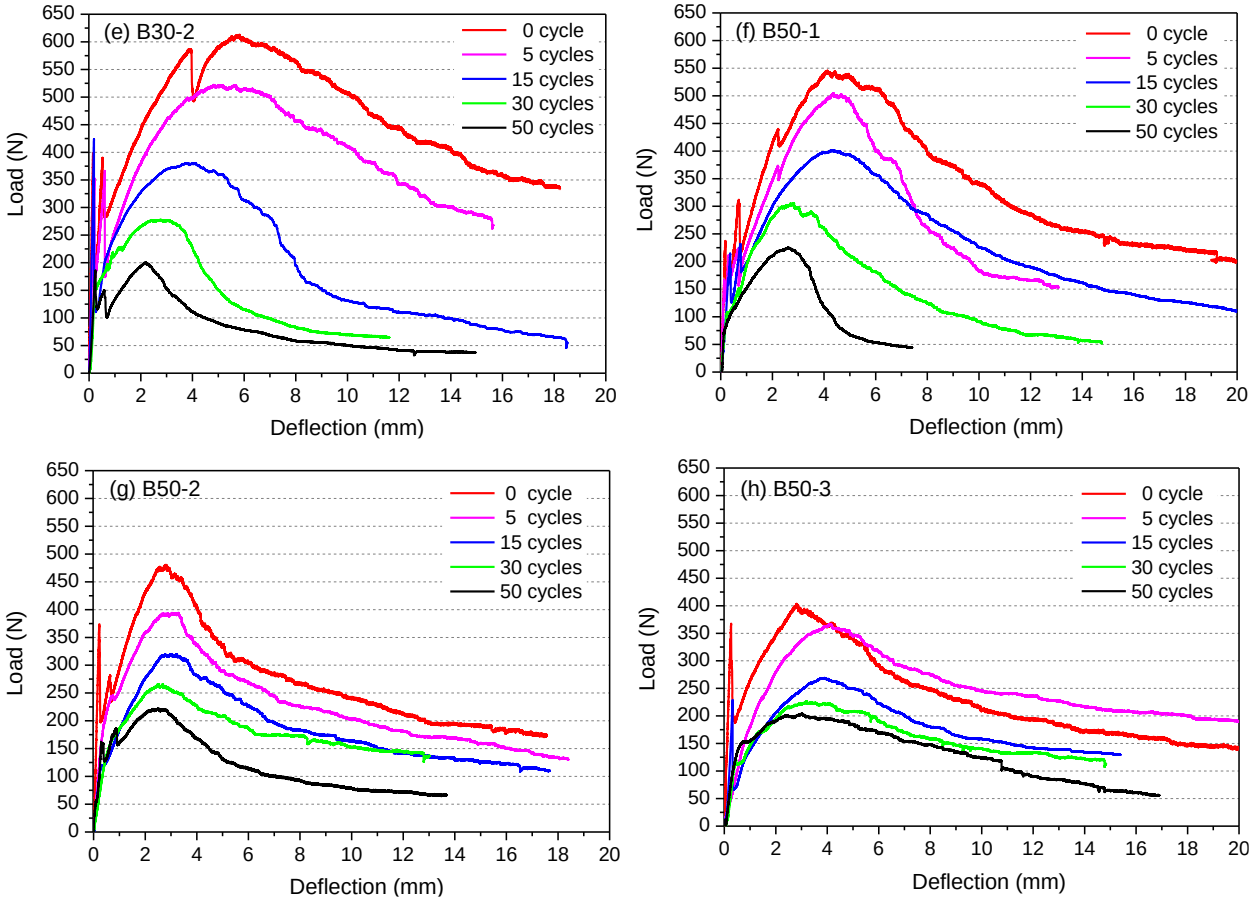

Figure 5.12: Typical load-deflection curves (one selected for each data point) for the blends subjected to cycles of wetting and drying

Fig. 5.13 shows the post-cracking strength and toughness of the samples subjected to increasing numbers of wetting and drying cycles. The post-cracking strength σ_p increased at first and then gradually decreased with increasing replacement of PC by MK and NC. B30-2 yielded the maximum peak strength, which was 49.7% greater than that of PC. B10-1, B30-1, B50-1, and B50-2 exhibited 21.20%, 36.46%, 33.31%, and 17.38% greater post-cracking strength than fiber reinforced PC, respectively. However, B50-3 yielded a 1.47% lower post-cracking strength than PC. A similar trend was also detected for the post-cracking toughness. B30-2 showed a 77.71% greater toughness, and the toughness of B50-1 and B50-2 were 35.44% and 3.99% greater than that of PC. However, B50-3, which contained the maximum NC amount, exhibited a poor ductile

behaviour. Although MK and NC exhibited high pozzolanic activity and CH reducing effect in the cement matrix, they decreased the matrix strength and interfacial adhesion between sisal fiber and the matrix at high cement replacement levels. The difference between B30-1 and B30-2, and that between B50-1 and B50-3 show that NC also contributes to the improvement of the post-crack strength σ_p and toughness T_p. But for samples with 50 wt. % replacement of PC, the toughness T_p decreased with increasing NC.

For the samples exposed to wetting and drying cycles, MK and NC are contributing to the remaining strength and toughness. Among all samples, the sisal fiber reinforced PC encountered the most severe drop: after 5, 15, 30 and 50 cycles, the post-cracking strength decreased by 24.72%, 68.34%, 86.52% and 91.91%, respectively. After 50 cycles, B30-2 showed a post-cracking strength of 4.17 MPa, which was 67.34% less than its initial strength. The ultimate strength of B30-2 was also lower than those of B50-1, B50-2 and B50-3 after the same number of cycles, which were 58.74%, 53.85%, and 49.42% lower than the corresponding initial strength, respectively. A considerably better improvement of durability was indicated by the post-cracking toughness of the samples. After 50 wetting and drying cycles, sisal fiber reinforced PC, B10-1, B10-2, B30-1, B30-2, B50-1, B50-2, and B50-3 encountered toughness reductions of 99.08%, 99.26%, 95.33%, 89.56%, 84.31%, 81.61%, 64.61% and 48.41%, respectively. Although B50-3 exhibited poor initial flexural properties, it maintained both the post-cracking strength and toughness more effectively, and therefore showed the best durability among all samples. By comparing strength and toughness of initial and aged samples, it can be concluded that the best mechanism to improve sisal fiber's durability in blends is to restrain the fiber degradation by reducing the CH content in the matrices, which leads to both the alkaline hydrolysis and mineralization of natural fibers.

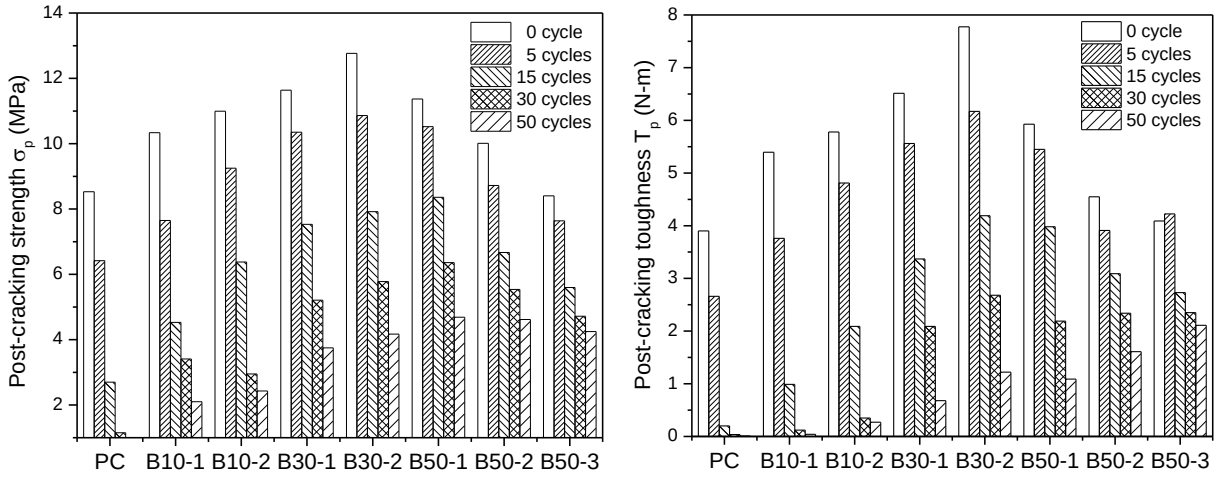

Figure 5.13: Post-cracking strength and toughness of blends subjected to wetting and drying cycles

In Fig. 5.14, the effects of replacing PC by a combination of MK and NC on T_{max} and $T_{0.5}$ of samples before and after aging are presented. Like the post-cracking strength and toughness of samples before exposure to cycling, the two deflection indices increased first and then gradually decreased with increasing MK and NC substitution. The maximum initial T_{max} and $T_{0.5}$ were obtained by B30-2, which were 38.66 and 109.09, respectively. Unlike samples of the B10 and B30 blends, both the deflection indices of B50 samples experienced sharp declines with increasing replacement of MK by NC. The PC reinforced with sisal fiber yielded an initial T_{max} of 25.80 and $T_{0.5}$ of 82.02, which were 33.26% and 24.81% lower than the corresponding optimal values, but similar to those of B50-3. The results in Fig. 5.14 also indicate that in this study T_{max} and $T_{0.5}$ are more sensitive to the aggressive environment than post-cracking strength and toughness. After 30 cycles of wetting and drying, the maximum loads of sisal fiber reinforced PC and B10-1 equal the first cracking load. After 50 cycles, the two deflection indices of PC dropped by 96.12% and 98.70%, respectively. The maximum ultimate T_{max} and $T_{0.5}$ were obtained by B50-1 and B30-2, which are 11.35 and 12.38 times those of PC, respectively. Among the samples, sisal fiber

reinforced B50-3 samples encountered the least decrease of $T_{0.5}$, which constitutes the best improvement of durability.

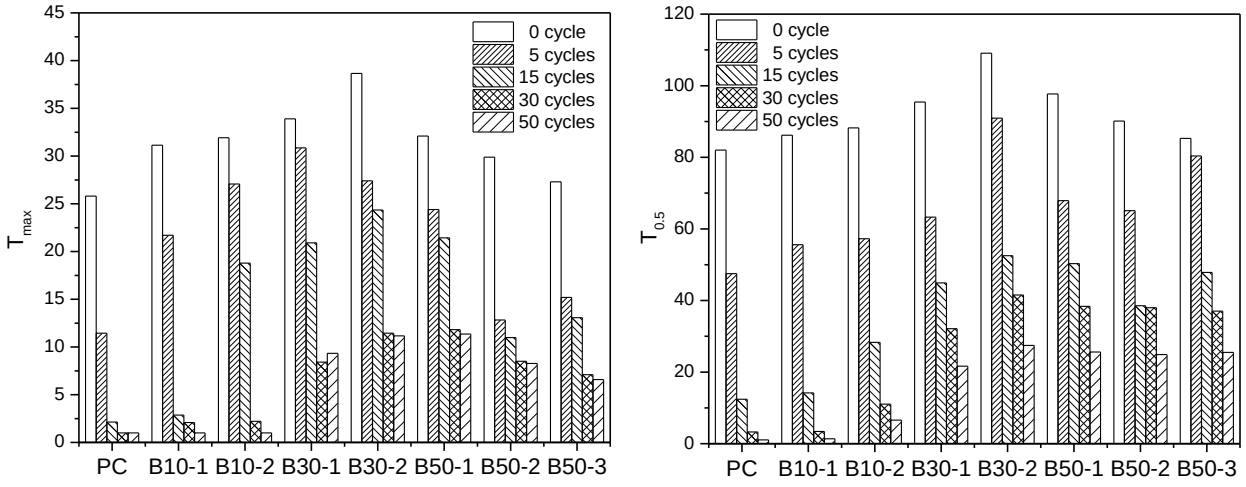

Figure 5.14: T_{max} and $T_{0.5}$ for the blends subjected to cycles of wetting and drying

The toughness indices I_{30} and I_{55} calculated from the load-deflection curves are shown in Fig. 5.15, which illustrates the beneficial effects of MK and NC on durability of SFRCC very clearly. PC exhibited the lowest initial I_{30} and I_{55} values and suffered the most severe declines when exposed to wetting and drying cycles. That means it has the worst durability of all cement blends studied here. B50-1 yielded the maximum values of I_{30} and I_{55} at each aging stage, but B50-2 and B50-3 exhibited the lowest rate of degradation for I_{30} and I_{55}, respectively. After 50 wetting and drying cycles, due to the poor durability, there was no residual I_{30} for sisal fiber reinforced PC and B10-1, and no residual I_{55} for PC, B10-1 and B10-2. The ultimate values of I_{30} for B10-2, B30-1, B30-2, B50-1, B50-2, and B50-3 were 19.1, 50.18, 55.89, 64.76, 63.2, and 57.7, which were 73.80%, 34.14%, 35.33%, 42.84%, 32.10%, and 34.10% lower than the initial values, respectively. The I_{55} toughness values for B30-2, B50-1, and B50-3, which exhibited higher ultimate values than the rest of the other samples, decreased by

43.93%, 35.62%, and 27.59%, respectively. By comparing the highest I_{30} and I_{55} values (B50-1), and the lowest rates of decline for I_{30} and I_{55} (B50-2 and B50-3), it can be concluded that a high level of combined substitution of MK and nanoclay NC for Portland cement can improve the durability of SFRCC significantly.

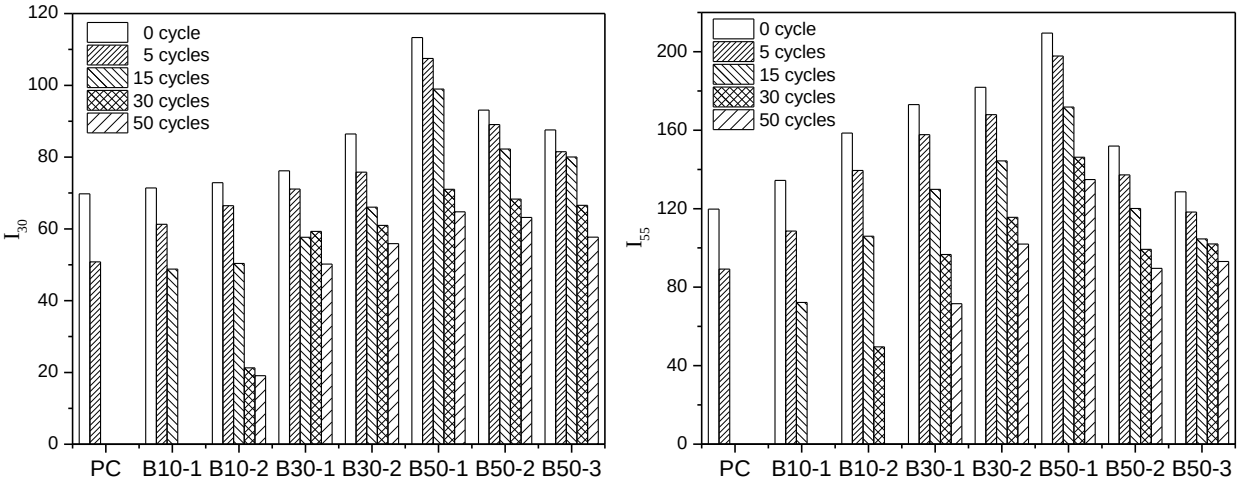

Figure 5.15: I_{30} and I_{55} for each blend subjected to wetting and drying cycles

5.3.8 Characterization of fiber degradation

5.3.8.1 Tensile behaviour of sisal fiber

Beside the flexural properties of SFRCC, the tensile properties of fibers embedded in the matrices subjected to identical aging conditions and durations were tested to evaluate the durability and fiber degradation rate directly. Compared with the mechanical properties of the composites, the direct testing of fiber behaviour in tension provides a better measure of the durability of fiber, because it is not affected by degradation of the cement matrix and the decline of adhesion between the reinforcing fiber and the surrounding matrix. Fig. 5.16 shows the Weibull plots and the corresponding regular residual of each sample after 5 and 30 cycles of wetting and drying. It

indicates that the Weibull distribution analysis of tensile strength showed a good fit with the experimental data evidenced by R^2>0.93. The distribution of test data was first more scattered and then gradually concentrated with the decreasing strength. Although with non-homogeneous structures, the raw sisal fiber showed a relatively high degree of concentration of test data owing to its high tensile strength. After 5 wetting and drying cycles, due to the encounter of serious attack of the fibers in a PC matrix, the tensile test results of fibers presented a low degree of concentration. However, the data of fibers embedded in PC after 30 cycles showed a high concentration because of the low tensile strength. This demonstrates that all fibers experienced severe degradation at this aging stage. On the other hand, the opposite was true for samples embedded in B30 and B50 matrices: the concentration after 5 cycles was much higher than that after 30 cycles. This indicates that the degradation of sisal fibers embedded in these matrices was considerably slowed at an early stage of aging and the fibers partially degraded, while the other fibers remained still intact later in the aging process. At each age, the Weibull modulus decreased with increasing replacement of MK by NC, which displayed lower pozzolanic activity at early age and higher CH reducing effect than MK due to the high SiO_2/Al_2O_3 ratio. Through the comparison of data concentration, the influence of the combination MK and NC on the degradation rate of sisal fiber in a cement matrix was confirmed.

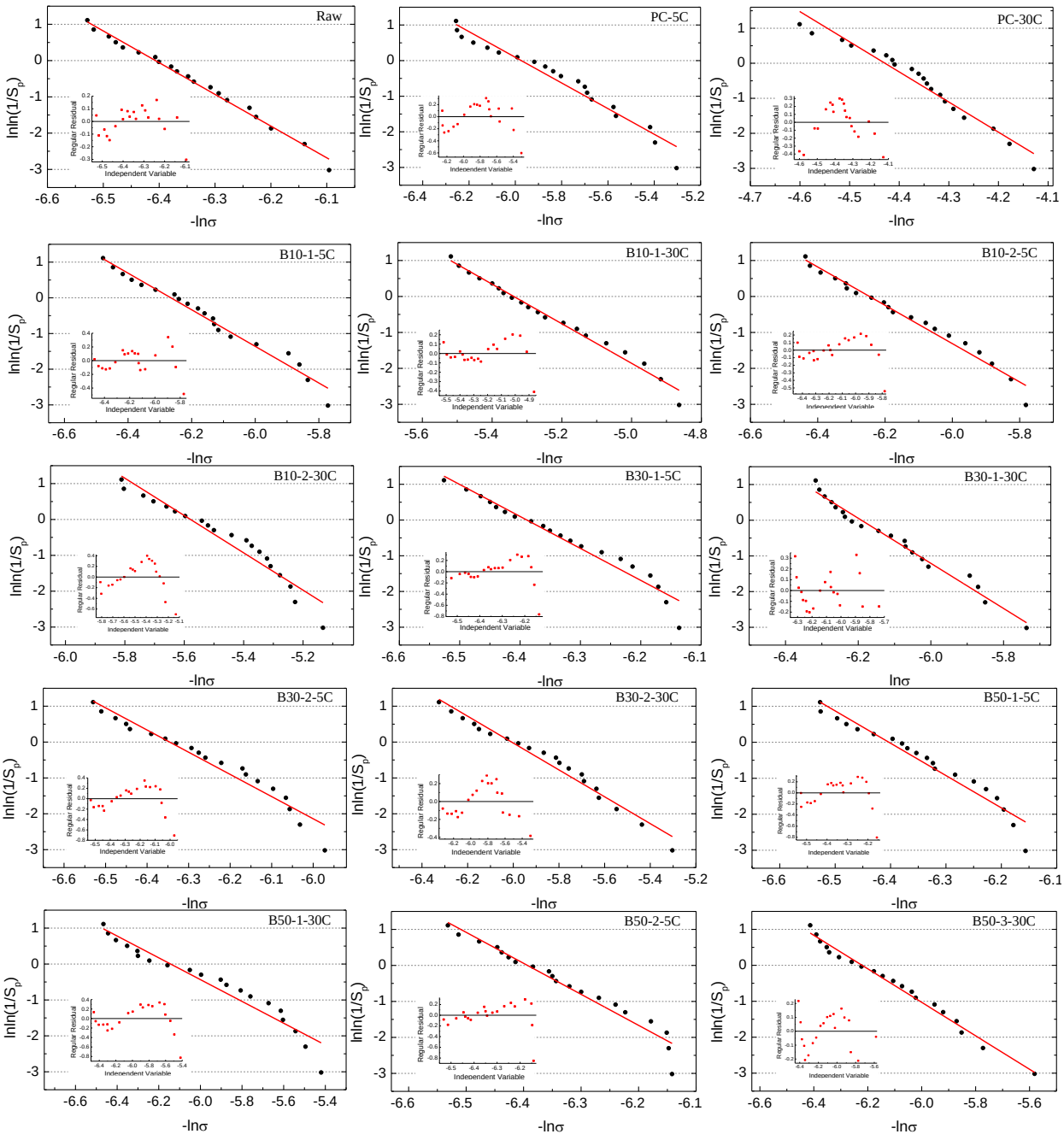

Figure 5.16: Weibull plots of raw and embedded fibers after 5 and 30 wetting and drying cycles

Table 5.1 shows the Weibull parameters calculated from the data of Fig. 5.16 and the tensile modulus, which can be used to estimate the deformability of sisal fibers. The data of Weibull modulus and characteristic strength show consistency in the analysis of the plots above: the raw

fiber had a maximum tensile strength of 605.88 MPa, while the strength of embedded fibers was lower due to the varying levels of alkaline attack in cement based matrices. The fibers embedded in PC encountered the most severe alkaline hydrolysis and mineralization evidenced by the lowest strength and maximum Young's modulus. Compared with the raw fibers, the strength and deformability of fibers in PC decreased by 35.11% and 10.77% after 5 wetting and drying cycles, and 86.17% and 22.13% after 30 cycles, respectively. The tensile strength of the embedded fibers increased with increasing replacement of PC by MK and NC at each aging stage due to their significant CH reducing effect as shown in Fig. 5.5. However, as analyzed above, due to lower aluminate amount and higher silicate content than MK, NC provides a delayed beneficial effect on durability of sisal fiber. After 5 cycles of wetting and drying, B50-1 reached the maximum tensile strength, which was 53.53% greater than that of fibers embedded in PC and was similar to the strength of raw fiber. Although the tensile strength decreased with increasing amount of NC at early aging stages, the deformability of fibers did not change by much, especially for the B50 series. After 30 wetting and drying cycles, the effectiveness of NC was demonstrated as the fibers embedded in the matrix of B50-3 yielded the maximum tensile strength and the best deformability, which were 500.36% and 19.15% greater than those of fiber embedded in PC. Compared with the raw fiber, the matrix of B50-3 reduced the strength and deformability of sisal fiber by only 16.94% and 7.22%, respectively, after 30 wetting and drying cycles. The results indicate that both MK and NC significantly slow down the degradation of sisal fiber in a cement matrix by reducing both the alkalinity and CH content of cement due to their high pozzolanic activity. The combination of these two supplementary cementitious materials validates their complementary and synergistic effect at different stages of aging.

Table 5.1: The Weibull parameters and deformability of sisal fibers in tensile test

Curing or Exposure duration	Samples	Weibull Modulus, m	R^2	Characteristic Strength, σ_0 (MPa)	Young's modulus, E (GPa)
-	Raw fiber	8.74	0.9893	605.88	15.41
5 cycles	PC	3.60	0.9546	393.15	17.27
	B10-1	5.13	0.9730	525.96	16.42
	B10-2	5.33	0.9752	516.05	16.51
	B30-1	8.95	0.9539	595.13	15.64
	B30-2	6.19	0.9453	570.05	15.73
	B50-1	8.98	0.9416	603.62	15.57
	B50-2	8.62	0.9486	597.79	15.59
	B50-3	8.57	0.9503	581.39	15.58
30 cycles	PC	8.60	0.9538	83.82	19.79
	B10-1	5.50	0.9846	208.07	17.73
	B10-2	5.20	0.9318	264.75	17.54
	B30-1	6.00	0.9149	385.02	17.32
	B30-2	3.74	0.9704	405.71	17.03
	B50-1	3.03	0.9288	465.45	16.79
	B50-2	4.72	0.9507	479.72	16.66
	B50-3	4.66	0.9858	503.22	16.61

5.3.8.2 Crystallization

The crystallinity indices of sisal fibers were determined by means of X-ray diffraction. Fig. 5.17 shows the XRD patterns of the raw sisal fiber and the fiber embedded in each blend subjected to 5, 15 and 30 wetting and drying cycles. It can be seen that due to the amorphous components, the sisal fiber is semi-crystalline.

The results also indicate that sisal fiber's crystallization mainly depends on cellulose, which presents an intensive peak at $2\theta \approx 22.5^{\circ}$ corresponding to its (002) lattice plane and a broad peak ranging from 13º to 18º corresponding to the $(\bar{1}10)$ and (110) lattice planes. The peaks of calcium hydroxide (18º and 34º) are present on curves of fiber embedded in a PC matrix and those embedded in other blends after 5 and 15 cycles of wetting and drying. Therefore, the CH

precipitation of sisal fiber in PC occurred much earlier than in other blends, which led to the increase of fiber embrittlement. In addition, the fiber pulled-out from series of B30 and B50 blends showed larger amounts of cement hydration products, such as ettringite, $CaCO_3$, C_2S, and C_3S, which points to a better interfacial bond between fiber and the matrix in these blends than that in pure PC. Due to the high amount of MgO in nanoclay, diffraction peaks of MgO phase (43º) were identified with a low intensity in blends of B30 and B50, especially the B30-1 and B50-3 after 15 and 30 wetting and drying cycles. Compared with the raw sisal fiber, the embedded fibers show recognizable peaks with higher intensity at each aging step, due to the decomposition of amorphous components (lignin and hemicellulose) in the alkaline environment of blends, especially the matrix of neat cement. After 30 cycles of wetting and drying, the main peaks of sisal fiber embedded in pure cement show the highest intensity, which means that the fiber encountered the most serious attack in PC, which contains the highest CH content as shown in Fig. 5.5.

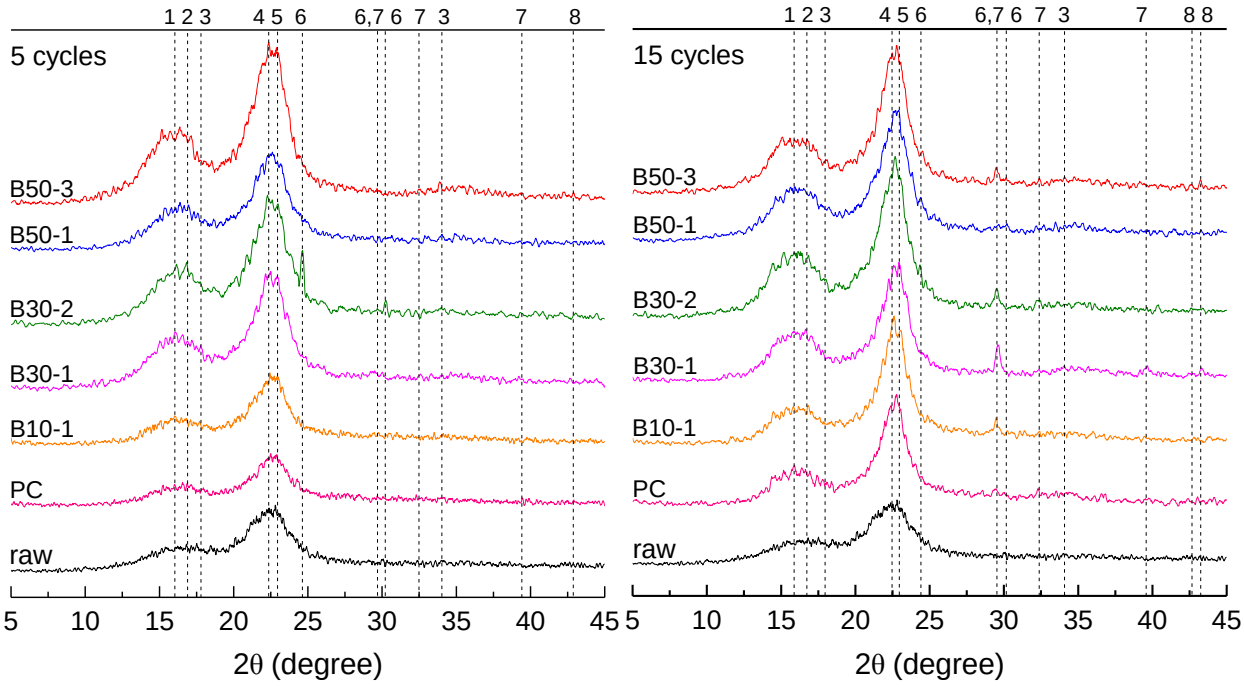

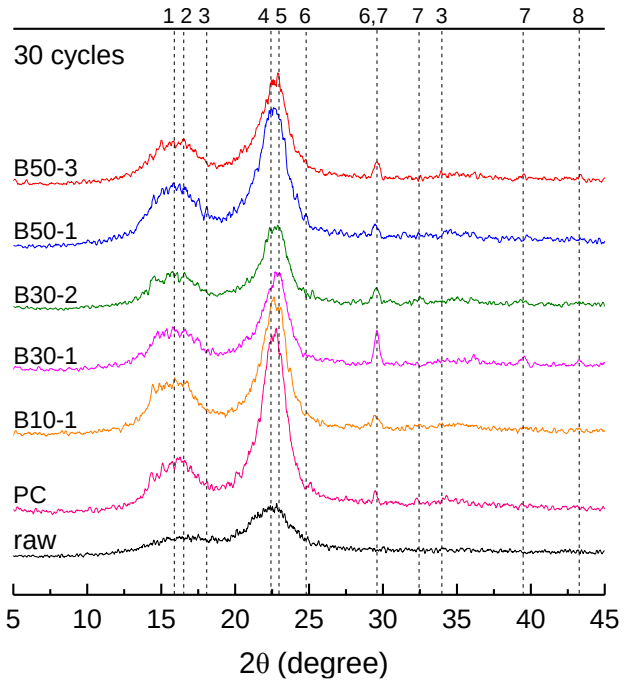

* 1, 2, 4: cellulose crystallographic plane ($\bar{1}10$), (110) and (002); 3: $Ca(OH)_2$; 5: ettringite; 6: $CaCO_3$; 7: C_2S, C_3S; 8: MgO.

Figure 5.17: XRD patterns of sisal fibers embedded in each blend after 5, 15, and 30 wetting and drying cycles compared to the raw fiber

The crystallinity index (Cr.I.), percentage of crystallinities (%Cr), and crystallite size (L), calculated from the corresponding diffraction peaks and FWHMs using the deconvolution method, are summarized in Table 5.2. Although it is affected by non-uniform strain, crystalline disorder, and some other uncertain factors, it still can be seen that the crystallite sizes for the two major peaks of embedded fiber are bigger than those of raw sisal fiber, and increase with aging duration. The removal of amorphous components is the main reason for the enhanced crystallite size of natural fiber (Sinha and Rout 2009), and it can also lead to the increase of the crystallinity index and percentage of crystallinities.

Table 5.2: Calculated crystalline parameters of sisal fiber

Curing or Exposure duration	Samples	Peak position (2θ)	FWHM(β) (2θ)	L (nm)	%Cr	Cr.I.
-	Raw fiber	16.68 22.41	4.58 3.69	1.73 2.17	77.67	0.7126
5 cycles	PC	16.61 22.56	4.11 3.37	1.93 2.38	79.70	0.7553
	B10-1	16.59 22.48	4.28 3.19	1.86 2.51	81.00	0.7655
	B10-2	16.57 22.50	4.31 3.23	1.84 2.48	81.03	0.7663
	B30-1	16.42 22.47	4.36 3.17	1.82 2.53	79.54	0.7427
	B30-2	16.46 22.50	4.06 3.35	1.80 2.39	79.69	0.7452
	B50-1	16.53 22.48	4.38 3.25	1.81 2.4	79.45	0.7414
	B50-2	16.32 22.45	4.41 3.26	1.80 2.46	79.51	0.7516
	B50-3	16.14 22.41	4.42 3.28	1.79 2.44	79.69	0.7608
15 cycles	PC	16.46 22.56	4.37 2.64	1.82 3.03	85.29	0.8276
	B10-1	16.53 22.61	4.10 2.29	1.94 3.50	85.17	0.8258
	B10-2	16.51 22.56	4.33 2.30	1.83 3.48	85.20	0.8249
	B30-1	16.21 22.63	4.04 2.53	1.96 3.17	84.41	0.8153
	B30-2	16.15 22.52	4.35 2.73	1.82 2.93	84.29	0.8139
	B50-1	16.36 22.59	4.29 2.75	1.85 2.91	84.13	0.8113
	B50-2	16.30 22.57	4.34 2.67	1.83 3.00	83.69	0.8109
	B50-3	16.21 22.56	4.47 2.60	1.78 3.08	83.37	0.8101
30 cycles	PC	16.47 22.59	4.58 2.30	1.73 3.48	86.76	0.8474
	B10-1	16.08 22.61	4.14 2.38	1.92 3.37	85.73	0.8336
	B10-2	16.12 22.60	4.16 2.40	1.91 3.34	85.65	0.8321
	B30-1	16.19 22.69	4.13 2.42	1.92 3.31	84.61	0.8181
	B30-2	16.11 22.64	4.12 2.44	1.93 3.28	84.37	0.8147
	B50-1	16.16 22.53	4.35 2.69	1.82 2.98	84.25	0.8119
	B50-2	16.16 22.57	4.29 2.67	1.85 3.00	83.81	0.8115
	B50-3	16.18 22.60	4.25 2.63	1.88 3.05	83.60	0.8110

As shown in Table 5.2, the raw sisal fiber has the lowest values of both, crystallinity index and percentage of crystallinities. Due to the alkaline hydrolysis of the amorphous components (lignin and hemicellulose) both parameters increase with age. After 5 wetting and drying cycles, B10-2 presented the maximum percentage of crystallinities and crystallinity index, which were 4.33% and 7.54% greater than those of raw fiber. Both %Cr and C.I. decreased with increasing replacement of PC. On each level of substitution, the replacement of MK by NC enhanced these two crystalline parameters. After 15 wetting and drying cycles, the fibers embedded in PC showed the highest indices among all samples. The percentages of crystallinities and crystallinity index were increased by 9.81% and 16.14% for 15 cycles, and 11.70% and 19.92% for 30 cycles, respectively. Although the two parameters of blends with high amounts of supplementary cementitious materials were enhanced, it is in contrast to the results obtained after 5 cycles that NC took a more active role in reducing the degree of fiber crystallinity. Due to the high amount of Al_2O_3, MK displayed a higher pozzolanic reactivity (as shown in Fig. 5.1) and slowed down the fiber degradation significantly at early age. The high amount of silicon minerals promotes the NC's complementary effect on reducing the alkalinity of the matrix for a long duration and therefore mitigates the corrosion of sisal fiber in the cement matrix.

5.3.8.3 Thermal analysis

The overall thermal decomposition process of sisal fiber embedded in each blend was investigated in the form of TGA and DTG curves and is shown in Figs. 5.18 and 5.19. Three stages of weight loss caused by the thermal decomposition of fiber components can be found in the TGA curves as follows:

(i) Slight weight loss due to evaporation of moisture in the fibers from 50 to 110 ºC.

(ii) Decomposition of hemicelluloses and the main part of lignin at temperatures between 270 and 360 ºC.

(iii) The maximum weight loss under higher temperature caused by the degradation of cellulose and the rest of lignin from 335 to 500 ºC.

A distinct DTG peak corresponding to the major loss of weight displayed by the TGA curve, due to the decomposition of cellulose, can be observed for each sample. However, the "shoulder", normally caused by the thermal decomposition of hemicellulose, is made visible only in the DTG curves of the raw fibers. These low-temperature hemicellulose shoulder peaks were overlapped in the cellulose main peaks (Yao, Wu et al. 2008), consequently they are not obvious in the other samples. The extensive temperature range of the lignin decomposing in two or three stages (Jakab, Faix et al. 1997, Sun, Lu et al. 2001) makes the analysis more difficult. Unlike the sharper DTG peaks of cellulose and the "shoulders" of hemicellulose, decomposition of lignin does not present any obvious peak in the DTG curve but is divided into three steps: the first one from 280 to 390 ºC, the second one at the higher temperature of 420 ºC, and the third one is a long tail beyond 500 ºC (Brebu and Vasile 2010). From the TGA curves (Fig. 5.18), the weight losses according to the decomposition of cellulose indicate that the raw fiber has a cellulose content of 74.21%, while the amount of cellulose for fiber embedded in a PC matrix after 30 wetting and drying cycles is 41.60% lower. The amount of cellulose in the fiber embedded in B10-1 is 29.49% higher than that of fibers embedded in PC. Therefore, 10 wt.% replacement of cement by MK slows down the decomposition of cellulose considerably. In addition, the moisture contents of the raw sample and fibers in B10-1 are 90.91% and 9.09% greater than those of fibers in the PC matrix. The significant differences in moisture indicate two facts. On one hand the embedded fibers experienced severe dewatering in the cementitious matrices due to the high hydroscopicity of cement and the drying

phase of each cycle. On the other hand, the decomposition of amorphous components in sisal fiber significantly decreases the water retained in the fiber cell walls. Here we make an assumption that the long tail of the curves beyond 500 ºC is caused by the thermal decomposition of lignin and that each sample decomposed the same amount of lignin. Therefore the extra weight loss of the embedded fibers in the range of temperature from 500 ºC to 600 ºC is due to the decomposition of CH, which immerses and precipitates in the cell walls of sisal fiber. The fiber embedded in PC shows a CH precipitation of 6.08%, which is 5.14 times more than that of fibers embedded in B10-1. Therefore, sisal fiber encountered the most serious alkaline attack in pure cement due to the high alkalinity and the largest amount of precipitated CH caused by the high CH content of the matrix. The 10 wt.% replacement of Portland cement by MK not only slows down the fiber's degradation, but also effectively protects the fiber from calcium hydroxide precipitation or mineralization, which tends to cause the brittleness of fibers.

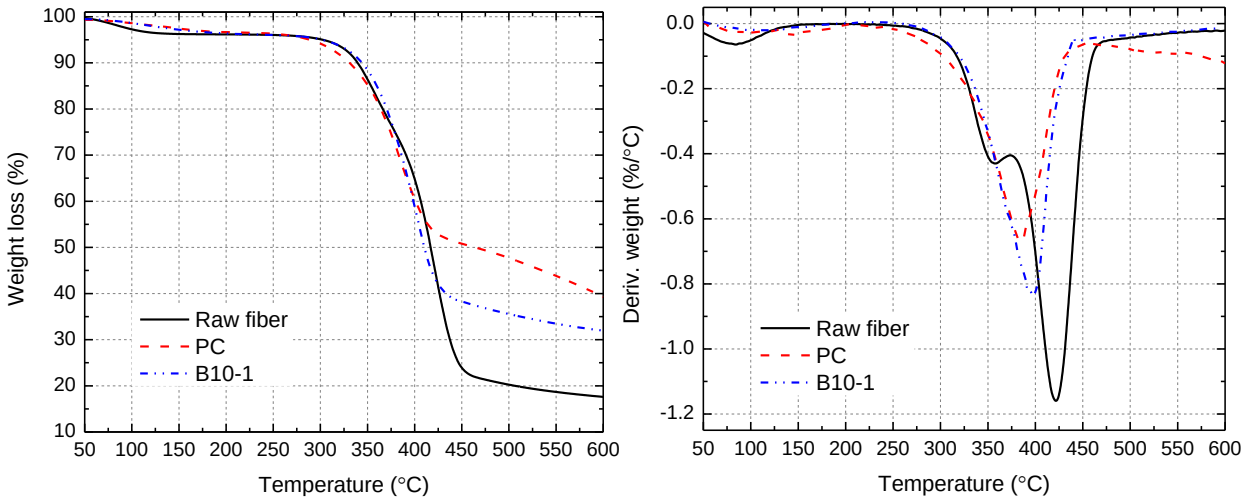

Figure 5.18: TGA and DTG curves of the raw sisal fiber and fibers pulled out from the matrix of PC, and B10-1 after 30 wetting and drying cycles

Fig. 5.19 shows the TGA and DTG curves of fibers embedded in the matrices of B30-1, B30-2, B50-1 and B50-3. From the weight loss between 50 and 270 ºC in the TGA curves, it can be seen that both hemicellulose and cellulose contents of the samples are increased with increasing cement replacement level and NC content. The fiber embedded in B50-3 shows a hemicellulose amount of 10.99%, which is 19.78% less than that of the raw fiber, but 2.90%, 4.17%, %, 5.76%, and 5.72% greater than those of fibers embedded in the matrices of B50-1, B30-2, B30-1, B10-1, and pure cement, respectively. B50-3 shows a cellulose content of 57.41%, which is 13.26% less than that of the raw sisal fiber but is the maximum among the pulled out fibers. Compared with fiber pulled out from PC, the samples embedded in B50-1, B30-2, and B30-1 experienced 45.47%, 40.88% and 38.32 greater weight losses, respectively, for the temperature range from 350 to 500 ºC.

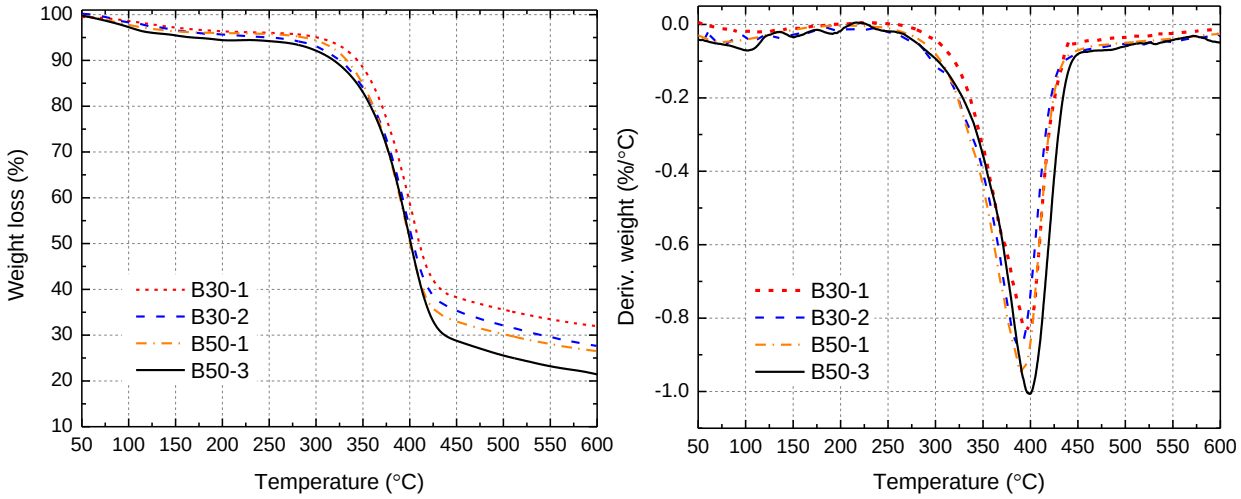

Figure 5.19: TGA and DTG curves of the fibers pulled out from the matrices of B30-1, B30-2, B50-1, and B50-3 after 30 cycles of wetting and drying

In addition, the temperatures for the maximum decomposition rate (T_m) represent a considerable trend of shifting forward with the increasing degradation degree of the sisal fibers.

From the DTG curve in Fig.5.18, the raw fiber shows a T_m of 421.06 ºC, which is the highest one among the samples. Due to the decomposition of hemicellulose and lignin and the reduced cellulose amount, the temperature range of thermal decomposition tends to finish earlier. Therefore, the main peaks of the samples are becoming narrower with a similar starting point at about 270 ºC. If the precipitation of CH in cell walls is ignored, the amount of lignin can be simply calculated by subtracting the holocellulose amount (hemicellulose and cellulose) from the whole weight loss at the temperature between 200 and 600 ºC. The fiber embedded in PC has the lowest amount of lignin (80.99% less than that of the raw fiber), which indicates that it experienced the most severe alkali attack. Among the embedded samples, the fiber pulled out from B50-3 yields a maximum preserved amount of lignin, which is 43% greater than that of the fiber embedded in the PC matrix. Therefore, the cement substitution by 45wt.% MK and 5wt.% NC leads to the most effective arrest of the fiber degradation.

5.3.9 Microstructure Analysis

Micro-analyses of typical fracture surfaces of sisal fiber-reinforced PC and PC-MK-NC blends were performed by using SEM to study the effect of MK and NC on the degradation of sisal fiber in a cement matrix. Fig. 5.20 shows SEM images of raw (28 day curing) and aged sisal fiber reinforced PC. The image of Fig. 5.20 a (PC-28d) illustrates that the uniformly distributed sisal fibers have no signs of mineralization. However, the micro-fibrils were partially dispersed due to the slight alkaline hydrolysis of lignin and hemicellulose. An evident stripping space, caused by the dry shrinkage, is found between each fiber and the surrounding cement matrix. During 15 wetting and drying cycles, the fibers experience serious degradation evidenced by the scattered cellulose fibrils (Fig. 5.20 b). The amorphous components, lignin and hemicellulose were totally decomposed due to the high alkalinity of the pore solution in a pure cement matrix. The enlarged

image indicates that the cell walls of sisal fiber are mineralized. Due to the precipitation of Ca^{2+}, both plates of calcium hydroxide and needles of ettringite are detected in the fracture section of the fiber. The more serious fibre corrosion is visible after 30 cycles of wetting and drying (Fig. 5.20 c). The space of micro-fibrils is split and filled with cement hydration products, which further erode the residual amorphous phases and cellulose in the fiber. The severe mineralization not only causes the strength loss, but also leads to the brittleness of the fiber as evidenced by the highest fiber tensile modulus detected in the PC matrix as summarized in Table 5.1.

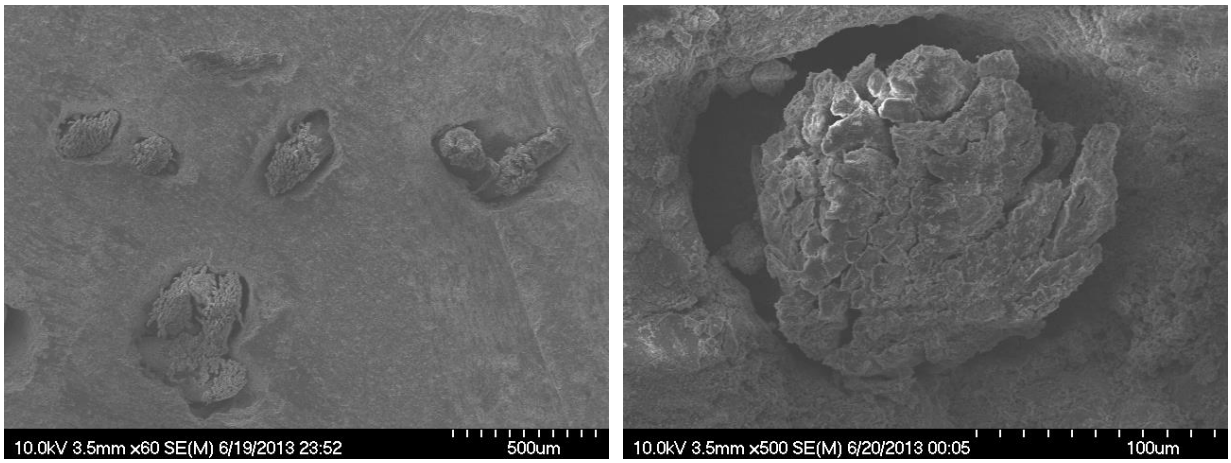

(a) PC-28d

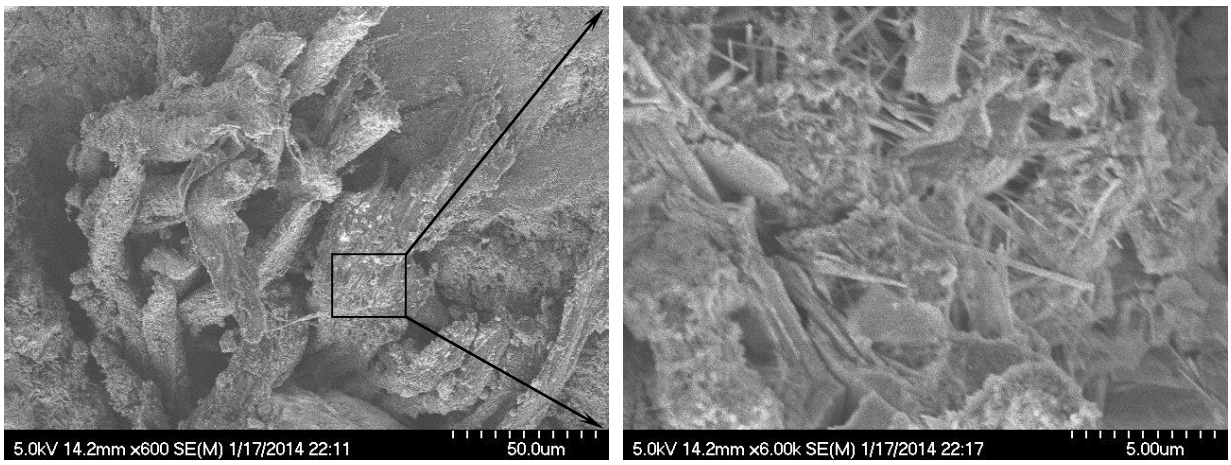

(b) PC-15c

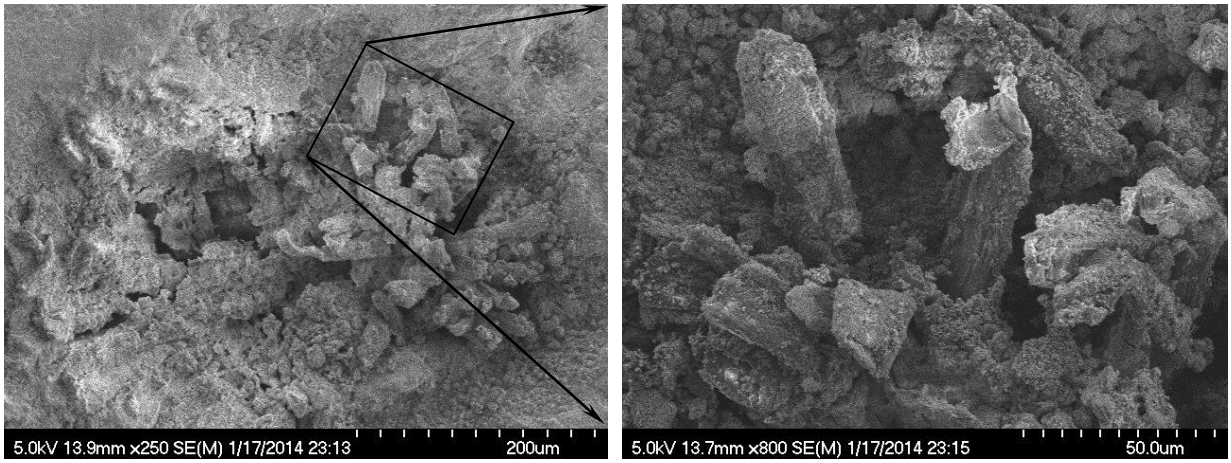

(c) PC-30c

Figure 5.20: SEM micrographs of the fracture surface for sisal fiber reinforced pure Portland cement at 28 days of curing, and after 15 and 30 cycles of wetting and dying

Fig. 5.21 shows the microstructure of the fracture sections for B30-2 after 15 and 30 wetting and drying cycles. Compared with that of PC, the degradation of sisal fiber in B30-2 is effectively restrained at this age. Although the fiber surface encounters slight attack after 15 wetting and drying cycles, the fibers remain intact without the sign of CH precipitation in fiber cells. After 30 wetting and drying cycles, the sediment of cement hydration products is detected on the fiber surface, which not only demonstrates the better interfacial adhesion between fiber and the matrix, but also indicates the high residual strength of the fiber. The replacement of cement by MK and NC improves the durability of fiber in cement in two ways: keeping the integrity of fiber by reducing the alkalinity of the matrix, and slowing the mineralization of cell walls by reducing CH and ettringite contents.

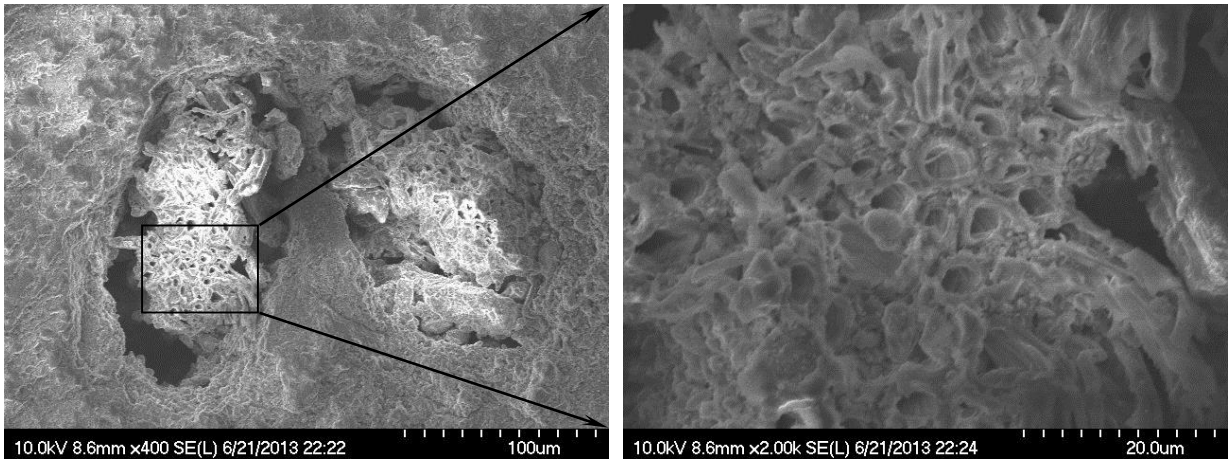

B30-2-15C

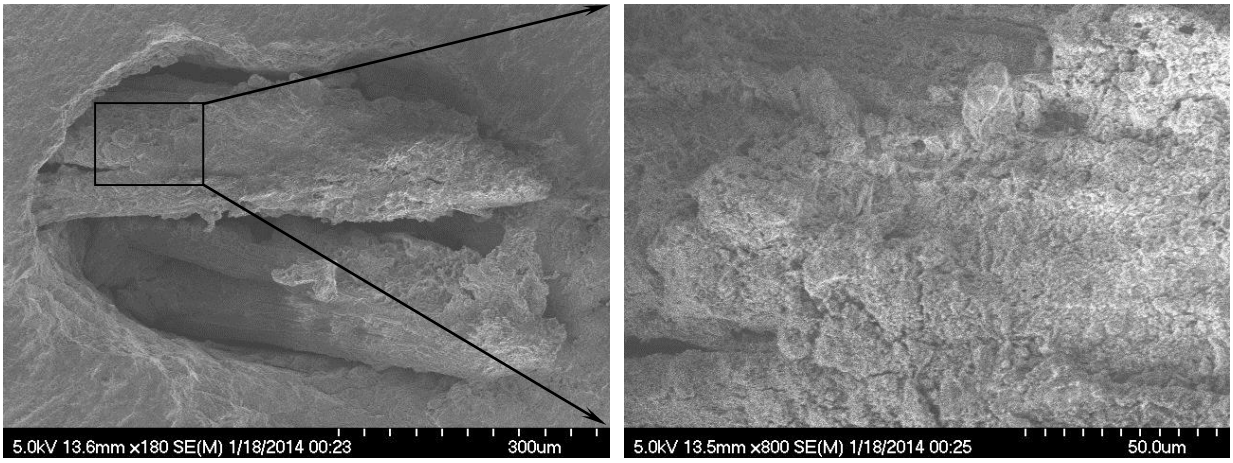

B30-2-30C

Figure 5.21: SEM micrographs of the fracture surface for sisal fiber reinforced B30-2 after 15 and 30 wetting and dying cycles

The microstructures of B50-1 and B50-3 after 30 wetting and drying cycles are compared in Fig. 5.22. In the fracture surface of B50-1, a pulled out fiber with neat fracture section is detected. On the one hand, the enlargement of the fiber section indicates the low alkaline hydrolysis degree of the amorphous phases. On the other hand, it shows a sign of mineralization in fiber cell walls. In B50-3, the fiber is more intact than that in B50-1. Both of the sieve tubes and vessels of the sisal fiber are detectable. Although there is no sign of mineralization in the center of the fiber, a small quantity of cement hydration products is found in the cell walls close to the fiber surface. The

results indicate that the combined partial substitution of MK and NC for Portland cement significantly improves the durability of sisal fiber in a cement matrix. The role of NC is more noticeable than MK for keeping the fiber intact and reducing mineralization of a fiber cell after 30 cycles of wetting and drying.

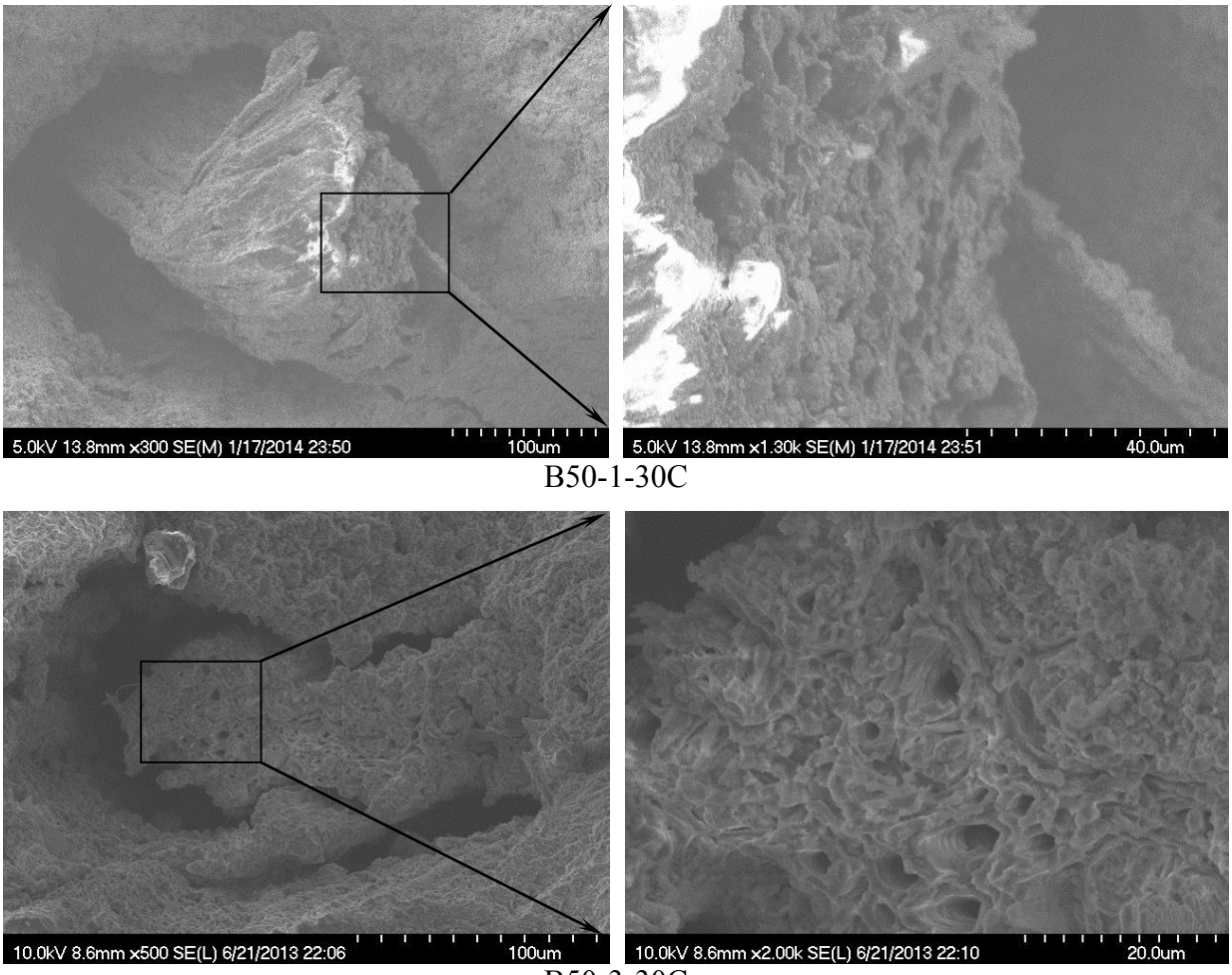

Figure 5.22: SEM micrographs of the fracture surface of sisal fiber reinforced B50-1 and B50-3 after 30 wetting and drying cycles

5.4 Utilization of Rice Husk Ash (RHA) to Mitigate Deterioration of Sisal Fiber

As shown in Table 2.2 and Fig.2.3, owing to the high amorphous silica content (> 90wt.%) and high specific surface area, RHA, with high pozzolanic reactivity, have been used in construction materials as supplementary cementitious material. RHA has a desirable modifying effect on cement composites, being associated with higher compressive and flexural strengths (Zhang 1996, Rodríguez de Sensale 2006), enhanced workability (Habeeb 2009), increased degree of cement hydration at later age (Van Tuan, Ye et al. 2011), and reduced $Ca(OH)_2$ (Zhang, Lastra et al. 1996). However, the effect of RHA on the degradation rate of natural fiber in the matrix of cement composites still lacks in-depth and systematic investigation. The modifying effects of the fine rice husk ash (RHA) and the coarse RHA (CRHA) were investigated in this section by replacing from 5 to 30wt.% cement.

5.4.1 Effect of RHA on the durability of SFRCC

The degradation of SFRCC exposed to wetting and drying cycles as determined by flexural testing can be used as an indirect measure of the deterioration of the embedded sisal fibers. Fig. 5.23 presents typical load-deflection curves for each blend after 0, 5, 15, and 30 wetting and drying cycles.

Ductile behaviour is displayed by all fiber-reinforced specimens. However, with increasing replacement of cement by RHA, the peak loads and the corresponding deflections ς_{max} increase at first and then gradually decrease. Therefore, the post cracking shoulders become broad at first and then narrow after RHA20 for specimens not subjected to wetting and drying cycling. Due to the pozzolanic reaction, the replacement of cement by the CRHA also leads to an increased flexural strength and post-cracking toughness, but their rates of increase are smaller than for samples with

the same amount of RHA. The replacement of 5 wt.% RHA by limestone (LS) led to a worse flexural behavior. From the differences identified between RHA5, RHA5-LS, and RHA10, it can be concluded that RHA is mostly responsible for the cement matrix beneficiation.

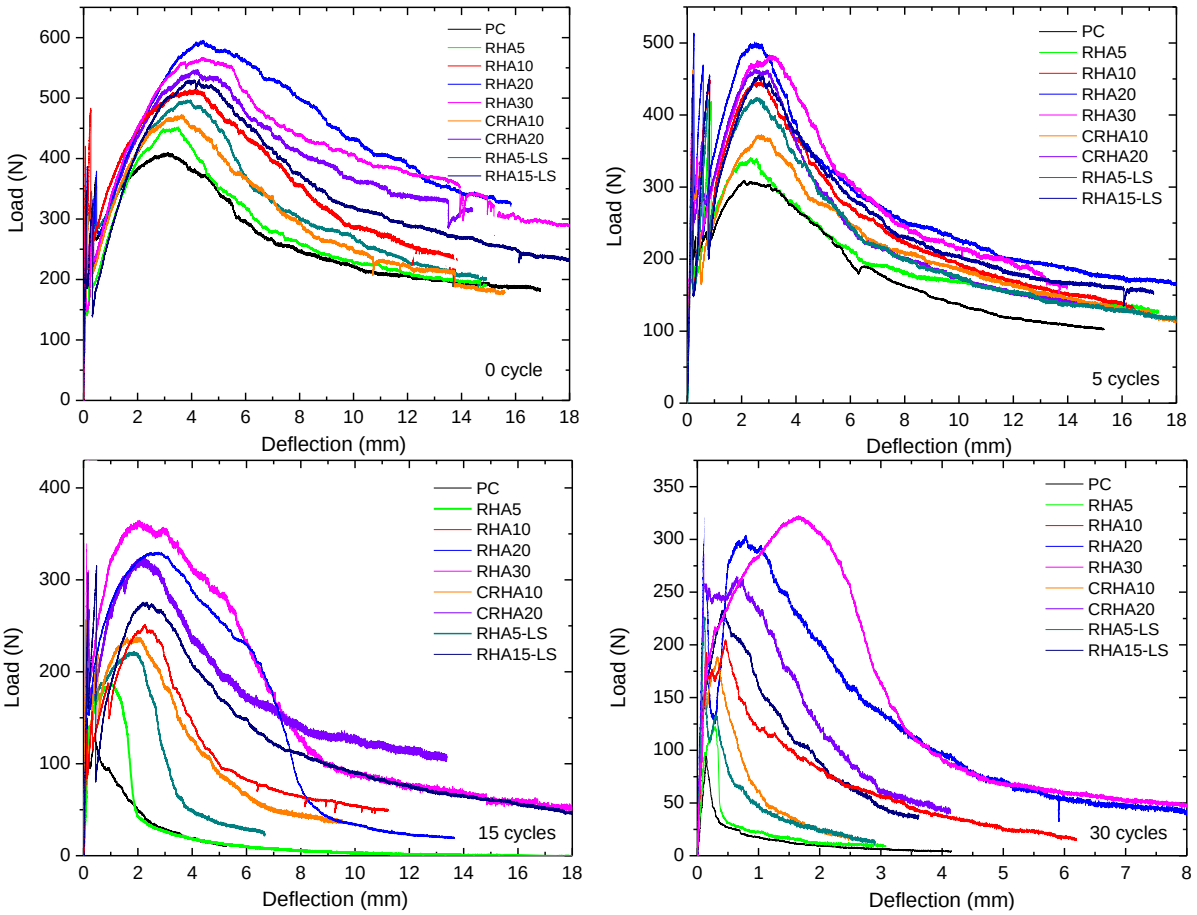

* PC: neat cement; RHA5: 95% cement+5% RHA; RHA10: 90% cement+10% RHA; RHA20: 80% cement+20% RHA; RHA30: 70% cement+30% RHA; CRHA10: 90% cement+10% CRHA; CRHA20: 80%cement+20%RHA; RHA5-LS: 90%cement+5%RHA+5%LS; RHA15-LS: 80%cement+15%RHA+5%LS. (Table 2.4)

Figure 5.23: Typical load-deflection curves for various cement blends subjected to cycles of wetting and drying

The flexural strength and toughness of sisal fiber reinforced PC samples experience the sharpest decline with increasing numbers of cycles. But with increasing level of cement replacement by RHA, the decrease of flexural properties can be effectively arrested. Although

RHA20 led to optimal flexural strength and toughness among the samples without aging, its durability is worse than that of RHA30, which presents the optimal post-cracking toughness after 5, 15, and 30 wetting and drying cycles of all the specimens. Therefore, the partial substitution of RHA for Portland cement not only increases the initial mechanical properties of SFRCC, but also significantly improves the durability of the composites by reducing the alkaline degradation of the fiber embedded in modified matrices.

According to the flexural parameters given in Table 5.3, the flexural strength of SFRCC subjected to 5, 15 and 30 wetting and drying cycles, decreases by 15.58%, 68.35% and 86.52%, respectively, compared to the initial value. The post-cracking toughness of PC declines more severely than the strength: after 30 wetting and drying cycles, the toughness indices T_p, I_{30}, and T_{JCI} decrease by 99.08%, 84.26%, and 98.87%, respectively. The I_{55} of PC after 15 cycles and that of all other specimens except RHA20 and RHA30 after 30 cycles disappear, due to the severe degradation of the sisal fiber. In addition, the deflection indices P_{max} and $P_{0.5}$ also show declines of 96.12% and 96.03%, respectively. The value of P_{max} (1.0) indicates that, after 30 wetting and drying cycles, the maximum load was reached at the first crack and there was no post-cracking toughening behavior. The JCI strength of sisal fiber reinforced PC after 30 cycles shows a 98.84% lower value than the specimens without aging.

Prior to cycling, the replacement of 20 wt.% cement by RHA leads to an increase of post-cracking strength and toughness by 45.02% and 63.33%, respectively. RHA30 shows a 38.34% greater strength and a 55.13% greater toughness than PC. Due to the smaller particle sizes and higher pozzolanic activity, the specimens with cement replacement by RHA show improved flexural properties compared with those with the same amount of CRHA. CRHA10 and CRHA20 yield 14.77% and 32.94% greater strength than PC, but 8.16% and 8.33% lower strength than

RHA10 and RHA20, respectively. Similar results can also be found for the toughness of the unaged samples.

All composites listed experienced decreases in flexural strength (σ_p and F_{JCI}), toughness (T_p, I_{30}, I_{50}, and T_{JCI}), and the deflection indices (P_{max} and $P_{0.5}$) when subjected to increasing wetting and drying cycles. However, the replacement of cement by RHA effectively improves the durability of SFRCC. After 30 cycles, the peak strength of RHA5, RHA10, RHA20 and RHA30 are 120.87%, 270.44%, 450.44%, and 480.87% greater, respectively, than the control. Although CRHA10 and CRHA20 yield relatively lower strength than RHA10 and RHA20, they still show 240.87% and 378.26% higher final strength than the control. RHA5-LS and RHA15-LS yield 221.74% and 321.74% greater strength than the control, which indicates that the replacement of 5wt.% RHA by LS leads to a slight decline of durability.

In terms of post-cracking toughness, RHA30 also shows the most effective enhancement in durability. By 30 wetting and drying cycles, the 30 wt.% replacement of cement by RHA leads to increases of T_p, P_{max}, $P_{0.5}$, I_{30}, and T_{JCI} by 270.56%, 1040.00%, 642.95%, 317.32%, and 3414.29%, respectively. All the other composites show considerable improvement of durability, however, similar as flexural strength, the replacement of cement by RHA leads to a better durability, as measured by toughness, than CRHA and that with replacement of RHA by LS.

Table 5.3. Durability of sisal fiber-reinforced cement mortar determined by flexural indices

Sample	Aging cycles	σ_p (MPa)	T_p (N-m)	P_{max}	$P_{0.5}$	I_{30}	I_{55}	T_{JCI} (N-m)	F_{JCI} (MPa)
PC	0	8.53	3.90	25.8	82.02	60.15	119.78	3.10	6.46
	5	6.42	2.66	11.44	47.49	50.81	89.21	2.20	4.59
	15	2.70	0.20	2.14	12.40	20.16	-	0.19	0.39
	30	1.15	0.036	1.0	3.26	9.47	-	0.035	0.075
RHA5	0	9.41	4.20	35.16	102.89	62.78	122.80	3.19	6.65
	5	7.07	2.96	12.57	53.20	52.26	91.44	2.38	4.95
	15	3.88	0.38	4.84	15.08	24.89	26.48	0.39	0.82
	30	2.54	0.039	2.29	2.90	11.80	-	0.037	0.076
RHA10	0	10.66	5.06	39.73	132.36	72.80	134.75	4.08	8.49
	5	9.29	3.66	14.07	65.15	56.04	110.83	3.01	6.27
	15	5.22	1.29	10.23	33.03	33.38	54.03	1.24	2.58
	30	4.26	0.35	3.04	9.87	27.11	-	0.32	0.66
RHA20	0	12.37	6.37	62.73	182.77	79.73	150.05	4.85	10.11
	5	10.40	4.11	14.95	83.04	60.19	124.89	3.36	6.99
	15	6.86	2.33	12.38	46.31	40.87	86.96	2.08	4.32
	30	6.33	0.86	6.65	22.46	35.38	61.19	1.07	2.22
RHA30	0	11.80	6.05	51.02	222.68	76.18	141.37	4.56	9.50
	5	10.04	4.01	18.17	109.14	59.95	121.02	3.29	6.85
	15	7.56	2.67	12.19	47.45	43.21	89.59	2.41	5.01
	30	6.68	1.01	11.40	24.22	39.52	74.98	1.23	2.57
CRHA10	0	9.79	4.38	36.25	116.61	64.91	130.78	3.52	7.33
	5	7.74	3.25	13.84	57.36	53.65	99.99	2.65	5.51
	15	4.95	1.01	8.16	21.18	31.35	51.26	0.95	1.98
	30	3.92	0.13	2.47	5.43	13.78	-	0.12	0.26
CRHA20	0	11.34	5.69	58.12	171.55	71.82	139.62	4.35	9.06
	5	9.65	3.71	14.87	67.91	59.20	108.73	2.92	6.09
	15	6.69	2.43	10.26	39.95	39.95	87.86	2.06	4.29
	30	5.50	0.51	5.41	15.87	32.48	-	0.49	1.01
RHA5-LS	0	10.31	4.61	38.56	87.51	71.26	132.43	3.69	7.70
	5	8.83	3.36	12.95	46.11	54.19	106.38	2.77	5.77
	15	4.59	0.63	7.28	26.05	29.57	41.07	0.60	1.25
	30	3.70	0.077	1.0	3.22	12.30	-	0.076	0.16
RHA15-LS	0	11.02	5.21	44.26	150.98	71.52	136.85	4.05	8.45
	5	9.49	3.76	14.54	56.52	57.05	111.81	3.07	6.40
	15	5.73	1.99	10.24	37.44	34.97	75.73	1.71	3.55
	30	4.85	0.37	4.02	12.33	28.97	-	0.34	0.72

5.4.2 Degradation of embedded sisal fibers

5.4.2.1 Tensile behavior of sisal fiber

In order to investigate directly the degradation degree of sisal fiber in aged specimens, the uniaxial tensile properties of the embedded fibers were determined. Fig. 5.24 shows the Weibull plots and the corresponding regular residuals of test data for the raw sisal fiber and those embedded in samples subjected to 30 cycles of wetting and drying. It can be seen that, except for the fibers embedded in PC and RHA5, the concentrations of test data of the other samples after 5 cycles are much higher than those after 30 cycles. This indicates that the degradation of sisal fiber embedded in these matrices was effectively arrested at early stages of aging and that the fibers were partially degraded later.

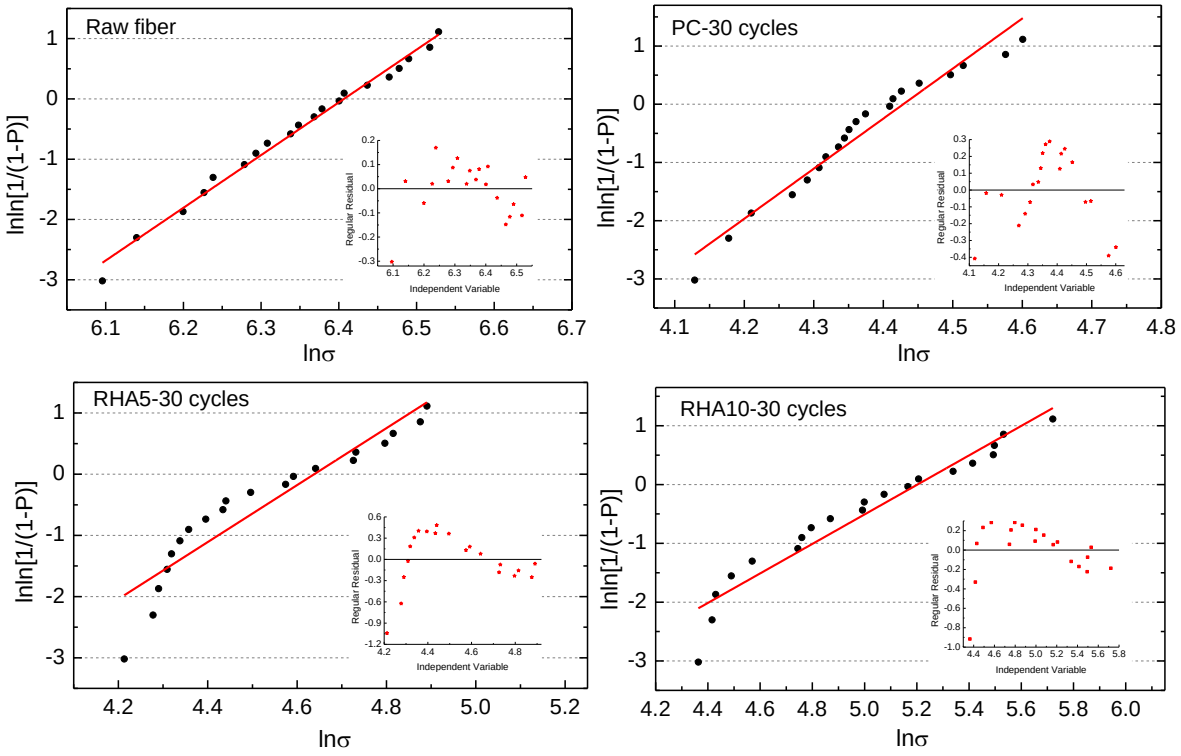

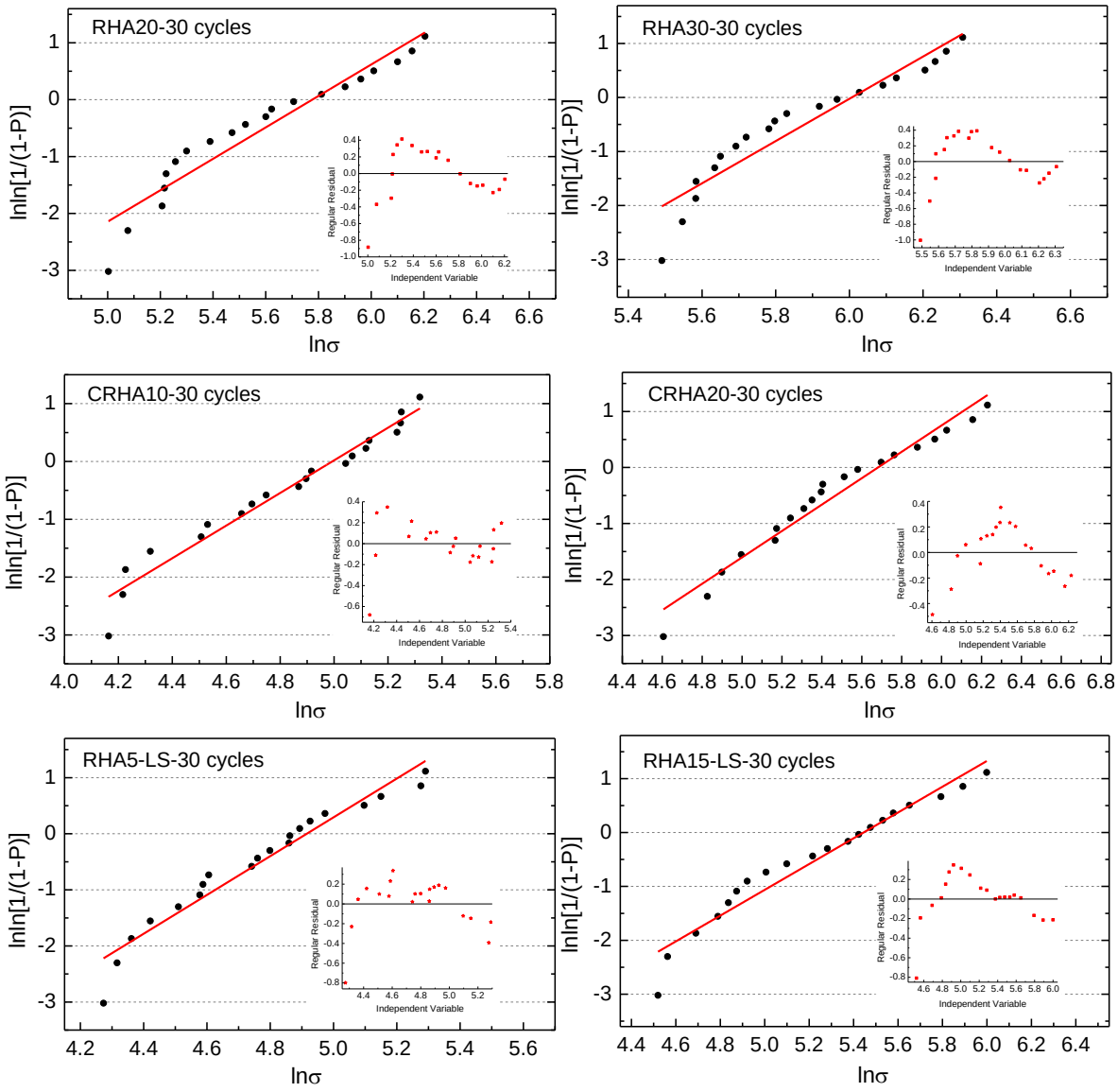

Figure 5.24: The Weibull plots of raw fiber and embedded fibers after 30 wetting and drying cycles

Table 5.4 shows the Weibull parameters calculated from Fig. 5.24. Due to the varying levels of alkaline attack in cement based matrices, the tensile strengths of embedded fibers are lower than the raw fiber. The fibers embedded in PC encounter the most severe alkaline hydrolysis and mineralization evidenced by the lowest strength and maximum Young's modulus. Compared with the raw fiber, the tensile strength of fiber in PC decreased by 35.11%, 78.04%, and 86.17%, after 5, 15 and 30 cycles, respectively. The Young's modulus of the fiber increased by 28.42% after 30

wetting and drying cycles. The replacement of cement by RHA effectively arrests the degradation of sisal fiber in mortar. After 30 wetting and drying cycles, the strengths of the fibers embedded in RHA5, RHA10, RHA20, and RHA30 are 23.53%, 116.82%, 284.86%, and 384.38% greater, respectively, than that of fiber in PC.

Table 5.4: The Weibull parameters and deformability of sisal fibers in tensile test

Sample	Number of cycles	Characteristic Strength σ_0 (MPa)	Weibull Modulus, m	R^2	Young's modulus, E (GPa)
Raw	0	605.88	8.74	0.9893	15.41
PC	5	393.15	3.60	0.9546	17.27
	15	133.06	5.47	0.9712	18.66
	30	83.82	8.60	0.9538	19.79
RHA5	5	403.61	3.67	0.9607	17.01
	15	179.16	2.71	0.9436	17.94
	30	103.54	4.65	0.8726	18.81
RHA10	5	486.33	5.06	0.9129	16.67
	15	236.62	2.40	0.9431	17.59
	30	181.74	2.51	0.9299	17.87
RHA20	5	556.79	5.37	0.9501	15.82
	15	413.73	4.16	0.9302	16.94
	30	322.59	2.76	0.9124	17.37
RHA30	5	561.41	5.41	0.9266	15.77
	15	507.22	5.15	0.9318	16.31
	30	406.01	3.91	0.9127	16.97
CRHA10	5	414.29	4.02	0.9644	16.90
	15	207.55	2.52	0.9437	17.75
	30	146.94	2.82	0.9571	18.20
CRHA20	5	524.39	5.26	0.9710	16.09
	15	385.16	3.62	0.9361	17.32
	30	293.30	2.36	0.9599	17.52
RHA5-LS	5	422.32	4.07	0.9618	16.78
	15	194.51	2.49	0.9523	17.79
	30	136.37	3.46	0.9412	18.26
RHA15-LS	5	517.16	5.19	0.9463	16.17
	15	319.57	2.70	0.9517	17.41
	30	231.53	2.39	0.9431	17.63

CRHA also plays an effective role of slowing down the degradation of sisal fiber in a cement matrix: the ultimate strengths of fibers in CRHA10 and CRHA20 are 75.30% and 249.92% higher than the control (PC), respectively, however they are lower than those with same amount of RHA. The replacement of RHA by LS slightly weakened the enhancing effect of RHA on durability of sisal fiber in the cement matrix.

5.4.2.2 Crystallization analysis (X-ray diffraction)

A crystallization analysis of sisal fibers was also performed to determine the effects of mineralization and alkaline hydrolysis. As a natural fiber, sisal is semi-crystalline and the tensile strength and elastic modulus have an evident relationship with its crystal content. Here, the intensity of the ($\bar{1}10$), (110), and (002) interference and the amorphous scatter between 18º and 19º were measured. Fig. 5.25 shows the XRD diagrams of raw sisal fibers and those embedded in PC and blends after 30 wetting and drying cycles. The cellulose has a crystalline nature with an intensive peak at $2\theta \approx 22.5$º corresponding to its (002) lattice plane and a broad peak between 13º and 18º corresponding to the ($\bar{1}10$) and (110) lattice planes. Peaks of ettringite and calcium carbonate are found in all fibers except the raw one, while the peaks of CH are only detected in fibers embedded in a neat PC matrix. Due to the dilution effect and pozzolanic activity of RHA, CH and ettringite are effectively consumed, and therefore less re-precipitation of these two hydration products in the lumen of natural fibers was identified.

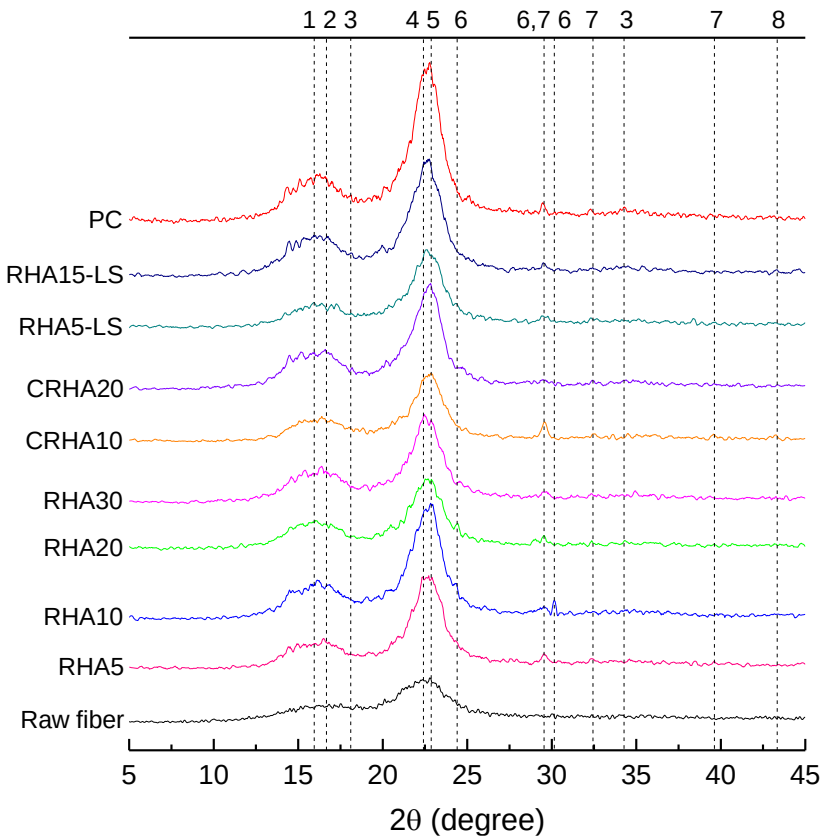

* 1, 2, 4: cellulose crystallographic plane ($\bar{1}10$), (110) and (002); 3: $Ca(OH)_2$; 5: ettringite; 6: $CaCO_3$; 7: C_2S, C_3S; 8: MgO.

Figure 5.25: XRD pattern of raw and embedded sisal fibers

The percent crystalline materials of the fibers, expressed by "percentage of crystallinity" (%Cr), "crystallinity index" (Cr.I.) and "crystallite size" (L), calculated from the corresponding diffraction peaks and corresponding FWHMs, are summarized in Table 5.5. Although they are affected by non-uniform strain, crystalline disorder, and some other uncertain factors, the crystallite sizes for the two major peaks of embedded fiber are bigger than those of raw sisal fiber. The removal of amorphous components is the main reason for the big crystallite size of natural fiber (Sinha and Rout 2009), and it can also lead to the increase of the crystallinity index and percentage of crystallinities.

Table 5.5: Calculated crystalline parameters of sisal fiber

Curing or Exposure duration	Samples	Peak position (2θ)	FWHM* (β) (2θ)	L (nm)	%Cr	Cr.I.
-	Raw fiber	15.83 22.32	5.62 3.43	1.45 2.48	68.95	0.5498
30 cycles	PC**	16.47 22.59	4.58 2.30	1.79 3.70	85.69	0.8330
	RHA5	16.46 22.64	4.27 2.48	1.92 3.43	85.29	0.8275
	RHA10	16.54 22.60	4.64 2.45	1.77 3.47	84.07	0.8106
	RHA20	16.14 22.58	3.92 2.67	2.09 3.19	83.82	0.8070
	RHA30	16.38 22.56	4.17 2.50	1.96 3.40	83.20	0.7980
	CRHA10	16.52 22.68	4.15 2.39	1.97 3.56	85.12	0.8180
	CRHA20	16.29 22.61	4.48 2.44	1.83 3.49	84.40	0.8151
	RHA5-LS	16.62 22.64	4.39 2.55	1.87 3.34	84.74	0.8175
	RHA15-LS	16.33 22.55	4.47 2.52	1.83 3.38	84.16	0.8118

* Full width of the peak at its half maximum height.
** The control group

Among all samples, the raw sisal fibers show the lowest values in both crystallinity index and percentage of crystallinities. Due to the alkaline hydrolysis of the amorphous components (lignin and hemicellulose) both parameters were increased. After 30 wetting and drying cycles, the fiber embedded in PC shows the maximum percentage of crystallinities and crystallinity index, which are 24.28% and 51.51% greater than those of raw fiber. Both %Cr and Cr.I. decreased with increasing replacement of cement by RHA. The fiber embedded in RHA shows the minimum percentage of crystallinities and crystallinity index, which are 20.67% and 45.14% greater than those of raw fiber, but 2.91% and 4.20% lower than the control, respectively. Like the fibers' tensile strength, CRHA shows a relatively lower effect on arresting the alkali hydrolysis of lignin and

hemicellulose than RHA. It is the large amount of silicon minerals of RHA that reduces the alkalinity of the matrix and protects the embedded fiber from the alkali attack in the cement matrix. Therefore the replacement of RHA by LS leads to an increased crystallinity index.

5.4.2.3 Thermal analysis: thermogravimetric analysis (TGA)

The alkali hydrolysis of the three components of sisal fiber is the main reason for the degradation of natural fiber in alkali environments. The overall thermal decomposition process of sisal fibers embedded in cementitious matrices was analyzed in terms of TGA and DTG curves to determine the composition changes. In Fig. 5.26, similar thermal degradation behavior of raw and embedded sisal fibers after 30 wetting and drying cycles can be noticed. Three stages of weight loss caused by the thermal decomposition of fiber components were identified in the TGA and DTG curves due to: (i) evaporation of moisture, (ii) decomposition of hemicelluloses, and (iii) degradation of cellulose. In each DTG curve, a distinct peak, due to the decomposition of cellulose, is observed, which corresponds to the major loss of weight in the TGA curve. A "shoulder", normally caused by the thermal decomposition of hemicellulose, is identified only on the raw sisal fiber's DTG curve. Unlike the sharper DTG peaks of cellulose and the "shoulders" of hemicellulose, there is no distinguished step for lignin's weight loss at a particular temperature.

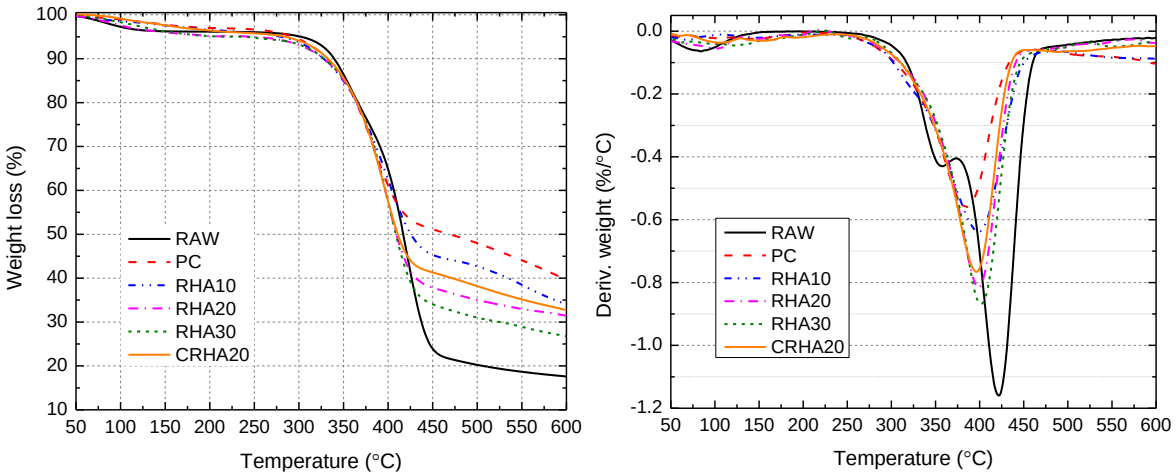

* The fiber embedded in PC is the control group.

Figure 5.26: TGA and DTG curves of the raw and embedded fibers after 30 cycles of wetting and drying

The decomposition profiles indicate the differences of thermal stability. As shown in Fig. 5.26, the DTG peaks shift to lower temperatures, which indicates that thermal stability of sisal fiber was reduced. The raw fiber has a cellulose content of 74.21%, which is 71.23% greater than that of the fiber embedded in the PC matrix after 30 wetting and drying cycles. The replacement of cement by RHA effectively arrests the alkali hydrolysis of natural fibers: the cellulose contents of the fibers embedded in RHA10, RHA20, and RHA30 are 12.51%, 28.47%, and 38.95% greater, respectively, than the control. Lignin and hemicellulose are more sensitive to the alkaline pore solution and are in direct contact with the hydration products of the matrix. Therefore, their degradation is more impressionable than that of cellulose. On the other hand, the decomposition of lignin and hemicellulose, which form the protective layer of cellulose micro fibrils, results in the more severe alkali attack on cellulose and therefore the failure of the fiber embedded in the cement matrix. In addition, the precipitation of calcium hydroxide among cellulose micro fibrils,

through the gap of lignin and hemicellulose, also accelerates the embrittlement and decomposition of cellulose.

5.4.3 Surface topography analysis by scanning electron microscopy (SEM)

Micro-analyses of typical fracture surfaces of sisal fiber-reinforced PC and PC-RHA blends were performed by using SEM to study the effect of RHA on the degradation of sisal fiber in a cement matrix. As shown in Fig. 5.27, after 30 wetting and drying cycles, the sisal fibers suffered severe corrosion in the cement matrix. The decomposition of amorphous components (lignin, hemicellulose, and pectin) led to a considerable migration and precipitation of cement hydration products in the fiber's cell walls. As a result, the cellulose micro-fibrils were partially dispersed and filled with cement hydration products, such as calcium hydroxide, calcium carbonate, and calcium silicate hydrate (C-S-H). The effect of RHA on improving the durability of sisal fiber in the cement matrix is clearly visible. In RHA10, the cellulose fibrils were partially dispersed and the fiber could still play a role bridging micro-cracks. The replacement of 20wt.% cement by RHA and CRHA, significantly mitigated the degradation of sisal fiber. As can be seen, the fiber in RHA20 shows a better integrity than that in CRHA20. The optimal durability of sisal fiber was obtained in RHA30, which not only effectively arrested the degradation of sisal fiber but also preserved a compact fracture surface. Owing to the high pozzolanic activity, the replacement of cement by RHA improved the mechanical properties of fiber-reinforced cement composites. This was made possible by a considerable reduction of the alkalinity of the cement matrix, which promises good integrity and excellent reinforcing potential of sisal fiber in cement composites, even if subjected to accelerated aging treatment.

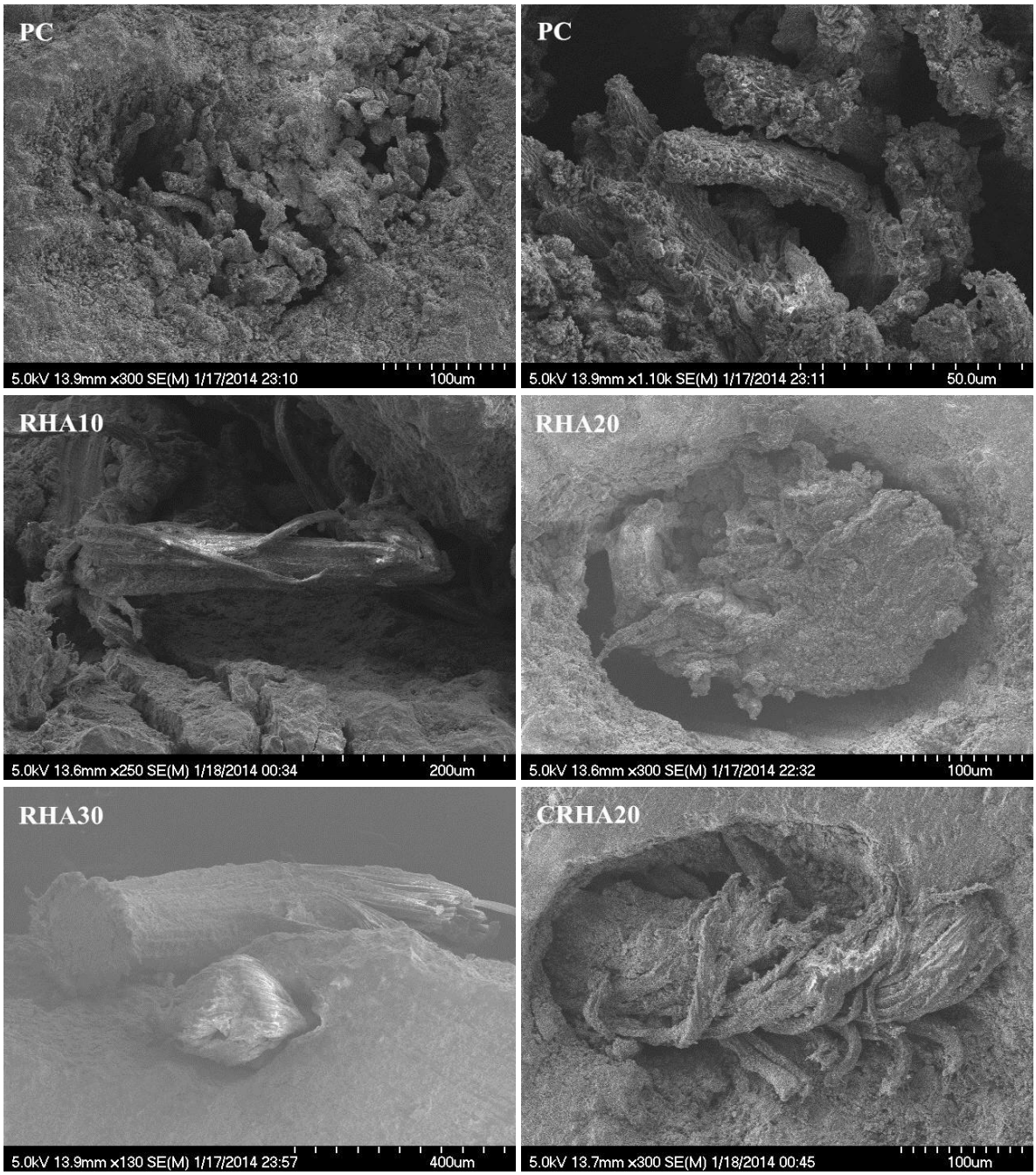

Figure 5.27: SEM micrographs of fiber fracture surfaces of sisal fiber-reinforced cement mortar after 30 wetting and drying cycles

5.5 Summary

This chapter describes the investigation of effective means to improve the durability of sisal fiber-reinforced cement composites and the mitigation of sisal fiber's degradation through modification of the cement matrix. Portland cement was partially replaced by supplementary cementitious materials, such as metakaolin, nanoclay, limestone, rice husk ash, and various combinations of them. The degradation of sisal fiber in cement matrices was investigated indirectly by testing the flexural behavior of SFRCC, and directly by testing the uniaxial tensile properties, thermal decomposition, crystallinity indices, and microstructures of embedded fibers. These properties were determined by means of uniaxial tension tests, thermalgravimetric analyses (TGA), X-ray diffraction (XRD), and scanning electron microscopy (SEM), respectively. The following conclusions can be drawn from the results:

1. The early age (< 20 h) hydration of cement is significantly affected by both physical and chemical features of MK. The existence of NC not only relieves the rapid hydration, but also reduces the total released heat by adjusting the "filler" size and balancing the Ca-Si-Al ratio of the blends. With the increasing replacement of PC by MK, which is rich in aluminide, the "shoulders" in the various graphs, caused by the tricalcium aluminate reactions to form ettringite and subsequently conversion into monosulfate, become more sharp and higher than those of silicate reactions. The fine MK powders provide a considerable amount of new surface for heterogeneous nucleation of C-S-H and monocarboaluminate. The replacement of MK by NC leads to a lower peak value and later peak position of the heat flow, and lower total heat released, because of the quick end of both acceleration and deceleration periods.
2. The neat PC paste has the highest CH and bound water content, but lowest normalized non-evaporable water content among all the pastes after 300 days of hydration. The replacement

of PC by MK leads to an increased normalized non-evaporable water content, while the replacement of MK by NC decreases it. Both MK and NC play an effective role in reducing CH content.

3. The combined partial substitution of MK and NC for Portland cement not only improves the initial flexural properties of SFRCC, but also significantly improves its durability by mitigating the alkaline degradation of the fiber in modified matrices.
4. The uniaxial tensile properties of the embedded fibers improve with increasing cement replacement level, which indicates that both MK and NC significantly restrain the degradation of sisal fiber by reducing both the alkalinity and CH content of cement due to their high pozzolanic activity. The combination of these two supplementary cementitious materials validates their complementary and synergistic effect at different stages of aging.
5. Due to the severe alkaline hydrolysis of the amorphous components (lignin and hemicellulose), the fiber embedded in a neat cement matrix shows the highest crystallinity indices. MK arrests the fiber degradation more effectively at early age, while the high amounts of silicon minerals promote the complementary effect of NC on reducing alkalinity of the matrix for a long-term and therefore relieve the corrosion of sisal fiber at later stage.
6. The results of thermal analysis indicate that the cement substitution by a combination of MK and NC considerably mitigates the alkali hydrolysis of amorphous components (lignin and hemicellulose) of sisal fiber by reducing the alkalinity of the cement matrix.
7. RHA shows a better modifying effect than CRHA on improving both the mechanical properties and durability of SFRCC. The replacement of 30wt.% cement by RHA effectively arrests the degradation of sisal fiber. Replacing RHA by LS shows that the role of RHA in cement modification is mainly as the active cementitious supplementary material.

CHAPTER 6: IMPROVING DEGRADATION RESISTANCE OF SISAL FIBER IN CEMENT MATRIX THROUGH FIBER SURFACE PRETREATMENT

6.1 Introduction

Because of the low corrosion resistance of lignin and hemicelluloses in the middle lamellae of the fibers and cellulose molecules in high alkali environments (Singh 1985, Tolêdo Filho, Scrivener et al. 2000), sisal fibers gradually degrade and lose their reinforcing capacity in cement matrices in later stages of their service life. These deterioration mechanisms have attracted the interest of researchers, and substantial efforts have been undertaken in recent years to improve the degradation resistance of sisal fiber in alkaline environments. Fibers were treated with alkali solutions (Yang, Zeng et al. 1996, Barreto, Esmeraldo et al. 2010, Esmeraldo Milena A. 2010, 2011) for previous hornification to partially remove the lignin, hemicelluloses and to improve the mechanical properties of both the fiber and their composites. Also isocyanate treatment, benzoyl peroxide and permanganate treatment, dicumyl peroxide (1996), as well as mixed treatments, were studied. Almost all of these treatments referred to above have been studied specifically to improve the properties of sisal fiber embedded in polymer matrices.

It was the purpose of the work reported in this chapter to identify treatment methods that improve the corrosion resistance of sisal fiber in the alkali environment of concrete and the durability of natural fiber reinforced-concrete in aggressive environments.

Unlike the previous chapter, the presented work here is to investigate the effect of degradation resistance of sisal fiber in concrete, which is the ultimate purpose of this research. The addition of coarse aggregate made it more difficult to precisely assess the degradation degree of

sisal fiber through flexural properties. Therefore, in this chapter, the durability of sisal fiber-reinforced concrete (SFRC) was determined by testing the compressive and splitting tensile strengths of the samples exposed to wetting and drying cycles. This work was part of a larger ongoing project at Columbia University to develop an ultra-low cost housing system that utilizes concrete composed of ingredients that are not only of low cost but also environmentally friendly and sustainable. This is the reason why recycled concrete was used exclusively as aggregate, thereby improving the sustainability of the composite and lowering the cost at the same time. Thermal treatment and Na_2CO_3 treatment were carried out to improve the degradation resistance of sisal fiber, the interface bond between fiber and cement matrix, and the durability of SFRCC. For thermal treatment, sisal fibers were placed in a ventilated oven at 150 ℃ for 8 h. For Na_2CO_3 treatment, sisal fibers were embedded in a Na_2CO_3 saturated solution for either 7 days (N7) or 10 days (N10).

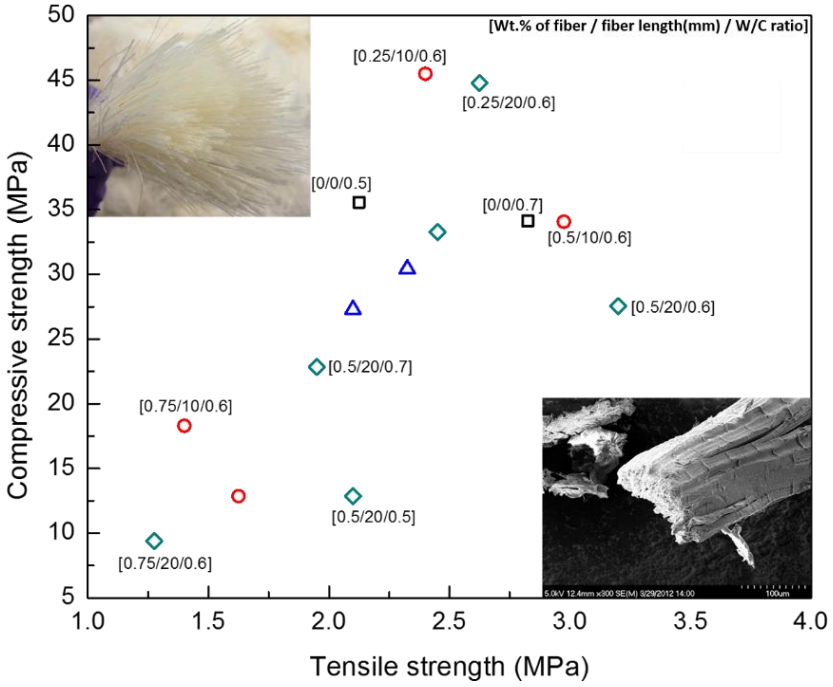

Figure 6.1: Effects of fiber content, fiber length and water/cement ratio on the mechanical properties of sisal fiber-reinforced concrete (SFCC)

The fiber with thermal, N7 and N10 treatment were used to reinforce concrete. Previous experiment results, shown in Fig. 6.1, illustrate the effects of sisal fiber content, fiber length, and water/cement ratio on tensile and compressive strength of concrete, as well as the morphology and microstructure of sisal fiber. It can be seen that the best results were achieved with 20 mm sisal fiber with 0.25 wt. %, and a W/C ratio of 0.6.

6.2 Microstructure Observations

Thermal treatment: In order to observe the microstructural changes caused by thermal treatment, a scanning electron microscope (SEM) was used to study the surface and cross section of the fibers, Fig. 6.2. In these figures, no obvious changes in the microstructure of surface and cross section were found, except for some decomposition of waxes (the cuticle layer). Actually, the degradation of hemicellulose and cellulose of sisal fiber starts at 186 ℃ (Martin, Martins et al. 2010), which is higher than the temperature used in our thermal treatment.

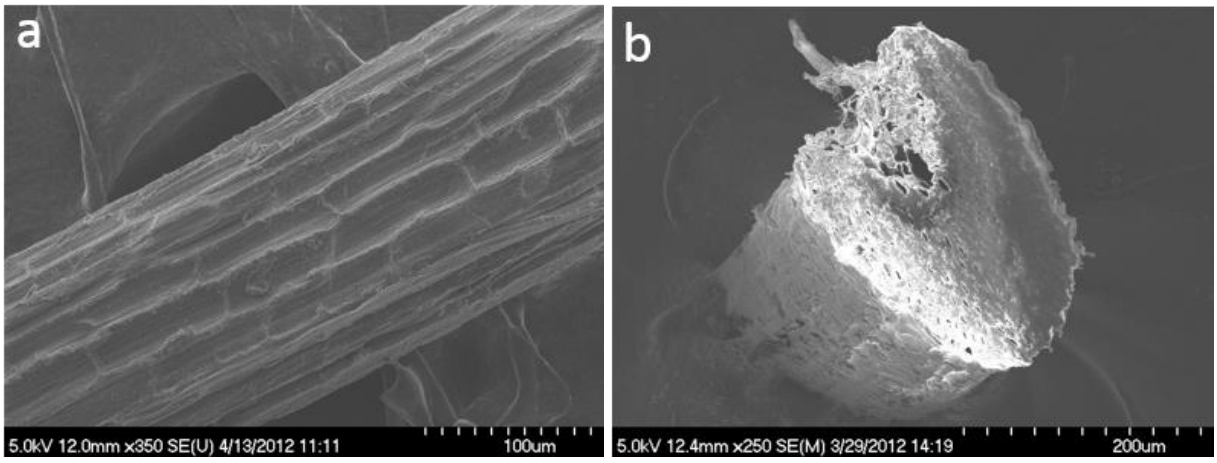

(a) Untreated fiber

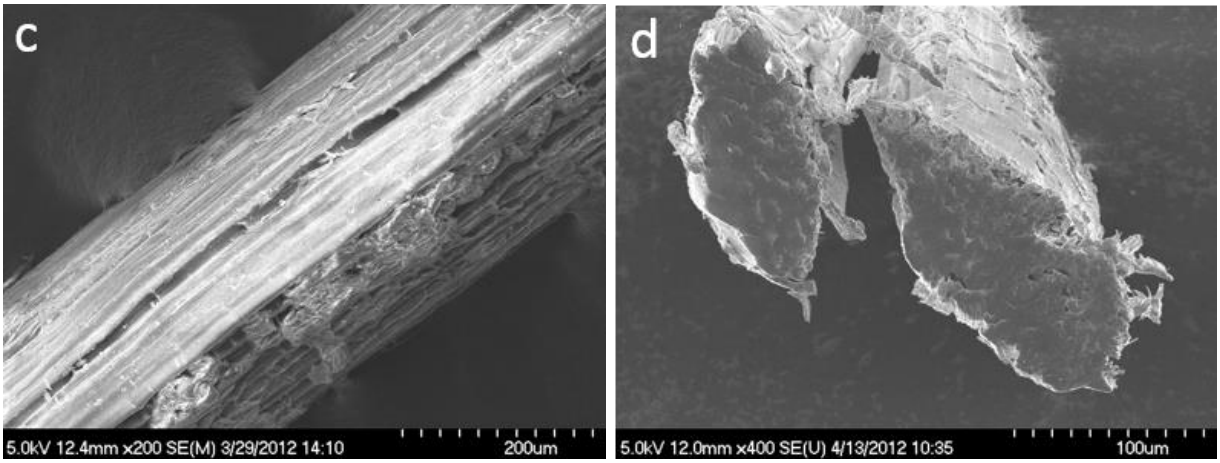

(b) Thermal treated fiber

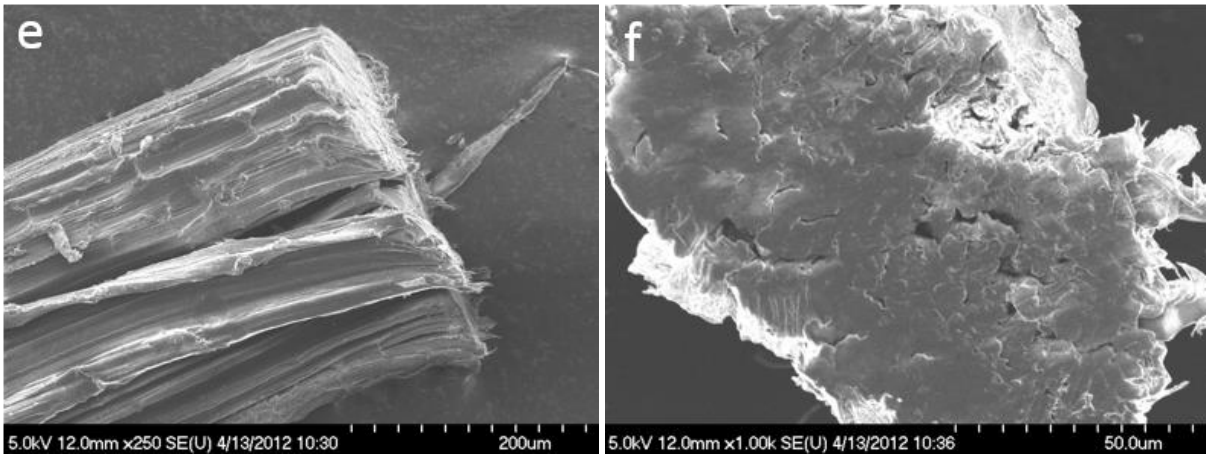

(c) N7 treated fiber

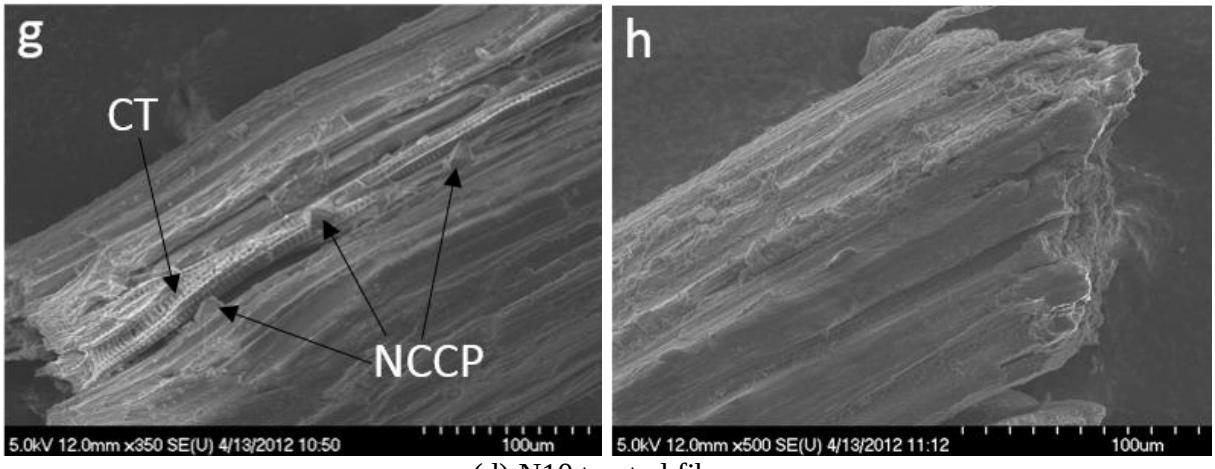

(d) N10 treated fiber

Figure 6.2: The microstructure of fiber surface and cross section

Na_2CO_3 treatment: The microstructural changes of sisal fiber caused by different Na_2CO_3 treatment durations are shown in Figs. 6.2-e to h. The fibers treated with Na_2CO_3 solution were washed with water and dried in air. There were no obvious changes in the microstructure of surface of fibers with N7 treatment, and the cross sections were found to be more compact than the raw fibers. The surface of sisal fiber after N10 treatment was very rough and conducting tissue (CT-tracheid and vessel element constituted as xylem), was found due to the degradation of hemi-cellulose, lignin in the primary cell wall of sisal fiber. Some Na_2CO_3 crystal particles (NCCP) were found on the fiber surface after washing.

6.3 Tensile Strength and Young's Modulus

Thermal treatment: The stress–strain curves of a single fiber with and without thermal treatment are shown in Fig. 6.3, and the numerical values are listed in Table 6.1.

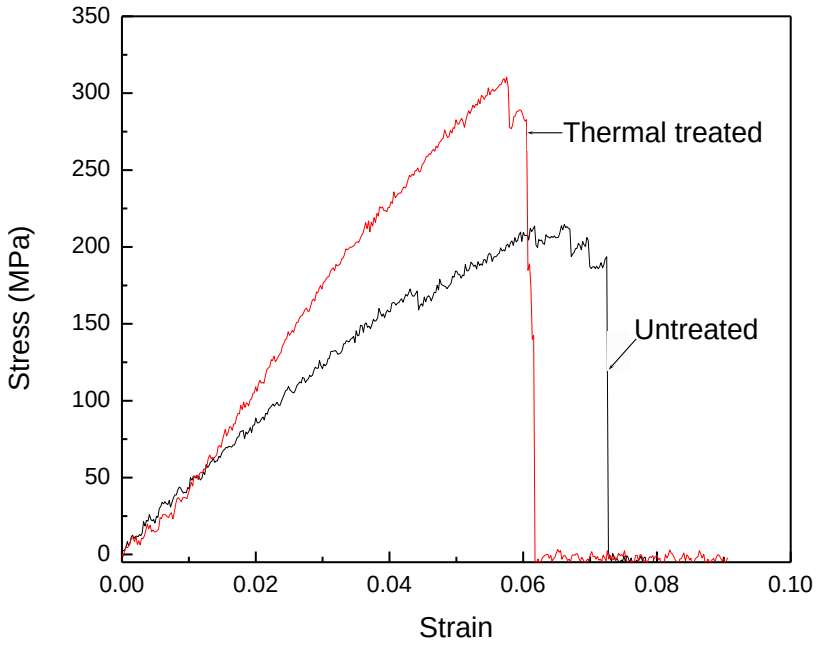

Figure 6.3: Effect of thermal treatment on stress–strain curve of sisal fiber

Table 6.1: Mechanical properties of sisal fiber with and without thermal treatment

Properties	Untreated	Thermal treated
Tensile strength (MPa)	214.65	310.54
Young's modulus (GPa)	19.979	33.988

These results indicate that the thermal treatment led to a significant 45% increase of tensile strength and an increase of Young's modulus of 70%.

Na_2CO_3 treatment: The stress–strain curves for single fibers with and without Na_2CO_3 treatment are shown in Fig. 6.4, and the numerical values are listed in Table 6.2. The cases of 7-day and 10-day treatment of fibers are identified as N7 and N10, respectively. According to these results a 7-day treatment caused a negligible 1% increase of the tensile strength, but a significant 37% increase of Young's modulus. On the other hand, the 10-day treatment reduced the tensile strength by a significant 36% and increased the Young's modulus by a moderate 12%. Thus it appears that the 7-day treatment is clearly superior to 10-day treatment with Na_2CO_3.

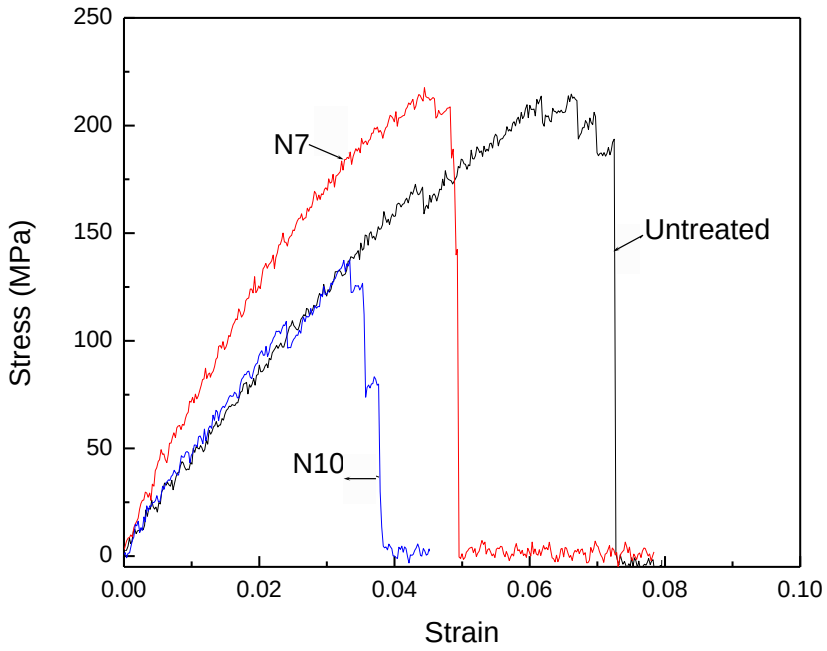

Figure 6.4: Effect of Na_2CO_3 treatment on stress–strain curves of sisal fiber

Table 6.2: Mechanical properties of sisal fiber with and without Na_2CO_3 treatment

Properties	Untreated	N7	N10
Tensile strength (MPa)	214.7	217.6	137.6
Young's modulus (GPa)	20.0	27.4	22.4

6.4 Weight Loss of Concrete Specimens

The actual weight losses of specimens should be able to serve as a measure of the durability of concrete (Otieno, Beushausen et al. 2012). The weight loss of concrete specimens with untreated and treated fibers was determined after subjecting the specimens to a certain number of wetting/drying cycles. The results are shown in Fig. 6.5. As can be seen, the weight of almost all specimens increased slightly after the first wetting/drying cycle, followed by a steady decrease with increasing number of cycles. After 15 cycles the average rate of weight loss of 10 specimens with thermal treated fibers was a negligibly small 0.5%. The average rate of weight loss of specimens with N7 treated fibers was 1.5%, while the largest rate of weight loss of 2.5% was experienced by specimens containing N10 treated fibers. The average weight loss rate of fibers with N7 treatment after 15 wetting/drying cycles was smaller than that of the untreated fiber group. As can be seen in Fig. 6.5, the weight of concrete reinforced with N7 treated sisal fibers increased after 20 cycles. This may be caused by a testing error, but it also illustrates the fact that the concrete with N7 treated sisal fiber does not suffer a severe weight loss.

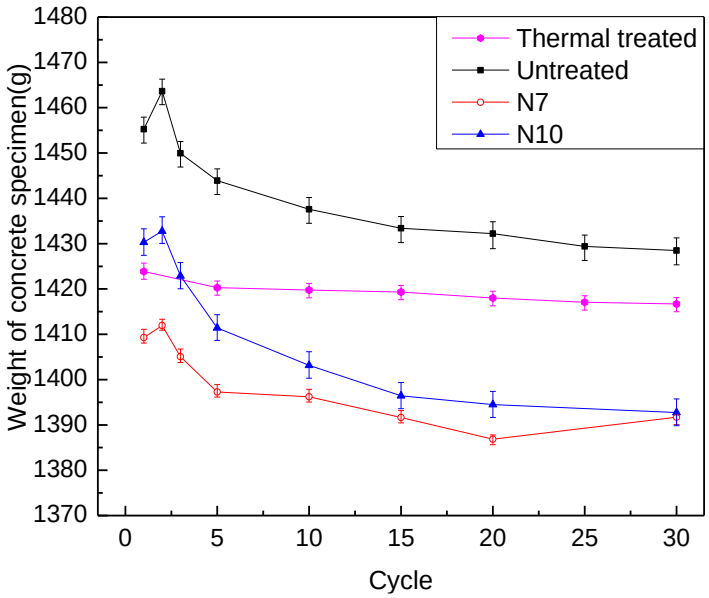

Figure 6.5: Change of weight of SFRC specimens with wetting/drying cycles

6.5 Durability of Concrete Reinforced with Treated Sisal Fiber

Thermal treatment: The durability of SFRC was evaluated using the rate at which the strength was reduced by wetting/drying cycles. The 7-day strength of concrete specimens reinforced with untreated and heat-treated sisal fibers served as reference, Fig. 6.6 and Table 6.3. As can be seen, the compressive strength increased slightly during the first five wetting/drying cycles before undergoing a steady decline. The rate of strength reduction caused by wetting/drying cycles was larger for the splitting tensile strength than for the compressive strength. The strength increase due to thermal treatment of the fibers was significant and consistent.

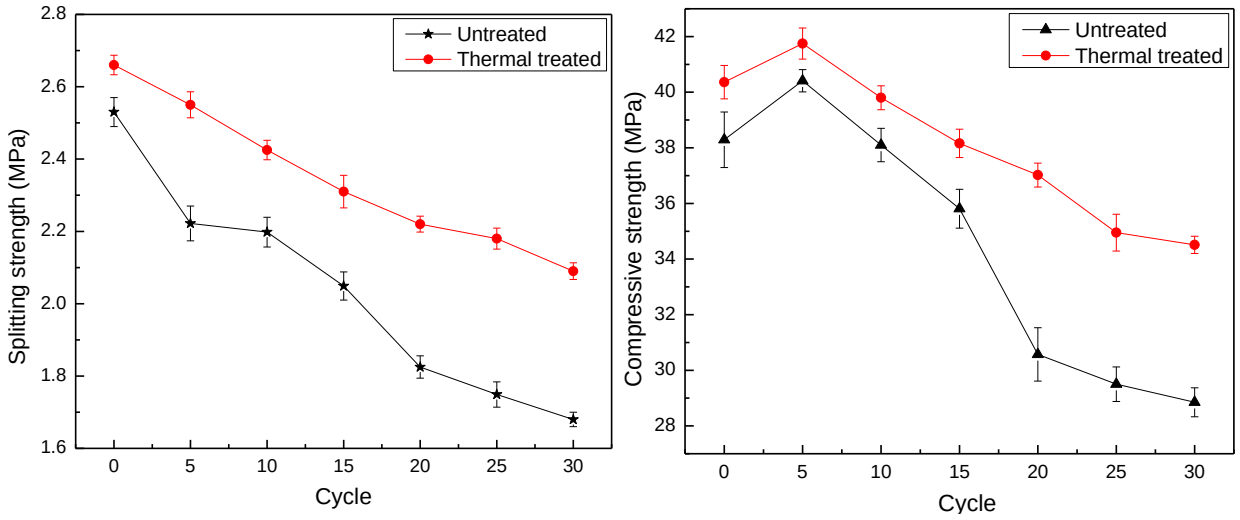

(a) Splitting tensile strength (b) Compressive strength

Figure 6.6: Effect of thermal treatment on durability of SFRC

Table 6.3: Effect of accelerated aging and fiber heat treatment on tensile and compressive strength

	Group	Initial strength (MPa)	Final strength (MPa)	Strength reduction	Average reduction rate per cycle
Splitting	Untreated	2.53	1.68	33.6%	1.12%
	Thermal	2.66	2.09	21.4%	0.71%
Compressive	Untreated	38.29	28.85	24.7%	0.82%
	Thermal	41.76	34.51	17.4%	0.58%

Na_2CO_3 treatment: The durability of concrete reinforced with sisal fiber with and without Na_2CO_3 treatment was also evaluated using the strength reduction caused by wetting/drying cycles as indicator, Fig. 6.7 and Table 6.4 According to these results, the splitting tensile and compressive strengths undergo steady reductions as functions of wetting/drying cycles, except for the specimens with untreated fibers, which experienced a small strength increase during the first five wetting/drying cycles. Specimens reinforced with N7 treated fibers had a little lower initial strengths than specimens with untreated fibers. The largest differences can be seen between specimens with fibers that had undergone N7 and N10 treatments. The effect of N7 treatment on compressive strength was far superior to that of N10 treatment. Whereas the N7 treatment resulted

in splitting tensile strengths exceeding those of specimens reinforced with both untreated and N10 treated fibers, the compressive strengths were comparable to those of the specimens with untreated fibers, both being superior to the performance of specimens with N10 treated fibers. Due to the lower tensile strength, the durability of N10 treated fiber reinforced concrete was lowest for compressive strength, and similar as untreated fiber reinforced concrete for splitting tensile strength.

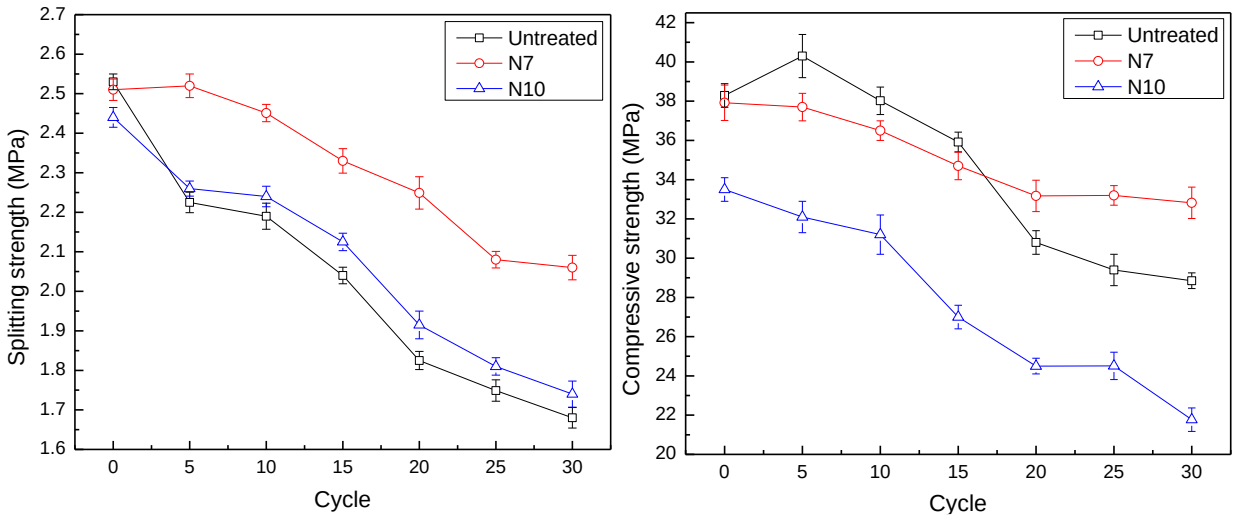

(a) Splitting tensile strength b) Compressive strength

Figure 6.7: Effect of Na_2CO_3 treatment on durability of SFRC

Table 6.4: Effect of Na_2CO_3 treatment on durability of SFRC

	Group	Initial strength (MPa)	Final strength (MPa)	Strength reduct.	Average reduct. rate per cycle
Splitting	Untreated	2.53	1.68	33.6%	1.12%
	N7	2.51	2.06	17.9%	0.60%
	N10	2.44	1.74	28.7%	0.96%
Compressive	Untreated	38.29	28.85	24.7%	0.82%
	N7	37.92	32.82	13.4%	0.45%
	N10	33.50	21.77	35.0%	1.17 %

6.6 Discussion of Treatment Mechanisms

6.6.1 Degradation of sisal fiber in concrete

The cement matrix has three different effects on the degradation of sisal fiber at the same time: (i) Alkaline pore water, produced by PC hydration, dissolves the amorphous materials of fiber, such as waxes, fats, hemicelluloses and lignin, which are sensitive to $Ca(OH)_2$ and high alkalinity and can be decomposed in an alkali environment (Tolêdo Filho, Scrivener et al. 2000, Sedan, Pagnoux et al. 2007). This weakens the link between individual fiber cells and leads to the reduction of tensile strength. (ii) Alkaline hydrolysis of cellulose molecules, which leads to degradation of molecular chains and then a reduction in the degree of polymerisation and lower tensile strength (Tolêdo Filho, Scrivener et al. 2000), because the strength of fiber mainly depends on the content of crystalline cellulose (Azwa, Yousif et al. 2013), which can also account for the increased tensile strength of thermal treated fiber. (iii) Crystallization of lime in the lumen, walls of the individual fibers and middle lamellae leading to a decrease in the technical fiber flexibility and strength (Singh 1985, Tolêdo Filho, Scrivener et al. 2000), which is also referred to as fiber mineralization. The detection of the deterioration causes becomes complicated, because all three effects influence the degradation of sisal fiber.

A microstructure analysis was performed to investigate the effect of wetting and drying cycles on the degradation of sisal fiber. Figs. 6.8-a, b, and c show micrographs of a composite fractured face obtained in compressive testing after 5, 15, and 30 wet/dry cycles, respectively. In Fig. 6.8-a, it can be seen that the sisal fiber, after being pulled out from the cement matrix, still remained intact without any indication of mineralization on the surface and decomposition of amorphous materials, which is likely to account for the remaining strength of untreated fiber reinforced concrete after the first five cycles. After 15 wetting and drying cycles, some fibers still

kept their original appearance, except for a minor sign of mineralization on the fiber surface caused by deposition of cement hydration products, especially calcium hydroxide. However, the other parts were seriously degraded on both the surface and in the lumen, due to the three degradation mechanisms discussed above. As shown in Fig. 6.8-b, the damaged fiber surface was mineralized and stripped from lumen, which was also decomposed due to the alkaline hydrolysis of hemicelluloses and lignin. With further aggravation of mineralization, decomposition and alkaline hydrolysis, sisal fibers were fully degraded. As can be seen in Fig. 6.8-c, after 30 wetting and drying cycles, the fiber surface was fully decomposed and the lumen was saturated with the cement hydration products. The hydration products on the surface and in the lumen caused degradation of the fibers and as a result the fibers lost their reinforcement capacity (Claramunt, Ardanuy et al. 2011). This is the reason for the reduction of both compressive and splitting tensile strength of untreated sisal fiber reinforced composites, as shown in Fig. 6.6 and Fig. 6.7.

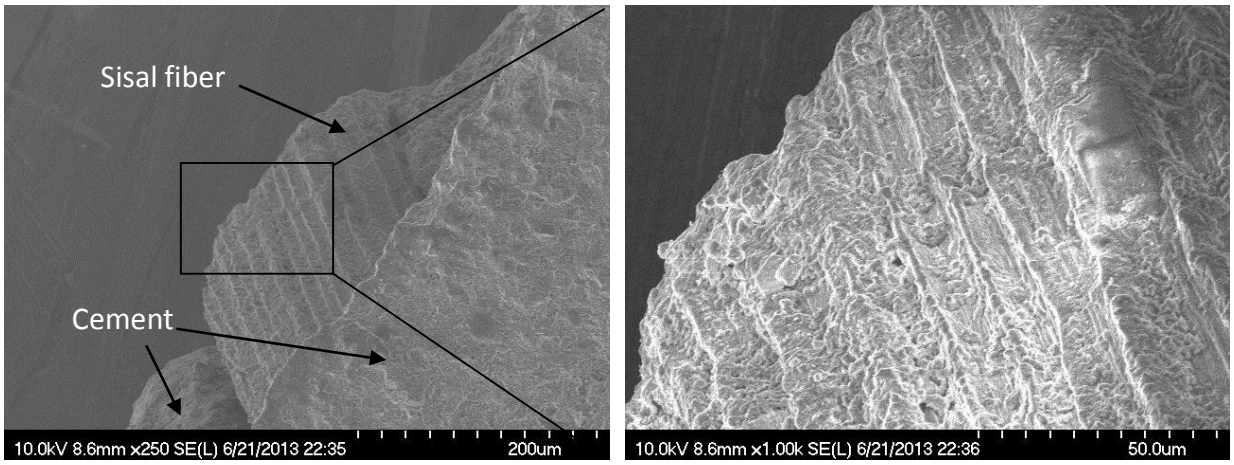

(a) after 5 cycles

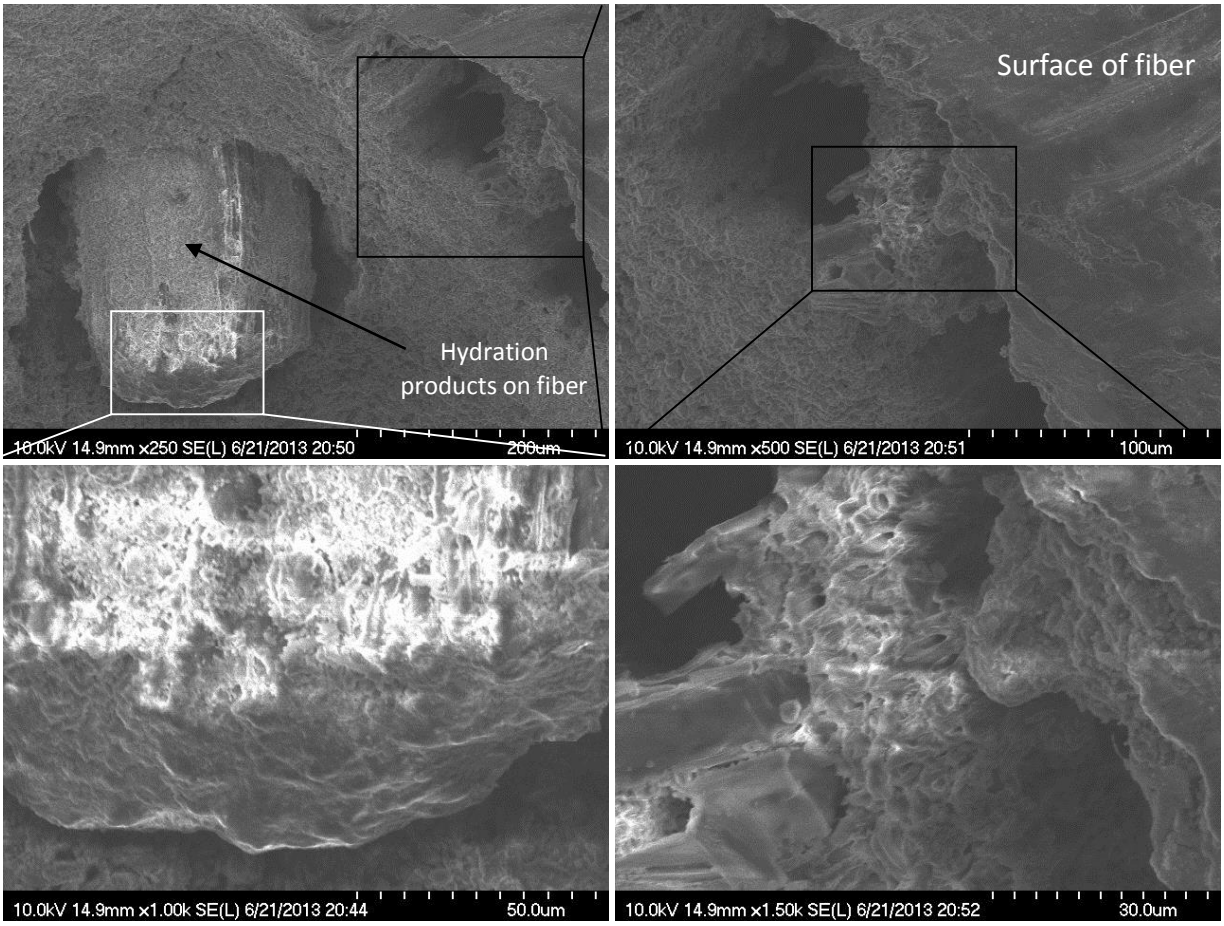

(b) after 15 cycles

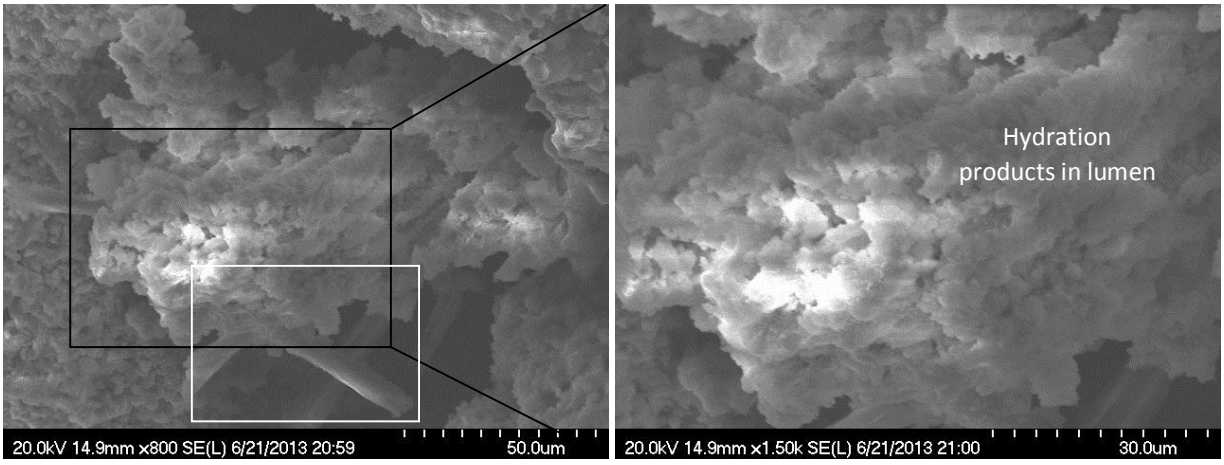

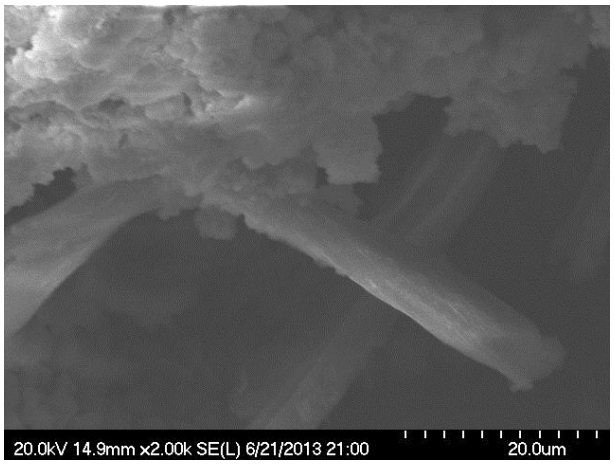

(c) after 30 cycles

Figure 6.8: SEM micrographs of the fracture surface of the aged concrete reinforced with untreated sisal fiber

6.6.2 Thermal treatment

Sisal fiber consists principally of 65.8%~78%) cellulose, 8%~10% lignin and 10%, ~12% hemicellulose (Wilson 1971, Walker 1993, Gassan 1996). Although lignin has the lowest initial decomposition temperature, it has the highest char yield (the percent mass that is retained at the end of the high temperature process stage) of 42%; this is attributable to a higher thermal stability, which is a consequence of lignin's aromatic structure (Abdel-Rahman, Al-Juruf et al. 1988). The results of X-ray diffraction presented in Fig. 6.9 reflect the effects of thermal and Na_2CO_3 treatment on sisal fiber's crystalline fraction. It can be seen that raw sisal fibers had similar spectra as treated ones, but the latter had higher intensity, thus the crystallinity and crystallite size of cellulose were greatly improved. The raw sisal fiber's cellulose crystallinity was 20.27%, and a slight improvement of it was obtained for sisal fiber immersed in Na_2CO_3 saturated solution, the percentage of crystallinity of which was 22.69%. The investigation results showed that thermal treatments have a superior enhancing effect on sisal fiber's crystallinity: their $\%Cr_2$ was improved from 20.27% to 22.67%, 26.42%, and 23.86%, owing to the thermal treatment under 150 ℃ for 4,

8, and 16 h, respectively, which means the highest degree of crystallinity was achieved by thermal treatment for 8 h for the maximum increase in the intensity of the crystalline peak at 22.5 °and the least one is thermal treatment for 4 h. This is also the reason for selecting fibers that were thermal treated for 8 h as reinforcement in concrete. Cellulose provides mechanical strength to the fibers (Patra, Bisoyi et al. 2012) and it is the most reactive constituent, which can be crystallized easily at a relative low temperature, therefore thermal treated sisal fiber showed a significant improvement of mechanical properties (as shown in Fig. 6.3) due to the improved crystallinity of cellulose, which assures higher initial strength and improved durability of sisal fiber in concrete.

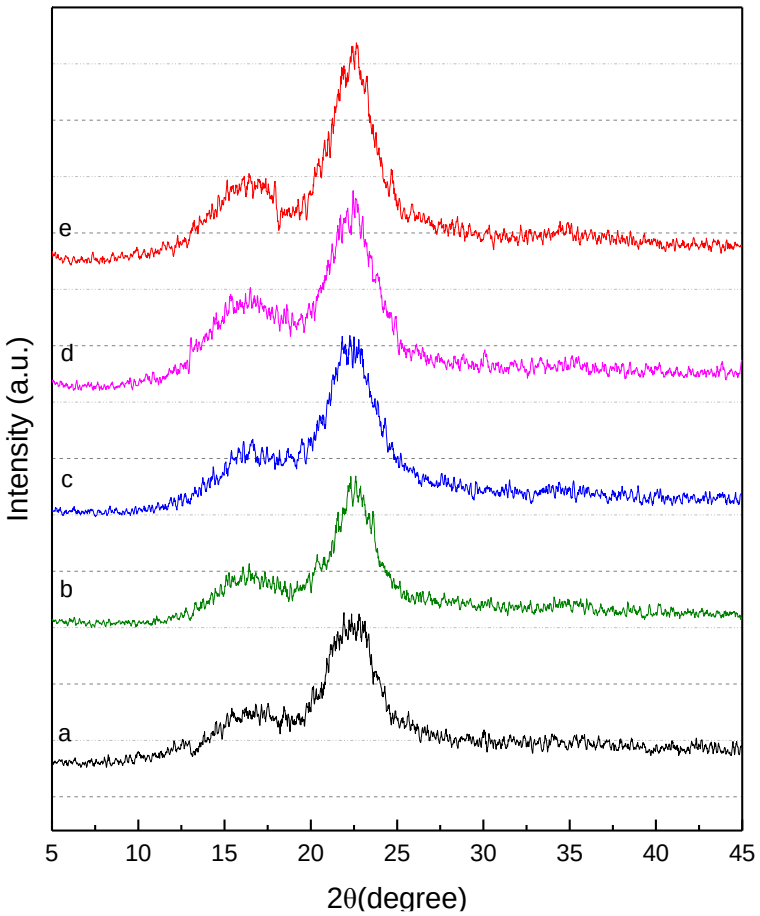

* a: untreated, b: Na_2CO_3 treated, c: thermal treated for 4 h, d: thermal treated for 8 h, e: thermal treated for 16 h.

Figure 6.9: X-ray diffraction spectra of sisal fiber

The results of thermal analysis (TGA and DTA) are shown in Fig. 6.10, which illustrates similar thermal degradation behavior differences between raw and thermal treated (8 h) fibers under temperatures between 25 and 600 ℃. Three main stages of weight loss were observed: (i) slight weight loss from 50 to 110 ℃ caused by evaporation of moisture in the fibers; (ii) weight loss for decomposition of hemicelluloses under temperature between 270 and 360 ℃; (iii) the maximum weight loss under higher temperatures reflecting the degradation of lignin and cellulose, the two of which account for over 80% of total fiber components.

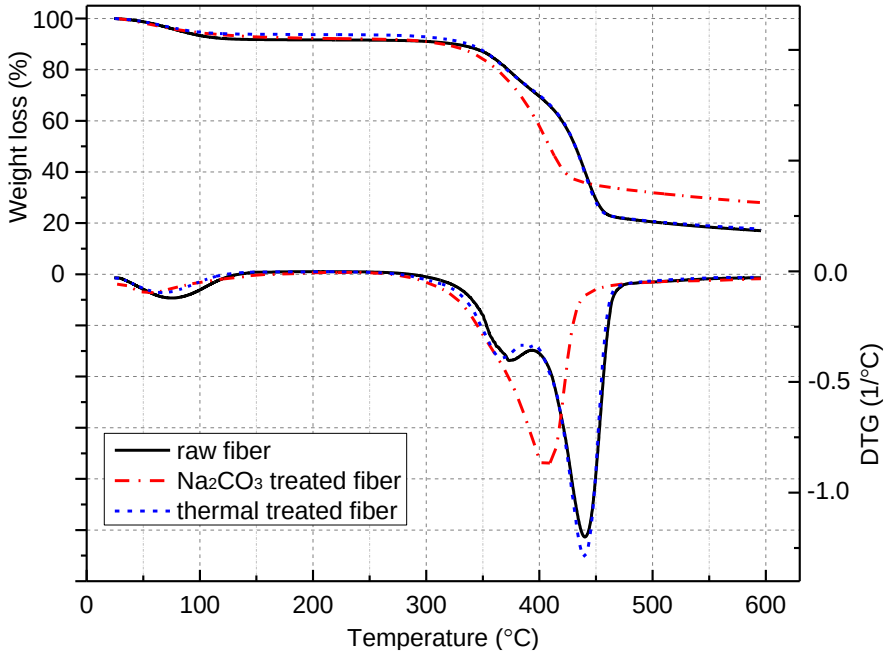

Figure 6.10: TGA (upper) and DTG (lower) curves of raw sisal fiber, Na_2CO_3 treated fiber (N10), and thermal treated fiber

The similar thermal degradation behaviors prove that thermal treatment does not reduce any component or decompose the molecules of sisal fiber, except for the slight reduction of moisture: a percentage weight loss of 7.08 % for untreated sisal fiber, and the weight loss of thermal treated sisal fiber is 4.57% (TGA curves between 50 and 110 ℃). Step 3 of N10 treated sisal fiber has a

weight loss, which is 27.77% and 26.68% less than that of untreated and thermal treated fiber. In addition, the DTG peak positions indicate that, compared with the untreated and thermal treated fibers, the decomposition of N10 treated sisal fiber finishes at a lower temperature (420 ℃). This means that Na_2CO_3 treatment removed some amorphous materials of sisal fiber, especially lignin, whose main function is to cement the cellulose fibers in plants. Therefore a slight improvement of fiber crystallinity caused by Na_2CO_3 was seen in Fig. 6.9. The result of TGA combined with XRD analysis above explains the reason for reduced mechanical properties of N10 treated sisal fiber and why we selected N7 treatment for comparison.

Fig. 6.11 shows the microstructure of the fracture surface of a composite after 30 wetting and drying cycles. Although the surface of sisal fiber was damaged and the links between individual fiber cells were broken in the accelerated aging process, it can be seen that there is no sign of mineralization caused by calcium hydroxide deposited in fiber lumen and voids, thus fiber cells with high crystallinity remained intact and retained part of the reinforcement capacity in concrete.

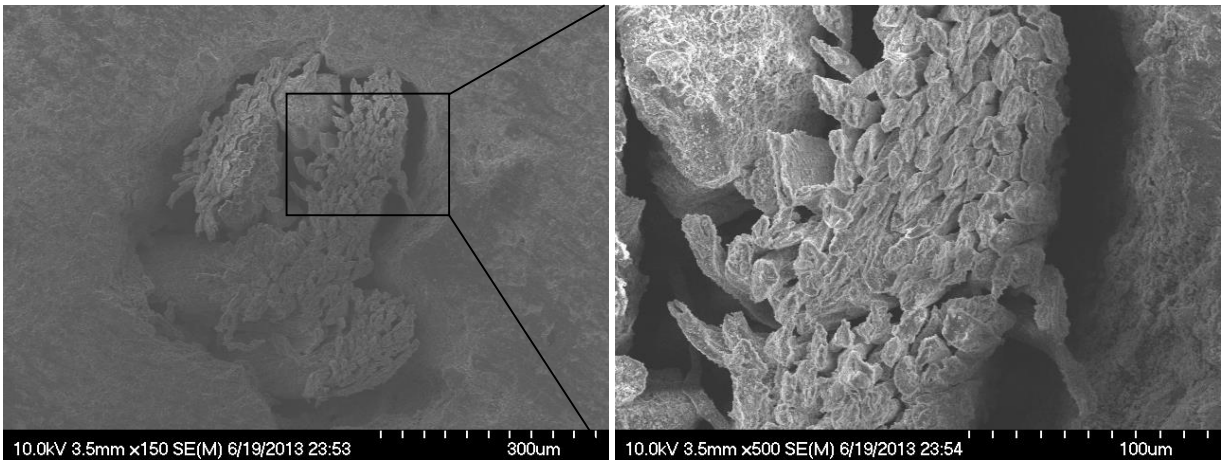

Figure 6.11: SEM micrographs of the fracture surface of the aged concrete reinforced with thermal treated sisal fiber after 30 wet/dry cycles

6.6.3 Na_2CO_3 treatment

Figs. 6.4 and 6.10 show that after N10 treatment, sisal fiber's tensile strength was reduced, due to the alkaline degradation of the three main components (lignin, hemicellulose and cellulose) of sisal in Na_2CO_3, therefore the durability of N10 treated SFRC is lower than that of the control group. In contrast, the fiber after N7 treatment did not lose tensile strength, and N7 treatment obviously improved the durability of fiber reinforced concrete. The major cause of the alkalinity of concrete is the following chemical reaction:

$$\mathrm{Ca(OH)_2} \rightarrow Ca^{2+} + 2OH^{-} \tag{6.1}$$

Utilizing the water absorption of sisal fiber, Na_2CO_3 solution was introduced to soak the dry fiber. After treatment in sodium carbonate saturated solution for several days, there will be a large number of Na^+ and CO_3^{2-} ions deposited on the fiber surface. When fibers are added to fresh concrete, there will be a chemical reaction on the fiber surface, due to the Ca^{2+} in the cement:

$$Ca^{2+} + \mathrm{CO_3^{2-}} \rightarrow \mathrm{CaCO_3}\downarrow \tag{6.2}$$

A layer consisting of calcium carbonate sediments, which protects the interior of a fiber from the strong alkali solution formed during the cement hydration process, was created and filled in pits and holes of the sisal fiber's surface (Fig. 6.12-a). The alkalinity of concrete restrains the ionization of the sediments, so that the protective layer can exist for a long time and provide good durability. The dissolution of the lignin and hemicelluloses existing in the middle lamellae of the fibers and hydrolysis of cellulose molecules caused by the alkaline pore solution can be effectively resisted, as presented in Fig. 6.12-b. Besides, Na^+ ions, which are harmful to the properties of concrete because they can trigger an alkali-aggregate reaction, are effectively prevented by the

protective layer from transferring into the concrete. Therefore, sisal fiber may achieve good durability when used as reinforcement of concrete and the detrimental effects of Na^+ ions can be kept to a minimum.

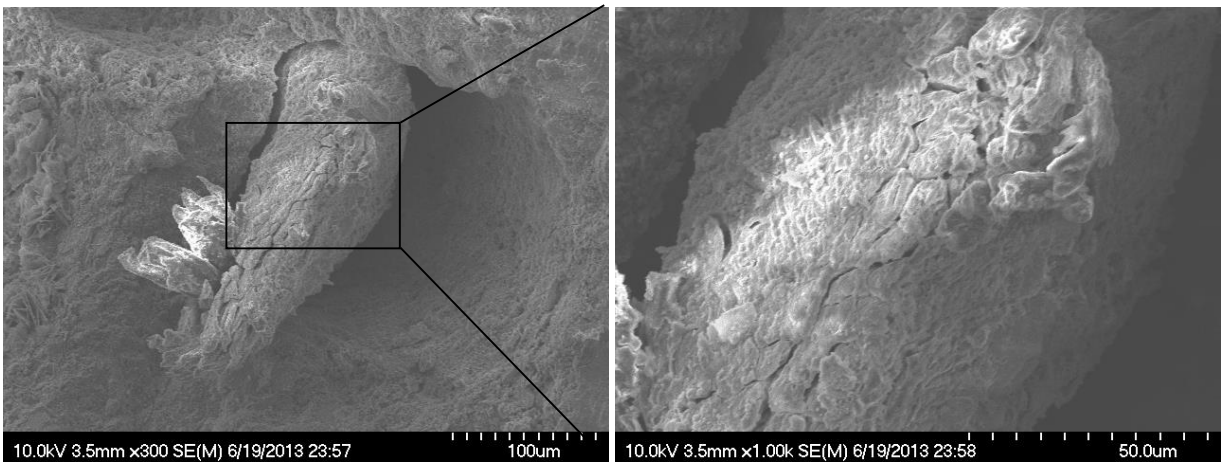

(a) The sediment layer around sisal fiber

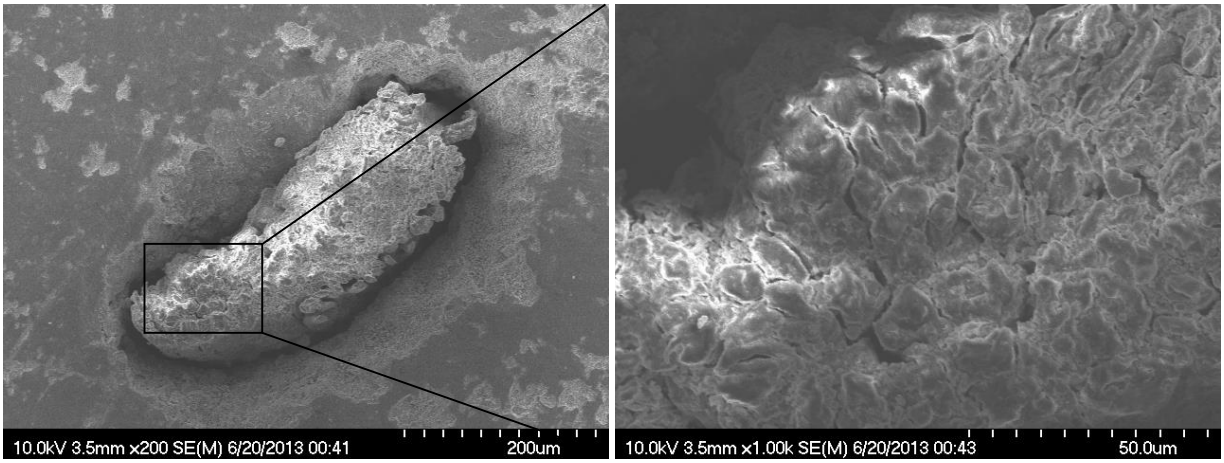

(b) Cross section of sisal fiber.

Figure 6.12: SEM micrographs of the fracture surface of the aged concrete reinforced with Na_2CO_3 treated sisal fiber after 30 wet/dry cycles

6.7 Summary

In order to improve the durability of sisal fiber in the alkali environment of concrete, two treatment methods were studied – thermal treatment and Na_2CO_3 treatment.

- The positive effects of thermal treatment on tensile strength and Young's modulus were obvious. Compared with untreated sisal fiber, thermal treatment increased the tensile strength and Young's modulus of fiber by 45% and 70%, respectively. N7 treatment improved the fiber's tensile strength and Young's modulus by 1.3% and 37.0%, respectively; N10 treatment reduced the tensile strength by 35.9%, but increased Young's modulus by 12.0%.
- The average weight loss rate of concrete reinforced with untreated fiber after 15 wetting/drying cycles was 1.6%, while the average weight loss rate of specimens with thermal treated fibers was a negligible 0.5%. The average weight loss rates due to N7 and N10 treatment were 1.6% and 2.5%, respectively.
- The durability of the sisal fiber in concrete was investigated by determining the effect of accelerated aging on the splitting and compressive strength of the SFRC. Concrete reinforced with thermal treated sisal fiber had higher splitting tensile and compressive strength than concrete reinforced with untreated fiber. Thermal treatment of the fiber improved the composite's splitting tensile strength by 24% and the compressive strength by 20%, after the specimens had been exposed to 30 wetting/drying cycles. The splitting tensile strength after 30 wetting/drying cycles was improved by N7 treatment by 45%, whereas N10 treatment improved it only by 14%. After 30 wetting/drying cycles, the compressive strength increased with N7 treatment by 45%, while N10 treatment reduced it by 42%.
- Treatment mechanisms were analyzed through XRD, TGA and microscopic investigation. Thermal treated sisal fiber showed a significant improvement of mechanical properties due to the improved crystallinity of cellulose, which assures higher initial strength and improved durability of sisal fiber in concrete. In the alkali environment of a concrete matrix, a layer consisting of calcium carbonate sediments was formed and filled in the pits and cavities on

the surface of Na_2CO_3 treated sisal fiber to improve the durability of the fiber and reduce the detrimental effects of Na^+ ions on concrete.

In conclusion, both thermal treatment and Na_2CO_3 treatment for 7 days were shown to have the potential of improving the durability of sisal as reinforcement of concrete. Both treatments have their advantages and disadvantages. Thermal treatment was shown to improve the mechanical properties of sisal fiber, thereby increasing the initial strength of SFRC, whereas the N7 treatment does not improve the initial strength of the fibers, but appears to improve the durability of SFRC. Therefore, both thermal and chemical treatments are economical and easy to apply and therefore deserve to be studied further. At present, our sisal fibers have been physically or chemically treated, respectively; indeed, a more effective reduction of Na^+ ions in the Na_2CO_3 treated sisal fibers should improve durability with less potential hazards. Further study of thermal-Na_2CO_3 dual processing can be expected to find that Na^+ reduction will be achieved through post processing with cation exchange resin.

CHAPTER 7: CONCLUSIONS AND FUTURE WORK

This dissertation presents a comprehensive series of novel experimental investigations and theoretical analyses to better understand the degradation behavior of natural fiber embedded in a cement matrix and to mitigate the fiber degradation and thereby improving the durability of natural fiber-reinforced cement composites. This chapter summarizes the primary findings of this study and identifies areas for future research. The main findings are grouped into six sections as follows: (i) a novel investigation to gain a deep understanding of natural fibers' degradation mechanisms and kinetics in the cement matrix; (ii) a separate investigation to directly determine the degradation rate of the embedded fibers by testing their tensile properties, thermal decompositions, and crystallinity indices; (iii) an innovative model proposed to predict the degradation rate of cellulose of natural fibers embedded in cementitious matrices; (iv) a novel and scientific method to determine accelerated aging conditions, to evaluate sisal fiber's degradation rate and durability of natural fiber-reinforced cement composites (NFRCC); (v) an innovative cement matrix modification to mitigate sisal fiber's deterioration through partial cement replacement by metakalin, nanoclay, limestone, biomass by-products (rice husk ash), and various combinations of them; (vi) two novel, simple, and economical treatment methods (thermal treatment and Na_2CO_3 surface treatment) of sisal fiber to improve its degradation resistance in the alkali environment of cement composites.

7.1 Mechanisms and Kinetics of Natural Fiber's Degradation in A Cement Matrix

- By partially replacing Portland cement with metakaolin (MK), amounts of calcium hydroxide (CH), ettringite and bound water of the solid phase, and concentrations of K, Na, Ca, Si and

OH^- of the pore solution of the cement matrix were significantly reduced. Therefore both the alkalinity and mineral environment of the cement matrix were effectively relieved. The substitution of MK not only decreases the autogenous shrinkage, but also significantly improves the compressive strength of the cement matrix.

- The chemical composition of sisal fiber is made up of pectin, extractive, lignin, hemicellulose, and cellulose, which is the main structural component in cell walls. Compared to fibers that were soaked in tap water, the fibers immersed in $Ca(OH)_2$ solution have a higher water absorption capacity.
- The substitution of 30 wt. % MK improved the durability of sisal fiber reinforced cement mortar. Therefore, controlling the pH value of the pore solution and the CH content at a relatively low level by using pozzolanic supplementary material is an effective way to arrest the degradation of natural fiber.
- The degradation of sisal fiber was also studied separately by tensile testing, crystallinity characterization, and components analysis. In blends with 10 and 30 wt.% metakaolin (MK10 and MK30), the fiber's degradation was effectively arrested, with higher amounts of residual lignin, hemicellulose and cellulose, and smaller crystallinity indices than the fibers embedded in pure cement.
- Due to the high amounts of residual lignin and hemicellulose and their protective barrier roles for arresting precipitation of portlandite in cell walls, the mineralization of natural fiber in MK modified cement matrices is effectively mitigated. The microstructure analysis also verified the better fiber integrity in MK30 than that in PC.
- Lignin and hemicellulose are amorphous and easily undergo the alkaline hydrolysis. Four interactional alternate steps were identified: (i) Degradation of lignin and part of hemicellulose

leading to the exposure of holocellulose; (ii) degradation of hemicellulose causing the decrease of integrity and stability of cell walls; (iii) degradation of intra-molecular hydrogen bonding leading to the dispersion of cellulose microfibrils; (iv) alkaline hydrolysis of amorphous regions containing reducing end (a latent aldehyde), and as a result, complete degradation of cellulose micro-fibrils. As the degradation proceeds, the hydration products, such as soluble C-S-H and portlandite, gradually infiltrate into the cell wall, which in turn will lead to mineralization and embrittlement of natural fiber.

- The alkali degradation of cellulose mainly depends on the reducing end in amorphous regions and can be simply generalized as the disconnection of discrete cellulose nano-crystals caused by decomposition of reducing end through four processes: peeling-off reaction, chemical stopping reaction, physical stopping reaction, and alkaline hydrolysis.
- Cell wall mineralization was found to be an important degradation mechanism which leads to the fiber embrittlement and the reduction of strength and strain capacity. In contrast to the reviews presented in the literature, two mineralization mechanisms are proposed in this study: CH-mineralization and self-mineralization. CH-mineralization: the crystallization of CH through nucleation and growth processes in cell walls not only seriously damage the bond between the various components but also corrode cellulose micro-fibrils, which leads to increased brittleness and reduction of strength. Self-mineralization: the slight hydrolysis of lignin and hemicellulose has no significant effect on Young's modulus of sisal fiber, however, when Cr.I exceeds 0.80, the deformability of fiber is reduced considerably.
- Four steps of fiber degradation were found in the modeling curve of cellulose degradation embedded in the MK30 matrix: primary stage, initial acceleration stage, deceleration stage, and final acceleration stage. The low degradation rates, especially the existence of a

deceleration stage, indicate that in the cement matrix with low alkalinity and CH amount, the deterioration of cellulose can be slowed significantly. The time needed to completely degrade the cellulose in MK30 is 13 times longer than in a matrix of pure cement.

7.2 Determination of Accelerated Aging Conditions for Evaluating Sisal Fiber's Degradation

- The most effective static approach for accelerating the degradation of natural fiber in cement composites is to soak the samples in tap water or change the humidity at 70 ℃ and higher temperature. The dynamic wetting and drying cycling has a more accelerating effect on strength and toughness decline of SFRCC.
- The results of a separate investigation of sisal fiber's degradation indicate that, compared with the static conditions, W&D treatment had a more accelerating effect on the alkali hydrolysis of fiber's amorphous components, as evidenced by the highest crystallinity indices, minimum content of holocellulose, and lowest tensile strength.
- The embedded fibers exposed to W&D cycling also suffer the most severe mineralization of cell walls. Therefore, the cyclic changes of humidity at a relative high temperature ($\geq$ 70 ºC) should be selected as the most effective accelerating condition for evaluating both the degradation of natural fiber in cement matrix and the durability of NFRCC.

7.3 Cement Matrix Modification to Mitigate Fiber Degradation

- With the increasing replacement of PC by MK, the second shoulder, caused by the tricalcium aluminate reactions, becomes more sharp and higher than that of silicate reaction. The replacement of MK by NC leads to a lower peak value and later peak position of the heat flow,

and lower total heat released. The combination of these two minerals significantly decreases the CH amount in the cement matrix.

- The combined partial substitution of MK and NC for Portland cement not only improves the initial flexural properties of SFRCC, but also significantly improves its durability.
- Both MK and NC significantly restrain the degradation of sisal fiber, while the combination of these two supplementary cementitious materials validates their complementary and synergistic effect at different stages of aging. MK arrests the fiber degradation more effectively at early age, while the high amount of silicon minerals promotes the complementary effect of NC on mitigating the deterioration of sisal fiber at later stages.
- RHA shows a better modifying effect than CRHA on improving both the initial mechanical properties and durability of SFRCC. Replacing 30wt.% cement by RHA effectively arrests the degradation of sisal fiber. The contrast test for replacing RHA by LS shows that the role of RHA in cement modification is mainly that of an active cementitious supplementary material.

7.4 Improving Fiber Degradation Resistance through Fiber Pretreatment

- Compared with Na_2CO_3 treatment, thermal treated sisal fibers obtain a higher tensile strength and Young's modulus. A decline of fiber strength was found for the fiber treated in Na_2CO_3 solution for 10 days.
- Concrete reinforced with thermal treated sisal fibers experiences a smaller average weight loss rate than concrete reinforced with untreated and Na_2CO_3 treated fibers.
- The durability of sisal fiber in concrete was investigated by determining the effect of accelerated aging on the splitting tensile and compressive strengths of the SFRC. The results

indicate that both thermal treatment and Na_2CO_3 treatment effectively improve the durability of SFRC.

- Thermal treated sisal fiber showed a significant improvement of mechanical properties due to the improved crystallinity of cellulose, which assures higher initial strength and maintains the reinforcing effect of sisal fiber in concrete for a long time.
- In the alkali environment of a concrete matrix, a layer consisting of calcium carbonate sediments was formed and filled in the pits and cavities on the surface of Na_2CO_3 treated sisal fiber to improve the degradation resistance of sisal fiber in the cement matrix and reduce the detrimental effects of Na^+ ions on concrete.

7.5 Recommendations for Future Work

- The degradation mechanisms and kinetics of natural fiber indicate the effect of alkalinity of the cement pore solution on the decomposition of its three components. Because of the uncertainties of the kinetics data and the lack of parameterization of mineralization, further investigation of the natural fiber degradation in cement matrices is necessary. The effects of temperature, concentration of Ca^{2+}, water/cement ratio, as well as their influences on mineralization, peeling-off reaction, and alkaline hydrolysis of lignin and hemicellulose, and especially the cellulose, need to be studied in more detail.
- The model proposed in Chapter 3 focuses on the degradation of cellulose in sisal fibers embedded in cement matrices. The model should be extended to predict the degradation rate of the entire natural fiber, including the hydrolysis rate of the other two components, lignin and hemicellulose.
- The partial replacement of Portland cement by combinations of metakaolin and nanoclay, as

well as rice husk ash, effectively mitigated the sisal fiber's degradation. Further investigation of cement modification using supplementary cementitious materials, such as fly ash, colloidal silicate, should be performed to produce calcium hydroxide free matrices.

- Both thermal and chemical treatments are economical and easy to apply and therefore deserve to be studied further. At present, our sisal fibers have been physically or chemically treated; indeed, a more effective reduction of Na^+ ions in the Na_2CO_3 treated sisal fibers should improve durability with less potential hazards. It is expected that Na^+ reduction will be achieved through post processing with cation exchange resin.

REFERENCES

Abdel-Hamid, A. M., J. O. Solbiati and I. K. O. Cann (2013). Chapter One - Insights into Lignin Degradation and its Potential Industrial Applications. Advances in Applied Microbiology. S. Sima and M. G. Geoffrey, Academic Press. Volume 82: 1-28.

Abdel-Rahman, H. H., R. Al-Juruf, F. Ahmad and I. Alam (1988). "Physical, mechanical and durability characteristics of date palm frond stalks as reinforcement in structural concrete." International Journal of Cement Composites and Lightweight Concrete 10(3): 175-181.

Adler, E. F., Ingemar; Marton, Joseph; Halvarson, Hans (1964). "The Behaviour of Lignin in Alkaline Pulping. II. Model Experiments with Arylalkyl-beta-aryl Ethers." Acta Chem. Scand 18: 1313-1314.

Agopyan, V., H. Savastano, V. John and M. Cincotto (2005). "Developments on vegetable fibre–cement based materials in São Paulo, Brazil: an overview." Cem Concr Compos 27: 527-536.

Al-Ghamdy, D. O., J. K. Wight and E. Tons (1994). "Flexural Toughness of Steel Fiber Reinforced Concrete." JKAU:Eng. Sci. 6: 81-97

Amato, I. (2013). "Green cement: Concrete solutions." Nature 494: 300-301.

Ambroise, J., S. Maximilien and J. Pera (1994). "Properties of Metakaolin blended cements." Advanced Cement Based Materials 1(4): 161-168.

Andersson, K., B. Allard, M. Bengtsson and B. Magnusson (1989). "Chemical composition of cement pore solutions." Cement and Concrete Research 19(3): 327-332.

Andonian, R., Y. Mai and B. Cotterell (1979). "Strength and fracture properties of cellulose fibre reinforced cement composites." International Journal of Cement Composites 1(4): 151-158.

Antoni, M., J. Rossen, F. Martirena and K. Scrivener (2012). "Cement substitution by a combination of metakaolin and limestone." Cement and Concrete Research 42(12): 1579-1589.

Anwar, M., Miyagawa, T., and Gaweesh, M. (2001). Using rice husk ash as a cement replacement material in concrete. The first International Conference on Ecological Building Structure. San Rafael, California: 671- 684.

Arabani, M., A. K. Haghi, A. Mohammadzade Sani and N. Kamboozia (2012). "Use of Nanoclay for Improvement the Microstructure and Mechanical Properties of Soil Stabilized by Cement." Proceedings of the 4th International Conference on Nanostructures (ICNS4) 12-14 March, Kish Island, I.R. Iran.

Aziz, M. A., P. Paramasivam and S. L. Lee (1981). "Prospects for natural fibre reinforced concretes in construction." International Journal of Cement Composites and Lightweight Concrete 3(2): 123-132.

Azwa, Z. N., B. F. Yousif, A. C. Manalo and W. Karunasena (2013). "A review on the degradability of polymeric composites based on natural fibres." Materials & Design 47(0): 424-442.

Bach, T. T. H., C. C. D. Coumes, I. Pochard, C. Mercier, B. Revel and A. Nonat (2012). "Influence of temperature on the hydration products of low pH cements." Cement and Concrete Research 42(6): 805-817.

Bakare, I. O., F. E. Okieimen, C. Pavithran, H. P. S. Abdul Khalil and M. Brahmakumar (2010). "Mechanical and thermal properties of sisal fiber-reinforced rubber seed oil-based polyurethane composites." Materials & Design 31(9): 4274-4280.

Balaguru, P. N. and S. P. Shah (1992.). Fiber-reinforced cement composites. New York, McGraw-Hill.

Baley, C., F. Busnel, Y. Grohens and O. Sire (2006). "Influence of chemical treatments on surface properties and adhesion of flax fibre–polyester resin." Composites Part A: Applied Science and Manufacturing 37(10): 1626-1637.

Barneyback Jr, R. S. and S. Diamond (1981). "Expression and analysis of pore fluids from hardened cement pastes and mortars." Cement and Concrete Research 11(2): 279-285.

Barreto, A. C. H., M. M. Costa, A. S. B. Sombra, D. S. Rosa, R. F. Nascimento, S. E. Mazzetto and P. B. A. Fechine (2010). "Chemically Modified Banana Fiber: Structure, Dielectrical Properties and Biodegradability." Journal of Polymers and the Environment 18(4): 523-531.

Barreto, A. C. H., M. A. Esmeraldo, D. S. Rosa, P. B. A. Fechine and S. E. Mazzetto (2010). "Cardanol biocomposites reinforced with jute fiber: Microstructure, biodegradability, and mechanical properties." Polymer Composites 31(11): 1928-1937.

Barreto, A. C. H., D. S. Rosa, P. B. A. Fechine and S. E. Mazzetto (2011). "Properties of sisal fibers treated by alkali solution and their application into cardanol-based biocomposites." Composites Part A: Applied Science and Manufacturing 42(5): 492-500.

Batis, G., P. Pantazopoulou, S. Tsivilis and E. Badogiannis (2005). "The effect of metakaolin on the corrosion behavior of cement mortars." Cement and Concrete Composites 27(1): 125-130.

Belaadi, A., A. Bezazi, M. Bourchak and F. Scarpa (2013). "Tensile static and fatigue behaviour of sisal fibres." Materials & Design 46(0): 76-83.

Bensted, J. and P. Barnes (2002). Structure and performance of cements (Second Edition). New York, NY,USA, Spon Press.

Benzerzour, M., N. Sebaibi, N. E. Abriak and C. Binetruy (2012). "Waste fibre–cement matrix bond characteristics improved by using silane-treated fibres." Construction and Building Materials 37(0): 1-6.

Bergström, S. G. and H.-E. Gram (1984). "Durability of alkali-sensitive fibres in concrete." International Journal of Cement Composites and Lightweight Concrete 6(2): 75-80.

Berhane Z, G. H. (1987). Effect of cement composition on the durability of natural fibres in mortar. Proc of the Fourth Intl Conf on Durability of Building Materials and Components. Singapore: 203–210.

Bessell, T. J. and S. M. Mutuli (1982). "The interfacial bond strength of sisal—cement composites using a tensile test." Journal of Materials Science Letters 1(6): 244-246.

Bilba, K. and M. A. Arsene (2008). "Silane treatment of bagasse fiber for reinforcement of cementitious composites." Composites Part A: Applied Science and Manufacturing 39(9): 1488-1495.

Bindu, C. S. B., K. S. (2009). "Utilization of coir fibre in bituminous concrete mixes." Indian Coconut Journal 52(8): 18-22.

Blankenhorn, P. R., B. D. Blankenhorn, M. R. Silsbee and M. DiCola (2001). "Effects of fiber surface treatments on mechanical properties of wood fiber–cement composites." Cement and Concrete Research 31(7): 1049-1055.

Blazej, A., M. Kosík, J. F. JKennedy, G. O. Phillips, D. J. Wedlock and P. A. Williams (1985). Cellulose and its Derivates: Chemistry, Biochemistry and Application. New York, Ellis Horwood Limited.

Blears, M. J., G. Machell and G. N. Richards (1957). "Alkaline Degradation of 4-0-Substituted Glucose Derivatives." Chem. and Ind: 1150-1151.

Bledzki, A. K. and J. Gassan (1999). "Composites reinforced with cellulose based fibres." Progress in Polymer Science 24(2): 221-274.

Bourbigot, S., S. Chlebicki and V. Mamleev (2002). "Thermal degradation of cotton under linear heating." Polymer Degradation and Stability 78(1): 57-62.

Brebu, M. and C. Vasile (2010). "Thermal degradation of lignin - A review." Cellulose Chem. Technol. 44(9): 353-363.

Browning, B. L. (1967). Methods in wood chemistry. New York, Interscience Publishers.

C1018, A. (1997). "ASTM C1018-97 Standard Test Method for Flexural Toughness and First-Crack Strength of Fiber-Reinforced Concrete (Using Beam With Third-Point Loading)."

C1185, A. (2012). Standard Test Methods for Sampling and Testing Non-Asbestos Fiber-Cement Flat Sheet, Roofing and Siding Shingles, and Clapboards. West Conshohocken, PA, ASTM International.

Caldaron, A. A. and R. G. Burg (1994). "High-reactivity metakaolin: A new generation mineral." Concr. Int. 11: 37-40.

Campbell, M. D. and R. S. P. Coutts (1980). "Wood fibre-reinforced cement composites." Journal of Materials Science 15(8): 1962-1970.

Carvalho, M. A., C. Calil Júnior, H. Savastano Junior, R. Tubino and M. T. Carvalho (2008). "Microstructure and mechanical properties of gypsum composites reinforced with recycled cellulose pulp." Materials Research 11: 391-397.

Chand, N., R. K. Tiwary and P. K. Rohatgi (1988). "Bibliography Resource structure properties of natural cellulosic fibres - an annotated bibliography." Journal of Materials Science 23(2): 381-387.

Charles, E. W., R. D. Stephen, E. H. Michael, W. B. John, E. S. Catherine and V. Liisa (2004). Hydrolysis of Cellulose and Hemicellulose. Polysaccharides, CRC Press.

Chindaprasirt, P., P. Kanchanda, A. Sathonsaowaphak and H. T. Cao (2007). "Sulfate resistance of blended cements containing fly ash and rice husk ash." Construction and Building Materials 21(6): 1356-1361.

Claramunt, J., M. Ardanuy, J. A. Garc á-Hortal and R. D. T. Filho (2011). "The hornification of vegetable fibers to improve the durability of cement mortar composites." Cement and Concrete Composites 33(5): 586-595.

Coleman, N. J. and W. R. McWhinnie (2000). "The solid state chemistry of metakaolin-blended ordinary Portland cement." Journal of Materials Science 35: 2701-2710.

Coleman, N. J. and C. L. Page (1997). "Aspects of the pore solution chemistry of hydrated cement pastes containing metakaolin." Cement and Concrete Research 27(1): 147-154.

Cooke, A. M. "Durability of Autoclaved Cellulose Fiber Cement Composites."

Courard, L., A. Darimont, M. Schouterden, F. Ferauche, X. Willem and R. Degeimbre (2003). "Durability of mortars modified with metakaolin." Cement and Concrete Research 33(9): 1473-1479.

Coutts, R. S. P. (1987). "Fibre-matrix interface in air-cured wood-pulp fibre-cement composites." Journal of Materials Science Letters 6(2): 140-142.

Coutts, R. S. P. and M. D. Campbell (1979). "Coupling agents in wood fibre-reinforced cement composites." Composites 10(4): 228-232.

Coutts, R. S. P. and P. Kightly (1982). "Microstructure of autoclaved refined wood-fibre cement mortars." Journal of Materials Science 17(6): 1801-1806.

Coutts, R. S. P. and P. G. Warden (1992). "Sisal pulp reinforced cement mortar." Cement and Concrete Composites 14(1): 17-21.

Cunha, V., J. Barros and J. Sena-Cruz (2010). "Pullout Behavior of Steel Fibers in Self-Compacting Concrete." Journal of Materials in Civil Engineering 22(1): 1-9.

D'Almeida, A. L. F. S., J. A. Melo Filho and R. D. Toledo Filho (2009). "Use of curaua fibers as reinforcement in cement composites " Chemical Engineering Transactions 17: 1717-1722.

D. Garvin, V. B. P., H.J. White (1987). CODATA Thermodynamic Tables. Selections for Some Compounds of Calcium and Related Mixtures: A Prototype Set of Tables. Berlin.

Dahlman, O., A. Jacobs and J. Sjöberg (2003). "Molecular properties of hemicelluloses located in the surface and inner layers of hardwood and softwood pulps." Cellulose 10(4): 325-334.

Das, B. R. and P. K. Banerjee (2013). "Interface bond and compatibility of jute with asphalt." Composites Part B: Engineering 53(0): 69-75.

Dasong Dai, M. F. (2010). "Characteristic and Performance of Elementary Hemp Fibre." Materials Sciences and Applications 1(6): 336-342.

de Guti érrez, R. M., L. N. D áz and S. Delvasto (2005). "Effect of pozzolans on the performance of fiber-reinforced mortars." Cement and Concrete Composites 27(5): 593-598.

De Rosa, I. M., J. M. Kenny, D. Puglia, C. Santulli and F. Sarasini (2010). "Morphological, thermal and mechanical characterization of okra (Abelmoschus esculentus) fibres as potential reinforcement in polymer composites." Composites Science and Technology 70(1): 116-122.

De Weerdt, K., M. B. Haha, G. Le Saout, K. O. Kjellsen, H. Justnes and B. Lothenbach (2011). "Hydration mechanisms of ternary Portland cements containing limestone powder and fly ash." Cement and Concrete Research 41(3): 279-291.

Delgado H, A. L. (2011). Investigation of the fatigue properties of asphalt mixtures reinforced with natural fibres. 5thInt conf bituminous mixtures and Pavements. Thessaloniki, Greece.

Deniel James I, G. V. S., Melvyn A. Galinat, et al. (2003). . 544.1R-96 State-of-the-Art Report on Fiber Reinforced Concrete. . ACI Manual of concrete practice-Part 6.

Deschner, F., F. Winnefeld, B. Lothenbach, S. Seufert, P. Schwesig, S. Dittrich, F. Goetz-Neunhoeffer and J. Neubauer (2012). "Hydration of Portland cement with high replacement by siliceous fly ash." Cement and Concrete Research 42(10): 1389-1400.

Ding, Z., D. Zhang, H. Shao, K. Wu and X. Zhang (1997). "Influence of metakaolin on properties of Portland cement." China Concr. Cem. Prod. 25(281-287).

Do Vale, A., M. J. Casagrande and J. Soares (2013). "A study of behaviour of natural fibre in stone matrix asphalt using two design methods." J Mater Civ Eng. 10: 1061.

Duchesne, J. and M. A. Be ŕube ´(1995). "Effect of supplementary cementing materials on the composition of cement hydration products." Advanced Cement Based Materials 2(2): 43-52.

Ebringerova, A., Z. Hromadkova and T. Heinze (2005). "Hemicellulose." Adv. Polym. Sci. 128: 1-67.

Elenga, R. G., G. F. Dirras, J. Goma Maniongui, P. Djemia and M. P. Biget (2009). "On the microstructure and physical properties of untreated raffia textilis fiber." Composites Part A: Applied Science and Manufacturing 40(4): 418-422.

Elie Awwad, D. C., Helmi Khatib (2013). Concrete masonry blocks reinforced with local industrial hemp fibers and hurds. Third International Conference on Sustainable Construction Materials and Technologies. Kyoto, Japan.

Erdtman, H. (1972). "Lignins: Occurrence, formation, structure and reactions, K. V. Sarkanen and C. H. Ludwig, Eds., John Wiley & Sons, Inc., New York, 1971. 916 pp. $35.00." Journal of Polymer Science Part B: Polymer Letters 10(3): 228-230.

Esmeraldo Milena A., B. A. C. H., Jos é E. B. Freitas, et al. (2010). "Dwarf-green coconut fibers: a versatile natural renewable raw bioresource." BioResources 4: 2478-2501.

Farzadnia, N., A. A. Abang Ali, R. Demirboga and M. P. Anwar (2013). "Effect of halloysite nanoclay on mechanical properties, thermal behavior and microstructure of cement mortars." Cement and Concrete Research 48(0): 97-104.

Fernandes, E. M., J. F. Mano and R. L. Reis (2013). "Hybrid cork–polymer composites containing sisal fibre: Morphology, effect of the fibre treatment on the mechanical properties and tensile failure prediction." Composite Structures 105(0): 153-162.

Fernandez, R., F. Martirena and K. L. Scrivener (2011). "The origin of the pozzolanic activity of calcined clay minerals: A comparison between kaolinite, illite and montmorillonite." Cement and Concrete Research 41(1): 113-122.

Flávio de Andrade Silva, B. M., Romildo Dias de Toledo Filho (2009). Advances in Natural Fiber Cement Composites: A Material for the Sustainable Construction Industry. 4th Colloquium on Textile Reinforced Structures (CTRS4). Dresden, Germany: 377-388.

Franzon, O. a. S., O. (1957). "Degradation of Cellulose by Alkali Cooking." Svensk Papperstidning 23: 872-877.

G. Ramakrishna, T. S. a. a. S. K. (2010). "EVALUA TION OF DURABILITY OF NATUR A L FIBRE REINF ORCED CEMENT MORTAR COMPOS ITE - A NEW APPR OACH " Journal of Engineering and A pplied Sciences 5(6).

Garvey, C. J., I. H. Parker and G. P. Simon (2005). "On the Interpretation of X-Ray Diffraction Powder Patterns in Terms of the Nanostructure of Cellulose I Fibres." Macromolecular Chemistry and Physics 206(15): 1568-1575.

Gassan, J., Bledzki, A. K. (1996). "Modification methods on nature fibers and their influence on the properties of the composites." J Eng Appl Sci 2: 2552–2557.

Gierer, J. L., Bernard; Wallin, Nils-Håkan (1964). "The Reactions of Lignin During Sulphate Cooking. Part V. Model Experiments on the Splitting of Aryl-alkyl Ether Linkages by 2N Sodium Hydroxide and by White Liquor." Acta Chem. Scand. 18: 1469-1476.

Gleize, P. J. P., M. Cyr and G. Escadeillas (2007). "Effects of metakaolin on autogenous shrinkage of cement pastes." Cement and Concrete Composites 29(2): 80-87.

Goring, D. A. I., T. E. Timell (1962). Tappi 45: 454.

Gram, H. E. (1983). Durability of natural fibers in concrete. Stockholm, Swedish Cement and Concrete Research Institute. Research Fo. 1:83.

Gram HE, N. P. (1987). Durability of natural fibres in cement-based roofing sheets. Proc of the Symp on Building Materials for Low-income Housing: Asia and Pacific Region. Bangkok, Thailand, NewDelhi: Oxford & IBH Publ: 328–334.

Gu, H. (2009). "Tensile behaviours of the coir fibre and related composites after NaOH treatment." Materials & Design 30(9): 3931-3934.

Gustavo Henrique Denzin Tonoli, A. E. F. d. S. A., Marcelo Assumpção Pereira-da-Silva, Alexandre Bassa, Danilo Oyakawa, Holmer Savastano Jr (2010). "Surface properties of eucalyptus pulp fibres as reinforcement of cement-based composites." Holzforschung 64(5): 595-601.

Haas, D. W., B. F. Hrutfiord and K. V. Sarkanen (1967). "Kinetic study on the alkaline degradation of cotton hydrocellulose." Journal of Applied Polymer Science 11(4): 587-600.

Habeeb, G. A. F., M. M. (2009). "Rice Husk Ash Concrete: the Effect of RHA Average Particle Size on Mechanical Properties and Drying Shrinkage." Australian Journal of Basic & Applied Sciences 3(3): 1616-1622.

Hamzeh, Y., K. P. Ziabari, J. Torkaman, A. Ashori and M. Jafari (2013). "Study on the effects of white rice husk ash and fibrous materials additions on some properties of fiber–cement composites." Journal of Environmental Management 117(0): 263-267.

Hatfield, R. and W. Vermerris (2001). "Lignin formation in plants. The dilemma of linkage specificity." Plant Physiology 126: 1351–1357.

He, C., B. Osbaeck and E. Makovicky (1995). "Pozzolanic reactions of six principal clay minerals: Activation, reactivity assessments and technological effects." Cement and Concrete Research 25(8): 1691-1702.

He, J., S. Cui and S.-y. Wang (2008). "Preparation and crystalline analysis of high-grade bamboo dissolving pulp for cellulose acetate." Journal of Applied Polymer Science 107(2): 1029-1038.

He, Z. Y. and F. X. Liu (2003). "Research on anti-fatigue ability of Sisal Fiber Asphalt Mixture Pavement." Applied Mechanics and Materials 405-408: 1782-1785.

Hernández-Olivares, F., I. Oteiza and L. de Villanueva (1992). "Experimental analysis of toughness and modulus of rupture increase of sisal short fiber reinforced hemihydrated gypsum." Composite Structures 22(3): 123-137.

Hewlett, P. (2004). Lea's Chemistry of Cement and Concrete. San Diego., Butterworth-Heinemann.

Hidalgo, A., J. L. Garcia, M. C. Cruz, L. Fernadez, L. Fernandez and C. Andrade (2005). Testing methodology for pH determination of cementitious materials—application to low pH binders for use in HLNWR. Proc. 2nd Workshop on R&D on Low-pH Cement for a Geological Repository. Madrid, Spain.

Hindeleh, A. M. and D. J. Johnson (1980). "An empirical estimation of Scherrer parameters for the evaluation of true crystallite size in fibrous polymers." Polymer 21(8): 929-935.

Hong, S.-Y. and F. P. Glasser (1999). "Alkali binding in cement pastes: Part I. The C-S-H phase." Cement and Concrete Research 29(12): 1893-1903.

Hult, E.-L., T. Iversen and J. Sugiyama (2003). "Characterization of the supermolecular structure of cellulose in wood pulp fibres." Cellulose 10(2): 103-110.

Humphreys, P. N., A. Laws and J. Dawson (2010). A review of cellulose degradation and the fate of degradation products und. Oxfordshire, UK Serco: 1-55.

Jahromi, S. G. and A. Khodaii (2009). "Effects of nanoclay on rheological properties of bitumen binder." Construction and Building Materials 23(8): 2894-2904.

Jakab, E., O. Faix and F. Till (1997). "Thermal decomposition of milled wood lignins studied by thermogravimetry/mass spectrometry." Journal of Analytical and Applied Pyrolysis 40–41(0): 171-186.

Jensen, O. M. (1993). Autogenous deformation and RH-change—self-desiccation and self-desiccation shrinkage. Lyngby, Denmark, Building Materials Laboratory, The Technical University of Denmark.

Johnston, C. D. and Å. Skarendahl (1992). "Comparative flexural performance evaluation of steel fibre-reinforced concretes acoording to ASTM C1018 shows importance of fibre parameters." Materials and Structures 25(4): 191-200.

Joseleau, J. P. C. J. R. K. (1992). Chemical structure of xylans and their interaction in the plant cell walls. Amsterdam, Elsevier.

Joseph, K., B. Kuriakose, C. K. Premalatha, S. Thomas and C. Pavithran (1994). "Melt rheological behavior of short sisal fibre reinforced polyethylene composites." Plastics, Rubber and Composites Processing and Applications 21(4): 237-245.

Joseph, K., S. Thomas and C. Pavithran (1992). "Viscoelastic properties of short-sisal-fiber-filled low-density polyethylene composites: effect of fiber length and orientation." Materials Letters 15(3): 224-228.

Joseph, K., S. Thomas and C. Pavithran (1993). "Dynamic Mechanical Properties of Short Sisal Fiber Reinforced Low Density Polyethylene Composites." Journal of Reinforced Plastics and Composites 12(2): 139-155.

Joseph, K., S. Thomas and C. Pavithran (1995). "Effect of ageing on the physical and mechanical properties of sisal-fiber-reinforced polyethylene composites." Composites Science and Technology 53(1): 99-110.

Joseph, K., S. Thomas and C. Pavithran (1996). "Effect of chemical treatment on the tensile properties of short sisal fibre-reinforced polyethylene composites." Polymer 37(23): 5139-5149.

Joseph, K., S. Thomas, C. Pavithran and M. Brahmakumar (1993). "Tensile properties of short sisal fiber-reinforced polyethylene composites." Journal of Applied Polymer Science 47(10): 1731-1739.

Joshi, S. V., L. T. Drzal, A. K. Mohanty and S. Arora (2004). "Are natural fiber composites environmentally superior to glass fiber reinforced composites?" Composites Part A: Applied Science and Manufacturing 35(3): 371-376.

Juárez, C., A. Durán, P. Valdez and G. Fajardo (2007). Performance of "Agave lecheguilla" natural fiber in portland cement composites exposed to severe environment conditions. Building and Environment.

Junli, R., P. Xinwen, Z. Linxin, P. Feng and S. Runcang (2012). "Novel hydrophobic hemicelluloses: Synthesis and characteristic." Carbohydrate Polymers 89(1): 152-157.

Kalaprasad, G., K. Joseph, S. Thomas and C. Pavithran (1997). "Theoretical modelling of tensile properties of short sisal fibre-reinforced low-density polyethylene composites." Journal of Materials Science 32(16): 4261-4267.

Kallapur, S. K. (1962). Bark and Leaf Fibres of India. Irla Road, Vile Parle, Bombay, Directorate of Publicity, KVIC.

Karihaloo, B. L. and J. Wang (2000). "Micromechanics of Fiber-Reinforced Cementitious Composites." Advanced Engineering Materials 2(11): 726-732.

Kawashima, S., P. Hou, D. J. Corr and S. P. Shah (2013). "Modification of cement-based materials with nanoparticles." Cement and Concrete Composites 36(0): 8-15.

Kennedy, J. F., G. O. Phillips, D. J. Wed-lock and P. A. Williams (1985). Cellulose and Its Derivatives: Chemistry, Biochemistry and Applications,. New York, Chichester, Brisbane,, Marcel Dekker.

Khan, M. N., D. K. Bisoyi, J. Shuckla and R. Sahoo (2011). "Structural aspects of alkali treated sisal fiber — A SAXS investigation." Fibers and Polymers 12(6): 765-770.

Korpa, A., T. Kowald and R. Trettin (2008). "Hydration behaviour, structure and morphology of hydration phases in advanced cement-based systems containing micro and nanoscale pozzolanic additives." Cement and Concrete Research 38(7): 955-962.

Kulik, D. (2002). GEMS-PSI 2.0, PSI, Villigen, Switzerland.

Kumar R., S. S., Singh O.V. (2008). "Bioconversion of lignocellulosic biomass: Biochemical and molecular perspectives." Journal of Industrial Microbiology and Biotechnology 35(5): 377-391.

Kumar, R. P., M. L. G. Amma and S. Thomas (1995). "Short sisal fiber reinforced styrene-butadiene rubber composites." Journal of Applied Polymer Science 58(3): 597-612.

Lai, Y. Z. (1991). Wood and Cellulosic Chemistry. New York and Basel, Marcel Dekker.

Lai, Y. Z. and K. V. Sarkanen (1967). "Kinetics of Alkaline Hydrolysis of Glycosidic Bonds in Cotton Cellulose." Cellulose Chem. Technol. 1(517-527).

Lawrence, C. D. (2003). 4 - The Constitution and Specification of Portland Cements. Lea's Chemistry of Cement and Concrete (Fourth Edition). Oxford, Butterworth-Heinemann: 131-193.

Le Saoût, G. and M. Ben Haha (2011). Effect of filler on early hydration XIII International Congress on the Chemistry of Cement. Madrid.

Le Troedec, M., D. Sedan, C. Peyratout, J. P. Bonnet, A. Smith, R. Guinebretiere, V. Gloaguen and P. Krausz (2008). "Influence of various chemical treatments on the composition and structure of hemp fibres." Composites Part A: Applied Science and Manufacturing 39(3): 514-522.

Li, G., Y. Yu, Z. Zhao, J. Li and C. Li (2003). "Properties study of cotton stalk fiber/gypsum composite." Cement and Concrete Research 33(1): 43-46.

Li, Y., Y.-W. Mai and L. Ye (2000). "Sisal fibre and its composites: a review of recent developments." Composites Science and Technology 60(11): 2037-2055.

Li, Z. and Z. Ding (2003). "Property improvement of Portland cement by incorporating with metakaolin and slag." Cement and Concrete Research 33(4): 579-584.

Litherland, K. L., D. R. Oakley and B. A. Proctor (1981). "The use of accelerated ageing procedures to predict the long term strength of GRC composites." Cement and Concrete Research 11(3): 455-466.

Liu, C.-H. and J. A. Nairn (1999). "Analytical and experimental methods for a fracture mechanics interpretation of the microbond test including the effects of friction and thermal stresses." International Journal of Adhesion and Adhesives 19(1): 59-70.

Loon, L. R. and M. A. Glaus (1997). "Review of the kinetics of alkaline degradation of cellulose in view of its relevance for safety assessment of radioactive waste repositories." Journal of environmental polymer degradation 5(2): 97-109.

Lora, J. H. G., W.G. (2002). "Recent industrial applications of lignin: a sustainable alternative to nonrenewable materials." J. Polym. Environ. 10: 39–48.

Lothenbach, B., K. Scrivener and R. D. Hooton (2011). "Supplementary cementitious materials." Cement and Concrete Research 41(12): 1244-1256.

Lothenbach, B. and F. Winnefeld (2006). "Thermodynamic modelling of the hydration of Portland cement." Cement and Concrete Research 36(2): 209-226.

Lu, F. and J. Ralph (2010). Chapter 6 - Lignin. Cereal Straw as a Resource for Sustainable Biomaterials and Biofuels. Amsterdam, Elsevier: 169-207.

Lura, P., O. M. Jensen and K. van Breugel (2003). "Autogenous shrinkage in high-performance cement paste: An evaluation of basic mechanisms." Cement and Concrete Research 33(2): 223-232.

Machell, G. and G. N. Richards (1960). "385. Mechanism of saccharinic acid formation. Part II. The [small alpha][small beta]-dicarbonyl intermediate in formation of D-glucoisosaccharinic acid." Journal of the Chemical Society (Resumed)(0): 1932-1938.

Madzhidova, V. E., G. N. Dalimova and B. K. Pulatov (1996). "Alkaline hydrolysis of the natural lignin of cottonplant stems in the presence of anthraquinone." Chemistry of Natural Compounds 32(5): 723-727.

Manzano, H., A. N. Enyashin, J. S. Dolado, A. Ayuela, J. Frenzel and G. Seifert (2012). "Do Cement Nanotubes exist?" Advanced Materials 24(24): 3239-3245.

Martin, A. R., M. A. Martins, O. R. R. F. da Silva and L. H. C. Mattoso (2010). "Studies on the thermal properties of sisal fiber and its constituents." Thermochimica Acta 506(1–2): 14-19.

Marx-Figini, V. M. (1963). "Kinetische Untersuchungen zur Biosynthese der Cellulose in der Baumwolle." Die Makromolekulare Chemie 68(1): 227-231.

Marx-Figini, V. M. and G. V. Schulz (1963). "Neuere untersuchungen über größe und größenverteilung der β-glukosidischen ketten nativer cellulosen." Die Makromolekulare Chemie 62(1): 49-65.

Marx-Figini, V. M. and G. V. Schulz (1963). "Neuere untersuchungen über größe und größenverteilung der β-glukosidischen ketten nativer cellulosen." Maka'omol. Chem 62.

Melo Filho, J. d. A., F. d. A. Silva and R. D. Toledo Filho (2013). "Degradation kinetics and aging mechanisms on sisal fiber cement composite systems." Cement and Concrete Composites 40(0): 30-39.

Mohr, B. J., J. J. Biernacki and K. E. Kurtis (2006). "Microstructural and chemical effects of wet/dry cycling on pulp fiber–cement composites." Cement and Concrete Research 36(7): 1240-1251.

Mohr, B. J., J. J. Biernacki and K. E. Kurtis (2007). "Supplementary cementitious materials for mitigating degradation of kraft pulp fiber-cement composites." Cement and Concrete Research 37(11): 1531-1543.

Mohr, B. J., H. Nanko and K. E. Kurtis (2005). "Durability of kraft pulp fiber–cement composites to wet/dry cycling." Cement and Concrete Composites 27(4): 435-448.

Mukherjee, P. S. and K. G. Satyanarayana (1984). "Structure and properties of some vegetable fibres." Journal of Materials Science 19(12): 3925-3934.

Murat, M. and C. Comel (1983). "Hydration reaction and hardening of calcined clays and related minerals III. Influence of calcination process of kaolinite on mechanical strengths of hardened metakaolinite." Cement and Concrete Research 13(5): 631-637.

Mwaikambo, L. Y. and M. P. Ansell (2002). "Chemical modification of hemp, sisal, jute, and kapok fibers by alkalization." Journal of Applied Polymer Science 84(12): 2222-2234.

Nadji, H., P. N. Diouf, A. Benaboura, Y. Bedard, B. Riedl and T. Stevanovic (2009). "Comparative study of lignins isolated from Alfa grass (Stipa tenacissima L.)." Bioresource Technology 100(14): 3585-3592.

Nair, K. C. M., S. M. Diwan and S. Thomas (1996). "Tensile properties of short sisal fiber reinforced polystyrene composites." Journal of Applied Polymer Science 60(9): 1483-1497.

Neville, A. and P.-C. Aïtcin (1998). "High performance concrete—An overview." Materials and Structures 31(2): 111-117.

Novo-Uzal, E., F. Pomar, L. V. Gómez Ros, J. M. Espiñeira and A. Ros Barceló (2012). Chapter 9 - Evolutionary History of Lignins. Advances in Botanical Research. J. Lise and L. Catherine, Academic Press. Volume 61: 309-350.

Oda, S., J. Leomar Fernandes Jr and J. S. Ildefonso (2012). "Analysis of use of natural fibers and asphalt rubber binder in discontinuous asphalt mixtures." Construction and Building Materials 26(1): 13-20.

Oksman, K., L. Wallström, L. A. Berglund and R. D. T. Filho (2002). "Morphology and mechanical properties of unidirectional sisal– epoxy composites." Journal of Applied Polymer Science 84(13): 2358-2365.

Otieno, M., H. Beushausen and M. Alexander (2012). "Prediction of corrosion rate in reinforced concrete structures – a critical review and preliminary results." Materials and Corrosion 63(9): 777-790.

P. Kumar, P. K. S., S. Bose, S. Chandra (2004). "Use of jute fibre in stone matrix asphalt." Road Mater Pav Des 5(2): 239–249.

P.K. Banerjee, M. G. (2008). "Studies on jute-asphalt composites." J Appl Polym Sci 109(5): 3165–3172.

Park, S., J. O. Baker, M. E. Himmel, P. A. Parilla and D. K. Johnson (2010). "Cellulose crystallinity index: measurement techniques and their impact on interpreting cellulase performance." Biotechnol Biofuels 3(10): 1-10.

Patra, A., D. Bisoyi, P. Manda and A. K. Singh (2012). "Effect of microwave radiation on the macromolecular, morphological and crystallographic structures of sisal fiber." Applied Physics A: 1-9.

Pavasars, I., J. Hagberg, H. Borén and B. Allard (2003). "Alkaline Degradation of Cellulose: Mechanisms and Kinetics." Journal of Polymers and the Environment 11(2): 39-47.

Pavithran, C., P. S. Mukherjee, M. Brahmakumar and A. D. Damodaran (1987). "Impact properties of natural fibre composites." Journal of Materials Science Letters 6(8): 882-884.

Pavithran, C., P. S. Mukherjee, M. Brahmakumar and A. D. Damodaran (1988). "Impact performance of sisal-polyester composites." Journal of Materials Science Letters 7(8): 825-826.

Pehanich, J. L., P. R. Blankenhorn and M. R. Silsbee (2004). "Wood fiber surface treatment level effects on selected mechanical properties of wood fiber–cement composites." Cement and Concrete Research 34(1): 59-65.

Phillips, M. (1934). "The Chemistry of Lignin." Chemical Reviews 14(1): 103-170.

Pimentel, L., A. Beraldo and H. Savastano (2006). "Durability of cellulose–cement composites modified by polymer." Eng Agr 26: 344-353.

Pollitt, H. W. W. and A. W. Brown (1969). The distribution of alkalis in Portland cement clinker. 5th ICCC: 322–333.

Ramakrishna, G. and T. Sundararajan (2005). "Studies on the durability of natural fibres and the effect of corroded fibres on the strength of mortar." Cement and Concrete Composites 27(5): 575-582.

Ramezanianpour, A. A. and H. Bahrami Jovein (2012). "Influence of metakaolin as supplementary cementing material on strength and durability of concretes." Construction and Building Materials 30(0): 470-479.

Ramli, M., W. H. Kwan and N. F. Abas (2013). "Strength and durability of coconut-fiber-reinforced concrete in aggressive environments." Construction and Building Materials 38(0): 554-566.

Ramlochan, T., M. D. A. Thomas and R. D. Hooton (2004). "The effect of pozzolans and slag on the expansion of mortars cured at elevated temperature: Part II: Microstructural and microchemical investigations." Cement and Concrete Research 34(8): 1341-1356.

Ray, D. and B. K. Sarkar (2001). "Characterization of alkali-treated jute fibers for physical and mechanical properties." Journal of Applied Polymer Science 80(7): 1013-1020.

Ren, J. L. and R. C. Sun (2010). Chapter 4 - Hemicelluloses. Cereal Straw as a Resource for Sustainable Biomaterials and Biofuels. Amsterdam, Elsevier: 73-130.

Ridi, F., E. Fratini and P. Baglioni (2011). "Cement: A two thousand year old nano-colloid." Journal of Colloid and Interface Science 357(2): 255-264.

Rocha, J. and J. Klinowski (1990). "Festkörper-NMR-Untersuchungen zur Struktur und Reaktivität von Metakaolinit." Angewandte Chemie 102: 539-541.

Rodríguez de Sensale, G. (2006). "Strength development of concrete with rice-husk ash." Cement and Concrete Composites 28(2): 158-160.

Roncero, M. B., A. L. Torres, J. F. Colom and T. Vidal (2005). "The effect of xylanase on lignocellulosic components during the bleaching of wood pulps." Bioresource Technology 96(1): 21-30.

Rong, M. Z., M. Q. Zhang, Y. Liu, G. C. Yang and H. M. Zeng (2001). "The effect of fiber treatment on the mechanical properties of unidirectional sisal-reinforced epoxy composites." Composites Science and Technology 61(10): 1437-1447.

Rothstein, D., J. J. Thomas, B. J. Christensen and H. M. Jennings (2002). "Solubility behavior of Ca-, S-, Al-, and Si-bearing solid phases in Portland cement pore solutions as a function of hydration time." Cement and Concrete Research 32(10): 1663-1671.

Roy, A., S. Chakraborty, S. P. Kundu, R. K. Basak, S. Basu Majumder and B. Adhikari (2012). "Improvement in mechanical properties of jute fibres through mild alkali treatment as demonstrated by utilisation of the Weibull distribution model." Bioresource Technology 107(0): 222-228.

Saha, B. C. (2000). "α-l-Arabinofuranosidases: biochemistry, molecular biology and application in biotechnology." Biotechnology Advances 18(5): 403-423.

Satyanarayana, K. G., K. Sukumaran, P. S. Mukherjee, C. Pavithran and S. G. K. Pillai (1990). "Natural fibre-polymer composites." Cement and Concrete Composites 12(2): 117-136.

Savastano Jr, H. and V. Agopyan (1999). "Transition zone studies of vegetable fibre-cement paste composites." Cement and Concrete Composites 21(1): 49-57.

Savastano Jr, H., P. G. Warden and R. S. P. Coutts (2003). "Potential of alternative fibre cements as building materials for developing areas." Cement and Concrete Composites 25(6): 585-592.

Sedan, D., C. Pagnoux, T. Chotard, A. Smith, D. Lejolly, V. Gloaguen and P. Krausz (2007). "Effect of calcium rich and alkaline solutions on the chemical behaviour of hemp fibres." Journal of Materials Science 42(22): 9336-9342.

Segal, L., J. J. Creely, A. E. Martin and C. M. Conrad (1959). "An Empirical Method for Estimating the Degree of Crystallinity of Native Cellulose Using the X-Ray Diffractometer." Textile Research Journal 29(10): 786-794.

SF4, J. (1984). Method of Tests for Flexural Strength and Flexural Toughness of Fibre Reinforced Concrete, Japan Concrete Institute.

Sha, W. (2002). Differential scanning calorimetry study of the hydration products in portland cement pastes with metakaolin replacement. Advances in Building Technology. M. Anson, J. M. Ko and E. S. S. Lam. Oxford, Elsevier: 881-888.

Sha, W. and G. B. Pereira (2001). "Differential scanning calorimetry study of ordinary Portland cement paste containing metakaolin and theoretical approach of metakaolin activity." Cement and Concrete Composites 23(6): 455-461.

Silva, F., J. A. Melo Filho and R. D. Toledo Filho (2006). Fairbairn EMR. Mechanical behavior and durability of compression moulded sisal fiber cement mortar laminates (SFCML). 1st International RILEM conference on textile reinforced concrete(ICTRC), Rilem Publications S.A.R.L: 171-180.

Silva, F. d. A., N. Chawla and R. D. d. T. Filho (2008). "Tensile behavior of high performance natural (sisal) fibers." Composites Science and Technology 68(15–16): 3438-3443.

Silva, F. d. A., B. Mobasher, C. Soranakom and R. D. T. Filho (2011). "Effect of fiber shape and morphology on interfacial bond and cracking behaviors of sisal fiber cement based composites." Cement and Concrete Composites 33(8): 814-823.

Singh (1985). "Alkali resistance of some vegetables fibers and their adhesion with Portland Cement." Research and Industry 15: 121-126.

Singh, M. and M. Garg (1994). "Gypsum-based fibre-reinforced composites: an alternative to timber." Construction and Building Materials 8(3): 155-160.

Singh, S. M. (1985). "Alkali resistance of some vegetable fibers and their adhesion with Portland cement." Res Ind . 15: 121-126.

Sinha, E. and S. K. Rout (2009). "Influence of fibre-surface treatment on structural, thermal and mechanical properties of jute fibre and its composite." Bulletin of Materials Science 32(1): 65-76.

Sjöström, E. (1993). Wood Chemistry: Fundamentals and Applications (second edition). San Diego, California, USA., Academic Press.

Soroushian, P., J.-P. Won and M. Hassan (2012). "Durability characteristics of CO2-cured cellulose fiber reinforced cement composites." Construction and Building Materials 34(0): 44-53.

Sousa Coutinho, J. (2003). "The combined benefits of CPF and RHA in improving the durability of concrete structures." Cement and Concrete Composites 25(1): 51-59.

Stein, H. N. and J. M. Stevels (1964). "Influence of silica on the hydration of 3 CaO,SiO2." Journal of Applied Chemistry 14(8): 338-346.

Suchismita, A. A Study of Effects of Binder Quality and Natural Fiber on Stone Matrix Asphalt Mixtures Master of Technology, National Institute of Technology, Rourkela.

Sugimoto, T., T. Akiyama, Y. Matsumoto and G. Meshitsuka (2002). "The erythro/threo ratio of beta-O-4 structures as an important structural characteristic of lignin – Part 2. Changes in erythro/threo (E/T) ratio of beta-O-4 structures during delignification reactions." Holzforschung 56: 416–421.

Sun, J. X., X. F. Sun, H. Zhao and R. C. Sun (2004). "Isolation and characterization of cellulose from sugarcane bagasse." Polymer Degradation and Stability 84(2): 331-339.

Sun, R., Q. Lu and X. F. Sun (2001). "Physico-chemical and thermal characterization of lignins from Caligonum monogoliacum and Tamarix spp." Polymer Degradation and Stability 72(2): 229-238.

Swift, D. G. and R. B. L. Smith (1979). "The flexural strength of cement-based composites using low modulus (sisal) fibres." Composites 10(3): 145-148.

Theander, O. and D. A. Nelson (1988). Aqueous, High-Temperature Transformation of Carbohydrates Relative to Utilization of Biomass. Advances in Carbohydrate Chemistry and Biochemistry. R. S. Tipson and D. Horton, Academic Press. Volume 46: 273-326.

Thulsairajan, K. and V. L. Narasimha (2011). "Studies on coir fibre reinforced bituminous concrete." Int J Earth Sci Eng. 4(6): 835-838.

Timell, T. E. (1967). "Recent progress in the chemistry of wood hemicelluloses." Wood Science and Technology 1(1): 45-70.

Tolêdo Filho, R. D., K. Ghavami, G. L. England and K. Scrivener (2003). "Development of vegetable fibre–mortar composites of improved durability." Cement and Concrete Composites 25(2): 185-196.

Tolêdo Filho, R. D., K. Scrivener, G. L. England and K. Ghavami (2000). "Durability of alkali-sensitive sisal and coconut fibres in cement mortar composites." Cement and Concrete Composites 22(2): 127-143.

Toledo Filho, R. D., F. d. A. Silva, E. M. R. Fairbairn and J. d. A. M. Filho (2009). "Durability of compression molded sisal fiber reinforced mortar laminates." Construction and Building Materials 23(6): 2409-2420.

Tonoli, G. H. D., U. P. Rodrigues Filho, H. Savastano Jr, J. Bras, M. N. Belgacem and F. A. Rocco Lahr (2009). "Cellulose modified fibres in cement based composites." Composites Part A: Applied Science and Manufacturing 40(12): 2046-2053.

Tonoli, G. H. D., S. F. Santos, A. P. Joaquim and H. Savastano Jr (2010). "Effect of accelerated carbonation on cementitious roofing tiles reinforced with lignocellulosic fibre." Construction and Building Materials 24(2): 193-201.

Torkaman, J., A. Ashori and A. Sadr Momtazi (2014). "Using wood fiber waste, rice husk ash, and limestone powder waste as cement replacement materials for lightweight concrete blocks." Construction and Building Materials 50(0): 432-436.

van Hazendonk, J. M., J. C. van der Putten, J. T. F. Keurentjes and A. Prins (1993). "A simple experimental method for the measurement of the surface tension of cellulosic fibres and its relation with chemical composition." Colloids and Surfaces A: Physicochemical and Engineering Aspects 81(0): 251-261.

Van Loon, L. R. and M. A. Glaus (1998). TECHNICAL REPORT 97-04-Experimental and TheoreticalStudies on Alkaline Degradationof Cellulose and its Impact onthe Sorption of Radionuclides, Wurenlingen, Switzerland, Paul Scherrer Institut.

Van Tuan, N., G. Ye, K. van Breugel and O. Copuroglu (2011). "Hydration and microstructure of ultra high performance concrete incorporating rice husk ash." Cement and Concrete Research 41(11): 1104-1111.

Vance, K., M. Aguayo, T. Oey, G. Sant and N. Neithalath (2013). "Hydration and strength development in ternary portland cement blends containing limestone and fly ash or metakaolin." Cement and Concrete Composites 39(0): 93-103.

Viera, R. G. P., G. R. Filho, R. M. N. de Assunção, C. d. S. Meireles, J. G. Vieira and G. S. de Oliveira (2007). "Synthesis and characterization of methylcellulose from sugar cane bagasse cellulose." Carbohydrate Polymers 67(2): 182-189.

Vijay K. Kaushik, A. K., Susheel Kalia (2012). "Effect of Mercerization and Benzoyl Peroxide Treatment on Morphology, Thermal Stability and Crystallinity of Sisal Fibers." International Journal of Textile Science 1(6): 101-105

Walker, J. C. F. (1993). Primary wood processing: principles and practice, Chapman and Hall.

Wardrop, A. B. (1964). The Formation of Wood in Forest Trees. New York, Academic Press.

Wei, J. Q. and C. Meyer (2014). "Improving degradation resistance of sisal fiber in concrete through fiber surface treatment." Applied Surface Science 289(0): 511-523.

Whistler, R. L. and J. N. BeMiller (1958). Alkaline Degradation of Polysaccharides. Advances in Carbohydrate Chemistry. L. W. Melville, Academic Press. Volume 13: 289-329.

Wild, S., J. M. Khatib and A. Jones (1996). "Relative strength, pozzolanic activity and cement hydration in superplasticised metakaolin concrete." Cement and Concrete Research 26(10): 1537-1544.

Wild, S., J. M. Khatib and L. J. Roose (1998). "Chemical shrinkage and autogenous shrinkage of Portland cement–metakaolin pastes." Adv Cem Res 10: 109-119.

William, H. (1975). Official methods of analysis of the Association of Official Analytical Chemists. Birmingham, AL, U.S.A., Association of Official Analytical Chemists.

Wilson, P. I. (1971). Sisal. Hard Fibres Research Series, No. 8. 11.

Word, W. s. (2006) "Major part of chemical compounds in plants & animals – Part II Phenolic compounds glycosides & alkaloids."

Wu, Z.-Q. and J. F. Young (1984). "The hydration of tricalcium silicate in the presence of colloidal silica." Journal of Materials Science 19(11): 3477-3486.

Xu, F., J. X. Sun, C. F. Liu and R. C. Sun (2006). "Comparative study of alkali- and acidic organic solvent-soluble hemicellulosic polysaccharides from sugarcane bagasse." Carbohydrate Research 341(2): 253-261.

Yang, G. C., H. M. Zeng, J. J. Li, N. B. Jian and W. B. Zhang (1996). "Relation of modification and tensile properties of sisal fibre." Acta Scientiarum Naturalium Universitatis Sunyatseni 35: 53-57.

Yao, F., Q. Wu, Y. Lei, W. Guo and Y. Xu (2008). "Thermal decomposition kinetics of natural fibers: Activation energy with dynamic thermogravimetric analysis." Polymer Degradation and Stability 93(1): 90-98.

Zhandarov, S. and E. Mäder (2005). "Characterization of fiber/matrix interface strength: applicability of different tests, approaches and parameters." Composites Science and Technology 65(1): 149-160.

Zhang, M. H., R. Lastra and V. M. Malhotra (1996). "Rice-husk ash paste and concrete: Some aspects of hydration and the microstructure of the interfacial zone between the aggregate and paste." Cement and Concrete Research 26(6): 963-977.

Zhang, M. H. a. M., M.V. (1996). "High-Performance Concrete Incorporating Rice Husk Ash as a Supplementary Cementing Material." ACI Materials Journal 93(6): 629-636.

Ziderman, I. and J. Bel-Ayche (1978). "Kinetics for unidirectional endwise chain depolymerizations. Experiments with amylose in aqueous alkaline solutions." Journal of Applied Polymer Science 22(4): 1151-1158.

Ziderman, I. I. and J. Belayche (1986). "Using disaccharides as a kinetic model for alkaline degradation of celluloses and starches." Journal of Applied Polymer Science 32(1): 3255-3261.